Factors controlling the formation and occurrence of petroleum in Norwegian petroleum systems, as revealed by considerations of chemical and isotopic compositions

vorgelegt von
M. Sc. Geologin
Wendy Murillo Hernandez
ORCID: 0000-0002-8391-5390

von der Fakultät VI – Planen Bauen Umwelt
der Technischen Universität Berlin
zur Erlangung des akademischen Grades

Doktor der Naturwissenschaften
- Dr. rer. nat. -

genehmigte Dissertation

Promotionsausschuss:

Vorsitzender: Prof. Dr. Thomas Neumann
Gutachter: Prof. Dr. Brian Horsfield
Gutachter: Prof. Dr. Jan Schwarzbauer

Tag der wissenschaftlichen Aussprache: 23. Oktober 2020

Berlin 2021

Dedicated to my beloved daughter Shany

Statement of Original Authorship

I, Wendy A. Murillo, hereby state that the work contained in this thesis or any parts thereof has not previously been submitted to the Fakultät VI - Planen, Bauen, Umwelt at the Technical University of Berlin or any other institution except where explicitly acknowledged. To the best of my knowledge and belief, the thesis does not contain any previously published material which has been written by another person except where due reference is made.

Hiermit erkläre ich, Wendy A. Murillo, dass diese Arbeit bisher von mir weder an der Fakultät VI - Planen, Bauen, Umwelt der Technischen Universität Berlin noch einer anderen wissenschaftlichen Einrichtung zum Zwecke der Promotion eingereicht wurde. Ferner erkläre ich, dass ich diese Arbeit selbständig verfasst und keine weiteren als die darin angegebenen Quellen und Hilfsmittel benutzt habe.

Wendy A. Murillo

June 2020

Acknowledgements

First and foremost, I would like to thank God for the life, his strength, sustenance and above all his faithfulness and love through the best and toughest years of my life. Thank God for giving me the strength, knowledge and ability to undertake this research study and to persevere until being able to complete it satisfactorily. He has made this possible.

I would like to express my sincere gratitude and deep appreciation to my academic tutor and supervisor Professor Dr. Brian Horsfield for giving me the opportunity to join his Organic Geochemistry research group, helping me to acquire the isotope data for my third research article, reading publications and this dissertation and offering constructive comments, as well as helping me to finish my PhD study. Many thanks also to Dr. Andrea Vieth and Dr. Heinz Wilkes for letting me to research into the stable isotope field and giving me a space to develop my ideas. I am grateful to Prof. Jan Schwarzbauer (Aachen University) and Prof. Thomas Neumann (TU Berlin) for reviewing the thesis and attending dissertation defense. My sincere thanks also go to Prof. Katja Deckart, head of Geology department at the University of Chile, for her support and collaboration to conduct the scientific defense of my doctoral dissertation.

I greatly acknowledge the financial support of the German Academic Exchange Service (DAAD) to pursue my doctoral degree. My deep gratitude is also extended to the Norwegian Petroleum Directorate (NPD) for the kind contribution of oil, core and cuttings samples for my doctoral research.

I am very grateful to Anika Zabel, Anke Kaminski, Cornelia Karger, Doreen Noack and Kristin Günther for their technical support and help to do lab work. My sincere gratitude goes to Claudia Engelhardt for her support and dealing with all my queries. Further thanks are to my colleagues at GFZ, especially Yaling Zhu, Yuanjia Han and Ricardo Ruiz for all their kind support during my doctoral studies. A very special word of thanks goes to my friend Clelia Medina from the FU Berlin for her friendship and for always cheering me up. I will always appreciate the time we spent together during our PhD studies.

Finally, I want to express my special gratitude to my beloved daughter Shany. It is your love that has got me through when I wanted to give up. I dedicate this thesis to you, my Shany.

List of Publications

Articles in peer-reviewed journals

Paper 1 - **Murillo, W.A.**, Vieth-Hillebrand, A., Horsfield, B., Wilkes, H., 2016. Petroleum source, maturity, alteration and mixing in the southwestern Barents Sea: New insights from geochemical and isotope data. Marine and Petroleum Geology, 70, 119-143, https://doi.org/10.1016/j.marpetgeo.2015.11.009.

Paper 2 - **Murillo, W.A.**, Horsfield, B., Vieth-Hillebrand, A., 2019. Unraveling petroleum mixtures from the South Viking Graben, North Sea: A study based on $\delta^{13}C$ of individual hydrocarbons and molecular data. Organic Geochemistry, 137, https://doi.org/10.1016/j.orggeochem.2019.103900.

Paper 3 - **Murillo, W.A.**, Horsfield, B., Garcin, Y., Vieth, A., Sachse, D., 2021. Compound-specific $\delta^{2}H$ and $\delta^{13}C$ values of *n*-alkanes as a tool to unravel complex petroleum mixtures in the South Viking Graben, Norway. Organic Geochemistry, *In Press,* published online, https://doi.org/10.1016/j.orggeochem.2020.104167.

Presentations at international conferences

- **Murillo, W.A.**, Vieth-Hillebrand, A., Horsfield, B., 2018. Petroleum in the Gullfaks Area, Northern North Sea: A New Appraisal of Source Indicators from Molecular and Isotope Data. Second EAGE Workshop on Geochemistry in Petroleum Operations and Production, Muscat, Oman. Extended Abstract, pp. 1-5, https://doi.org/10.3997/2214-4609.201803094.

- **Murillo, W.A.,** Horsfield, B., Vieth-Hillebrand, A., Wilkes, H., 2017. Source Indicators to Unravel Mixtures of Oils in the South Viking Graben, North Sea: A Study based on $\delta^{13}C$ of Individual Hydrocarbons, PAHs and Sulfur Aromatic Hydrocarbons. AAPG Annual Convention and Exhibition, Search and Discovery Article Nº 90291, Houston, Texas, USA.

- **Murillo, W.A.**, Vieth-Hillebrand, A., Horsfield, B., Wilkes, H., 2017. Petroleum Correlation in the Tampen Spur Area, North Sea: A New Approach from Molecular and Stable Carbon Isotopic Data of Light Hydrocarbons. AAPG Annual Convention and Exhibition, Search and Discovery Article Nº 90291, Houston, Texas, USA.

- **Murillo, W.A**, Wilkes, H., Horsfield, B., Vieth-Hillebrand, A., 2014. Deciphering oil mixing from Jurassic, Triassic and Paleozoic source rocks in the Hammerfest Basin, SW Barents Sea. AAPG International Conference and Exhibition "The Spirit Between Continents: Energy Geosciences in a Changing World", Search and Discovery Article Nº 90194, Istanbul, Turkey.

- **Murillo, W.A.**, Wilkes, H., Vieth-Hillebrand, A., 2013. Assessing the effects of primary and in-reservoir processes using biomarkers and compound-specific isotopic compositions in crude oils from the Norwegian Viking Graben, North Sea. Book of Abstracts of the Communications; vol. 2, 26th International Meeting on Organic Geochemistry-IMOG, Costa Adeje, Tenerife Spain, pp. 100-101.

- **Murillo, W.A.**, Vieth-Hillebrand, A. and Wilkes, H., 2012. New insights into the effects of primary and in-reservoir processes in the Norwegian South Viking Graben using compound-specific carbon and hydrogen isotopic compositions in crude oils. Book of Abstracts, Joint European Stable Isotopes Users Group Meeting-JESIUM, Leipzig, Germany, pp. 177-178.

Abstract

Establishing genetic correlations between oils and between oils and their source rocks is especially difficult in basins with multiple source rocks where oil mixing has occurred. It is therefore of paramount importance to employ multiparameter approaches based on a combination of source-related molecular markers across different fractions of oils and source rock extracts in order to perform meaningful oil-oil and oil-source correlations rather than simply relying on classical correlation protocols based on biomarkers. Furthermore, the complexity of petroleum mixtures demands that compound-specific isotope analysis (CSIA) rather than bulk isotope analysis are implemented, as CSIA enables the identification of multiple organic matter sources in oils, condensates and source rock extracts by comparing the isotopic compositions of individual hydrocarbons of different chain length. The main objective of this dissertation has been to investigate the source, maturation, alteration and mixing of petroleum in two basin-specific case studies, (1) the Hammerfest Basin (HB), Norwegian Barents Sea and (2) the South Viking Graben (SVG), Norwegian North Sea. For this purpose, multiparameter approaches that combine the molecular composition of different petroleum components, such as light hydrocarbons, *n*-alkanes, sterane and triterpane biomarkers, resin-derived biomarkers, heterocyclic and polycyclic aromatic hydrocarbons in conjunction with compound-specific stable carbon and hydrogen isotope compositions of alkanes have been employed. The present research work also addresses the issue of how best to unravel and quantify the relative input of different source rocks contributing to mixed oils using $\delta^{13}C$ values of individual petroleum hydrocarbons.

Molecular and isotopic evidence revealed distinct petroleum mixing processes involving source, age and thermal maturity variations in reservoirs of the HB. The mixtures originated from hydrocarbons derived from Type-II and Type-III kerogen-rich source rocks, which displayed only small maturity variation within the main stage of oil generation or between the peak and late-oil generation stages. Nonetheless, mixtures of hydrocarbons generated from source rocks at multiple levels of maturity were identified in the Goliat field. $\delta^{13}C$ values of *n*-alkanes ($>C_{15}$) were valuable for oil-source rock correlation and even quantification of the relative contribution from distinct source rocks. They enabled the

differentiation of Triassic and Jurassic source contribution and also provided new insights into an additional Paleozoic-source input in the HB. Moreover, several petroleum alteration processes were recognized in Jurassic and Triassic reservoirs, including microbial degradation, water washing, evaporative fractionation, influx of gas-condensate charge and advance level of thermal maturation.

In the SVG, heterocyclic and polycyclic aromatic compounds proved useful in the differentiation of mixed petroleum from Jurassic source rocks of distinct organic matter types, depositional environments and lithologies. According to the relative contribution of oils from Type-III kerogen rich source rocks, seven populations of mixed petroleum were identified by combining source-related ratios of heterocyclic and polycyclic hydrocarbons and $\delta^{13}C$ values of *n*-alkanes, pristane (Pr) and phytane (Ph). The ^{13}C-enrichments of (C_{10}-C_{14}) *n*-alkanes, and Pr and Ph were good indicators of the scale of the terrigenous source contribution and allowed the quantitative determination of the proportional contribution of hydrocarbons from Jurassic source rocks enriched in Type-II and Type-III kerogens to complex mixtures of petroleum. The estimated mixing proportions correlated linearly with concentration data, supporting the use of compound-specific stable carbon isotope composition for quantitative assignment of sources in mixed oils generated at moderate thermal maturity. Furthermore, hydrogen CSIA of *n*-alkanes proved to be a powerful tool to discriminate petroleum mixtures and provided an improved resolution to unravel complex petroleum mixtures from multiple Jurassic source rocks in the SVG. Multiparameter approaches that include the molecular composition of different petroleum fractions as well as $\delta^{13}C$ and δD values of individual alkanes allowed to gain new insights into the source origins of petroleum mixtures and the assessment of diverse secondary alteration processes as well as a more complete and comprehensive understanding of the multiple petroleum systems in the HB and SVG.

Zusammenfassung

Die Herstellung genetischer Korrelationen zwischen Ölen und zwischen Ölen und ihren Quellgesteinen wird in einem Becken mit mehreren Quellgesteinen aufgrund der Ölmischung im Reservoir schwieriger. Es ist daher von größter Bedeutung, Multiparameter-Ansätze zu verwenden, die auf einer Kombination von quell-bezogenen molekularen Markern in verschiedenen Fraktionen von Ölen und Quellgesteinsextrakten basieren, um aussagekräftige Öl zu Öl- und Öl zu Quellen-Korrelationen anstelle der auf Biomarkern basierenden klassischen Korrelationsstudien aufzuzeigen. Darüber hinaus erfordert das Auftreten komplexer Erdölmischungen die Durchführung einer verbindungsspezifischen Isotopenanalyse (CSIA) anstelle einer Massenisotopenanalyse, da CSIA die Identifizierung mehrerer Quellen organischer Stoffe in Ölen, Kondensaten und Quellgesteinsextrakten durch Vergleich der Isotopenzusammensetzungen von einzelnen Kohlenwasserstoffen unterschiedlicher Kettenlänge ermöglicht. Das Hauptziel dieser Dissertation ist es, die Herkunft, Reifung, Veränderung und Vermischung von Erdöl in zwei beckenbezogenen Fallstudien zu untersuchen: (1) das Hammerfest-Becken (HB) in der norwegischen Barentssee und (2) dem Süd-Viking-Graben (SVG) in der norwegischen Nordsee. Zu diesem Zweck werden Multiparameter-Ansätze verwendet, die die molekulare Zusammensetzung verschiedener Erdölkomponenten wie leichte Kohlenwasserstoffe, *n*-Alkane, Steran- und Triterpan-Biomarker, von Harz abgeleitete Biomarker, heterocyclische und polycyclische aromatische Kohlenwasserstoffe in Verbindung mit verbindungsspezifischem stabilem Kohlenstoff und Wasserstoff Isotopenzusammensetzungen von Alkanen betrachten. Die vorliegende Forschungsarbeit befasst sich auch mit dem Problem der Entschlüsselung und Quantifizierung des relativen Beitrags verschiedener Quellgesteine zu den gemischten Ölen unter Verwendung von $\delta^{13}C$-Werten einzelner Erdölkohlenwasserstoffe.

Molekulare und isotopische Hinweise ergaben unterschiedliche Erdölmischprozesse, bei denen Schwankungen der Quelle, des Alters und der thermischen Reife in den HB-Reservoirs auftreten. Gemische resultierten aus Kohlenwasserstoffen, die aus kerogenreichen Quellgesteinen vom Typ II und Typ III mit geringen Reifegradschwankungen innerhalb der Hauptstufe der Ölentstehung oder zwischen der Spitzen- und der späten Ölentstehungsstufe stammen. Dennoch wurden im Goliat-Feld Gemische von Kohlenwasserstoffen identifiziert,

die aus Quellgesteinen mit unterschiedlichen Reifegraden entsprangen. $\delta^{13}C$-Werte von *n*-Alkanen (>C_{15}) waren für die Korrelation von Ölquellgesteinen und sogar für die Quantifizierung des relativen Beitrags von verschiedenen Quellgesteinen hilfreich. Sie ermöglichten die Unterscheidung des Beitrags von Trias- und Juraquellen und lieferten neue Einblicke in einen zusätzlichen Beitrag aus paläozoischen Quellen in der HB. Darüber hinaus wurden in jurassischen und triassischen Reservoirsverschiedene Erdölveränderungsprozesse erkannt, darunter mikrobieller Abbau, Wasserauswaschungen, Verdunstungsfraktionierung, Einströmen von Gaskondensatladungen und fortschreitende thermische Reifung.

In dem SVG erwiesen sich heterocyclische und polycyclische aromatische Verbindungen als nützlich bei der Differenzierung von gemischtem Erdöl aus jurassischen Quellgesteinen mit unterschiedlichen Arten organischer Stoffe, Ablagerungsumgebungen und Lithologien. Entsprechend dem relativen Beitrag von Ölen aus kerogenreichen Quellgesteinen des Typs III wurden sieben Populationen von gemischtem Erdöl identifiziert, indem quellbezogene Verhältnisse von heterocyclischen und polycyclischen Kohlenwasserstoffen und $\delta^{13}C$-Werten von *n*-Alkanen, Pristan (Pr) und Phytan (Ph) kombiniert wurden. Die ^{13}C-Anreicherungen von (C_{10}-C_{14}) *n*-Alkanen sowie Pr und Ph waren gute Indikatoren für das Ausmaß des Beitrags der terrigenen Quelle und ermöglichten die quantitative Bestimmung des proportionalen Beitrags von Kohlenwasserstoffen aus jurassischen Quellgesteinen, die mit Typ II und Typ III Kerogenen zu komplexen Erdölmischungen angereichert sind. Die geschätzten Mischungsverhältnisse korrelierten linear mit den Konzentrationsdaten, was die Verwendung einer verbindungsspezifischen stabilen Kohlenstoffisotopenzusammensetzung für die quantitative Zuordnung von Quellen in gemischten Ölen unterstützt, die bei mäßiger thermischer Reife erzeugt wurden. Darüber hinaus erwies sich die Wasserstoff-CSIA von *n*-Alkanen als leistungsstarkes Instrument zur Unterscheidung von Erdölmischungen und bot eine verbesserte Auflösung, um komplexe Erdölmischungen aus mehreren jurassischen Quellgesteinen im SVG zu entschlüsseln. Multiparameter-Ansätze, die molekulare Zusammensetzung verschiedener Erdölfraktionen sowie $\delta^{13}C$- und δD-Werte einzelner Alkane umfassen, ermöglichten neue Einblicke in die Herkunft von Erdölgemischen und die Bewertung verschiedener sekundärer Alterationsprozesse sowie ein vollständigeres und umfassenderes Verständnis der vielfältigen Erdölsysteme in der HB und SVG.

Contents

List of Figures

List of Tables

Abbreviations

API	**A**merican **P**etroleum **I**nstitute (measure of oil density)
BTEX	**B**enzene, **T**oluene, **E**thylbenzene and **X**ylene
CPI	**C**arbon **P**reference **I**ndex
DST	**D**rill **S**tem **T**est
GC-FID	**G**as **C**hromatography-**F**lame **I**onization **D**etector
GC-MS	**G**as **C**hromatography-**M**ass **S**pectrometry
GC-MS-IRMS	**G**as **C**hromatography-**M**ass **S**pectrometry-**I**sotope **R**atio **M**ass **S**pectrometry
HC	**H**ydrocarbon
HI	**H**ydrogen **I**ndex (mg HC/g TOC)
MD	**M**easured **D**epth (m)
MDR	**M**ethyl **D**ibenzothiophene **R**atio
MPDF	**M**ethyl **P**henanthrene **D**istribution **F**actor
MPI	**M**ethyl **P**henanthrene **I**ndex
MPLC	**M**edium **P**ressure **L**iquid **C**hromatography
PAHs	**P**olycyclic **A**romatic **H**ydrocarbons
Ph, Pr	**Ph**ytane, **Pr**istane
R_c	Calculated vitrinite reflectance (%)
R_o	Measured vitrinite reflectance (%)
T_{max}	Pyrolysis oven temperature during maximum generation of hydrocarbons
TOC	**T**otal **O**rganic **C**arbon
$\delta^{13}C$	Stable carbon isotope composition ($^{13}C/^{12}C$ ratio) relative the standard Peedee Belemnite (PDB)
δD or δ^2H	Hydrogen isotope composition ($^2H/^1H$ ratio) relative to the Vienna Standard Mean Ocean Water (VSMOW)

Chapter 1

Introduction

As a general background for the understanding of the present PhD research study, an explanation of the processes involved in petroleum formation as well as a detailed review of the main chemical and physical secondary processes that can alter its composition within the reservoir, and how stable carbon and hydrogen isotope compositions of individual petroleum hydrocarbons behave as a result of these processes, will be provided in the following sections. Furthermore, a description of multiparameter research approaches for geochemical correlation purposes based on source indicators across different fractions of oils and source rock extracts, will be developed in the current chapter.

1.1. The Origin of Petroleum

Petroleum is formed from organic matter occurring within the sediments of sedimentary basins, therefore it is important to know how and why organic-rich deposits form. The formation of organic-rich sediments depends on (1) a high supply of biogenic organic matter, which varies from partially degraded biomass extending from hydrogen-rich algal/bacterial material to hydrogen-poor woody fragments; (2) a low supply of oxygen-bearing water to favor the organic matter preservation; and (3) a supply of inorganic mineral matter that not overwhelm to organic matter in order to prevent its dilution significantly. Thus, the accumulation of organic matter represents a duality between the processes that preserve and concentrate organic matter and those that destroy and dilute it. Favorable conditions for the deposition of sediments rich in organic matter are found on the continental

shelves in areas of quiet waters, such as lagoons, estuaries, in the continental slopes and deep marine basins of restricted circulation (Littke et al., 1997).

After deposition, the organic matter composed primarily of biopolymers, such as carbohydrates, proteins, lipids and lignin is buried with the sediments and undergoes successive steps of thermal transformation to convert it in petroleum. The three major stages of petroleum formation are diagenesis, catagenesis and metagenesis (Tissot and Welte, 1978). Diagenesis is defined as changes that occur in sediments during the early stage of burial under conditions of relatively low pressure and temperature (up to 60-80 ºC) (e.g., Tissot et al., 1974; Tissot and Welte, 1984). During diagenesis some biopolymers are first degraded by microorganisms, then the residue not used by microbes recombines by polycondensation and polymerization to form complex high-molecular-weight geopolymers (Durand et al., 1980; Tissot and Welte, 1984), which along with undegraded biopolymers (e.g., Hunt, 1979; Tegelaar et al., 1989; Mösle et al., 1998), such as lignin, cutan, algaenan, tannin among others, become the precursors of kerogen. These precursors of kerogen undergo a whole series of low-temperature reactions, such as decarboxylation, deamination, polymerization and reduction, which result in the formation of kerogen through the loss of oxygen, nitrogen and sulfur (e.g., Tissot and Welte, 1984, Hunt, 1996). At this stage, the few hydrocarbons observed in extracts result from direct incorporation of hydrocarbon biomarkers into the sediments and their early diagenetic transformation of functionalized biomarkers (such as fatty acids and fatty alcohols) into more stable hydrocarbons (e.g., Hunt, 1996). The bitumen contains a high proportion of nitrogen, sulfur and oxygen (NSO) compounds. Besides, biogenic methane is also formed during diagenesis (e.g., Tissot et al., 1974; Durand et al., 1980; Rice and Claypool, 1981; Tissot and Welte, 1984). The kerogen formed during diagenesis, is commonly defined as the condensed macromolecular fraction of the organic mater in sediments, which is insoluble in organic solvents (Forsman and Hunt, 1958; Durand, 1980; Tissot and Welte, 1984, Tegelaar et al., 1989). In contrast, the fraction that is soluble in organic solvents is called bitumen (Tissot and Welte, 1984).

Catagenesis results from an increase in temperature during burial in sedimentary basins. During this stage, the kerogen produces first liquid hydrocarbons in the so-called oil

window. As thermal stress increases the cracking of both kerogen and oil results in the formation of wet gas and condensates. Oil, condensate and wet gas progressively degrade into significant amounts of methane as secondary cracking proceeds (e.g., Tissot and Welte, 1984; Behar and Vandenbroucke, 1987; Bordenave, 1993; Hunt, 1996). Metagenesis is the last stage in the thermal evolution of the sedimentary organic matter, and occurs in the temperature range of 200 to 250 ºC. Here, some methane is generated from the kerogen (e.g., Mahlstedt and Horsfield, 2012) and a graphitic structure begins to form.

Evidence suggests that kerogen is likely formed by a combination of the selective preservation of biopolymers that are resistant to microbial and chemical degradation, and the formation of new geopolymers (e.g., Tegelaar et al., 1989; Allard et al., 2002). Various resistant highly aliphatic, insoluble and non-hydrolyzable biopolymers have been found in organisms, of which algaenan from microalgae has a particularly high preservation potential (Tegelaar et al., 1989). Other resistant biopolymers known as sporopollenin, cutin and cutan have been found in spores and higher plants, respectively (e.g., Mösle et al., 1998; de Leeuw et al., 2006). Also, highly aliphatic biopolymers have been identified in cyanobacteria (e.g., Biller et al., 2015). The oxidative polymerization of low molecular weight lipids is another pathway explaining the presence of the aliphatic content in kerogens (de Leeuw et al., 2006). Gupta et al. (2014) have argued in favour of the formation of geopolymers from lipids also contributing to the aliphatic content of kerogens due to algaenan not being as widespread ecologically and phylogenetically.

Most petroleum forms from the thermal cracking of the kerogen, whose composition largely dictates the type of first generated petroleum (oil, condensate and gas). The composition and type of kerogen depend on the nature of the biological input, the environment of deposition and the preservation pathway (Briggs, 1999; de Leeuw et al., 2006). Based on their carbon, hydrogen and oxygen contents, kerogens have been classified as Type-I, II, III and IV (Tissot et al., 1974; Durand et al., 1980; Tissot and Welte, 1984). Types-I and II generate most of world oil reserves and Type-III generates mainly gas, condensate and some waxy oil. Type-IV generates only small amounts of methane and CO_2.

Kerogen Type-I occurs particularly in lacustrine environments, although it can also occur in marine environments. It is predominantly composed of the most hydrogen-rich organic matter, and initially has a high H/C ratio (≥1.5) and a low O/C ratio (<0.1). It contains a significant contribution from lipid and highly aliphatic biopolymers, especially long-chain aliphatics. These aliphatic components, especially in lacustrine kerogens, are predominantly derived from algaenan present in algae (e.g., Gelin et al., 1997; Goth et al., 1998) with contributions from amorphous bacterial material. The freshwater alga *Botryococcus braunii* is a major contributor to Type-I kerogens (Tegelaar et al., 1989). Compared to other kerogen types, the content of aromatic units and heteroatoms is low.

Kerogen Type-II is more common than Type-I, and has relatively high H/C and low O/C ratios. This kerogen is usually related to marine settings and derive from a mixture of autochthonous organic matter from phytoplankton (and possibly also zooplankton and bacteria) together with an allochtonous contribution of higher plants. It contains higher amounts of polyaromatic nuclei as compared to Type-I kerogen, and abundant aliphatic structures mostly with chains of moderate length (up to C_{25}). The sulfur-rich Type-II kerogens (Type-IIS) contain high organic sulfur (8-14 wt.%, atomic S/C≥0.04) (Orr, 1986). A model of the chemical structure of Type-II kerogen at the beginning of catagenesis is depicted in Figure 1.1.

Kerogen Type-III is formed essentially from lignocellulose biopolymers derived in the majority of vascular plants, containing land-plant debris, so vitrinite macerals predominate. Initially, it has a low H/C (<1.0) and a high O/C (up to 0.3) ratio, hence it generates less oil than do Type-I and II. A significant proportion of polyaromatic nuclei and minor amounts of aliphatic groups, often bound to oxygen-containing groups, are present in this kerogen type. Finally, kerogen Type-IV consists of primary or reworked oxidized organic material. This residual type of kerogen exhibits abnormally low H/C ratios associated with high O/C ratios, thus it cannot generate any hydrocarbons and is considered to be one form of “dead carbon”

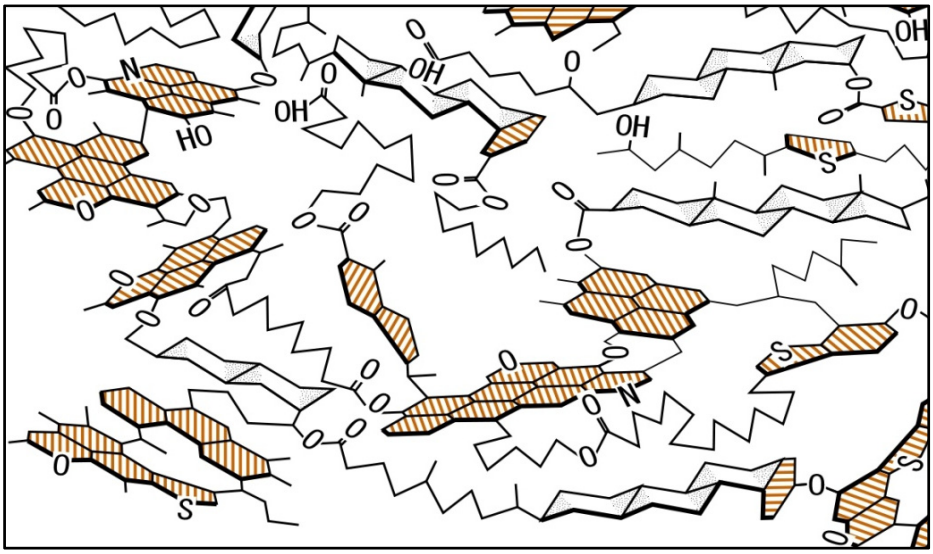

FIGURE 1.1. *Chemical structure of Type-II kerogen of the Lower Toarcian shales from the Paris Basin at the onset of oil generation. Redrawn from Tissot et al. (1987).*

1.2. Petroleum Migration, Accumulation and Alteration through Secondary Processes in the Reservoirs

Petroleum generated during the maturation of organic matter, may be expelled out of the source rock and find its way to traps where it can accumulate. The expulsion of petroleum from the source rock towards carrier beds is called primary migration. Subsequently, oil and natural gas move through the complex network of faults and carrier beds up to their accumulation into traps in a process called secondary migration. These traps consist of a permeable "reservoir rock" and a permeability barrier which retain the migration of hydrocarbons, allowing their accumulation in a reservoir. The traps can be stratigraphic or structural, but commonly they are located in the upper zones of the geological structures, such as the anticlines. The oil and gas can also escape from one trap to another or up to the surface, through faults, unconformities or not fully efficient cap rocks. This process is called tertiary migration.

Once the petroleum has been generated, expelled, migrated and trapped, various chemical and physical secondary processes can alter its composition within the reservoir. The understanding of their effects on petroleum quality is important in order to estimate the

economic value of the petroleum that might occur in a prospect. A schematic summary of the main factors influencing oil composition is shown in Figure 1.2. A brief review of the main in-reservoir alteration processes is described as follows.

1.2.1. Biodegradation and Water Washing

Biodegradation is the microbial alteration of crude oil (e.g., Milner et al., 1977; Connan, 1984; Palmer, 1993, Blanc and Connan, 1994), which usually occurs in reservoirs whose temperature have never exceeded 90 ºC (Wilhelms et al., 2001). Whereas, water washing applies to the removal of water soluble compounds (Connan, 1984; Palmer, 1984; Lafargue and Barker, 1988) and can accompany biodegradation. Highly saline formation waters may inhibit degradation of oils. Most biodegradation in shallow reservoirs was traditionally assumed to be due to aerobic activity (e.g., Connan, 1984; Palmer, 1993); indeed, the circulation of meteoric water may provide oxygen in deep, nutrient-depleted reservoir where metabolic rates are low (e.g., Horstad et al., 1992; Larter et al., 2000). However, anaerobic biodegradation has been shown in recent years to be the most important in subsurface degraded oil reservoirs (e.g., Coates et al., 1996; Caldwell et al., 1998; Zengler et al., 1999; Wilkes et al., 2000; Aitken et al., 2004; Jones et al., 2007).

Oil biodegradation occurs first among the light hydrocarbons, where *n*-alkanes and aromatics are removed, the latter by water washing as well as microbial action (Palmer, 1983). Then, oils that are more biodegraded show changes in the C_{15+} saturated hydrocarbon fraction. The susceptibility of saturated hydrocarbon classes to increasing biodegradation has been proposed as *n*-alkanes > *n*-alkylcyclohexanes > acyclic isoprenoids > regular steranes> hopanes > rearranged steranes > tricyclic terpanes (Volkman et al., 1984). Peters and Moldowan (1993) developed a quasi-stepwise biodegradation scale (levels 1-10) on the basis of factors that affect the occurrence of microbial activity and the compounds that are preferentially catabolized. With increasing biodegradation, oils become more viscous, richer in sulfur, resins, asphaltenes, and metals (e.g. vanadium and nickel). This leads to decreasing oil quality, and thus its economic value, by lowering API gravity.

Bacterial degradation likely obscures the effects of water washing. Based on solubilities of hydrocarbons, water washing involves a decrease of the most soluble aromatics (especially, benzene and toluene), then light alkanes and then naphthenes (Connan, 1984; Palmer, 1984; Lafargue and Barker, 1988). A decrease in sulfur-bearing aromatics (especially dibenzothiophene) while the C_{15}-C_{20} saturate fraction remains unchanged has been proposed to assess a water washing phase without a biodegradation process (Lafargue and Barker, 1988).

1.2.2. Evaporative Fractionation

Thompson (1987) described two types of gas-condensates systems, the first is the "primary" gas condensates or "thermal" gas condensates, which originate by thermal cracking; and the second called "secondary" gas condensates or "evaporative" gas condensates. Evaporative condensates came from the vertical migration of gas and light-oil fractions formed by partial vaporization or gas-stripping processes of gas-saturated oil accumulations at greater depths. Evaporative fractionation involves the addition or injection of gas into an oil accumulation at elevated pressure, followed by phase separation and escape of only the gas, carrying in solution an enhanced burden of condensable liquid derived from the oil (Thompson, 1987, 1988). Consequently, the shallowest condensates are slightly less aromatic (more paraffinic) than the parent oil, and the successive condensates become highly aromatic and naphthenic by repeated recharging of the residual oil with methane. In addition, this results in shallower oils having higher API gravities than deeper oils, and it is in contrast to thermal condensates that usually show the general trend of increasing API gravities at greater depths. Other writers have used the terms "phase fractionation", e.g., van Graas et al. (2000), "gas washing", e.g., Losh et al. (2002), or "stripping", for these phenomena. Van Graas et al., 2000 performed experiments of simple phase fractionations without addition of excess dry gas. In the experiments, they simulated the behavior of a single-charge petroleum during upward migration or in a reservoir undergoing uplift and they reported that the changes observed in the C_6-C_9 hydrocarbons are similar to those reported by Thompson (1987), with condensates having higher paraffinicity and lower aromaticity than corresponding oils.

Evaporative fractionation has been reported in numerous basins and some examples of cases have been described by: Murillo et al. (2016) for the Hammerfest Basin, Norwegian Barents Sea; Akinlua et al. (2006) for the Niger Delta; Sharaf and El Nady (2006) for the north and north central Sinai, Egypt; Volk et al. (2002) for the Barrandian Basin, Czech Republic; Su et al. (2003) for the Qaidam Basin, China; Masterson et al. (2000) for the Prudhoe Bay region of Alaska; Matyasik et al. (2000) for the Eastern Carpathians, Poland; Napitupulu et al. (2000) for the Northwest Java Basin; Dzou and Hughes (1993) for the K field, offshore Taiwan; Knudsen and Meisingset (1991) for the Gullfaks South field, Norwegian North Sea; Thompson (1987, 1988) for the Gulf Coast and Shelf, the U.S.

1.2.3. Thermal Alteration

Using the kinetic parameters of Waples (2000) the maximum temperature where oil is preserved varies from 170 ºC at geologically slow heating rates to over 200 ºC at geologically fast heating rates. At high temperatures, the thermodynamically favored reactions of aromatic condensation can make hydrogen available to form smaller paraffin molecules by thermal alteration of oils in reservoirs (Hunt, 1996), whereas polycondensed aromatic hydrocarbon are converted to an asphaltite or pyrobitumen. Thus, crude oil cracks to light oil, condensate, and finally gas and pyrobitumen in reservoir with increasing temperature. The formation of pyrobitumen can cause production problems by decreasing the permeability and porosity in deep reservoirs. Huc et al. (2000) studied a sandstone reservoir in Oman, where up to 40% of the reservoir porosity was filled by pyrobitumen.

1.2.4. Natural Deasphalting

Deasphalting of an oil occurs when a large volume of gas dissolves in a crude oil and causes the asphaltene fraction to be precipitated in reservoir pore spaces. Deasphalting may explain many tar mats at the base of reservoirs in the North Sea (Dahl and Speers, 1986; Wilhelms and Larter, 1994a). Dahl and Speers (1986) reported that natural deasphalting is the major cause of the thick tar mats at the base of the Oseberg field in the Norwegian sector of the North Sea. They indicated that the tar mats found below the oil-water contact are geochemically related to the pooled oil in the overlying oil column, as revealed by the similar distribution of *n*-alkanes (>C_{15}), biomarker content (steranes, triterpanes and aromatic

steroids) and carbon isotope composition. In contrast, the tar mat extract has about 50 wt% of asphaltenes, whereas the overlying oil has less than 5%. All of these features indicated that natural deasphalting rather than biodegradation formed the tar mat. Similarly, Wilhelms and Larter (1994b, 1995) studied other cases of tar mats at the Oseberg and Ula fields of the North Sea and a North American field. They proposed the gas injection and the influx of an asphaltic-rich oil as the main mechanisms of tar mat formation.

1.2.5. Oil Segregation by Gravity

The tendency of fluids to stratify into different layers because of density is referred to as gravity segregation. Generally, this process requires high permeability and most often occurs in steeply dipping reservoirs where heavy-end components from the oil settle near the bottom and the light end components rise to the top of the reservoir (Wenger et al., 2002), thereby API gravity of oils decreases with depth. Gravity segregation explains the increase in specific gravity in the Vic Bilh oil field in the Aquitaine Basin. In this case, the relative proportion of alkanes and aromatics remained constant, while an increase in polar compounds (resins and asphaltenes) together with a decrease in API gravity was observed with depth (Blanc and Connan, 1993).

1.2.6. Dysmigration

Some changes in the accumulated oil composition can be related to the efficiency of the seal rock. Dysmigration occurs along a permeable fault or through cap of rocks in which the capillary pressure barrier becomes weaker than the buoyancy forces. Leakage can be related to tectonic events that cause movements along a major fault that traps oils, producing significant losses of the lightest hydrocarbons, which move toward the surface or toward another trap. Dysmigration was described as a “separation-migration” process by Silverman (1965), in which the pressure release causes a phase-separation where a gas cap forms above the oils. Then, this gas is lost through the leak along with light oils and migrate to shallower traps. A new pool is formed containing a fluid with a high API gravity, whereas the oil left behind in the original pool has a low API gravity. The two oil accumulations, therefore, show significant differences in chemical and physical properties despite its same level of maturity.

An example of dysmigration has been found in the Lagrave area in the Aquitaine Basin, where upward-migrating hydrocarbon fluids of high quality accumulated in a shallower trap. The Emeraude area offshore of the Congo in Africa is an example of intense leakage through the seal rock of deeper accumulations (Blanc and Connan, 1993). Pockmarks are generally accepted as morphological expressions of leakage from active subsurface petroleum systems attributed mainly to expulsion of gas and/or pore fluids from underlying sediment rocks. They have been reported in many Norwegian offshore areas, including the Barents Sea (e.g., Hovland, 1982; Jud and Hovland, 2007, Chand et al., 2009; Ostanin et al., 2013).

1.2.7. Thermochemical Sulfate Reduction (TSR)

Thermochemical sulfate reduction (TSR) is the abiological reduction of sulfate by hydrocarbons in reservoirs close to anhydrite at high temperature (e.g., Worden et al., 1995). During TSR reactions, the sulfur in the sulfate is mainly transferred into sulfur-rich solid bitumen, H_2S, and some solid sulfides (pyrite). In addition, the concentration of aromatic sulfur compounds increases with H_2S content because these compounds are formed as by-products (Orr, 1974). Some authors suggest that TSR starts in the range from 127 to 140 ºC, and that higher temperatures are required to initiated TSR for methane than for heavier hydrocarbons (Machel et al., 1995; Worden et al., 1995; Rooney, 1995). With increasing thermal maturation of crude oil, saturated hydrocarbons increase relative to aromatics; nonetheless, the opposite trend occurs during TSR due to the greater reactivity of saturated compared to aromatic hydrocarbons.

Some cases of TSR have been documented in: The Smackover Trend in the Gulf of Mexico (Claypool and Mancini, 1989); the Western Canada Basin (Krouse et al., 1989); the Big Horn Basin in Wyoming (Orr, 1974); the Permian Zechstein Formation in northwestern Germany (Orr, 1977); the Aquitaine Basin in France (Connan and Lacrampe-Coloume, 1993); reservoirs of the Permian Khuff Formation of Abu Dhabi (Worden et al., 1995).

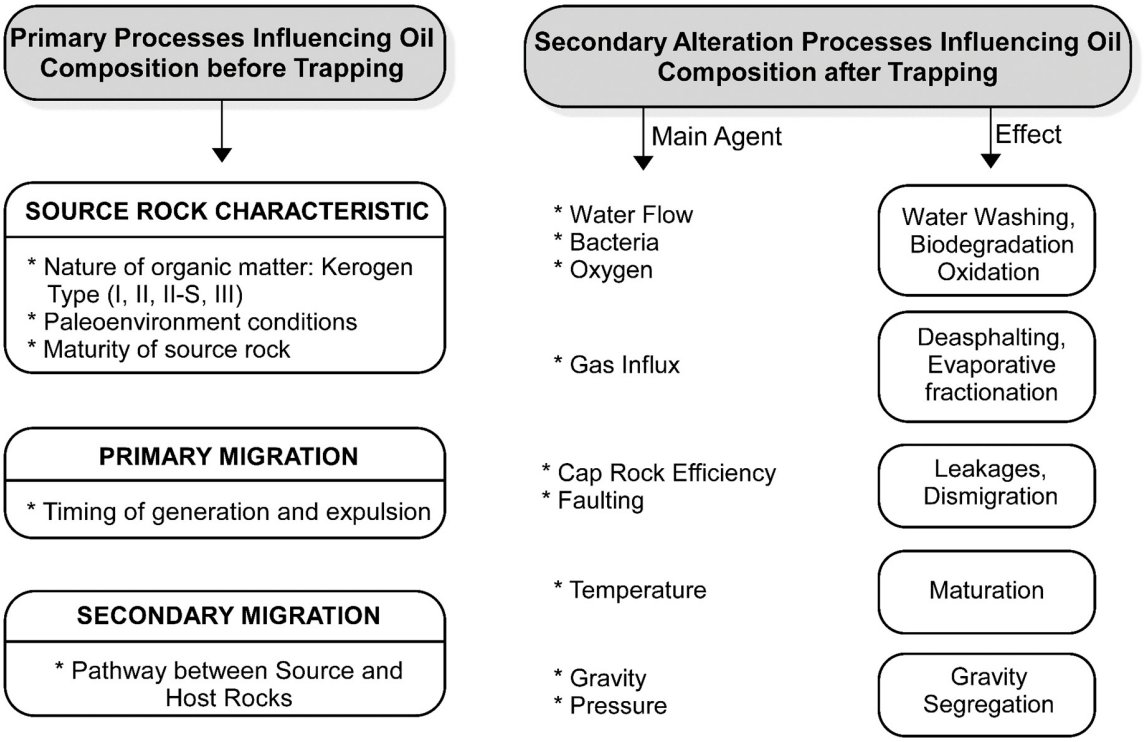

FIGURE 1.2. *Schematic summary of the main factors influencing oil composition (Modified from Bordenave, 1993)*

1.2.8. In-Reservoir Oil Mixing

Overall, petroleum are mixtures of different components charged from source rocks at different temperatures. In many petroleum traps, mixtures of petroleum expelled from: (1) similar organic facies source rocks at different maturities and (2) two or more different source rocks can be distinguished. Wilhelms and Larter (2004) indicated that not all the components of petroleum are able to reliably track facies or maturity signals in mixed oil situations. They indicated that the concentrations of biomarkers change greatly in petroleum sourced from different source rock types and in petroleum sourced from single facies source rocks of different maturities, thus they are not reliable to distinguish compositional differences in mixed oils with different mixing ratios. Most biomarkers are generated from kerogen early in the oil window (before 0.8% R_o) and are then diluted by later petroleum charges, which are depleted in biomarkers (e.g., Larter et al., 1979; Rullköter et al., 1984; Øygard et al., 1988; Larter, 1990). Li et al. (1995) and Jiang and Li (2002) found that mixed maturity oils interpreted previously as immature oils resulted to be mixtures of oils with a wide range of

maturity. They concluded that interpretations of facies and maturities in oil mixtures using biomarker parameters is not possible without a detailed quantitative study of component concentrations in end member oils. Peters et al. (2008) performed hypothetical mixing experiments for oils A and B having different initial amounts of biomarker compounds in the range C_{19}-C_{35}. They found that mixtures yield straight lines on plots of the fraction of oil A versus the concentration of any compounds. In contrast, mixtures commonly yield curves rather than lines on plots of the fraction of oil A versus X/Y, where X and Y are different compounds. Therefore, de-convolution of mixtures using ratios of compounds can be complicated because they vary as nonlinear functions of the amount of each oil type.

Some case studies of petroleum mixing have been studied in: The Cooper and Eromanga Basins, Australia (e.g., Boreham and Summons, 1999); the Tarim Basin, China (e.g., Jia et al., 2013); Pearl River Mouth Basin, China (e.g., Zhang et al., 2004); the Junggar Basin, China (e.g., Cao et al., 2006); the Prudhoe Bay Field, Alaska (e.g., Peters et al., 2008); the South Viking Graben, Norwegian North Sea (e.g., Isaksen et al., 2002; Justwan et al., 2006; Murillo et al. 2019); the Hammerfest Basin, Norwegian Barents Sea (e.g., Ohm et al., 2008; Duran et al., 2013; Murillo et al., 2016); the Potiguar Basin, Brazil (e.g., Trindade et al., 1992); the West Greenland (e.g., Bojesen-Koefoed et al., 1999).

1.3. Effects of the Main Secondary Alteration Processes on $\delta^{13}C$ and δD values of Individual Petroleum Hydrocarbons

1.3.1. Effects of Biodegradation

The effects of biodegradation on the $\delta^{13}C$ values of individual organic compounds have been investigated for applications in petroleum and environmental sciences (e.g., Boreham et al., 1995; Huang et al., 1997; Mansuy et al., 1997; Pond et al., 2000; Wilkes et al, 2000; Masterson et al., 2001; Mazeas et al., 2002; George et al., 2002; Sun et al., 2005). In general, no significant carbon isotopic fractionation for *n*-alkanes (>C_{12}) occurs during slight to moderate biodegradation in petroleum reservoirs (Boreham et al., 1995, Sun et al., 2005). Similarly, some laboratory studies using bacterial incubation have also demonstrated that the $\delta^{13}C$ of *n*-alkanes (>C_{12}) do not seem to be significantly altered during aerobic

microbial degradation (Huang et al., 1997; Mansuy et al., 1997; Mazeas et al., 2002). Nevertheless, Sun et al. (2005) observed a significant increase of up to 4‰ in the $\delta^{13}C$ values of *n*-alkanes (C_{15}-C_{18}) in crude oils, with identical source and thermal maturity, affected by heavy biodegradation. In contrast, the $\delta^{13}C$ values of higher molecular weight *n*-alkanes ($\geq C_{19}$) remains constant. Therefore, $\delta^{13}C$ values of higher molecular weight *n*-alkanes ($\geq C_{19}$) are effective tracers for source identification of heavily biodegraded oils.

With respect to the effects of biodegradation on the δD values of individual *n*-alkanes from crude oils, previous experiments of in vitro aerobic biodegradation (Pond et al., 2002) showed that *n*-alkanes (C_{15}-C_{18}) had the largest overall hydrogen isotopic fractionation, with an enrichment in deuterium (D) by ~12-25‰. On the other hand, δD values of longer chain *n*-alkanes (C_{19}-C_{27}) were relatively constant (<5‰ overall deuterium enrichment) during slight to moderate biodegradation of crude oils. δD data of *n*-alkanes in crude oils, representing a natural progressive biodegradation sequence (Sun et al., 2005) are consistent with laboratory studies in suggesting relatively small variations in δD values of longer chain *n*-alkanes ($\geq C_{19}$) during slight to moderate levels of biodegradation. *n*-Alkanes ($\geq C_{19}$), however, show a significant enrichment in D by up to ~35‰ as moderate biodegradation proceeds. Asif et al. (2009) reported that *n*-alkanes (C_{14}-C_{22}) exhibit the largest D-enrichment of up to 50‰, whereas *n*-alkanes ($>C_{23}$) show a smaller D-enrichment (~20‰), and pristane and phytane exhibit no isotopic changes in crude oils altered by low levels of biodegradation. Therefore, in reservoirs where biodegradation has occurred, δD values of *n*-alkanes are less conserved and can be quite useful in understanding the impact of biodegradation.

1.3.2. Effects of Evaporative Fractionation

Even though evaporative fractionation can change the relative abundance of *n*-alkanes in an oil, and thus, the isotope ratio of the bulk saturates; it cannot significantly affect the $\delta^{13}C$ values of individual *n*-alkanes. Dzou and Hughes (1993) showed differences of less than 0.5‰ between the $\delta^{13}C$ values of C_{12}-C_{14} *n*-alkanes in a condensate compared to those in the residual oil. Carpentier et al. (1996) based on experimental separation of liquid and gas phases (PVT experiments) reported that $\delta^{13}C$ values of C_6, C_7 and C_8 *n*-alkanes are identical in both the gas phase and the original oil, whereas the carbon isotopic variations in *n*-alkanes

(C_9-C_{14}) are very small and even close to the limits of the analysis, confirming results from Dzou and Hughes (1993). Mansuy et al. (1997) showed that despite the partial loss of *n*-alkanes, $\delta^{13}C$ values of *n*-alkanes $\geq C_{10}$ show good correlation between the evaporated and unweathered oils. Similarly, Wang and Huang (2003) found no significant carbon isotope fractionation, showing carbon isotope differences <0.3‰ for *n*-alkanes (C_{10}-C_{14}) during vaporization experiments. The $\delta^{13}C$ values of these *n*-alkanes can therefore be used in correlation studies in oils and condensates, because the effect of in-reservoir phase partitioning is not significant on their $\delta^{13}C$ values.

Evaporation of hydrocarbons is explained by an "inverse" deuterium isotope effect, where the vapor phase is D-enriched relative to the liquid (Hopfner, 1969; Kiss et al., 1972), hence, the liquid becomes depleted in D during evaporation. Wang and Huang (2003) determined the H isotope fractionation of common volatile petroleum hydrocarbons, including the *n*-alkanes (C_{10}-C_{14}), during progressive vaporization under simulated experimental conditions. Their results indicate that H isotope fractionation increases with *n*-alkane chain length, showing a decrease in δD values for *n*-alkanes of up to 33.3‰ when 99% of these substances has evaporated. Such fractionation patterns were interpreted in terms of competition between (1) the decreased intermolecular binding energy in D-enriched species, and (2) the isotope effect due to the mass difference. A field study showing the impact of evaporation/phase separation in naturally evaporated oils is shown in Murillo et al. (2016). In this study, condensates resulting from evaporative fractionation in the Hammerfest Basin, southwestern Barents Sea, exhibited a very strong and constant D-enrichment of *n*-alkanes with chain length.

1.3.3. Effects of Thermal Maturation

Reactions of oil generation are accompanied by kinetic isotope effects that favor reaction of ^{13}C- and D-depleted molecules, because ^{12}C–^{13}C and C–D bonds are stronger and react more slowly than ^{12}C–^{12}C and C–H bonds. Some authors have documented by bulk analyses that released hydrocarbons are consistently depleted in ^{13}C and D, whereas the residual kerogen becomes enriched in ^{13}C and D (Rigby et al., 1981; Schoell et al., 1983). Clayton (1991) differentiates the effects of oil generation (~100-150 ºC) from the effects of

oil to gas cracking (~150-180 ºC) for modelling carbon isotopic variations. This author indicates generation of oil from kerogen can increase $\delta^{13}C$ of the oil by between 0 and 1‰ (average 0.5‰) at about the end of oil generation. During oil and gas cracking, however, kinetic isotope effects become important and can further increase $\delta^{13}C$ of oil by up to 1.5‰ by 50% cracking. At higher degrees of cracking, the increase in $\delta^{13}C$ values should not exceed about 4‰. Clayton and Bjorøy, 1994 reported that maturity variations produce an increase in $\delta^{13}C$ values of individual hydrocarbons generally between 2 and 3‰ in North Sea oils. Similarly, during artificial thermal maturation of a North Sea crude oil under anhydrous conditions, Tang et al. (2005) found $\delta^{13}C$ values of C_{13} to C_{21} *n*-alkanes increased by ~4‰ and δD values increased by ~50‰ at an equivalent vitrinite reflectance of 1.5%. While the observed ^{13}C-enrichment showed no significant dependence on hydrocarbon chain length, thermally induced D-enrichment increased with increasing *n*-alkane carbon number. Tang et al, (2005) predicted that significant fractionations, due to kinetic isotope effects, should be expected only at relatively high maturity ($\%R_o$>1.5). On the other hand, Dawson et al. (2005) reported that *n*-alkanes generally remain at a constant isotopic composition until late maturity, where there is then a significant D-enrichment in *n*-alkanes that is attributed to hydrogen exchange reactions. Radke et al. (2005) showed that differences between δD values of phytane and *n*-alkanes in immature samples disappear by high level of thermal maturity ($\%R_o$~1.3).

Hydrogen exchange processes become important during late diagenesis, and may have partially or largely erased the original biological signal by the onset of oil generation (e.g., Schimmelmann et al., 1999, Sessions et al., 2004, Pedentchouk et al., 2006). Dawson et al. (2005); Pedentchouk et al. (2006) pointed out that pristane and phytane become more enriched in D relative to the *n*-alkanes with increasing maturity. The more rapid D-enrichment in isoprenoids relative to *n*-alkanes with maturation suggests that hydrogen isotopic exchange occurs via a mechanism involving carbocation-like intermediates (Dawson et al., 2005, 2007). Compared to *n*-alkanes, greater susceptibility of isoprenoids to hydrogen exchange/transfer makes that δD values of pristane and phytane may serve as a useful tool for assessing thermal maturity.

1.3.4. Effects of Thermochemical Sulfate Reduction (TSR)

Thermochemical sulfate reduction (TSR) alters petroleum composition until the complete oxidation of hydrocarbons to CO_2. In contrasts to thermal maturity, the TSR decreases the content of saturated hydrocarbons relative to aromatic, due to the greater reactivity of saturates compared to aromatic hydrocarbons (Peters and Fowler, 2002). Nevertheless, like thermal maturity, the remaining hydrocarbons becomes enriched in ^{13}C. Rooney (1995) found substantial variations in the $\delta^{13}C$ of some gasoline-range hydrocarbons in oils affected by TSR. This author reported that the $\delta^{13}C$ of the *n*-alkane and branched hydrocarbons increase 22‰ in oils affected by TSR compared to an increase of 2 and 3‰ observed in oils altered by high level of thermal maturity. Other compounds, such as toluene, showed much smaller variations (3-6‰) in $\delta^{13}C$ values.

1.4. Oil-Oil and Oil-Source Rock Correlations

Correlations are geochemical comparisons among oils or between oils and source rock extracts, and are used to determine whether a genetic relationship exists (Peters and Moldowan, 1993; Waples and Curiale, 1999). Crude oil correlations are based on the assumption that the same source material and environment of deposition produce the same oil. The accumulated oils, however, can be altered by secondary processes thus correlation parameters have to be little affected by them. On the other hand, oil-source rock correlations are more difficult than oil-oil correlations, nonetheless, these correlations are based on the fact that certain compositional parameters of migrated oil do not differ significantly from those of bitumen remaining in the source rock. Hence, the comparison of biomarkers is the preferred method of oil-source rock correlation. Nevertheless, in basins with multiple source rocks and complex charging histories, the presence of complex hydrocarbon mixtures can make oil-oil and oil-source correlations difficult. For this reason, the implementation of a multiparameter approach is important for geochemical correlation purposes with the main contributing source in the case of petroleum mixtures.

Although, the approach commonly used for correlation studies is gas chromatography-mass spectrometry (GC-MS) of biomarkers (Seifert and Moldowan, 1978, 1981; Mackenzie, 1984), a wide variety of sophisticated and sensitive analytical techniques have been

developed over the past two decades, such as the metastable-reaction monitoring-GC-MS, GC-MS/MS, and compound-specific isotope analysis (CSIA) by gas chromatography-isotope ratio-mass spectrometry (GC-IRMS). Multiparameter approaches used for genetic correlations utilize parameters of biomarkers, light hydrocarbons, polycyclic and heterocyclic aromatic hydrocarbons and CSIA, all of which will be briefly described in the following sections.

1.4.1. Biomarkers

Biomarkers are complex organic compounds found in sediments, rocks, and crude oils, and that show little or no change in carbon skeleton from their parent organic molecules, or so called biogenic precursors (for example, hopanoids and steroids), in living organisms (Peters and Moldowan, 1993). The two main controls on the biomarker composition of source rock extracts and crude oils are (1) the type of organic matter (algal, microbial and land plant organic matter), and (2) the depositional environment, i.e. source rock lithology, water column salinity, oxicity/anoxicity (Moldowan et al., 1985; Peters and Moldowan, 1993). Biomarkers in the oils can be used to infer the depositional environments, organic matter input, thermal maturity, and even the age of the source rocks. In addition, they can estimate the degree of microbial degradation. However, oil-oil correlation requires biomarker parameters that distinguish oils from different sources and are resistant to secondary processes, such as biodegradation and thermal maturation (Peters and Moldowan, 1993).

Certain biomarkers in oils are considered characteristic of different primary biomass components. For example, the extended hopanes are derived from precursors in bacterial cell membranes while steranes originate mainly from sterols present in the cell of eukaryotes (Moldowan et al., 1985). Other biomarkers reflect the oxicity variations occurring during the deposition of the source rocks, such as the distribution of the C_{31}-C_{35} homologs, in which oxidation reduces the length of the side chain (Peters and Moldowan, 1991). Whereas others can be used to indirectly predict the source rock lithology, as for example the extent of conversion of sterols to diasterenes, which reflect the catalytic effect of clay minerals (Rubinstein et al., 1975).

1.4.2. C_7 Hydrocarbons

The light hydrocarbons are a significant portion of most crude oils, and they are used to correlate oils and condensates, assess thermal maturity, and indicate various in-reservoir alteration processes. The C_7 parameters have been widely used to classify and correlate oils in many basins (e.g., Odden et al., 1998, Chung et al., 1998; ten Haven, 1996, Jarvie, 2001). Light hydrocarbon analysis complements biomarker correlations of crude oils, especially when high thermal maturity level decreases the usefulness of biomarkers. Moreover, they are particularly useful for mixtures where light and heavy ends may have different source rocks (Peters et al., 2005).

Mango (1987, 1990) indicates that ratios of isoalkanes are almost constant in all oils and invariant within oils from a common source. This author attributed differences in the isoheptane ratio (K_1= (2-MH + 2,3-DMP)/ (3-MH+2,4-DMP)) of oils to different kinetic reaction rates of solid-state catalysis associated with different kerogens and source rocks. Besides, Mango (1997) proposed parent-daughter ratio plots based on ring-preference reactions, which can be also used for oil-oil and oil-condensate correlations. Halpern (1995) proposed five C_7 parameters representing the proportion of individual C_7 alkylated pentanes to the sum of these compounds. These C_7 ratios based on the same solubility in water and the same susceptibility to microbial degradation of C_7 alkylated pentanes.

1.4.3. Heterocyclic and Polycyclic Aromatic Hydrocarbons

Several thermal maturity parameters have been proposed from the distribution of methylphenanthrenes (MPs), dimethylphenanthrenes (DMPs), and methyldibenzothiophenes (MDBTs) to assess the maturity of crude oils, condensates and sediments (Radke et al., 1982; Radke and Welte, 1983). Here, however, the use of the distribution and relative abundance of certain polycyclic aromatic hydrocarbons (PAHs), along with their methyl homologs, as source indicators will be presented.

The distribution of methyl, dimethyl and trimethylphenanthrenes is influenced by the type of organic matter and the environment in which it was deposited (Fan et al., 1990 and Budzinski et al., 1995). Diterpenoids with an abietane and pimarane skeleton are likely

biological precursors of alkylphenanthrenes (Simoneit et al., 1986). The most prominent alkylphenanthrene directly attributed to diterpenoids of the abietane type, is 1-methyl-7-isopropylphenanthrene (retene). 1,7-DMP derived likely from diterpenoids of the pimarane type present in resin material (Simoneit, 1977). Similarly, high proportions of 1-methylphenanthrene (1-MP) were preferentially found in the organic matter of terrestrial source rocks, while the dominance of 9-methylphenanthrene (9-MP) is related to marine organic matter (Radke et al., 1986; Heppenheimer et al., 1992). Some studies on coals have shown the predominance of 1,7-DMP over other isomers, in conjunction with retene and 1-MP (Heppenheimer et al., 1992; Alexander et al., 1992). Furthermore, the relative abundances of some isomers of alkylnaphthalenes have been associated with specific natural precursors and applied to differentiate terrigenous from marine source input (e.g., Püttmann and Villar, 1987; Strachan et al., 1988; Alexander et al., 1992). One example is 1,2,5-trimethylnaphthalene (1,2,5-TMN), which can be used to indicate higher-plant source input since it is a common product of aromatization of terpenoid precursors, such as bicyclic diterpenoids and pentacyclic triterpenoids (Strachan et al., 1988). Likely, 1,6-dimethylnaphthalene (1,6-DMN) and 1,6-dimethyl-4-isopropylnaphthalene (cadalene) are derived from fossil resins (e.g., Simoneit et al., 1986; Radke et al., 1986; van Aarssen et al., 1992). Simoneit (1985) and Alexander et al. (1988) indicated that the higher plant biomarker retene is derived from compounds produced by conifers, while specific higher plant markers like cadinane has been reported as a source for cadalene (van Aarssen et al., 1990; 1992) and it is thought to be derived from gymnosperm resins (Simoneit et al., 1986) or from fragmentation of polycadinene resins produced by angiosperms (van Aarssen et al., 1990).

Apart from the PAHs, the distribution of dibenzothiophene, dibenzofuran and fluorene and their methyl homologs are controlled by the source rock lithology and depositional environment (Hughes, 1984; Fan et al., 1990). The sulfur-containing heterocyclic aromatic hydrocarbons (i.e., dibenzothiophene and alkyldibenzothiophenes) are particularly abundant in marine oils and carbonates (Hughes, 1984; Fan et al., 1990), where they predominate over alkylfluorenes and alkyldibenzofurans. In contrast, abundant oxygen-containing heterocyclic aromatic hydrocarbons (i.e., dibenzofuran and alkyldibenzofurans) as well as fluorene and alkylfluorenes have been associated with source rocks from oxic/fresh

water environments (e.g., Fan et al., 1990; Radke et al., 2000). Various studies have proved the usefulness of the heterocyclic aromatic compounds for the assessment of organic facies and lithology in petroleum and source rocks (e.g., Radke et al., 2000; Asif and Fazeelat, 2012; Li et al., 2013; Asif and Wenger, 2019).

1.4.4. Compound-Specific Stable Isotope Analysis (CSIA)

The CSIA allows a rapid and precise determination of the isotope ratios of stable carbon and hydrogen of individual compounds ($^{13}C/^{12}C$ and $^{2}H/^{1}H$ or D/H expressed as $\delta^{13}C$ and $\delta^{2}H$ or δD, respectively), which is given in delta (δ) notation in parts per thousand (‰). Farquhar et al. (1989) and Hayes (1993) identified the main factors that control the $\delta^{13}C$ of biological organic matter: (a) the isotopic composition of the primary carbon source, (b) isotope effects associated with assimilation of carbon by producing organisms, (c) isotope effects due to metabolism and biosynthesis, and (d) cellular carbon budget. Even though carbon tends to be preserved during diagenesis and maturation (Hoefs, 1997); hydrogen is exchanged during various diagenetic reactions with environmental water. Therefore, δD values of organic compounds can provide information about processes during burial of sedimentary rocks (Sessions et al., 2004).

The $\delta^{13}C$ values of crude oils are mainly controlled by the isotopic composition of its source material (i.e., the type of kerogen and the depositional environment in which it has been formed) (e.g., Murray et al., 1994) and by its degree of thermal alteration (e.g., Tang et al., 2005). Nonetheless, their δD values are determined not only by the lipids δD values, but also by post-depositional processes that exchange hydrogen between organic matter and formation waters. The δD of sedimentary hydrocarbons represents a complex combination of different factors, such as: the environmental water δD values and physiologic and metabolic processes in organisms that transfer hydrogen derived from water into organic molecules (e.g., Sternberg, 1988; Sessions et al., 1999; Sauer et al., 2001; Chikaraishi et al., 2005; Li et al., 2009); hydrogen exchange processes that involve water (e.g., Schimmelmann et al., 1999, 2001; Sessions et al., 2004; Dawson et al., 2005; Pedentchouk et al., 2006) and/or clay minerals (Alexander et al., 1982, 1984); and kinetic isotopic fractionations that occur during liquid hydrocarbon generation (e.g., Tang et al., 2005).

The *n*-alkanes are among the most abundant hydrocarbon groups present in both source rock extracts and oils. Some *n*-alkanes are typically associated with algae and bacterial biomass (*n*-C_{16} to *n*-C_{19}); whereas others derived from terrestrial higher plants (*n*-C_{27} to *n*-C_{35}). Therefore, the stable carbon isotope composition of individual alkanes has the advantage of identifying different organic matter sources, as for example primary producers versus bacterially reworked organic matter, or algal versus higher plant input in oils, source rock extracts and kerogen pyrolysates (e.g., Freeman et al. 1990, Hayes et al. 1990, Rieley et al. 1991). Also, carbon isotope differences between the regular isoprenoids (pristane and phytane), for which a common origin from chlorophyll is generally assumed, denote different origins of these two components (Freeman et al., 1990). Furthermore, CSIA studies have also focused on light hydrocarbons, which can have carbon isotope composition that differs from the C_{15+} hydrocarbons. Unless altered by reservoir processes, oils and condensates generated from the same source rocks should have the same pattern of $\delta^{13}C$ values for individual light hydrocarbons (Peters et al., 2005). Hence, CSIA of light hydrocarbons is especially useful to correlate light oils and condensates.

In general, compound-specific stable carbon isotope composition of light hydrocarbons and *n*-alkanes have been applied as a powerful tool to: (1) distinguish oil families (e.g., Peters and Creaney, 2004; Samuel et al., 2009; Murillo et al., 2016, 2019); (2) better constrain and provide insights into oil-oil, oil-condensate and oil-source correlations (e.g., Bjorøy et al., 1994; Odden et al., 2002; Jia et al., 2013; Murillo et al., 2016, 2019); and (3) understand secondary processes that have affected the oil composition (e.g., George et al., 2002; Sun et al., 2005). On the other hand, compound-specific hydrogen isotope composition of *n*-alkanes has also been useful as a geochemical parameter for correlation studies in marine and terrestrially sourced oils (e.g., Li et al., 2001; Schimmelmann et al., 2004) and for the assessment of in-reservoir alteration processes (e.g., Sun et al., 2005; Asif et al., 2009; Murillo et al., 2016).

1.5. Scientific Scope of the Thesis

The current PhD project focused on petroleum mixing and alteration in reservoirs from two study areas that represent petroleum systems with multiple source rocks and complex charging histories. The first study area is the Hammerfest Basin (HB) located in the Norwegian Barents Sea (NBS). The NBS is a large geological province that is nearly twice the size of the Norwegian North Sea. This area represents an overfilled petroleum system, characterized by the occurrence of several source rock intervals ranging in age from Lower Carboniferous to Lower Cretaceous (e.g., Johansen et al., 1992; Larssen et al., 2002; Ohm et al., 2008), and thus, hydrocarbon generation over a long geologic history. Furthermore, the area has had a complex geological history with various episodes of uplift and erosion during the Cenozoic (e.g., Vorren et al., 1991; Faleide et al., 1993; Doré and Jensen, 1996) and prominent Pliocene-Pleistocene glacial cycles (e.g., Jansen and Sjoholm, 1991; Cavanagh et., 2006), which induced the main gas leakage events and sequestration of methane at the surface (e.g., Ostanin et al., 2013, 2017), affecting the petroleum accumulations in the region. Furthermore, this has not only resulted in a very complex history of petroleum generation, migration and trapping, but also on different scenarios of petroleum mixing and alteration in the HB reservoirs. In the HB, some authors have proposed the occurrence of petroleum mixtures from Triassic and Jurassic source rocks (Ohm et al., 2008; Duran et al., 2013a; Killops et al. 2014) and even from Paleozoic source rocks (Ohm et al., 2008).

The second studied area comprises the South Viking Graben (SVG), a prolific hydrocarbon province located in the Norwegian North Sea, whose petroleum systems include source rocks deposited mainly during the Late Jurassic to earliest Cretaceous (e.g., Isaksen et al., 2002; Justwan et al., 2005, 2006a). Previous studies (Isaksen et al., 2002; Justwan et al., 2005, 2006a) identified several hydrocarbon families in the SVG that correlated with different facies of the Upper Jurassic Draupne Formation, the Upper Jurassic Heather Formation and the Middle Jurassic Sleipner and Hugin formations. These authors indicated that petroleum traps in the Greater Sleipner Area, located in the southern part of the South Viking Graben, can be charged from different directions and from Jurassic source rocks with differing organic matter composition and lithology, which result in complex in-reservoir mixing.

In these two basin-specific case studies, mixing of petroleum can make oil-oil and oil-source correlations difficult. It therefore demands the implementation of additional and more specific geochemical and isotopic analyses to unravel complex hydrocarbon mixtures and to better understand the multiple petroleum systems. So far, previous authors have studied source rock extracts, oils and condensates using the composition of conventional biomarkers and the bulk $\delta^{13}C$ values of whole oils and oil fractions. Nevertheless, multiparameter approaches have not been performed to assess mixtures of petroleum in the Norwegian Barents and North Seas.

In order to assess the topics of scientific interest, it is therefore important that a detailed study is performed to decipher mixtures of petroleum using multiparameter approaches with the combination of different tools and analytical techniques. In this PhD research, the applied multiparameter approaches involve not only the molecular composition of sterane and triterpane biomarkers but also resin-derived biomarkers as well as other petroleum components, such as light hydrocarbons, *n*-alkanes and heterocyclic and polycyclic aromatic hydrocarbons as well as diamondoids in the case study of the HB. In addition, compound-specific stable carbon and hydrogen isotope compositions of individual petroleum hydrocarbons are used rather than isotopic compositions of bulk samples. Both molecular and isotope data are statistically examined by multivariate analysis, principal component analysis (PCA) and hierarchical cluster analysis (HCA), to classify petroleum families. The present PhD research also focuses on the appraisal of petroleum alteration processes. Special focus was given to evaporative fractionation process and the effect of evaporation on δD values of *n*-alkanes using field study cases in the HB and SVG.

Furthermore, increasing attention has been given to the identification and quantification of relative contributions from different source rocks to oil pools in basins containing more than one petroleum system. To quantify the relative source contribution to mixed oils, previous studies applied mathematical calculation based on the absolute concentrations of biomarkers (Chen et al., 2003; Peters et al., 2008) and individual aromatic hydrocarbons (Arouri and McKirdy, 2005), as well as carbon isotopic composition of whole oils and source rock extracts (Peters et al., 1989; Chen et al., 2003). Nonetheless, so far, no

studies have employed $\delta^{13}C$ values of individual alkanes to estimate the relative source contribution to reservoirs containing mixtures of petroleum. In the present PhD study, therefore, mixing proportions were estimated using $\delta^{13}C$ values of *n*-alkanes in two key case studies.

1.6. Project Objectives and Research Questions

The main goals of this PhD work are to: (1) investigate the origin, thermal maturity and mixing of oils and condensates; (2) appraise petroleum alteration processes; (3) apply multivariate statistics using molecular and compound-specific stable carbon isotope data to classify mixed petroleum according to the main contributing source rock; (4) better constrain oil-oil and oil-source correlations; (5) estimate the relative source contributions to mixed petroleum accumulations using $\delta^{13}C$ values of individual alkanes. The present PhD work also addresses the issue of how best to discriminate petroleum mixtures using different fractions and components of oils and how multiparameter approaches, integrating molecular and isotope data, can provide valuable additional information to improve our understanding of multiple petroleum systems.

As regards mixing, the following key questions are addressed retrospectively:

- Can the $\delta^{13}C$ values of individual alkanes be useful to estimate mixing proportions?
- What are the main factors that may control the δD values of individual hydrocarbons in Jurassic source rocks, oils and condensates from the SVG?
- Can the δD values of *n*-alkanes be used as geochemical parameters for oil-oil and oil-source correlations?
- Can the combination of the $\delta^{13}C$ and δD signatures of *n*-alkanes be employed as a tool to resolve mixtures of differently sourced petroleum?

Regarding secondary alteration processes and condensate formation, the following questions are also investigated:

- What is the effect of evaporation/phase separation on the δD values of individual *n*-alkanes in naturally evaporated hydrocarbon samples?
- What is the effect of maturation on the δD values of individual *n*-alkanes, and Pr and Ph in thermally generated condensates?
- How can a combined appraisal of $\delta^{13}C$ and δD values of individual hydrocarbons lead to a comprehensive understanding of the processes that have influenced petroleum fluid properties over time?

1.7. Structure of the Dissertation

This introduction presents a brief description of the origin, maturation, migration, and accumulation of petroleum (Sections 1.1 and 1.2). This is then followed by a review on the petroleum alteration and mixing processes in reservoirs (Sections 1.2.1 to 1.2.8), mentioning some case studies in the world. In addition, this introduction explains the effects of the main secondary alteration processes on $\delta^{13}C$ and δD values of individual petroleum hydrocarbons (Section 1.3). A description of multiparameter research approaches for correlation studies and unraveling mixtures of petroleum, on the basis of the molecular composition of different petroleum components and the stable carbon and hydrogen isotope compositions of individual hydrocarbons, is presented in Section 1.4. This general background provides an understanding of the reasons and the scientific interest of this PhD study (Sections 1.5 and 1.6). Subsequent to this introduction, the analytical methods and techniques applied in this research are described in Chapter 2. In order to achieve the objectives and to answer the research questions, the main findings of the present PhD research are addressed in three publications (Chapters 3, 4 and 5). A review of the next chapters is presented as follows.

Chapter 2 describes the analytical techniques applied for (1) evaluation of organic matter richness, type and thermal maturity of source rocks, including total organic carbon (TOC) and Rock-Eval pyrolysis; (2) separation of saturate and aromatic fractions (medium pressure liquid chromatography, MPLC); (3) identification and quantification of light

hydrocarbons, *n*-alkanes and regular isoprenoids (gas chromatography-flame ionization detection, GC-FID), biomarkers, diamondoids, and heterocyclic and polycyclic aromatic hydrocarbons (gas chromatography-mass spectrometry, GC-MS in full scan and metastable reaction monitoring, MRM modes); and (4) $\delta^{13}C$ and δD measurements of individual petroleum hydrocarbons in extracts, oils and condensates (gas chromatography-isotope ratio mass spectrometry, GC-IRMS).

In Chapter 3, multiparameter approaches that include light hydrocarbons, conventional biomarkers, higher-plant derived biomarkers, polycyclic aromatic hydrocarbons, diamondoids, as well as $\delta^{13}C$ and δD values of individual hydrocarbons, enable to identify hydrocarbon mixtures of distinct sources, thermal maturity levels, and geological ages in the HB, Northwestern Barents Sea. In addition, $\delta^{13}C$ values of *n*-alkanes ($>C_{20}$) are used for quantitative assessment of oil source contribution, allowing a good differentiation on Triassic *versus* Jurassic contributions. This integrated approach also provides new insights and a comprehensive understanding of the petroleum systems in the HB, showing molecular and isotope evidence for a possible Paleozoic source contribution, and for the occurrence of dry gas influx, evaporative fractionation, and gas-condensate charges, which may indicate the existence of deeper petroleum accumulations.

Chapter 4 focuses on unraveling mixtures of petroleum and quantifying mixing ratios of hydrocarbons generated from Jurassic source rocks in the SVG, Norwegian North Sea. For that, a multiparameter approach that comprises the molecular composition of light hydrocarbons and heterocyclic and polycyclic aromatic compounds as well as the $\delta^{13}C$ values of individual hydrocarbons is performed in Jurassic oils, condensates and source rock extracts. The ^{13}C-enrichments of (C_{10}-C_{14}) *n*-alkanes and pristane and phytane are good indicators of the scale of the terrigenous source contribution and are used to estimate the mixing proportions of hydrocarbons from Jurassic source rock enriched in Type-II and Type-III kerogens in petroleum mixtures at moderate level of thermal maturity from the southern part of the SVG. The applied multiparameter approach also provides valuable information to better understand the multiple petroleum systems in the SVG. This suggests a most widespread occurrence of hydrocarbons sourced from calcareous source facies of the Upper

Jurassic Draupne Formation, and Middle Jurassic coaly shales/coals from the Vestland Group in reservoirs from the southern half of the SVG, as well as a high relative input from siliciclastic shales enriched in Type-III kerogen (the Heather Fm. and/or the lower Draupne Fm.) in the northern half of the SVG.

In Chapter 5, carbon and hydrogen CSIA are applied to better understand sources of complex mixtures of petroleum generated from Upper and Middle Jurassic source rocks of distinct organic matter types, lithologies and depositational environments in the SVG. This study focuses on the main factors that may control the δD values for oils, condensates and analyzed extracts of Jurassic source rocks. With the increase in the estimated contribution of hydrocarbons from terrigenous source material to petroleum mixtures (Chapter 3) is found that *n*-alkanes of lower molecular weight (C_{10}-C_{15}) tend to be more prone to source variation, becoming more enriched in ^{13}C. In contrast, *n*-alkanes of higher molecular weight (>C_{20}) become more enriched in D. Likewise, differences between the weighted average δD values of *n*-alkanes and the weighted average δD values of Pr and Ph, in petroleum mixtures of similar thermal maturity, tend to increase. δD and $\delta^{13}C$ values of *n*-alkanes were, therefore, combined to unravel complex mixtures of petroleum from the SVG. δD values of *n*-alkanes (>C_{20}) allow a good discrimination between petroleum mixtures that were not well differentiated by $\delta^{13}C$ values.

Chapter 6 summarizes the results of the proceeding chapters and presents an outlook for future work.

Chapter 2

Analytical Techniques and Methods

2.1. Total Organic Carbon (TOC) and Rock-Eval Pyrolysis

For TOC analysis, finely crushed rock samples were firstly treated with diluted HCl in water (1:9) at 60 °C to remove carbonates. Then, the samples were rinsed to remove HCl and dried. Determination of the total carbon content (TOC) was achieved by measuring the carbon dioxide formed by combustion at 1350 °C using a Leco SC-632 IR-detector. Rock-Eval pyrolysis was performed on pulverized rock samples using a Rock-Eval 6 instrument to measure the free hydrocarbon fraction (S1), the fraction released by thermal cracking (S2), and the pyrolysis temperature (T_{max}) at the maximum rate of kerogen cracking measured at the crest of the S2 peak. The procedure for Rock Eval analysis is described in NIGOGA 4th edition (Weiss et al., 2000).

2.2. Solvent Extraction and Medium Pressure Liquid Chromatography (MPLC)

The source rock samples (7-10 g each) were powdered and extracted with 350 ml of dichloromethane-methanol (vol. 99:1) at approximately 40 °C for a period of 24 h using a Soxhlet apparatus. The solvent was removed using a TurboVap evaporator and the extracts were redissolved in 250 µl of the same solvent mixture. Asphaltenes were precipitated by adding 40 ml of *n*-hexane followed by filtering in a series of stages (Theuerkorn et al., 2008). The maltene fraction was concentrated using a TurboVap. Crude oils and maltene samples were separated into aliphatic, aromatic and polar fractions using an automated medium

pressure liquid chromatography (MPLC) procedure, as described by Radke et al. (1980). *n*-Alkanes and branched/cyclic alkanes were separated from an aliquot of saturate fractions by urea adduction for some source rock extracts with low concentrations of compounds. A saturated solution of urea in methanol was added to the aliphatic fraction (in 0.5 ml dichloromethane), heated and stored overnight in the fridge for complete adduction. After that, the solvent (non-adduct) was separated from the urea precipitate (adduct) by filtration. The filter residue was rinsed with distilled water several times. The *n*-alkanes were extracted by addition of *n*-hexane after dissolution of the urea crystals in water. Similarly, the non-adduct is extracted by addition of *n*-hexane. Then both fractions were analyzed by gas chromatography-isotope ratio mass spectrometry (GC-IRMS).

2.3. Gas Chromatography-Flame Ionization Detection (GC-FID)

Identification and quantification of individual *n*-alkanes and isoprenoids (pristane and phytane) was conducted using a GC-FID instrument (6890A, Agilent Technologies, USA) equipped with an Agilent-Ultra 1 capillary column (50 m x 0.20 mm i.d., 0.33 μm film thickness) for saturated fraction samples and a HP-PONA GC column (50 m x 0.20 mm i.d., 0.50 μm film thickness) for whole oil samples. The GC-FID used He as carrier gas at a constant flow rate of 1.0 ml/min. For saturated fraction analysis, samples were injected using a splitless mode and the initial temperature of injector was 40 °C. During injection, the injector was heated to 300 °C at a rate of 700 °C/min and held for 3 min at the final temperature. The initial GC oven temperature was held for 2 min at 40 °C, then raised to 300 °C at 5 °C/min and held for 65 min at the final temperature. For whole oil analysis, samples were injected using a split ratio of 1:50 and the injector was set at a constant temperature of 300 °C. The initial oven temperature was held for 10 min at 30 °C and was then increased to 60 °C at 2 °C/min, later to 320 °C at 4 °C/min and held for 35 min at the final temperature. Iso-octane was added to the samples of condensates and oils as an internal standard for quantification prior to GC-FID analysis.

2.4. Gas Chromatography-Mass Spectrometry (GC-MS) Full Scan

Full-scan GC-MS analysis was performed by using a Thermo Trace GC Ultra gas chromatograph coupled to a Thermo DSQ II single-quadrupole mass spectrometer and

controlled by a computer running XCalibur software. The GC was equipped with a BPX5 fused silica column (50 m x 0.22 mm i.d., 0.25 µm film thickness) using He as carrier gas at a constant flow rate of 1 ml/min. The injector was operated at 50 °C and heated to 300 °C at 600 °C/min in splitless mode. The initial GC oven temperature was 50 °C, which was held for 1 min, then raised to 310 °C at 3 °C/min and held for 30 min at the final temperature. The MS was operated in full scan electron ionization (EI) mode (*m/z* 100-330). The electron multiplier was operated at 70 eV and 260 °C source temperature. Identification and quantification were carried out using ions of *m/z* 128 for naphthalene, *m/z* 142 for methylnaphthalenes, *m/z* 156 for dimethylnaphthalenes, *m/z* 170 for trimethylnaphthalenes, *m/z* 178 for phenanthrene, *m/z* 183 for cadalene, *m/z* 184 for dibenzothiophenes, *m/z* 192 for methylphenanthrenes, *m/z* 219 for retene, *m/z* 231 for triaromatic steroids, *m/z* 253 for monoaromatic steroids, *m/z* 191 for terpanes and hopanes, *m/z* 217 for steranes. Diamondoids, which occur in the saturated fraction, were monitored using the following ions: *m/z* 135, 136, 149, 163 (adamantanes); *m/z* 187, 188 and 201 (diamantanes). The calculated concentrations of biomarkers and PAHs are relative to the concentration of the corresponding internal standards. The 5α-androstane (*m/z* 260) and 1-ethylpyrene (*m/z* 215+230) were used as the saturated and aromatic internal standard, respectively.

2.5. Gas Chromatography-Mass Spectrometry (GC-MS) Metastable Reaction Monitoring (MRM)

A Finnigan MAT 95XL spectrometer coupled to a HP 6890A gas chromatograph was employed, operating in MRM mode. A SGE BPX5 fused silica capillary column (50 m x 0.22 mm i.d., 0.25 µm film thickness) was used with He as carrier gas at a flow rate of 1 ml/min. The injector was operated at 52 °C and heated to 300 °C at 720 °C/min in splitless mode. The GC oven was programmed from 50 to 310 °C at 3 °C/min with initial and final hold times of 1 and 7 min, respectively. The metastable transitions used for identification of hopanes and steranes were *m/z* (370, 384, 398, 412, 426, 440, 454, 468, 482) →191 and *m/z* (372, 386, 400, 414) →217 respectively. Ion transitions were monitored with dwell times of 21 ms and an inter-dwell time of 20 ms per metastable transition. The total cycle time was 0.984 s for the detection of 24 ion transitions.

2.6. Gas Chromatography-Isotope Ratio Mass Spectrometry (GC- IRMS)

Compound-specific carbon isotope analysis was carried out using an Agilent Technology 6890 GC coupled to a MAT 253 isotope ratio mass spectrometer (Thermo Fisher Scientific) via a combustion interface (GC-C/TC III, Thermo Fisher Scientific) in samples of oils, condensates and source rock extracts. For oil and condensate samples, compound-specific hydrogen isotope analysis was performed using an Agilent Technology 6890 GC coupled to a Delta V Plus IRMS via a pyrolysis interface (GC-C/TC III, Thermo Fisher Scientific). Combustion was completed in a microvolume ceramic tube with CuO/Ni/Pt wires at 940 ºC. Pyrolysis was performed in a microvolume ceramic tube at 1440 ºC. In addition, δD values for *n*-alkanes from source rock extracts were measured using a Thermo Scientific Delta V Plus IRMS coupled to a Trace 1310 GC via an Isolink pyrolysis furnace operated at 1420 °C at the University of Potsdam. For saturated fraction analysis, the GC was equipped with a HP Ultra 1 column (50 m x 0.2 mm i.d., 0.33 µm film thickness). The temperature program started at 40 °C for 2 min and was then increased to 300 °C at 4 °C/min and held for 45 min. The injector was held at variable split ratios (splitless to split 1:50) and an initial temperature of 230 °C. During injection, the injector was heated to 300 °C at a rate of 700 °C/min and held at this temperature for the rest of the analysis time. For whole oil analysis, the GC was equipped with a HP Ultra 1 column (50 m x 0.32 mm i.d., 0.52 µm film thickness). The temperature program started at 30 °C for 10 min and was later increased to 60 °C at 2 °C/min, then to 300 °C at 4 °C/min and held for 30 min. The isotope data of individual hydrocarbons are reported in conventional delta notation (i.e., $\delta^{13}C$ and δD or $\delta^{2}H$ values) in per mil (‰) units. Each sample was analysed at least in triplicate. H_2 gas of a known isotopic composition was used as a working reference standard. The $\delta^{13}C$ and δD measurements were corrected to the Peedee Belemnite (PDB) and Vienna Standard Mean Ocean Water (VSMOW), respectively. The $\delta^{13}C$ and δD determinations were checked by regular measurements of certified standards containing mixtures of *n*-alkanes (Chiron, Norway and A. Schimmelmann, Indiana University, USA). The accuracy was monitored by routine measurements of the standard mixture after every six injections. Standard deviations of triplicate measurements for $\delta^{13}C$ and δD signatures were ≤0.5‰ and ≤5‰, respectively, in analyzed samples.

Chapter 3

Petroleum Source, Maturity, Alteration and Mixing in the Southwestern Barents Sea: New Insights from Geochemical and Isotope Data

3.1. Abstract

The Hammerfest Basin (HB) is an important area for petroleum exploration in the southwestern Norwegian Barents Sea. This contribution is aimed to characterize oils and condensates hosted in Triassic and Jurassic reservoirs, establish genetic relationships and to assess maturity, mixing and petroleum alteration processes. The research was based on geochemical as well as bulk and compound-specific stable carbon and hydrogen isotope analyses of oil and condensate samples from all major fields and discoveries in the HB, including extracts from Jurassic and Triassic source rocks. Interpretations of light hydrocarbon composition and isotope data clearly identify four main petroleum groups affected by microbial degradation, water washing, evaporative fractionation and high thermal maturity level. Based on polycyclic aromatic hydrocarbons (PAHs), marine and higher-plant-derived biomarkers and carbon isotopic composition ($\delta^{13}C$) of individual petroleum hydrocarbons, four petroleum families (I-IV) are recognized in the HB and a distinction can be made among oils and condensates from different stratigraphic levels and sectors of the Basin. Most oils and condensates from the HB consists of mixtures with small maturity variations; however, oils from Middle Triassic reservoirs in the Goliat field showed larger

This chapter has been published as: Murillo, W.A., Vieth-Hillebrand, A., Horsfield, B., Wilkes, H., 2016. Petroleum source, maturity, alteration and mixing in the southwestern Barents Sea: New insights from geochemical and isotope data. Marine and Petroleum Geology 70, 119-143. https://doi.org/10.1016/j.marpetgeo.2015.11.009

maturity variations according to biomarker, PAH and light hydrocarbon-maturity ratios. In the HB, geochemical and isotopic data allowed unraveling mixtures of hydrocarbons derived mainly from Jurassic, Triassic and Paleozoic source rocks.

3.2. Introduction

The Hammerfest Basin (HB) is located in the southwestern part of the Norwegian Barents Sea (NBS), a large geological province that is nearly twice the size of the Norwegian North Sea and that includes several sedimentary basins of Paleozoic and Mesozoic age (Fig. 3.1). The NBS is characterized by a complex tectonic history (e.g., Vorren et al., 1991; Faleide et al., 1993; Dimakis et al., 1998) and the occurrence of several source intervals ranging in age from Lower Carboniferous to Lower Cretaceous (e.g. Johansen et al., 1992; Larssen et al., 2002; Ohm et al., 2008). This has not only resulted in a very complex history of petroleum generation, migration and trapping, but also in different scenarios of petroleum mixing and alteration in the HB reservoirs.

Although many authors have assessed the potential source rocks from different source intervals in the NBS (e.g., Johansen et al., 1992; Larsen et al., 1992; Linjordet and Grung-Olsen, 1992; Larssen et al., 2002; Ohm et al., 2008; Van Koeverden et al., 2010), only a few geochemical studies have been carried out using oil and condensate samples from the HB (Ohm et al., 2008; Duran et al., 2013; Killops et al., 2014). Ohm et al. (2008) analyzed several samples of petroleum from the Norwegian Barents Sea and suggested mixing of oils from Upper Jurassic, Triassic and Paleozoic source rocks. The same authors also reported biodegradation and water washing in crude oils from the Goliat field, and suggested that the loss of water-soluble aromatic compounds was due to long-distance migration or migration through a carrier rock with a high surface to volume ratio. Duran et al. (2013a) compared basin modelling predictions and geochemical data of fluid samples from the Hammerfest Basin. They suggested that petroleum charges from Upper Jurassic and Triassic source rocks migrated from the western and northern margins of the HB to the Askeladd and Snøhvit fields, respectively; whereas the Albatross field was charged from both areas. Local and long distance migration from the north were suggested to be responsible for petroleum accumulations in the Goliat and Tornerose fields. Furthermore, they reported that

hydrocarbons from the Tornerose field also might have been slightly influenced by biodegradation. Killops et al. (2014) examined a wide range of age indicators in source rock extracts and oils from the NBS. They suggested that oils of Jurassic origin dominate in post-Triassic reservoirs of the central HB, whereas towards the margins of the basin, Triassic contributions seem to dominate in pre-Jurassic reservoirs.

The previous works have been based on light hydrocarbon composition, carbon isotopic composition of gas and oil fractions and biomarkers to assess source, thermal maturity, alteration and source age of petroleum from the HB. Nevertheless, the presence of complex hydrocarbon mixtures demands the implementation of additional and more specific geochemical and isotopic analyses to decipher them and to better understand the petroleum systems in the HB. A valuable tool used in the current study is the analysis of compound-specific carbon and hydrogen isotopic compositions, which has been successfully applied to better constrain oil-to-oil and oil-to-source correlations (e.g., Schoell and Hayes, 1994; Li et al., 2001; Schimmelmann et al., 2004) and to characterize and quantify oil mixtures (e.g., Peters et al., 1989; Chen et al., 2003). Furthermore, diamondoid data have been included because they are very suitable to determine high thermal maturity contributions from source rocks to petroleum fluids in reservoirs (e.g. Chen et al., 1996; Li et al., 2000; Fang et al., 2012).

The aims of the present paper are: (1) to investigate the origin, maturity and mixing of oils and condensates in the HB and (2) to appraise diverse petroleum alteration processes in Jurassic and Triassic reservoirs. The integrated approach followed in this study includes light hydrocarbons, conventional biomarkers, higher-plant-derived biomarkers, PAHs, diamondoids and stable carbon ($\delta^{13}C$) and hydrogen (δD) isotope compositions of branched, cyclic and *n*-alkanes, pristane and phytane. This detailed geochemical and isotopic study helps to identify hydrocarbon mixtures of distinct sources, thermal maturity levels and geological ages, thus providing a better understanding of the HB petroleum systems. This research also shows evidence for Paleozoic-source contribution, dry gas influx, evaporative fractionation and gas-condensate charges, which may indicate the existence of deeper petroleum accumulations.

3.3. Study Area and Geological Setting

The study area (Fig. 3.1) is situated in the Norwegian sector of the Barents Sea (NBS). The NBS, along with the Russian sector, together constitute one of the world's widest epicontinental seas covering an area of ~1.3 million km^2 (Renard and Malod, 1974; Doré, 1995). The HB is geographically delimited by latitudes 70°50'N to 72°15'N and by longitudes 20°E to 24°10'E (Gabrielsen et al., 1990). The basin is a relatively shallow, fault-bounded structure developed during the Early-Late Carboniferous transition, but with a main phase of subsidence in the Jurassic-Early Cretaceous (e.g., Gabrielsen et al., 1990). The HB is bounded on the north by the Loppa High (LH), on the northeast and east by the Bjarmeland Platform, on the south by the Finnmark Platform (FP) and on the west by the Tromsø Basin (TB) (Gabrielsen et al., 1990; Doré, 1995) (Fig. 3.1a). The FP and TB are separated from the HB by the Troms-Finnmark Fault Complex (TFFC) and the Ringvassøy-Loppa Fault Complex (RLFC), respectively.

It is beyond the scope of this paper to comprehensively synthesize the tectonic evolution of the NBS and the geological history of the HB; therefore, the reader is referred to Faleide et al. (1984), Berglund et al. (1986), Gabrielsen et al. (1990), Johansen et al. (1992), Doré (1995), Doré and Jensen (1996), Gudlaugsson et al. (1998), Brekke et al. (2001), Larsen et al. (2002), Riis et al. (2008), Worsley (2008), Henriksen et al. (2011) and references therein for details. Instead, some key aspects focused on the HB evolution and petroleum systems have been summarized as follows:

Stratigraphically, the NBS consists of a very thick, non-marine to marine Upper Paleozoic to Cenozoic sedimentary record resting on Precambrian to Early Triassic metamorphic rocks (e.g., Faleide et al., 1984, 2010; Gudlaugsson et al., 1998). This succession is characterized by both lateral and vertical variations in thickness and facies (Faleide et al., 2010). A summary of the lithostratigraphy, reservoir and source intervals and the major tectonic events of the southwestern Barents Sea are depicted in Fig. 3.2.

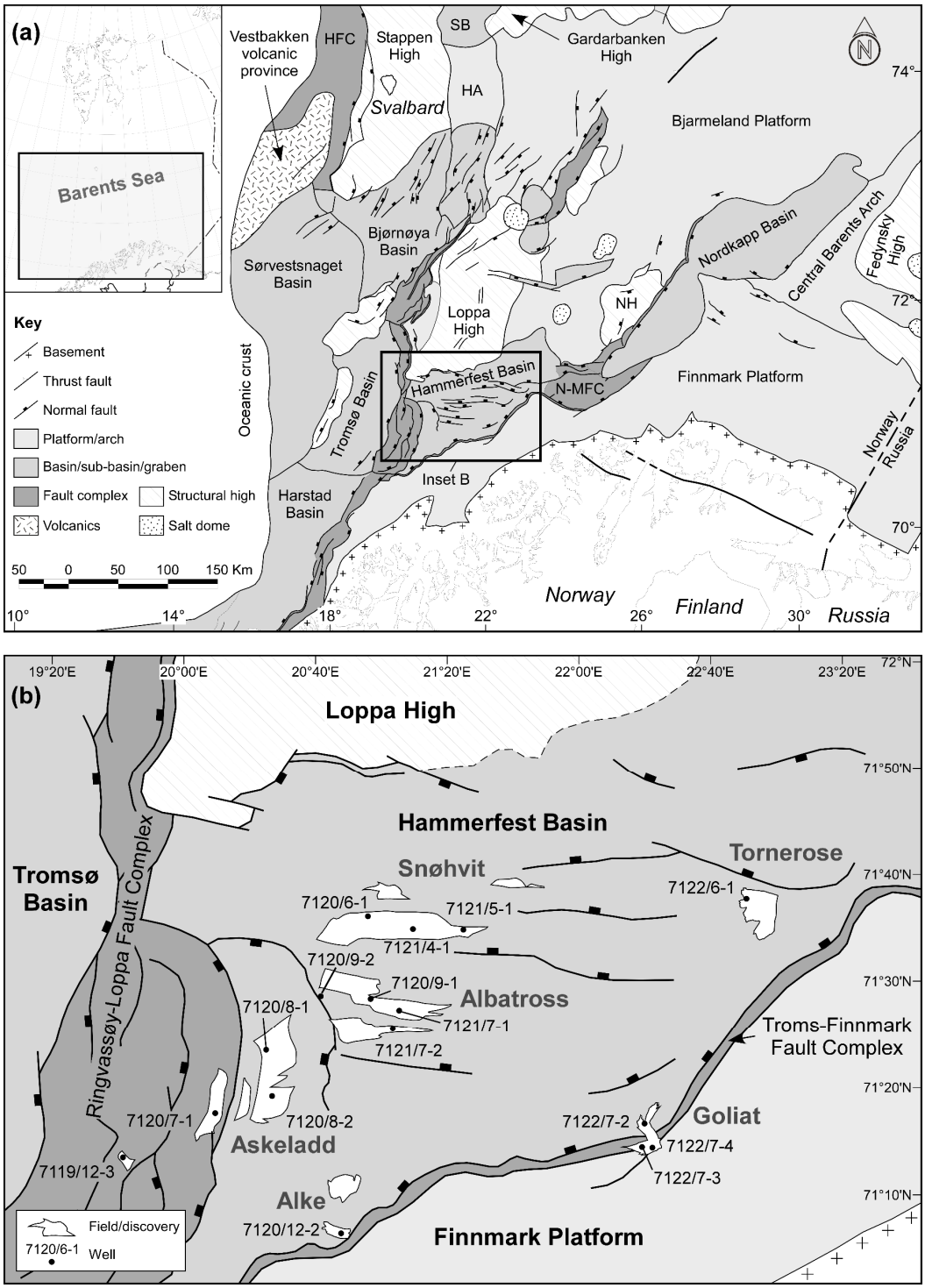

FIGURE 3.1. *(a) Index map showing major structural elements of the large Barents Sea geological province and the relative location of the Hammerfest Basin, boxed area expanded in (b) well location map with the major structural elements, fields, discoveries and sampled wells for fluids and rocks in the study area. HA = Hopenbanken Arch, HFC = Hornsund Fault Complex, NH = Norsel High, N-MFC = Nysleppen-Måsøy Fault Complex, SB = Sørkapp Basin. Map composed from Gabrielsen et al. (1990), Larsen et al. (2002), and Norwegian Petroleum Directorate (2014).*

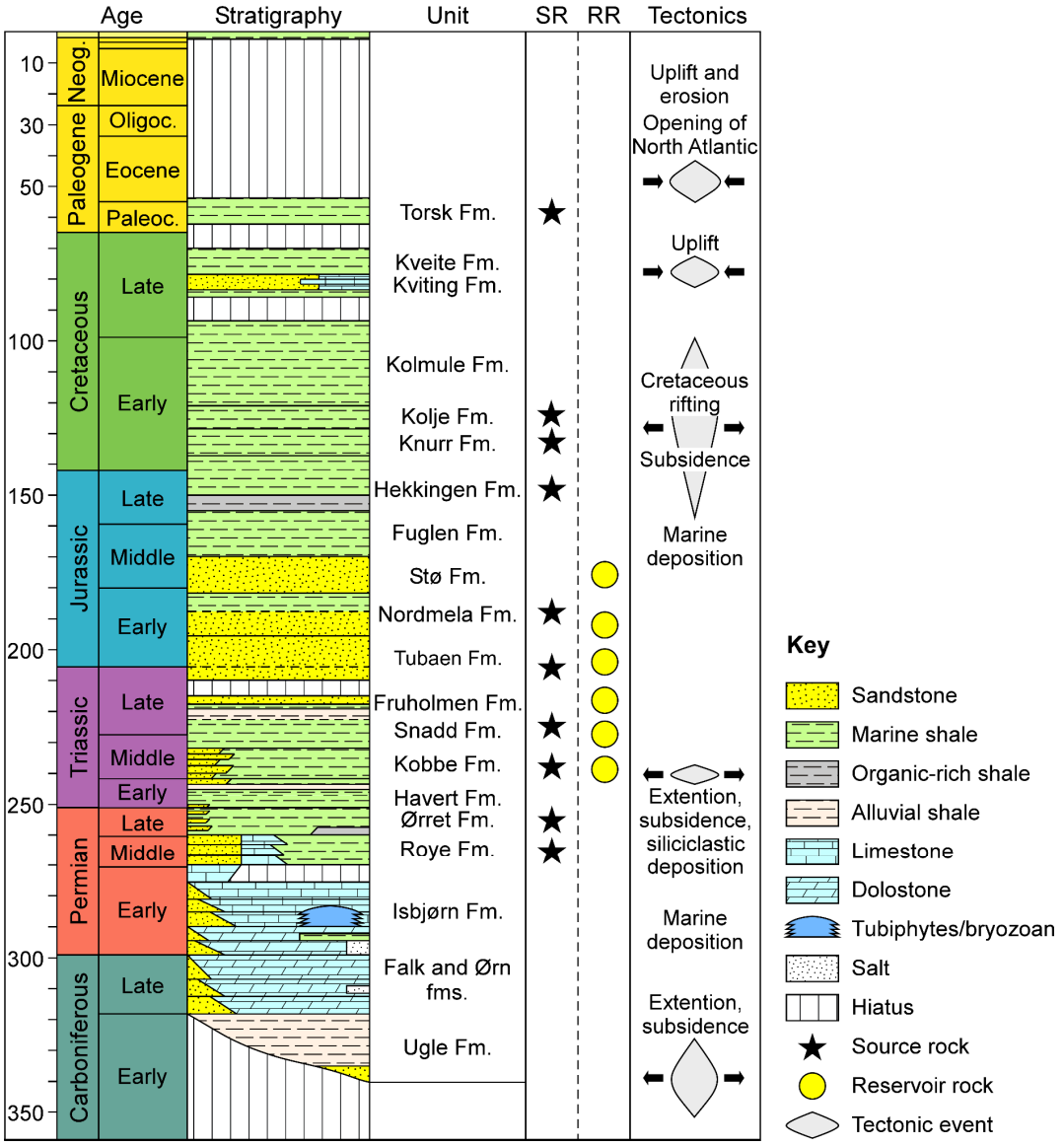

FIGURE 3.2. *Chronostratigraphic column of the Hammerfest Basin showing source and reservoir rock intervals and the major tectonic events composed from Doré (1995), Ohm et al. (2008) and Duran et al. (2013a).*

Drillings in the western part (wells 7120/9-2 and 7120/12-2) and on the southern margin (well 7122/7-3) of the HB have revealed a succession of up to 1000 m of Permian siliciclastic, carbonate and minor evaporite deposits above the basement (Norwegian Petroleum Directorate, 2014). This succession is associated with marine basinal to shelf sedimentation during a main phase of extension and thermal subsidence during Late Pennsylvanian to early Permian times (Faleide et al., 2010). After a renewed episode of faulting, uplifting and erosion in the latest Early Permian, deep-water sedimentation took

place under a relatively quiet tectonic setting for most of the Triassic (Gabrielsen et al., 1990; Riis et al., 2008; Faleide et al., 2010). The associated stratigraphy is dominated by fine-grained deposits that are locally organic-rich (e.g., the Snadd Formation) constituting important source rocks in the Basin (Ohm et al., 2008). The Lower-Middle Jurassic is dominated by shallow-marine to coastal sandstones of the Tubåen, Nordmela and Stø formations, which constitute the main petroleum reservoirs of the HB (Gjelberg, 1987; Worsley, 2008; Faleide et al., 2010). This succession is succeeded by predominantly shales of the Flugen, Hekkingen, Knurr, Kolje and Kolmule formations, deposited during a time of extension in Middle Jurassic-Early Cretaceous times; the Hekkingen Formation is considered the main source rock in the region (e.g., Doré, 1995; Ohm et al., 2008). During Late Cretaceous-middle Paleogene (earliest Eocene times), the HB has undergone uplift, erosion and then deposition of the fine-grained Torsk Formation. The rest of the Paleogene and most of the Neogene are characterized by volcanism, glaciation and uplift (Gabrielsen et al., 1990; Riss and Fjeldskaar, 1992; Worsley, 2008). The long-term Late Cenozoic uplift may have resulted in the erosion of up to 1500 m of sedimentary rocks in the Hammerfest Basin (e.g., Henriksen et al., 2011) and alteration of petroleum in the HB reservoirs (e.g., Doré and Jensen, 1996). The Pliocene-Pleistocene glacial-interglacial cycles resulted in significant overpressure fluctuations, which likely induced the main gas leakage events and sequestration of methane at the surface, affecting the petroleum accumulations in the region (Cavanagh et al., 2006; Duran et al., 2013b).

3.4. Samples

A total of 16 crude oil and condensate samples from 15 wells and source rock extracts of 10 cuttings and core samples from the Triassic Snadd and Kobbe formations and the Jurassic Hekkingen and Nordmela formations were collected. The locations of sampled wells used in this study are shown in Fig. 3.1b and basic sample information is included in Tables 3.1 and 3.2. A large number of petroleum wells (11) are located in the HB domain but some of them occupy marginal positions on the RLFC (2 wells) to the west and the TFFC (2 wells) to the south. Most of the wells are located in areas with commercial accumulations of gas and oil, which make the HB the most important hydrocarbon province of the NBS (e.g., Doré, 1995).

TABLE 3.1. *Sample details and assigned families for analyzed oils and condensates.*

Well	Test	Depth MD (m)	Field/Discovery	Reservoir Fm./Age	Family
7120/7-1	T2	2415-2435	Askeladd Vest	Stø Fm./ Early-Middle Jurassic	I
7120/8-1	DST1	2165-2172	Askeladd	Stø Fm./ Early-Middle Jurassic	I
7120/8-2	DST1	2092	Askeladd	Stø Fm./ Early-Middle Jurassic	I
7121/7-2	-	2153-2180	Albatross Sør	Fruholmen Fm./ Late Triassic	I
7120/9-1	DST2A	1869-1874	Albatross	Stø Fm./ Early-Middle Jurassic	II
7121/7-1	DST2	1866-1871	Albatross	Stø Fm./ Early-Middle Jurassic	II
7122/6-1	DST2	2424-2434	Tornerose	Snadd Fm./ Late Triassic	II
7120/6-1	DST2	2432-2436	Snøhvit	Stø Fm./ Early Jurassic	III-A
7121/4-1	DST3	2419-2434	Snøhvit	Nordmela Fm./ Early Jurassic	III-A
7121/5-1	DST1	2436-2439	Snøhvit	Stø Fm./ Early Jurassic	III-A
7122/7-2	-	1078-1106	Goliat	Tubåen Fm./ Late Triassic	III-B
7122/7-3(1)	DST1B	1195	Goliat	Snadd Fm./ Late Triassic	III-B
7122/7-3(2)	DST3C	1812	Goliat	Kobbe Fm./ Middle Triassic	IV
7122/7-4S	-	1911-1927	Goliat	Kobbe Fm./ MiddleTriassic	IV
7120/12-2[a]	DST2	1985-1991	Alke	Nordmela Fm./ Early Jurassic	-
7119/12-3	T1	3185-3195	7119/12-3	Stø Fm./ Early Jurassic	-

[a] Condensate sample from well 7120/12-2 (DST 2) is probably a mislabelled DST 1 or DST 3 sample (Norwegian Petroleum Directorate, 2013).

TABLE 3.2. *List of source rock samples sorted by well, formation, age, depth and field. Values of vitrinite reflectance calculated using methylphenanthrene distribution factors and the age-related parameter (extended tricyclic terpane ratio, ETR) are included.*

Well	Source rock Fm.	Age	Depth MD (m)	Field	$\%R_c$ (MPDF1)	$\%R_c$ (MPDF2)	ETR
7120/8-2 (1)	Hekkingen**	Late Jurassic-Early Cretaceous	1974	Askeladd	0.82	0.78	0.33
7120/8-2 (2)	Hekkingen**	Late Jurassic-Early Cretaceous	1995	Askeladd	0.86	0.76	0.48
7120/8-2 (3)	Hekkingen**	Late Jurassic-Early Cretaceous	2055	Askeladd	0.73	0.68	0.50
7120/9-2 (1)	Hekkingen**	Late Jurassic-Early Cretaceous	1943	Albatross	0.73	0.69	0.40
7120/6-1	Nordmela*	Early Jurassic	2531.15	Snøhvit	0.76	0.75	-
7120/9-2 (2)	Snadd**	Middle-Late Triassic	2708	Albatross	0.95	0.95	0.60
7120/9-2 (3)	Kobbe**	Middle Triassic	3993	Albatross	0.97	1.03	0.73
7122/7-4 (1)	Kobbe*	Middle Triassic	1815.15	Goliat	0.74	0.74	0.56
7122/7-4 (2)	Kobbe*	Middle Triassic	1820.15	Goliat	0.73	0.78	0.55
7120/12-2 (1)	Kobbe**	Middle Triassic	2940	Alke	0.97	0.98	0.56

Core samples (*); cuttings samples from wells with water-based drilling muds (**). $\%R_{c\,(MPDF1)}$: -0.166 + 2.242 F1, F1: (2-MP + 3-MP)/(2-MP + 3-MP + 1-MP + 9-MP); $\%R_{c\,(MPDF2)}$: -0.112 + 3.739 F2, F2: 2-MP/ 2-MP + 3-MP + 1-MP + 9-MP. Extended tricyclic terpane ratio (ETR): $(C_{28} + C_{29})/(C_{28}+C_{29}+Ts)$.

3.5. Methods

3.5.1. Analytical Methods

The analytical methods were described in the methodology section, see details of specific techniques, methods and tools in Chapter 2.

3.5.2. Multivariate Statistics

Statistical analysis was completed using the multivariate analysis tool Past version 3.04. All values for each parameter were normalized to the standard deviation of the variables. Computational and graphical display of the data was carried out using hierarchical cluster analysis and principal component analysis (PCA).

3.6. Results and Discussion

3.6.1. Geochemical Characteristics of Extracts from Triassic and Jurassic Source Rocks

To establish useful parameters for source-oil correlation, a study of organic matter source facies and depositional environment was conducted on Triassic and Jurassic formations, which contain organic rich shales and coaly shales at the same level of thermal maturation (Table 3.2). The thermal maturity of the source rock extracts was estimated using methylphenanthrene distribution factors (Kvalheim et al., 1987). Most analyzed extracts from source rock samples show values of calculated vitrinite reflectance ranging from 0.7-0.8% R_o. However, some Triassic source rocks have reached a higher maturity level (0.9-1.0% R_o) (Table 3.2). Typical examples of *m/z* 191 and *m/z* 218 mass fragmentograms for source rock extracts from the Triassic Kobbe Formation and the Jurassic Nordmela and Hekkingen formations are shown in Fig. A.1, Appendix A. Biomarker ratios and sterane percentages for the individual samples of source rock extracts are listed in Table B.1, Appendix B.

The ratio of pristane/phytane (Pr/Ph) has been widely used to assess redox conditions of the depositional environment for the source rock (e.g. Didyk et al. (1978)). In the analyzed

extracts of siliciclastic source rocks, the Pr/Ph values varied between 1.5 and 2.5 for the Hekkingen Formation and between 1.2 and 3.5 for the Kobbe Formation at the same level of thermal maturity (peak oil-generative window). The wide ranges of Pr/Ph ratios in these source rocks indicate redox condition variations during their deposition. In addition, the extracts show different ratios of Ts/Tm and Diast/St (Fig. 3.3a) despite similar maturities, which can also be the result of fluctuating oxygen levels during deposition (e.g., Moldowan et al., 1986). Analyzed intervals of Triassic and Jurassic source rocks show predominance of C_{29} steranes over C_{27} homologs (Fig. 3.3b), a high ratio of C_{30} moretane relative to C_{30} hopane (0.15-0.20) and presence of C_{30} steranes, which indicate that these formations have been influenced by mixed sources of marine algal and terrestrial organic material. In the HB, sterane ratios were useful to distinguish among source rock extracts. The C_{27}/C_{29} sterane ratio shows the highest values in source rock extracts from the Upper Jurassic Hekkingen Formation (Askeladd and Albatross fields), while lower values were found in those from the Lower Jurassic Nordmela Formation (Snøhvit field) and the Middle Triassic Kobbe Formation (Goliat field) (Fig. 3.3b), which have the highest percentages of C_{29} steranes (61-65%). Because source rock extracts from the Triassic Kobbe Formation contain a lower amount of C_{30} steranes (4-5%) relative to those from the Upper Jurassic Hekkingen Formation (9-13%), the ratios of regular steranes to C_{30} steranes were appropriate to discriminate between them (Fig. 3.3b and c). Moreover, the extract from the Nordmela Formation was differentiated readily from the Hekkingen and Kobbe formation extracts using a crossplot of C_{27}/C_{29} against C_{27}/C_{30} sterane ratios (Fig. 3.3b).

The extended tricyclic terpane ratio (ETR) has been considered as a conventional age indicator (Holba et al., 2001). Low values of ETR for Triassic source rocks in the Barents Sea were recorded by Ohm et al. (2008) and Killops et al. (2014). In this study, the ETR values allowed distinguishing between extracts from Triassic and Jurassic source rocks. Source rock extracts from the Hekkingen Formation have ETR values ranging from 0.33 to 0.50, while ETR values of the Kobbe and Snadd formations varied between 0.55 and 0.73 (Table 3.2). Killops et al. (2014) also suggested that ETR can differentiate Triassic from Jurassic sources in the Barents Sea.

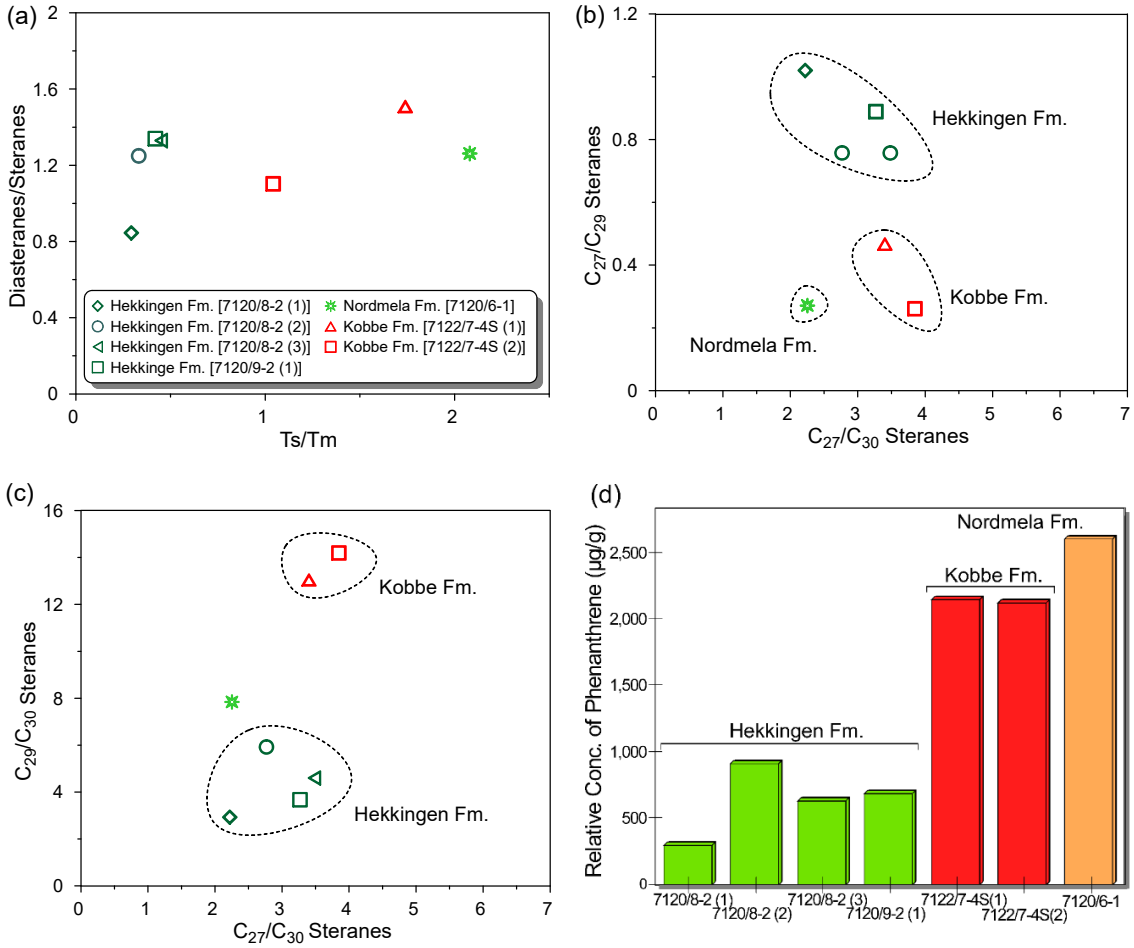

FIGURE 3.3. *Scatter plots of (a) diasterane/sterane ratio versus Ts/Tm ratio; (b) C_{27}/C_{29} versus C_{27}/C_{30} sterane ratios and (c) C_{29}/C_{30} versus C_{27}/C_{30} sterane ratios; (d) bar graph of phenanthrene relative concentration in source rock extracts.*

In order to assess the influence of terrestrial organic matter in Jurassic and Triassic source rocks, the relative abundances of three higher-plant-derived biomarkers, retene, cadalene and 6-isopropyl-1-isohexyl-2-methylnaphthalene (ip-iHMN), were measured. The relative abundance of these biomarkers are linked to different plant types (van Aarssen et al., 2000). Retene has been associated with input from conifer type plants (e.g., Simoneit, 1986). Cadalene is derived from higher land-plant biological precursors (e.g., Simoneit, 1986), however, also algal material has been proposed as a precursor for this marker (e.g., Elias et al., 1997). Although the ip-iHMN has an uncertain specific source, a higher plant origin has been recognized (Ellis et al., 1996). The ratio of retene to the sum of retene plus cadalene (HPP) has been used as an indicator of conifer contributions (van Aarssen et al., 2000).

Similar HPP values (0.80-0.97) were recognized in the analyzed Jurassic and Triassic source rocks found at the same level of thermal maturity (0.7-0.8% R_o), which seem to reflect no discrepancy in the terrestrial source input. Besides higher-plant-derived biomarkers, some aromatic compounds can also be used for differentiating the organic matter source input. Phenanthrene is an important component in the aromatic fraction of oils and previous studies have shown that marine source rocks and crude oils contain lower abundance of phenanthrene than their terrestrial counterparts (e.g., Fan et al., 1990). Under this premise, the concentration of phenanthrene was evaluated in extracts from Jurassic and Triassic source rocks at the same thermal maturity level. Source rock extracts from the Middle Triassic Kobbe Formation and Early Jurassic Nordmela Formation have a higher concentration of phenanthrene than those from the Upper Jurassic Hekkingen Formation, indicating that the former are more influenced by terrestrial organic material (Fig. 3.3d).

3.6.2. Evaluation of Petroleum Alteration Processes

Multivariate statistical analysis using the composition of cyclic alkanes, *n*-alkanes (C_5-C_9) and light aromatic hydrocarbons (Fig. 3.4a), including benzene, toluene, ethylbenzene and xylenes (BTEX), allowed to classify HB oils and condensates into four groups (A-D) according to their main secondary alteration processes. Compositional data of gasoline-range aromatic, paraffinic and cyclic hydrocarbons are represented in a ternary diagram (Fig. 3.4b), which depicts the different oil groups. Even though the samples were carefully handled and stored, this classification could have been affected by the high volatility of hydrocarbons $<C_7$. Because the C_7 hydrocarbons are less susceptible to evaporation than lighter hydrocarbons and they have notably different properties, such as boiling points, water solubilities and susceptibilities to bacterial attack (Halpern, 1995), their peak ratios can be effectively used for distinguishing compositional variations in oils caused by secondary alteration processes (Thompson, 1983; Halpern, 1995). The star plots of Halpern transformation parameters (Tr1-Tr8) for samples from the HB (Fig. 3.4c), support the oil groups established using the molecular composition of gasoline-range hydrocarbons (Fig. 3.4b). Light hydrocarbons were useful for describing petroleum alteration processes but not for correlation in mixed oils from the HB, where the ratios of C_7 hydrocarbons related to source (Halpern, 1995) did not allow a good differentiation based on contributing source

rocks. The C_7 ratios to differentiate hydrocarbon samples are shown in Table B.2, Appendix B.

- ***Group A (Biodegraded oils)***

This group includes oils hosted in the Tubåen and Snadd formations of the Goliat field (Fig. 3.1b; Table 3.1). These crude oils show the lowest concentrations of *n*-alkanes ($<C_{14}$) and methyl alkanes (Fig. 3.5), the highest percentage of cycloalkanes (Fig. 3.4b) and the lowest heptane (H) and isoheptane (I) ratios (Fig. 3.6a) interpreted as a result of microbial degradation. Some differences, however, were detected between the two biodegraded samples. The oil sample from well 7122/7-2 (Tubåen Formation) shows a higher concentration of toluene (Fig. 3.5) and thus higher ratios of toluene/*n*-heptane and toluene/benzene than oil sample from well 7122/7-3 (Snadd Formation). In contrast, the Snadd Formation hosted oil shows a higher concentration of benzene (Fig. 3.5) and a higher ratio of benzene/*n*-heptane. In addition, the Snadd Formation hosted oil has the lowest concentrations of iso- and methyl-alkanes (Fig. 3.5).

- ***Group B (Evaporative condensates)***

This group is represented by condensates from the Askeladd and Albatross fields (Fig. 3.1b; Table 3.1). The cross-plot of aromaticity ratio (toluene/*n*-heptane, *B*) and paraffinicity ratio (*n*-heptane/methylcyclohexane, *F*) suggests that condensates from the Askeladd and Albatross fields are caused by evaporative fractionation (Fig. 3.6b). The stratigraphically deeper condensates from the Askeladd and southern Albatross fields have a higher aromaticity ratio and a lower paraffinicity ratio than the stratigraphically shallower condensates from the northern Albatross field (Fig. 3.6b). To evaluate the degree of evaporative fractionation in oils and condensates, Dzou and Hughes (1993) developed the fractionation index (FI), which measures the distribution of light (*n*-C_{10}) versus heavy (*n*-C_{16} + *n*-C_{25}) hydrocarbons. In the HB, condensates from the northern Albatross field show the highest values of fractionation index (FI, 2.7-2.8), whereas the values for condensates from the Askeladd and southern Albatross fields are lower (0.7-1.2). All of these parameters strongly indicate evaporative fractionation in the Askeladd and Albatross fields. The FI values of hydrocarbon samples are listed in Table B.2, Appendix B.

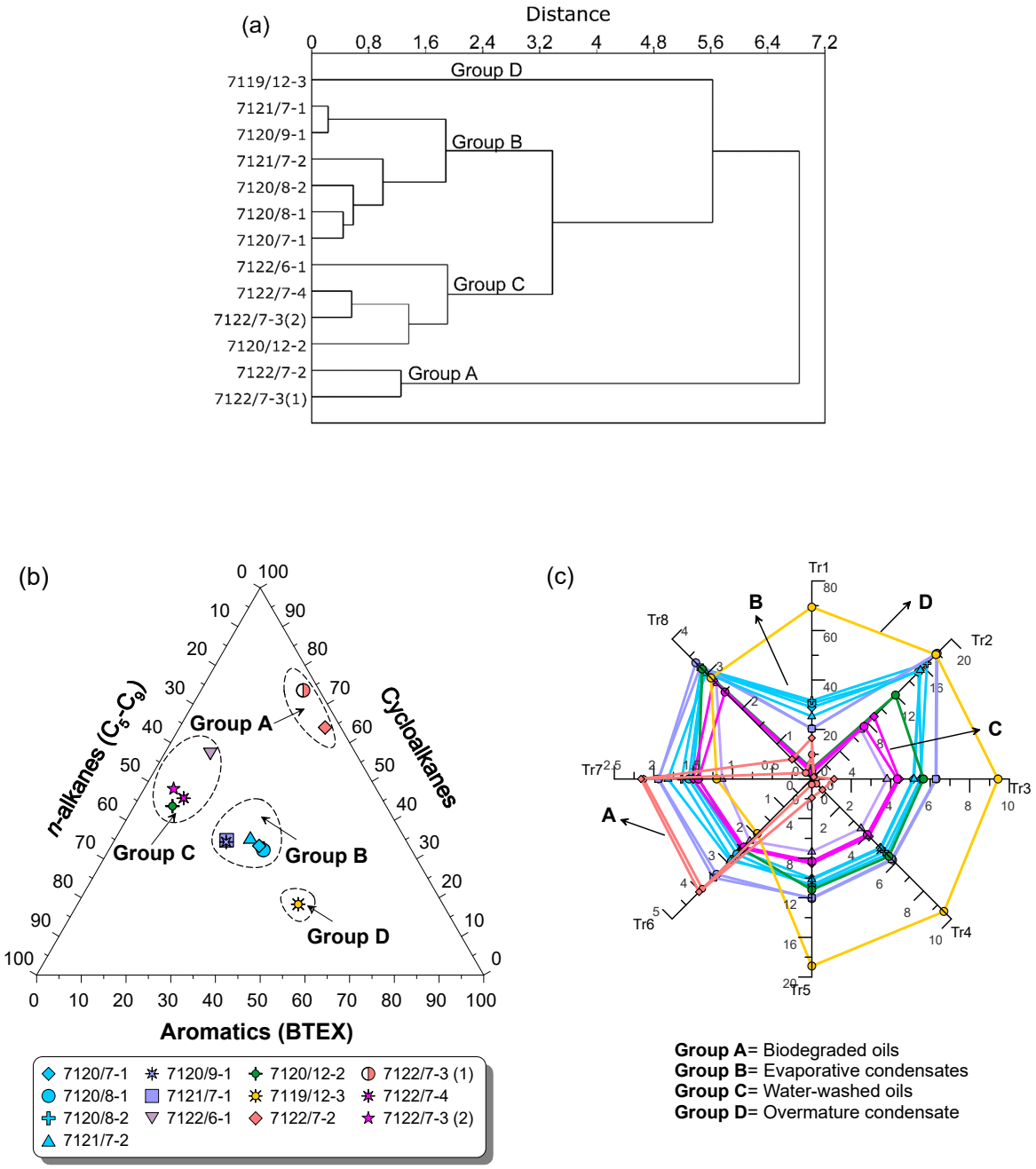

FIGURE 3.4. *Classification of hydrocarbon groups according to main petroleum alteration processes based on (a) Cluster analysis; (b) ternary diagram of gasoline range hydrocarbons; (c) C_7 oil transformation star diagram (Halpern, 1995). Halpern ratios are described as: Tr1: toluene/X; Tr2: n-C_7/X; Tr3: 3-MH/X; Tr4: 2-MH/X; Tr5: P2/X; Tr6: 1c2-DMCP/X; Tr7: 1t3-DMCP/X; Tr8: P2/P3. X: 1,1-DMCP; P2: (2-MH + 3-MH); P3: (2,2-DMP + 2,3-DMP + 2,4-DMP + 3,3-DMP + 3-EP). MH: methylhexane, DMCP: dimethylcyclopentane. DMP: dimethylpentane, EP: ethylpentane, c: cis, t: trans. Symbol color indicates the petroleum field/discoveries as follows: cyan blue – Askeladd and Southern Albatross fields; light blue – Northern Albatross field; pink – Goliat field (shallow reservoir); magenta – Goliat field (deep reservoir); light purple – Tornerose field; green – Alke field; yellow – discovery 7119/12-3.*

Snøhvit oils, which were not included in this classification, also show a high ratio of aromaticity (Fig. 3.6b), however, they show a lower fractionation index (0.08-0.10). The high aromaticity ratio may be associated with a high terrestrial organic matter input. High concentrations of toluene and xylenes (Fig. 3.5) are consistent with sources containing a high terrestrial input (e.g., von der Dick et al., 1989). In addition, the high concentration of methylcyclohexane in these oils (Fig. 3.5) seems to be related to input from terrigenous organic matter. Oils derived from terrigenous coals and coaly shales are enriched in methylcyclohexane (e.g., von der Dick et al., 1989, Clayton et al., 1991). However, it is important to note that hydrocarbon leakage has taken place from the Snøhvit reservoirs (e.g., Linjordet and Grung-Olsen et al., 1992).

- ***Group C (Water washed condensates and oils)***

Group C consists of condensate samples from the Tornerose and Alke fields and the Kobbe Formation hosted oils from the Goliat field (Fig. 3.1b; Table 3.1). These samples are characterized by very low concentrations of benzene, toluene and xylenes (Fig. 3.5), indicating that they were affected by water washing (e.g., Palmer et al., 1984). Except for oils in the Group A, the Tornerose condensate shows the lowest *n*-heptane/methylcyclohexane ratio (Fig. 3.6b), suggesting that it was also biodegraded but to a lesser degree than Group A oils. In addition, Tornerose and Alke condensates show a high FI (1.0 and 1.7, respectively) and the latter has an elevated concentration of gasoline-range paraffins (Fig. 3.5), suggesting they were also affected by migration-fractionation processes. The very low aromaticity ratio in the Alke condensate is mainly attributed to water washing, (Thompson, 1987) (Fig. 3.6b). The Kobbe Formation hosted oils from the Goliat field also exhibit anomalously high concentrations of gasoline-range hydrocarbons (C_5-C_9) interpreted as a result of a secondary gas-condensate charge (Fig. 3.5). The low concentrations of benzene, toluene and xylenes together with a high concentration of *n*-alkanes $<C_9$ suggest a water washing phase without biodegradation.

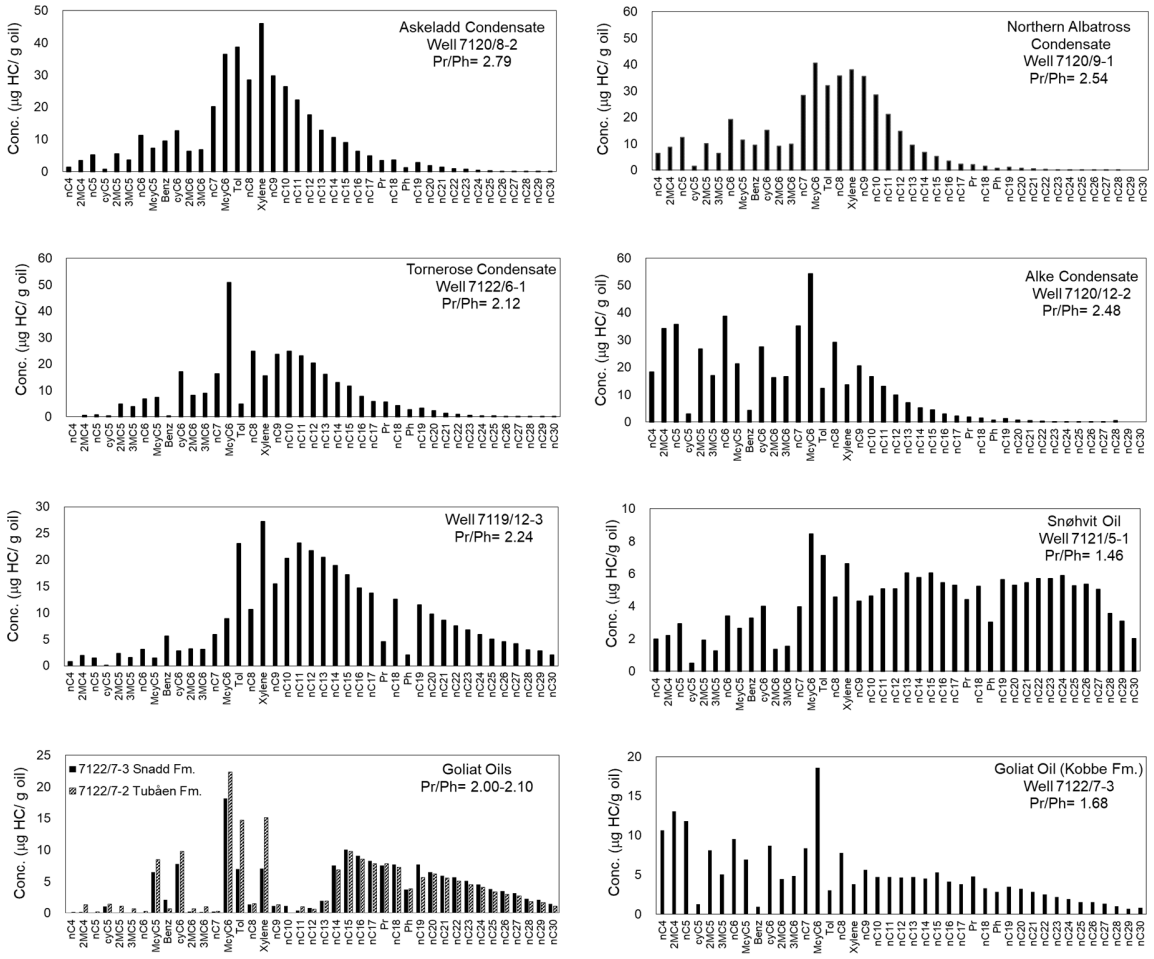

FIGURE 3.5. *Concentrations of light hydrocarbons and n-alkanes up to n-C_{30} in selected oils and condensates from the main fields and discoveries of the HB.*

- ***Group D (Thermally generated condensate)***

This group includes a condensate sample from well 7119/12-3 located on the Ringvassøy-Loppa Fault Complex (RLFC). This condensate shows a strong increase in light aromatics accompanied by a decrease in cycloalkanes (Fig. 3.4b), which are attributed to its high maturity level (condensate generation window). Despite its high maturity, the low heptane value found in this condensate (Fig. 3.6a) can be associated with type III kerogen-derived hydrocarbons (Thompson, 1983). The presence of long-chain *n*-alkanes (>C_{20}) (Fig. 3.5) typical for waxes of terrestrial higher plants (Eglinton and Hamilton, 1967) indicates that this condensate was derived mainly from a source containing a high terrigenous input.

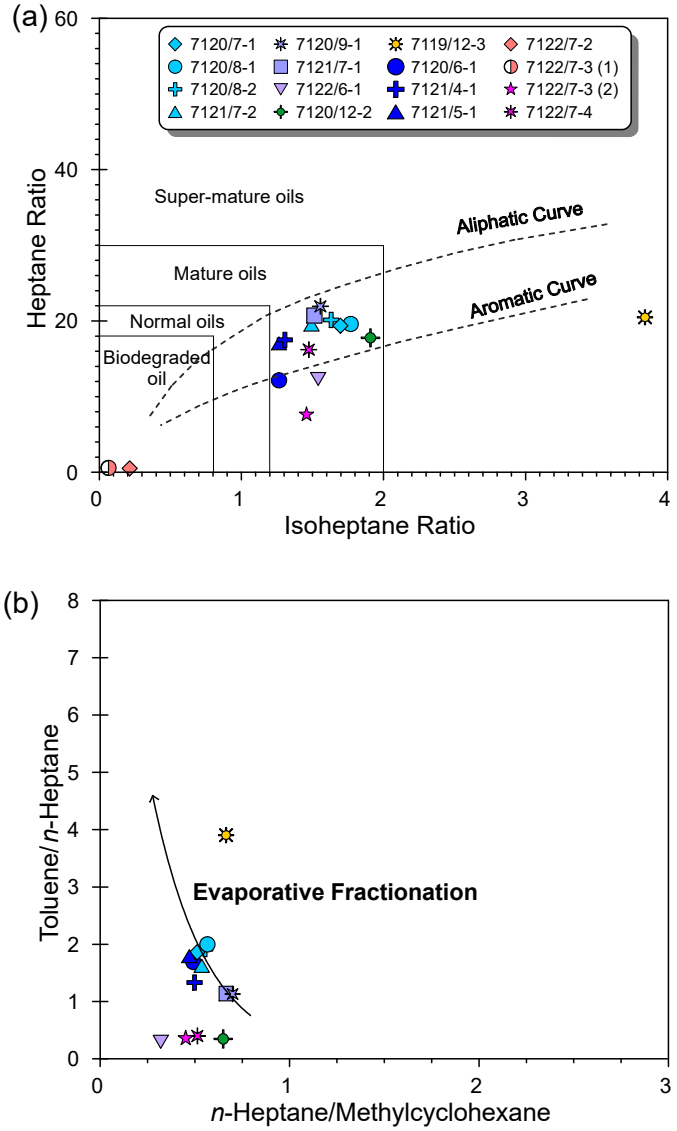

FIGURE 3.6. *(a) Heptane versus isoheptane ratios; (b) aromaticity ratio (toluene/n-heptane, B) versus paraffinicity ratio (n-heptane/methylcyclohexane, F), Thompson (1987). The arrow shows the changes in B and F ratios of condensates. Values of toluene/n-heptane ratio were not included for biodegraded oils from the Goliat field because of their elevated values.*

3.6.3. Evaluation of Thermal Maturity

In order to detect in-reservoir mixing of hydrocarbons of different thermal maturities in the HB, several maturity parameters based on composition of various petroleum components, such as light hydrocarbons, biomarkers, PAHs and diamondoid hydrocarbons were assessed in this study. Values of these maturity parameters for the individual oil and condensate samples are listed in Table B.3, Appendix B.

3.6.3.1. Light Hydrocarbons

High ratios of light-hydrocarbons containing quaternry to tertiary carbon species, C_7 isoheptanes and 2,2-dimethylbutane/2,3-dimethylbutane (Hunt et al., 1980; Hunt, 1984), were observed in oils affected by a secondary gas-condensate charge in the Middle Triassic reservoirs of the Goliat field. Even though biomarkers and PAHs do not give information related to an increase in oil maturity, these maturity parameters based on light hydrocarbons indicate hydrocarbon influx with a higher thermal maturity level. Furthermore, condensates from wells located on the RLFC and from the Alke and Tornerose fields show high values of quaternary to tertiary carbon species. An additional light hydrocarbon ratio, such as isopentane to *n*-pentane (*i*-C_5/*n*-C_5), also showed an increase with thermal maturity in non-biodegraded crude oils.

Vitrinite reflectance values calculated using Schafer's thermal maturation parameters (V) and (J) (Schaefer and Littke, 1988), exhibited a strong correlation between them (%R^2=0.97), when condensate and oil data affected by evaporative fractionation and biodegradation were excluded (Fig. 3.7a). In addition, good correlations were also obtained between vitrinite reflectance values calculated using Schaefer's parameters and some light-hydrocarbon ratios of quaternary to tertiary carbon species (Fig. 3.7b and c). Based on well-correlated plots, high maturity levels were encountered in the Kobbe Formation hosted oils from the Goliat field (1.1-1.2% R_o), condensates from the Tornerose and Alke fields (1.0-1.2% R_o, respectively) and condensates from wells located on the RLFC, such as well 7120/7-1 (1.1%R_o) and well 7119/12-3 (1.4%R_o) (Fig. 3.8). Moreover, light-hydrocarbon ratio of quaternary to tertiary C_7 isoheptanes suggests that oils hosted in the Snadd and Tubåen formations of the Goliat field were generated at the early stage of oil generation (0.55-0.6% R_o) (Fig. 3.8).

3.6.3.2. Saturated and Aromatic Biomarkers

Samples from the Snøhvit and Goliat fields are the only ones that show detectable amounts of biomarkers and have sterane isomerization ratios of 20S/(20S + 20R) and ββ/(αα+ββ) ranging from 0.4-0.52 and 0.55-0.62, respectively. These values suggest that hydrocarbons were generated at the main stage of oil generation. The values of

22S/(22S+22R) homohopane isomerization of C_{32} 17α-hopane range from 0.55 to 0.60. Although these values are not significantly deviated from the equilibrium values, the lowest values found in the Goliat oils hosted in the Kobbe Formation may suggest a contribution of less mature oils. That is also suggested by their higher ratios of Pr/*n*-C_{17} (1.2-1.3) and Ph/*n*-C_{18} (0.8-0.9) relative to those of Goliat oils hosted in the Snadd and Tubåen formations and Snøhvit oils, which show lower values. Values of equivalent vitrinite reflectance using maturity parameters of mono- and triaromatic steroids also suggest that Snøhvit and Goliat oils were generated at the main oil-generation stage, 0.65-0.75% R_o, (Peters et al., 2005).

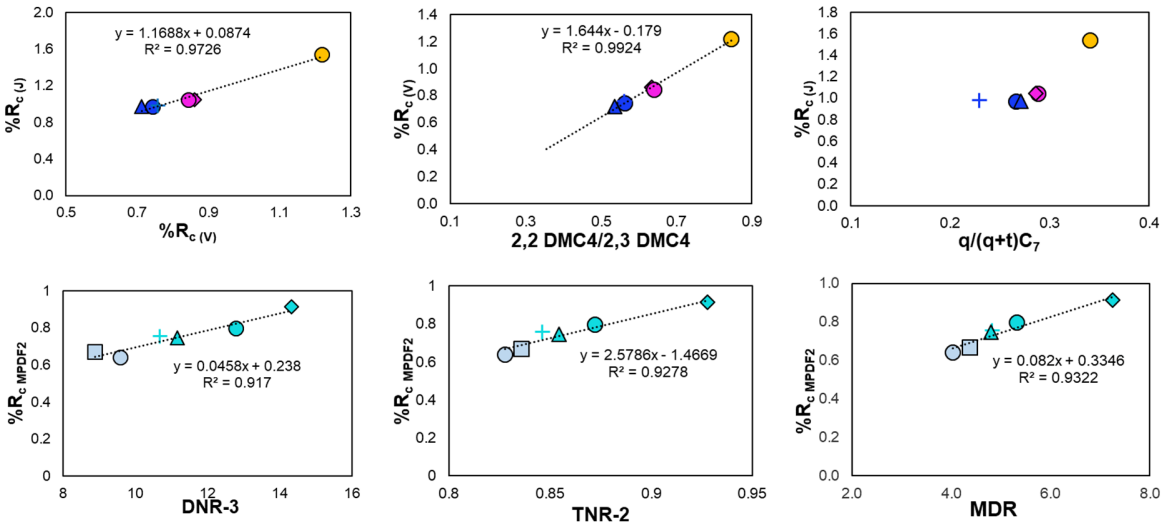

FIGURE 3.7. *Calibration cross-plot of (a) vitrinite reflectance values calculated using Schaefer-maturity parameters (V) and (J), $\%R_{c\,(V)}$ and $\%R_{c\,(J)}$, respectively; (b) $\%R_{c\,(V)}$ vs 2,2-DMC4/2,3-DMC4; (c) $\%R_{c\,(J)}$ vs q/(q+t) C_7 isoheptanes; (d) $\%R_{c\,(MPDF2)}$ vs dimethylnaphthalene ratio (DNR-3); (e) $\%R_{c\,(MPDF2)}$ vs trimethylnaphthalene ratio (TNR-2); and (f) $\%R_{c\,(MPDF2)}$ vs methyldibenzothiophene ratio (MDR) for oil and condensate samples from the HB. Maturity parameters are described as: $\%R_{c\,(V)}$: 1.0 + 1.8 logV, V: C_7 paraffins/ naphthenes; $\%R_{c\,(J)}$: 0.84 + 1.1 logJ, J: (2-methylhexane + 3-methylhexane)/(1,2-(cis + trans)- + 1,3 (cis + trans) dimethylpentanes); 2,2-DMC4/2,3-DMC4: 2,2-dimethylbutane/2,3-dimethylbutane; q/(q+t) C_7 isoheptanes: (2,2-DMP + 3,3-DMP)/ (2,2-DMP + 3,3-DMP + 3-EP + 2,3-DMP + 2,4-DMP) where DMP: dimethylpentane and EP: ethylpentane; $\%R_{c\,(MPDF2)}$: -0.112 + 3.739 F2, F2: 2-MP/ 2-MP + 3-MP + 1-MP + 9-MP where MP: methylphenanthrene; DNR-3: 2,6-DMN/1,8-DMN; TNR-2: (1,3,7-TMN + 2,3,6-TMN)/ (1,3,5-TMN + 1,3,6-TMN + 1,4,6-TMN); MDR: 4-MDBT/1-MDBT.*

3.6.3.3. Polycyclic Aromatic Hydrocarbons

The distribution of alkylated PAHs, including methyl-phenanthrene, -naphthalene and -dibenzothiophene homologs are very helpful in maturity assessment (e.g., Radke et al., 1982, 1983; Alexander et al., 1985). Kvalheim et al. (1987) found a predictive relationship

between vitrinite reflectance and the methylphenanthrene distribution factors, F1 and F2. Vitrinite reflectance values using these factors ($\%R_{c\ MPDF1}$, $\%R_{c\ MPDF2}$) and methylphenanthrene index ($\%R_{c\ MPI-1}$), suggest that condensates from the Alke, Askeladd, Albatross and Tornerose fields and oils from the Snøhvit and Goliat fields were generated at the main stage of oil generation. Condensates from well 7120/7-1 (Askeladd Vest field) and well 7119/12-3, both located on the RLFC, have the highest calculated vitrinite reflectance values (Fig. 3.8). Vitrinite reflectance values calculated using F1 and F2 yield a strong correlation coefficient between them, in Askeladd and Albatross condensates (R^2=0.97). Well correlated cross-plots of some trimethylnaphthalene and dimethylnaphthalene ratios and methyldibenzothiophene ratio against $\%R_{c\ MPDF2}$ were also obtained for the Askeladd and Albatross condensate samples (Fig. 3.7d-f).

3.6.3.4. Diamondoid Hydrocarbons

Due to their thermal stability, diamondoids are suitable for evaluating high thermal maturity levels (e.g. Chen et al., 1996; Li et al., 2000). The vitrinite reflectance values were estimated using dimethyl-, trimethyl- and ethyladamantane indexes (DMAI-1, TMAI-1 and EAI) along with well-correlated plots reported by Fang et al., 2012. The average values of vitrinite reflectance cover a maturity range from 2.0 to 2.5%, suggesting an influx of dry gas to all of HB reservoirs (Fig. 3.8). Typical examples of mass chromatograms showing the distribution of adamantanes for oils and condensates from the HB are represented in Fig. A.2, Appendix A.

According to Duran et al. (2013b), part of the gas accumulations may have been sourced from Triassic source rocks, mainly from the Kobbe Formation, which have reached overmature conditions in the western and northwestern parts of the basin. The same authors also predicted gas generation by secondary cracking when hydrocarbons started to accumulate in reservoirs (Paleocene times), supporting the occurrence of thermogenic gas in the basin. In addition, Ohm et al. (2008) reported the presence of non-cogenetic gases, which have migrated after the event of uplift and pressure release, implying a live petroleum system in the western HB.

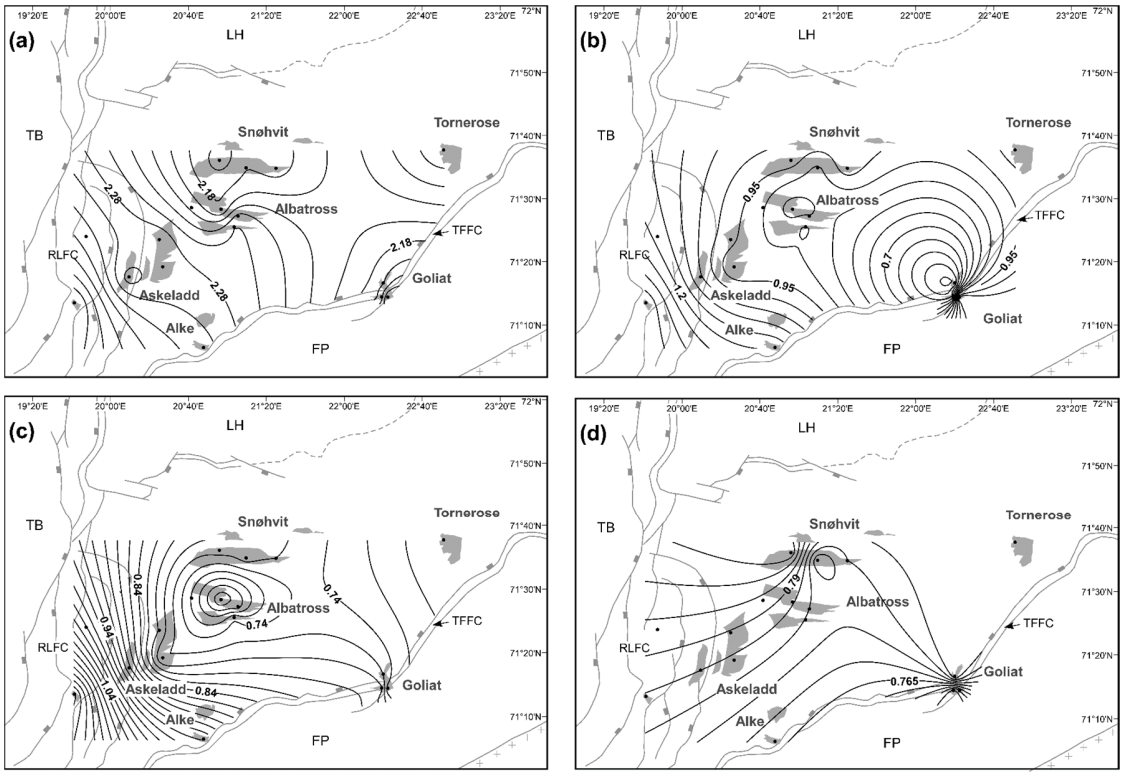

FIGURE 3.8. *Maps of %R_o calculated or equivalent using (a) dimethyl-, trimethyl- and ethyladamantane indexes (DMAI-1, TMAI-1 and EAI); (b) light hydrocarbon ratio of quaternary to tertiary isoheptanes; (c) methylphenanthrene distribution factor F_2; and (d) ratios of C_{29} sterane isomerization for oils and condensates hosted in Jurassic and Triassic reservoirs of the HB. DMAI-1: 1,3-DMA/ (1,2-DMA + 1,3-DMA); TMAI-1: 1,3,5-TMA/(1,3,5-TMA + 1,3,4-TMA); EAI: 2-EA/ (1-EA + 2-EA).*

In general, the variation of several maturity parameters suggests that most HB oils and condensates consist of hydrocarbon mixtures with small thermal maturity variations within the peak oil-generation stage, such as Snøhvit oils, Askeladd and Albatross condensates or between peak and late oil-generation stages, including condensates from the Tornerose, Askeladd Vest and Alke fields (Fig. 3.8). Condensates from wells 7120/12-2 (Alke field) and 7119/12-3 show the highest level of thermal maturity (1.2 and 1.4% R_o, respectively) (Fig. 3.8). Maturity parameters, however, cover a relatively larger variation in mixed oils hosted in the Kobbe Formation of the Goliat field, which were formed from multiple stages of generation (early to late oil-generation stages). In addition, the Snadd and Tubåen formation hosted oils from the Goliat field were formed from early to peak-oil generation stages (Fig. 3.8).

Apart from a petroleum contribution from long-distance migration to reservoirs of the Goliat field (Duran et al., 2013a), in this study oil maturity data (Fig. 3.8) confirm a local migration of oils from early-mature source rocks to the reservoirs of the Goliat field. Although the loss of gaseous and light hydrocarbons in the Goliat field has been associated with long-distance petroleum migration and leakage during uplift and erosion (e.g., Ohm et al., 2008; Duran et al., 2013b), the presence of a secondary gas-condensate charge, identified in the Goliat oils, may indicate a deeper petroleum accumulation (e.g., Dzou and Hughes, 1993; Holba et al., 1996). Furthermore, diamondoids indicate the occurrence of a late gas charge in the Goliat field (Fig. 3.8).

3.6.4. Correlations

3.6.4.1. Hydrocarbon Families: Oil-Oil Correlation

Multivariate statistical analyses (MVA), such as cluster and principal component analysis (PCA), were performed to establish the correlation degree of the oil and condensate data set and define the main geochemical and isotope variables responsible for the variation of the data. The data used for MVA include the average $\delta^{13}C$ values of Pr and Ph, cyclic alkanes and *n*-alkanes for different carbon number intervals $C_{10\text{-}14}$, C_{14}-C_{19}, and $>C_{20}$, and ratios of Pr/Ph and 4-MDBT/Phen for 14 oil and condensate samples (Table 3.3). The 4-MDBT/Phen ratio was used instead of the DBT/Phen ratio because the latter can be affected by water washing and both ratios correlate well. Considering the linear mixing behavior for Pr/Ph found by Wilhelms and Larter (2004) and that the ratios of Pr/Ph and DBT/Phen are convenient to infer oil source rock depositional enviroments and lithologies (Hughes et al., 1995), these parameters were selected for oil-oil correlations. The $\delta^{13}C$ data of branched and *n*-alkanes $\leq C_9$ were not considered for oil-oil correlations because they can be affected by maturation and secondary alteration processes more easily. Biomarker data were excluded because most of the samples are condensates and they do not have detectable amounts of biomarkers. Furthermore, Wilhelms and Larter (2004) reported that biomarker parameters were unable to resolve the effects of mixing differences because of their low abundance and very unequal concentration in the end member oils. The condensate sample from well 7119/12-3 was not included for correlations because most of the molecular and isotopic data were affected by a high level of thermal maturity (1.4% R_o). Similarly, data for the

evaporative condensate sample from the Alke field were also ruled out because it shows hydrocarbon contribution at a high maturity level (1.2% R_o) and absence of isotope data of *n*-alkanes>C_{16} due to their very low concentrations.

Four main genetic families of hydrocarbons were identified using cluster and PCA (Fig. 3.9a and b), and were classified on the basis of compositional variations associated with their contributing source rocks. The total variance in the data set (88%) is explained by the first and second principal components (PC1: 57% and PC2: 31%). The PC loadings, which measure the importance of each variable in accounting for the variability in the PC1 and PC2, are represented in Fig. 3.9c and d. The geographic distribution of these four main families is illustrated in Fig. 3.9e, and they are located in different fields and reservoirs. Typical examples of *m/z* 191 and *m/z* 218 mass chromatograms for the oil and condensate families are represented in Fig. A.1, Appendix A. Data of source, oil source rock depositional environment and lithology parameters for the individual samples of oils and condensates from the HB are listed in Table B.1, Appendix B.

- ***Family I (Askeladd and Southern Albatross condensates)***

Family I includes three condensate samples from wells 7120/7-1, 7120/8-1, 7120/8-2 of the Askeladd field and one condensate sample from well 7121/7-2 located in the southern part of the Albatross field (Fig. 3.1b; Table 3.1). Condensate samples from these fields show the highest values of Pr/Ph ratio (2.7-2.8) and a unimodal *n*-paraffin distribution with a predominance of *n*-alkanes (C_6-C_{15}) (Fig. 3.5). Family I condensates exhibit a pattern of ^{13}C-depletion with *n*-alkane carbon number, showing more positive $\delta^{13}C$ values for *n*-alkanes C_{10}-C_{14} (-28 to -30‰) and more negative ones for *n*-alkanes ≥C_{15} (-30 to -34‰), Fig. 3.10a and b. Average $\delta^{13}C$ values of Pr and Ph range from -31 to -32‰, having a slightly more positive value (<1‰) in the condensate from well 7120/7-1 (Fig. 3.10b). The $\delta^{13}C$ values of branched alkanes tend to become slightly more negative with increasing molecular weight; this pattern, however, was not observed in cyclic alkanes and light aromatic hydrocarbons (Fig. 3.10c).

In view of the fact that the $\delta^{13}C$ values of *n*-alkanes >C_{10} do not undergo significant carbon isotopic fractionation as a result of evaporation (Mansuy et al., 1997; Wang and Huang, 2003), the $\delta^{13}C$ values of *n*-alkanes >C_{10} in these evaporative condensates with similar thermal maturity are more likely related to source effects.

- ***Family II (Northern Albatross and Tornerose condensates)***

Family II includes two condensate samples from sandstones of the Middle Jurassic Stø Formation in the northern Albatross field (wells 7120/9-1 and 7121/7-1) and a condensate sample hosted in the Late Triassic Snadd Formation from well 7122/6-1 located in the Tornerose field (Fig. 3.1b; Table 3.1). Similar to Family I, Family II condensates are characterized by a high Pr/Ph ratio (2.1-2.6) and a unimodal distribution of *n*-alkanes with a dominance from C_6 to C_{15} (Fig. 3.5). Despite their similar thermal maturity, northern Albatross condensates show more negative isotope values of branched and *n*-alkanes up to 2 and 3‰ in relation to Family I condensates, suggesting a different organic matter source (Fig. 3.10a-c). Furthermore, Family II exhibits the most negative average $\delta^{13}C$ values of Pr and Ph, which range from -32.5 to -33.5‰ (Fig. 3.10b). Apart from the $\delta^{13}C$ variations, their intermediate values of DBT/Phen ratio (0.35-0.39) between the corresponding values for oils from the Snøhvit field (0.47-0.51) and condensates from the Askeladd and southern Albatross fields (0.12-0.25), support the hydrocarbon filling by fluids generated and expelled from both western and northern margins (Duran et al., 2013a), especially in the northern Albatross field.

- ***Family III (Snøhvit oils and shallow oils from the Goliat field)***

Based on small differences related to source, Family III oils can be divided into two subfamilies. Family III-A comprises oil samples from Lower-Middle Jurassic sandstones in the Snøhvit field (wells 7120/6-1, 7121/4-1 and 7121/5-1), and Family III-B includes oils hosted in the Middle-Late Triassic Snadd Formation and the Late Triassic-Early Jurassic Tubåen Formation in the Goliat field (Fig. 3.1b; Table 3.1). Snøhvit oils show the lowest Pr/Ph values (1.4-1.5) and a bimodal distribution of *n*-alkanes with maxima from *n*C_{11} to *n*C_{18} and *n*C_{20} to *n*C_{27} (Fig. 3.5). This *n*-alkane distribution suggests marine and terrestrial organic matter sources. In contrast, shallow oils from the Goliat field have a higher Pr/Ph ratio and have been degraded microbially (Figs. 3.4b, 3.5 and 3.6a).

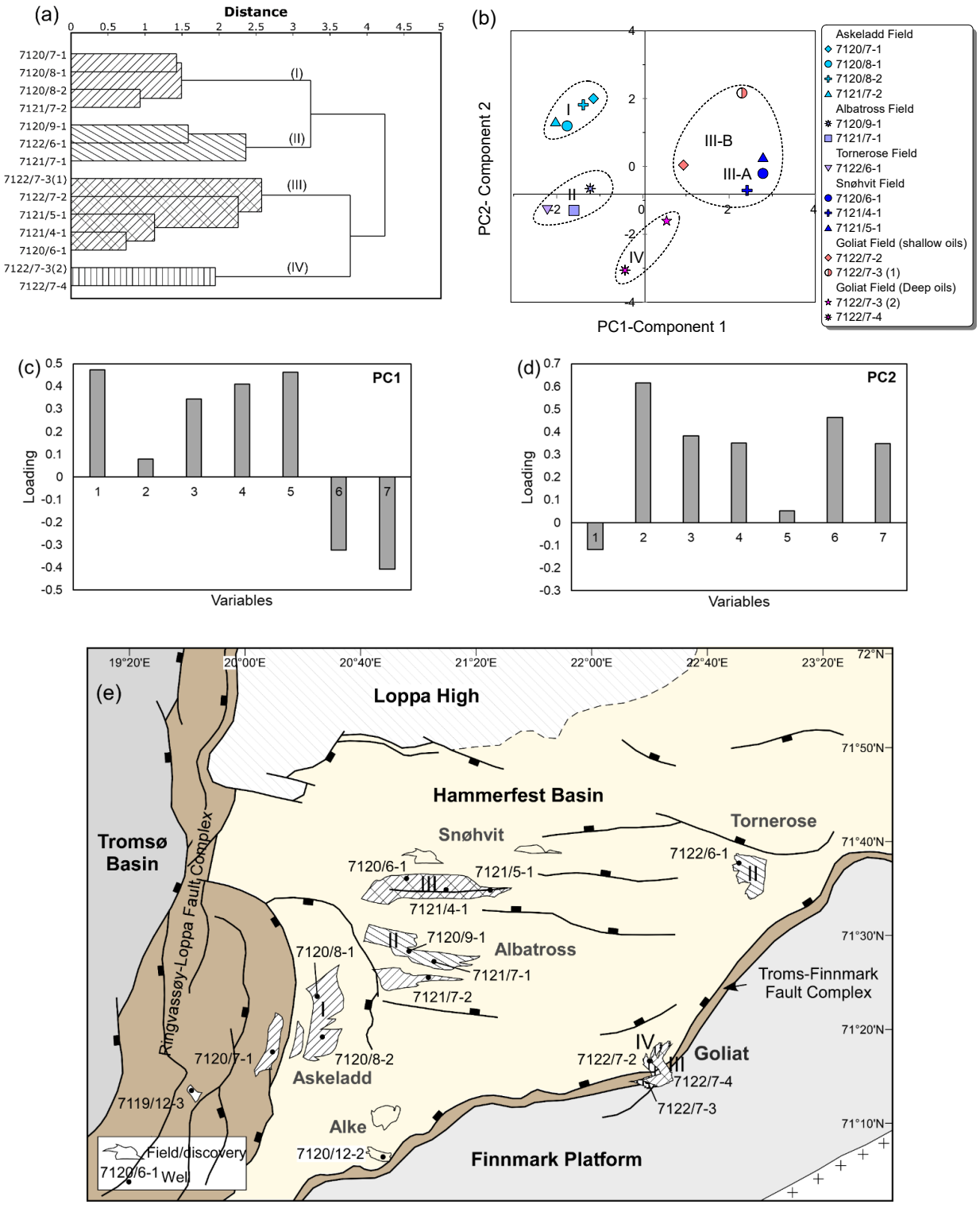

FIGURE 3.9. *Classification of genetic families of hydrocarbons based on (a) cluster analysis and (b) principal component analysis (PCA); (c) loading plots for the first principal component (PC1); (d) loading plots for the second principal component (PC2); (e) location map of hydrocarbon families in the HB. In the cluster, the length of the branches connecting each sample is an expression of their degree of correlation.*

Family III oils show a homogenous $\delta^{13}C$ pattern of *n*-alkanes with values ranging from -29 to -31‰ in oils from the Snøhvit field and shallow oils from the Goliat field (Fig. 3.10a and b). Average $\delta^{13}C$ values of Pr and Ph range from -30 to -31‰ with the exception of the oil sample from the Tubåen Formation of the Goliat field, which shows a more negative $\delta^{13}C$ value (-32‰) (Fig. 3.10b). $\delta^{13}C$ values range from -28 to -29‰ for branched alkanes and from -25 to -29‰ for cyclic alkanes in Family III oils (Fig. 3.10c). More positive $\delta^{13}C$ values of alkyl-cycloalkanes were found in oils hosted in the Snadd and Tubåen formations of the Goliat field (Fig. 3.10c).

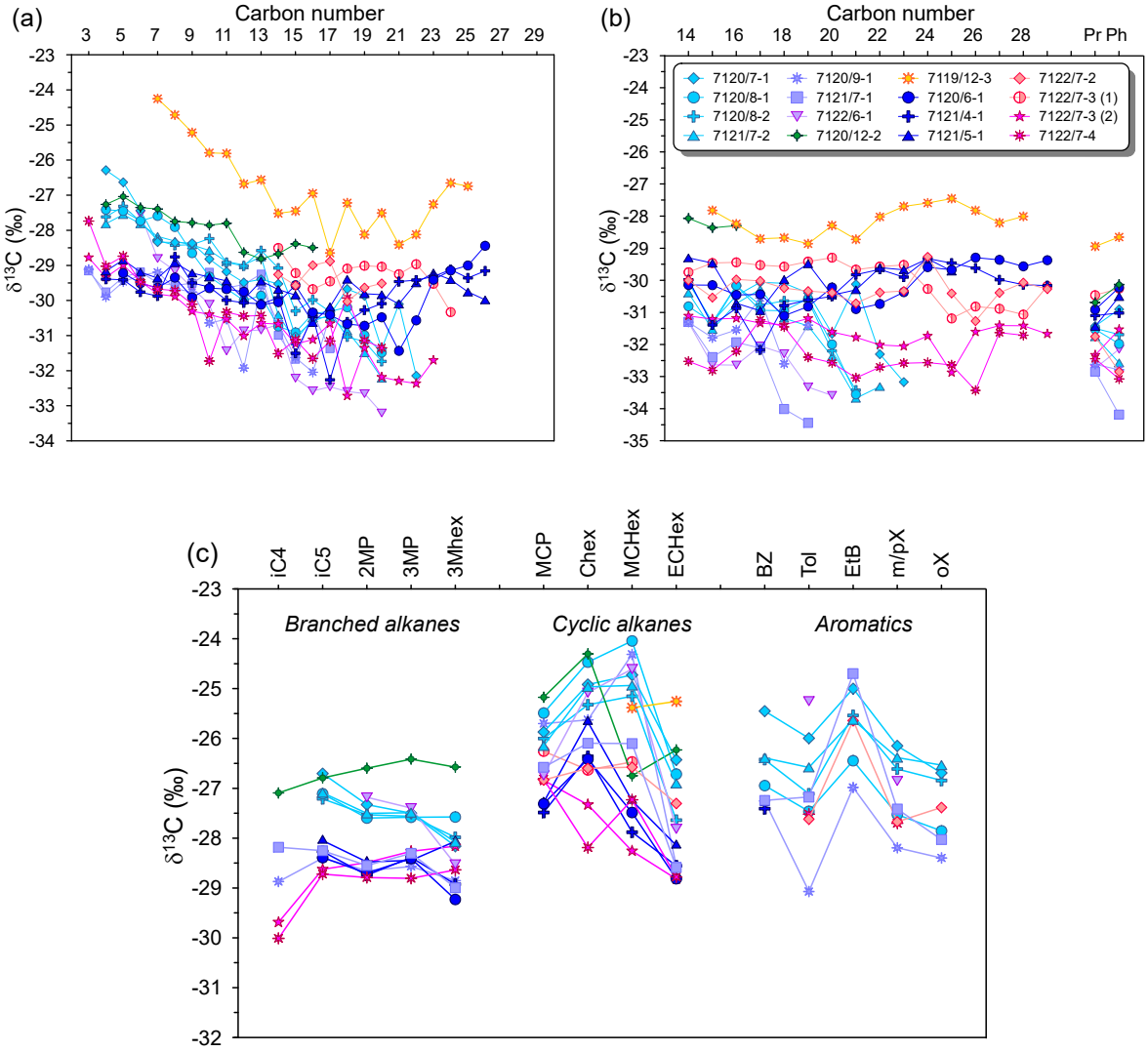

FIGURE 3.10. *Compound-specific $\delta^{13}C$ signatures for oils and condensates in the HB. (a) $\delta^{13}C$ values of n-alkanes in whole oils versus carbon number; (b) $\delta^{13}C$ values of (>C_{14}) n-alkanes, Pr and Ph in saturated fractions versus carbon number; (c) $\delta^{13}C$ values of branched and cyclic alkanes and aromatic hydrocarbons (BTEX) versus carbon number.*

Unlike hydrocarbons of other families, Family III shows typical features of oils derived from carbonate source facies (Murillo et al., 2014), such as a slight even-over-odd carbon number predominance of nC$_{20}$ to nC$_{25}$-alkanes in Snøhvit oils (Moldowan et al., 1985), lower concentrations of tricyclic terpanes >C$_{26}$ as compared with their C$_{21}$-C$_{25}$ homologs (Aquino-Neto et al., 1983), and the highest concentrations of dibenzothiophene and alkyl-dibenzothiophenes (Fan et al., 1990), (Fig. 3.11a-c). Considering that in the Barents Sea, the Upper Paleozoic was dominated by carbonate deposition (Stemmerik and Worsley, 1989; Brekke et al., 2001), all of the aforementioned characteristics would confirm a Paleozoic contribution, which was suggested by Ohm et al. (2008). It is important to note, that although DBT/Phen values are not as high as those reported for carbonate-source rocks (Hughes et al., 1995), Family III oils have the highest ratios of DBT/Phen (0.4-0.5), MDBT/MPhen (0.3-0.4) and 4-MDBT/Phen (0.5-0.7) as compared to Goliat oils hosted in the Kobbe Formation, which show values <0.2.

Family III oils show a relative predominance of C$_{29}$ steranes (40-46%), a low C$_{27}$/C$_{29}$ sterane ratio (0.7-0.9), a low bisnorhopane content (BNH%, 4-7), a low C$_{35}$ homohopane index (C$_{35}$S/C$_{34}$S homohopane ratio, 0.4-0.6), and a high content of higher-plant-derived biomarkers, including retene and tricyclic saturated diterpenoids. These features suggest input from terrestrial-dominated sources. Even though oils from the Snøhvit field and shallow oils from the Goliat field have comparable δ^{13}C signatures of long-chain *n*-alkanes, some differences related to source were recognized. Snøhvit oils show a slightly higher ratio of retene/retene+cadalene and concentrations of phenanthrene and tricyclic saturated diterpanes (Fig. 3.12a and b) than Goliat oils, especially those hosted in the Kobbe Formation, suggesting that they can have a higher terrestrial influence. Linjordet and Grung-Olsen (1992) reported that in the Snøhvit field, the waxy hydrocarbons were probably generated from coal and coaly shales of the Nordmela Formation. A significant amount of resin-derived biomarkers in the Snøhvit oils along with their lowest Pr/Ph ratio (Fig. 3.12c) demonstrate the presence of hydrocarbon mixtures derived from distinct sources.

Similar to Snøhvit oils, shallow oils from the Goliat field contain a higher C$_{30}$ sterane percentage (9-10%) in comparison to source rock extracts from the Middle Triassic Kobbe

Formation (4-5%) in the Goliat field, indicating an additional contribution of oils derived from more marine-influenced source rocks. In view of extracts from the Hekkingen Formation shales contain a great amount of C_{30} steranes (9-12%) and the fact that this formation is immature in the Goliat field, the high content of C_{30} steranes in Family III-B oils may confirm long-distance migration as suggested by Ohm et al. (2008) and Duran et al. (2013a).

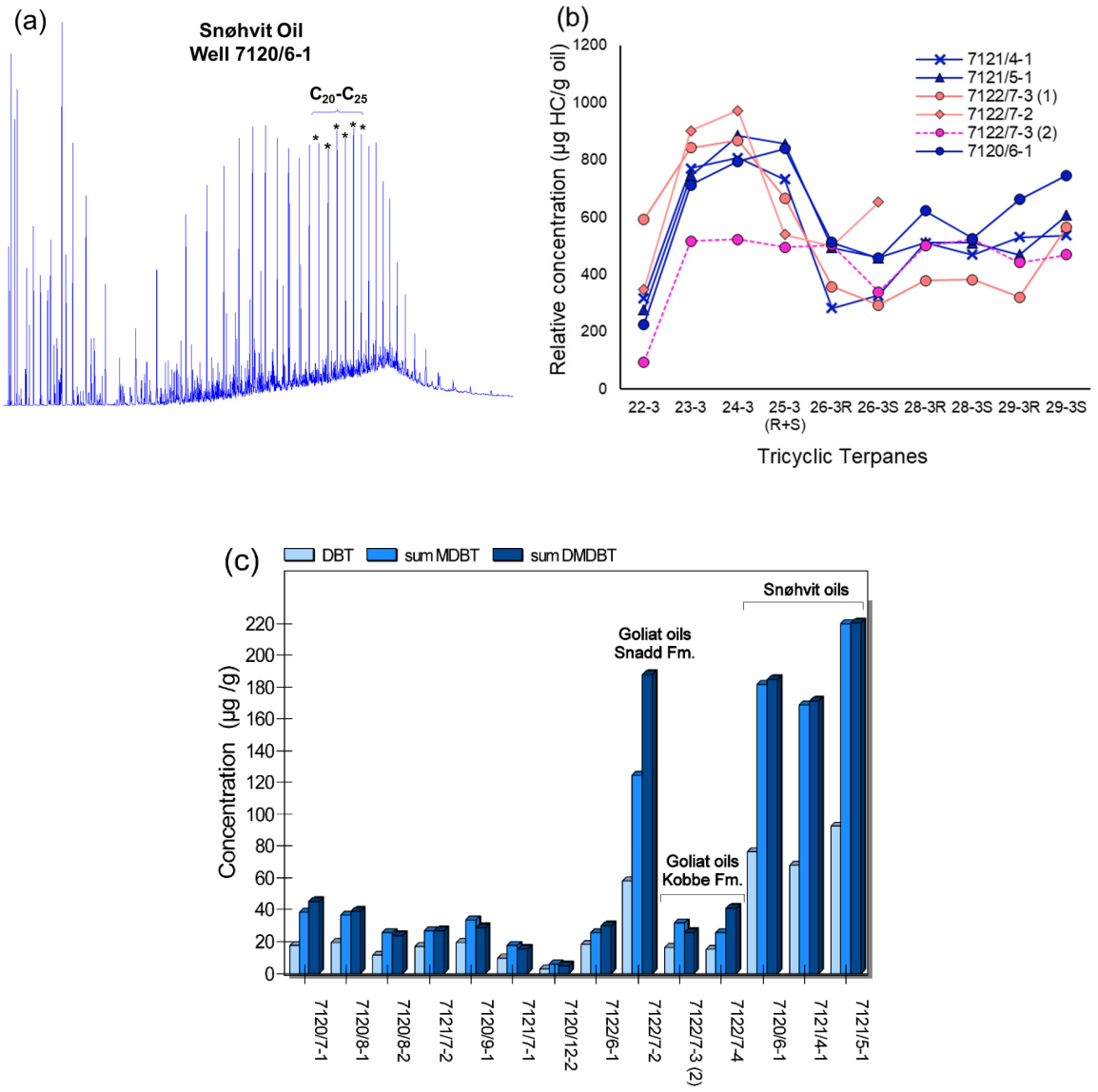

FIGURE 3.11. *(a) Example of whole oil-gas chromatogram for oil from well 7120/6-1, showing a slight even-over-odd carbon number predominance of n-C_{20} to n-C_{25} alkanes; (b) relative concentration of tricyclic terpanes for oils from the Snøhvit and Goliat fields; (c) relative concentration of DBT series for oils and condensates from the HB.*

- ***Family IV (Deep oils from the Goliat field)***

This family includes two crude oil samples from wells 7122/7-4 and 7122/7-3, hosted in the sandstones of the Middle Triassic Kobbe Formation, in the Goliat field (Fig. 3.1b; Table 1). $\delta^{13}C$ signatures of Family IV oils range from -28 to -31‰ for *n*-alkanes ($\leq C_{14}$) and from -31 to -33‰ for *n*-alkanes ($\geq C_{15}$) (Fig. 10a and b). The latter show isotopically lighter $\delta^{13}C$ values relative to those of Family III oils. Similar to *n*-alkanes ($\geq C_{15}$), the Pr and Ph are ^{13}C-depleted (-32 to -33‰) (Fig. 3.10b). The $\delta^{13}C$ values of branched alkanes range from -28 to -30‰ and tend to become isotopically heavier with increasing carbon number (Fig. 3.10c). Particularly, Family IV oils show the most negative $\delta^{13}C$ values of isobutane (-30‰) and one of the most negative $\delta^{13}C$ values of cyclic and alkyl cyclic alkanes, which may indicate a different source (Fig. 3.10c).

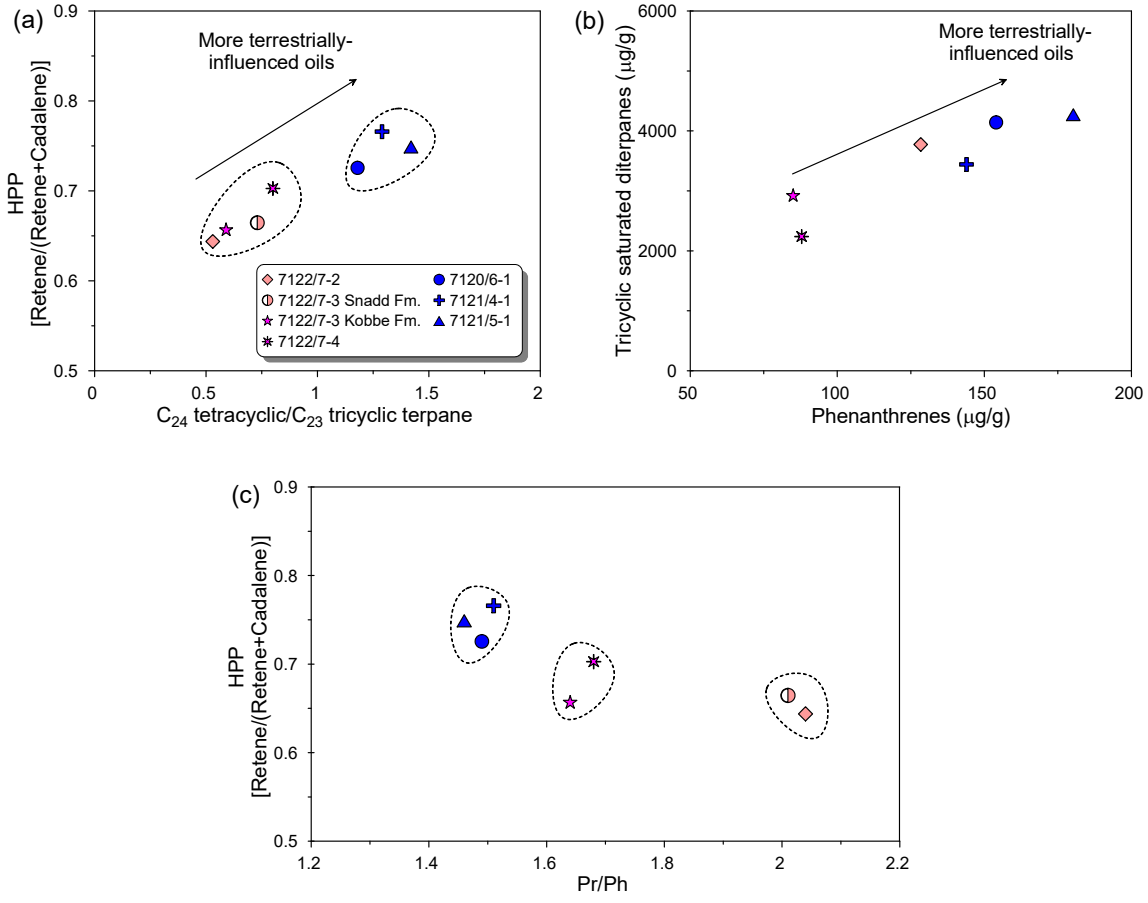

FIGURE 3.12. *(a) Cross-plots of retene/retene + cadalene ratio (HPP) versus C_{24} tetracyclic/C_{23} tricyclic terpane ratio; (b) tricyclic saturated diterpanes versus phenanthrene relative concentrations; (c) HPP versus Pr/Ph ratio for oils from the HB.*

In the Goliat field, the Kobbe Formation hosted oils differ isotopically from shallower oils in the $\delta^{13}C$ values of *n*-alkanes ($\geq C_{14}$), which are more negative up to 3‰. In addition, they show a lower Pr/Ph ratio (1.6-1.7), (Fig. 3.5). Similar to Family III, Family IV oils present a high abundance of C_{29} steranes (44-48%), low ratio of C_{27}/C_{29} steranes (0.6-0.8), a high content of C_{30} steranes (9-10%) and a low C_{35} homohopane index (0.4-0.7). Although Family IV oils show presence of higher-plant-derived biomarkers (Fig. 3.12a and b), which indicate a contribution derived from type-III kerogen-rich source rocks, they seem to be less terrestrially influenced (Fig. 3.12a and b). Unlike Snøhvit oils, Family IV oils do not show an even-over-odd carbon number predominance of *n*-alkanes (C_{20} to C_{25}) and they show lower relative concentrations of methyl- and dimethyl-dibenzothiophenes (Fig. 3.11c) and lower MDBT/Mphen and 4-MDBT/Phen ratios (<0.2), which might also be affected by an input of highly mature hydrocarbons. Nevertheless, the wide concentration ranges of DBT compounds between Family III and IV (Fig. 3.11c) together with the similar concentration of C_{26}-C_{29} and C_{21}-C_{25} tricyclic terpanes (Fig. 3.11b), indicate a larger influence of siliciclastic source rocks in Family IV. The very negative $\delta^{13}C$ values of long-chain *n*-alkanes (-31 to -33‰) from Family IV oils suggest a contribution of Paleozoic-derived oils, which can be related to shaly source rocks.

A particularly good discrimination among hydrocarbon families was achieved with a cross-plot of average $\delta^{13}C$ of Pr and Ph and Pr/Ph ratio (Fig. 3.13a). Families whose ranges of Pr/Ph ratios were not differentiable, as is the case for oils from Families III-A and IV and condensates from Families I and II, were discriminated using only the $\delta^{13}C$ of Pr and Ph. The most negative average $\delta^{13}C$ values of these isoprenoids were recognized in Family IV oils and Family II condensates, which were separated by a distinct Pr/Ph ratio.

The distribution of hydrocarbon families in the HB agrees with the 3D model of hydrocarbon charges proposed by Duran et al. (2013b), which was based on the analysis of migration pathways and drainage areas in the Basin. In this study, however, biomarker and isotope data support Paleozoic-source contribution, which was not considered by Duran et al. (2013a, b).

3.6.4.2. Oil-Source Correlation

Oil accumulations in the HB represent mixtures of oils from different stratigraphic source intervals, especially from the Triassic-Jurassic (Fig. 3.2). Although correlations of oil families to specific source rocks are not possible, a comparison of biomarker and PAH data from source rock extracts and oils could help to differentiate Triassic from Jurassic contributions. The identified oil families exhibit different values of Pr/Ph ratio; however, the wide and comparable range of Pr/Ph ratio together with the similar average $\delta^{13}C$ values of Pr and Ph for the analyzed intervals of Triassic and Jurassic shales (the Kobbe and Hekkingen formations, respectively), prevented discrimination of source contributions (Fig. 13a). Despite the high variability in Pr/Ph ratio represented by hydrocarbons and Triassic and Jurassic source rock extracts (1.0-3.5) in the HB, the differences in $\delta^{13}C$ values between the two isoprenoids are less than 1‰ (Fig. 3.13b). Isotope differences slightly higher were found in condensate from well 7121/7-1 (1.3‰) and Nordmela Formation extract (1.7‰). In general, over the range of redox condition variation for Jurassic and Triassic source rocks, the carbon isotope values of pristane and phytane are very similar (Fig. 3.13b). That is consistent with similar origin of the two isoprenoids (e.g., Hayes et al., 1990).

Although sterane ratios were useful to differentiate Jurassic from Triassic source rock extracts, they were not able to discriminate compositional differences in mixed oils from the Snøhvit and Goliat fields, which show comparable percentages of steranes (Fig. 3.14a). Nonetheless, as with the Jurassic and Triassic source rock extracts, the ETR values were convenient to discriminate Jurassic from Triassic contributions in the HB. Shallow oils from the Goliat field and oils from the Snøhvit field show lower ETR values (0.4-0.5) than deeper oils from the Goliat field (0.6), suggesting a higher Jurassic-source contribution (Fig. 3.14b). The higher ETR values in deep oils from the Goliat field seem to suggest a higher Triassic-source contribution. Besides ETR values, the C_{24}-nordiacholestane (NDR) and the C_{24}-norcholestane ratios (NCR) have been applied for appraising petroleum source age (Holba et al., 1998). However, the NDR and NCR values of Snøhvit and Goliat oils tend to be similar and range from 0.2 to 0.3 (Fig. 3.14b) and from 0.3 to 0.5, respectively. These values correlate mainly with reported values for source-rock extracts from Early Cretaceous and Jurassic ages (Holba et al., 1998).

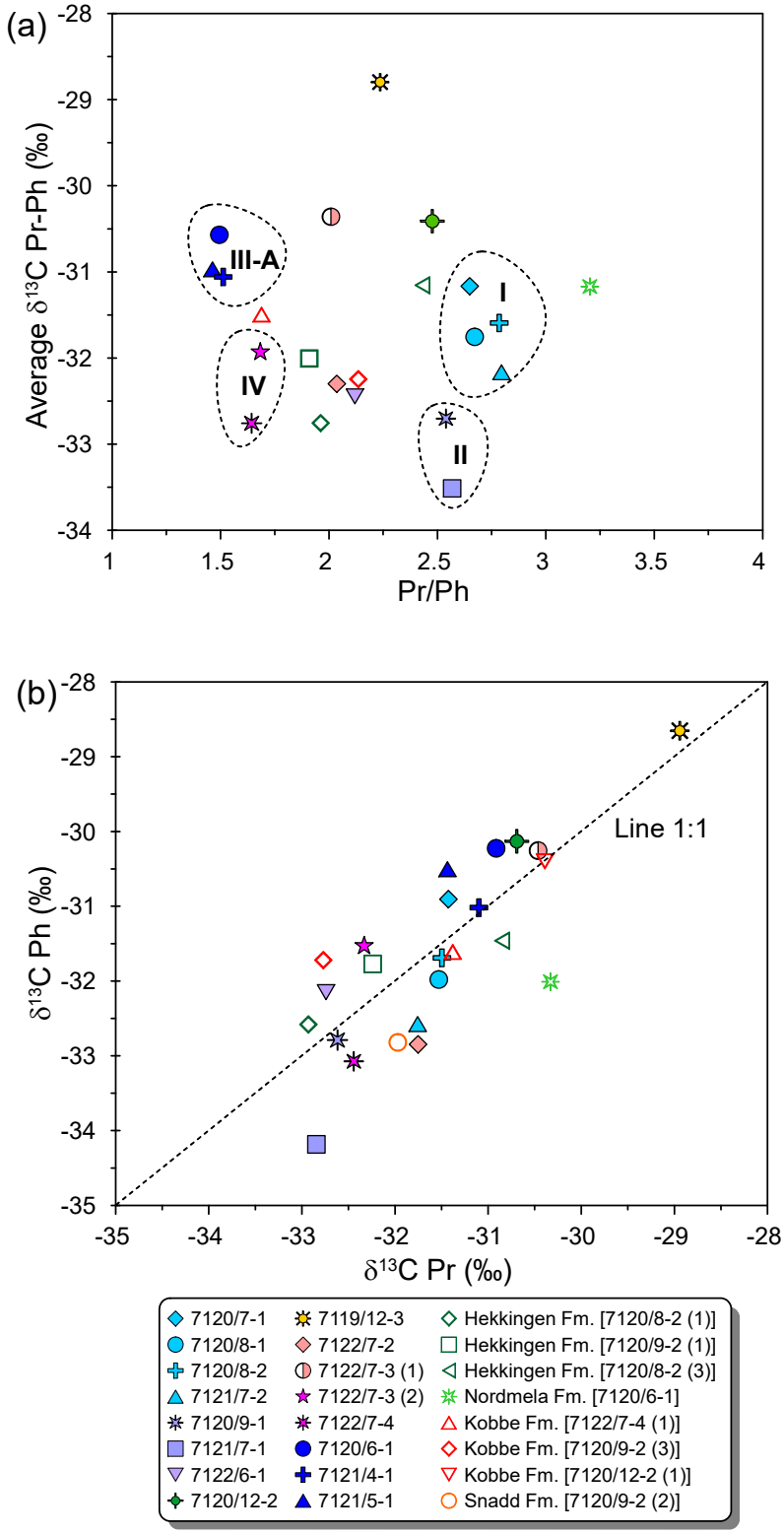

FIGURE 3.13. *(a) Average $\delta^{13}C$ values of Pr and Ph versus Pr/Ph ratio; (b) $\delta^{13}C$ values of Ph versus $\delta^{13}C$ values of Pr for samples of oils, condensates and source rock extracts from the HB. Filled symbols denote the oil and condensate samples, while unfilled ones denote the source rock extracts.*

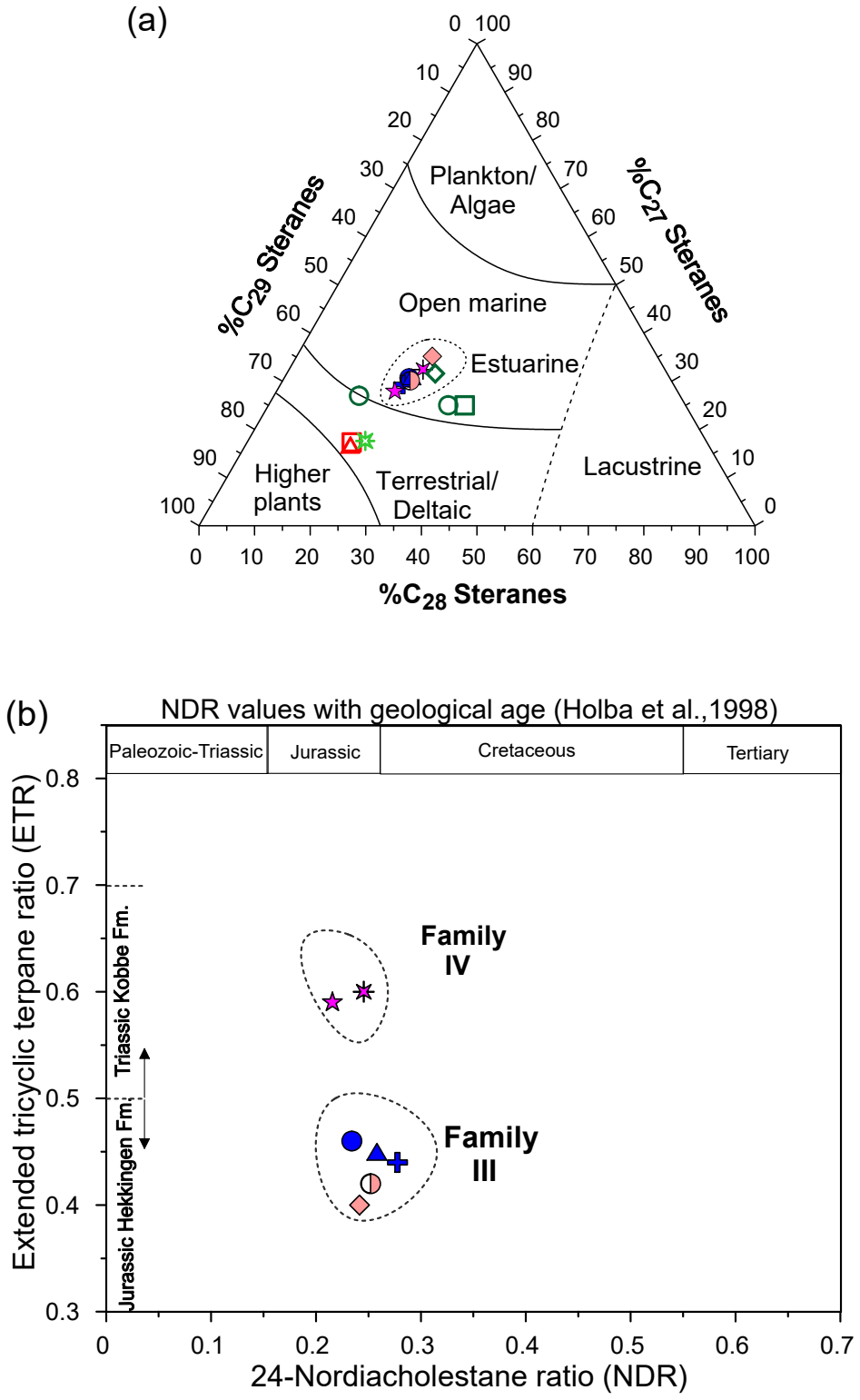

FIGURE 3.14. *(a) Ternary diagram of C_{27}-C_{29} sterane distribution; (b) cross-plot of extended tricyclic terpane ratio (ETR) versus 24-nordiacholestane ratio (NDR) for oils and source rock extracts from the HB.*

The relative abundances of higher-plant-derived biomarkers were measured in the crude oils to assess the terrestrial source influence. Like extracts from Triassic and Jurassic source rocks, the Snøhvit and Goliat oils show a predominance of retene over cadalene and ip-iHMN. In contrast, the condensates from the Albatross, Askeladd, Alke and Tornerose fields, which are also derived from the same source intervals, have higher relative abundance of cadalene with respect to retene, negligible abundances of ip-iHMN and the lowest higher-plant parameter (HPP) (Fig. 3.15a and b). Thus, the cadalene percentage increases with FI whereas the retene percentage decreases (Fig. 3.16).

A selective partitioning into the gas-condensate phase of lower molecular weight compounds (e.g. cadalene ($C_{15}H_{18}$) in comparison to higher molecular weight compounds, such as retene ($C_{18}H_{18}$) and iHMN ($C_{20}H_{28}$) seems to explain the changes in these source parameters. Selective physical partitioning of hydrocarbons between gas and liquid phase was found in other source indicators by Dzou and Hughes (1993). Furthermore, condensates from the Askeladd and Albatross fields show higher values of the Napht/Phen ratio (14-28) compared to oils from the Snøhvit and Goliat fields (1-5). Values of the naphthalene/ phenanthrene ratio in evaporative condensates from the Askeladd and Albatross fields increase with the FI (Fig. 3.16), suggesting that this ratio may also be affected by migration effects during evaporative fractionation.

Despite the fact that the analyzed Jurassic and Triassic source rocks show similar HPP values (0.80-0.97) (Fig. 3.15b), crude oils from the Snøhvit and Goliat fields have lower HPP values (0.6-0.8) (Fig. 3.15b). Particularly, the lowest HPP values found in evaporative condensates may be related to migration-fractionation. Phenanthrene concentration was also used for source assessment, showing important differences between Family III and IV oils (Fig. 3.12b). The lowest relative concentration of phenanthrene found in deep oils from the Goliat field (Fig. 3.12b), suggests a less terrestrial influence.

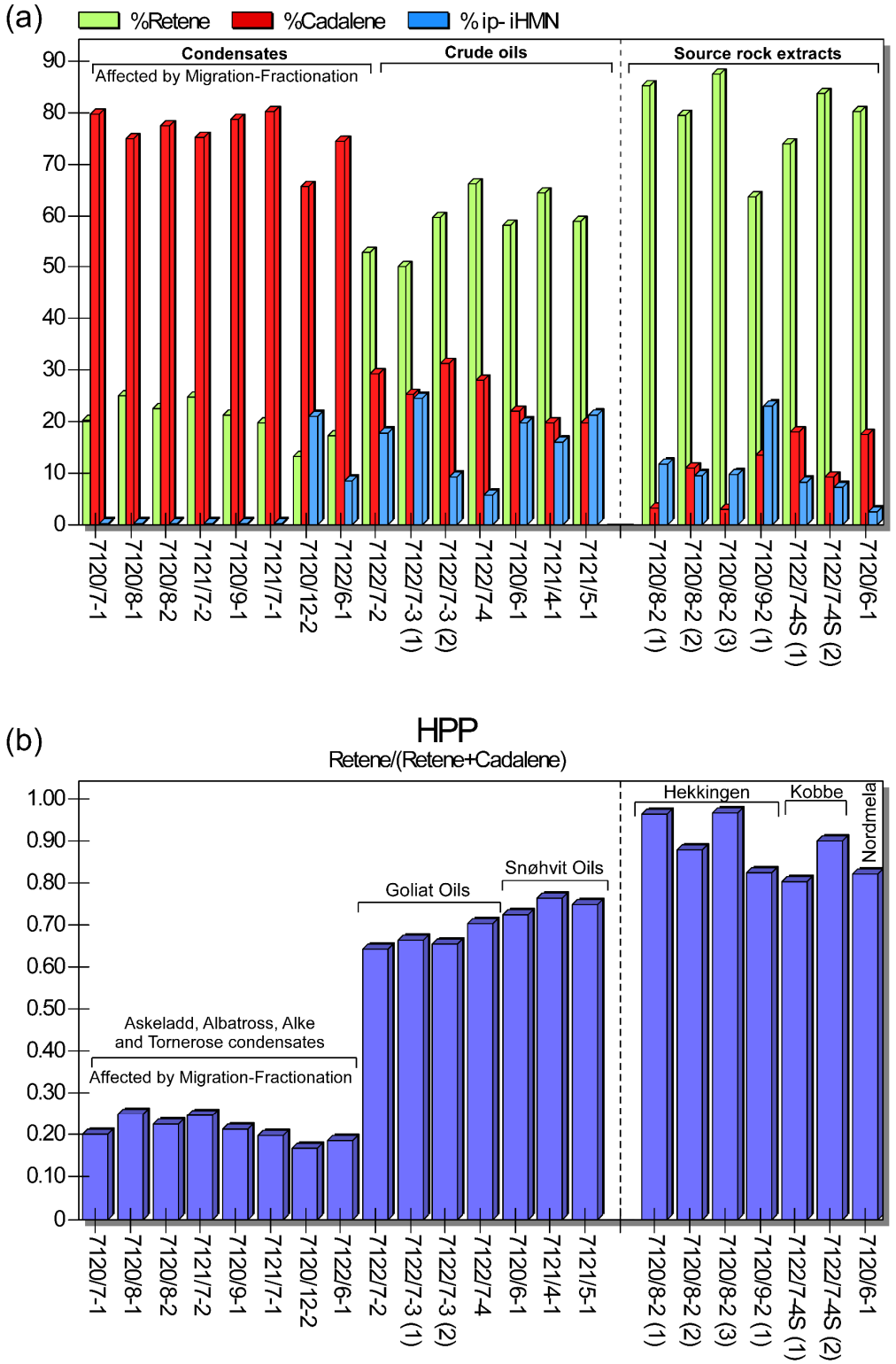

FIGURE 3.15. *Bar graphs of (a) percentages of retene, cadalene and 6-isopropyl-1-isohexyl-2-methylnaphthalene (ip-iHMN); (b) HPP for oils, condensates and source rock extracts.*

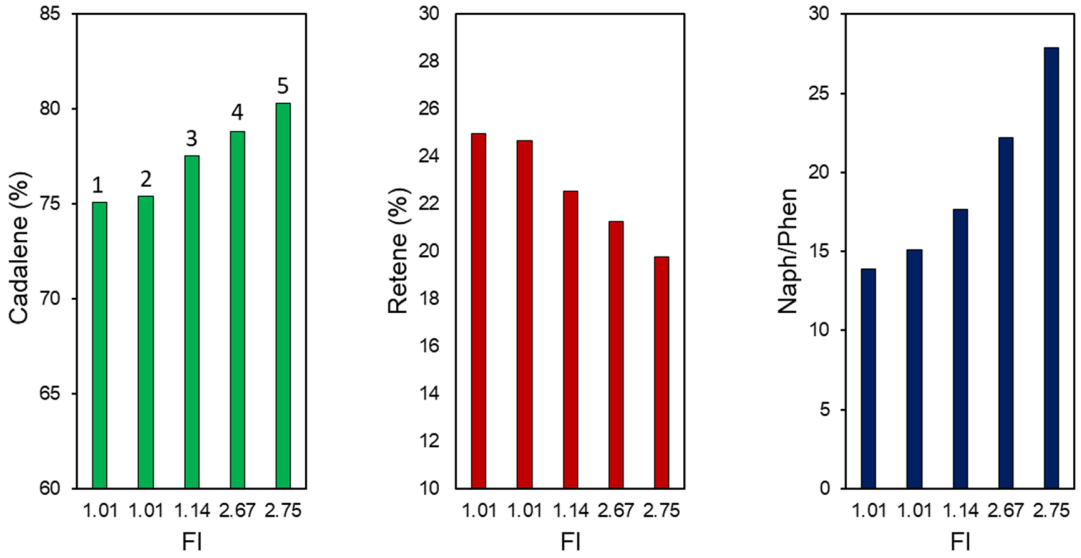

FIGURE 3.16. *Bar-plots of fractionation index (FI) versus (a) cadalene percentage; (b) retene percentage and (c) naphthalene/phenanthrene ratio (Naph/Phen) for Askeladd and Albatross condensates at the same level of thermal maturity. Fractionation index is defined as, FI: n-C_{10}/ ∑(n-C_{16} to n-C_{25}) alkanes. 1: Well 7120/8-1; 2: Well 7121/7-2; 3: Well 7120/8-2; 4: Well 7121/7-1; 5: Well 7120/9-1.*

3.6.5. Detailed Evaluation of Hydrocarbon Mixing Processes

Several scenarios of hydrocarbon mixing, involving different organic matter source types, maturity levels and geological ages, were recognized in the main accumulations of the HB. Determining the relative contributions of different sources to hydrocarbon mixtures in a complex basin with multiple source rocks, such as the Hammerfest Basin, is quite difficult. However, some clues about source contributions were obtained using $\delta^{13}C$ values of *n*-alkanes in extracts from the Jurassic and Triassic source rocks.

Source rock extracts from the Upper Jurassic Hekkingen Formation and the Middle Triassic Kobbe Formation show similar $\delta^{13}C$ values of *n*-alkanes in the range C_{14}-C_{19} (Fig. 3.17a). However, the $\delta^{13}C$ values of long chain *n*-alkanes (>C_{20}) show variations up to 4 and 6 ‰, and thus can be used to differentiate both extracts (Fig. 3.17a). Source rock extracts from the Upper Jurassic Hekkingen Formation have more positive average $\delta^{13}C$ values of (>C_{20}) *n*-alkanes (-28 to -31‰) than those from the Middle Triassic Kobbe Formation (-32 to -35‰) (Table 3.4). Since the $\delta^{13}C$ values of (>C_{20}) *n*-alkanes seem to be suitable for

distinguishing source rock extracts from Jurassic and Triassic ages, average $\delta^{13}C$ values of ($>C_{20}$) *n*-alkanes *vs* average $\delta^{13}C$ values of (C_{14}-C_{19}) *n*-alkanes for Jurassic and Triassic source rock extracts and hydrocarbon samples were cross plotted to look for any systematic relationships (Fig. 3.17b). Jurassic contribution is higher in oils from the Snøhvit field and the Snadd and Tubåen formation hosted oils from the Goliat field (Family III), while condensate samples from the Askeladd, Albatross and Tornerose fields (Families I and II) and the Kobbe Formation hosted oils from the Goliat field (Family IV) seem to have a greater Triassic contribution. Nonetheless, as aforementioned, in addition to Jurassic and Triassic contributions, evidences of Paleozoic contribution were recognized especially in Snøhvit and Goliat oils.

The $\delta^{13}C$ values of (C_{14}-C_{19}) *n*-alkanes in Askeladd condensates are comparable to those of extracts from the Snadd, Kobbe and Hekkingen formations, however, the $\delta^{13}C$ values of *n*-alkanes $>C_{20}$ are isotopically lighter as compared to those of the Hekkingen Formation, indicating a high Triassic contribution (Fig. 3.17b). Duran et al. (2013a) reported the relative contributions of the Jurassic Hekkingen Formation and the Triassic Snadd and Kobbe formations to the main accumulations in the HB using 3D basin modelling. For the Askeladd field, they estimated contribution percentages of 18, 49 and 33%, respectively. Based on the assertion that isotopic measurement of *n*-alkanes can be valuable for the quantitative assessment of oil source contribution (Schimmelmann et al., 2004); compound-specific stable carbon isotopic composition in mixed oils was used to estimate mixing relationships. In this study, the contribution of oils from Triassic and Jurassic source rocks to the Askeladd field was quantitatively estimated using the average $\delta^{13}C$ values of long-chain *n*-alkanes in source rock extracts and condensates generated at the same maturity level (0.7-0.9% R_o) (Tables 3.3 and 3.4). Considering that the Triassic Snadd and Kobbe formations have similar $\delta^{13}C$ values of ($>C_{20}$) *n*-alkanes, the following equation was employed to estimate contributions in two-source-mixed oils:

$$C = A(x) + B(1 - x)\ (0 \leq x \leq 1)$$

Where *A* stands for the average $\delta^{13}C$ values of *n*-alkanes (>C_{20}) of one source, whose relative contribution is (*x*), *B* for the average $\delta^{13}C$ values of *n*-alkanes (>C_{20}) of another source, whose relative contribution is (1-*x*) and *C* represents the average values of the measured $\delta^{13}C$ of *n*-alkanes (>C_{20}) of the mixed oil.

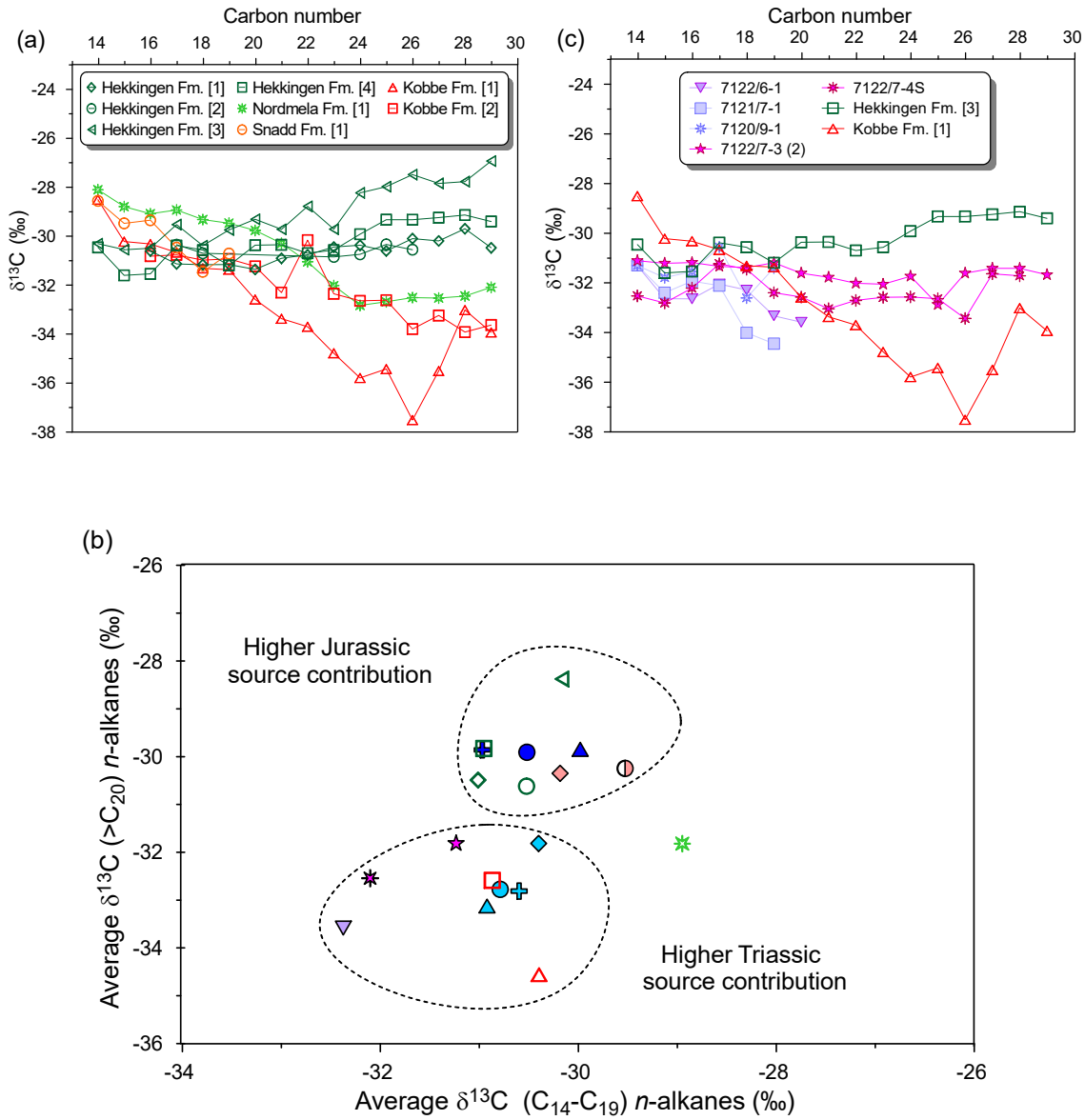

FIGURE 3.17. *(a) $\delta^{13}C$ profiles of (>C_{14}) n-alkanes for extracts from Jurassic and Triassic source rocks; (b) cross-plot of average $\delta^{13}C$ values of (>C_{20}) n-alkanes versus average $\delta^{13}C$ values of (C_{14}-C_{19}) n-alkanes for oils, condensates and source rock extracts; (c) $\delta^{13}C$ profiles of (>C_{14}) n-alkanes for hydrocarbon samples from Family II and Family IV compared with $\delta^{13}C$ profiles of (>C_{14}) n-alkanes for two extracts from the Hekkingen and Kobbe Fms in the HB. Filled symbols denote the oil and condensate samples, while unfilled ones denote the source rock extracts.*

The quantification results of source contribution in the Askeladd field using $\delta^{13}C$ values of *n*-alkanes (>C_{20}) indicate a proportion of 18-21% for Upper Jurassic and 79-82% for Triassic derived-oils (Tables 3 and 4). This estimation is quite consistent with that obtained from 3D basin modelling by Duran et al. (2013a) and demonstrates that $\delta^{13}C$ values of *n*-alkanes are useful for quantitative assignment of oil sources. The high ^{13}C-enrichment of (C_{10}-C_{14}) *n*-alkanes recognized in the Askeladd condensates, characterized by a high Triassic contribution, can be related to a higher input of terrestrial organic matter in the main source rock. The same pattern of ^{13}C-enrichment in (C_{10}-C_{14}) *n*-alkanes with the increase of terrestrial organic matter contribution was identified in Jurassic oils from the Viking Graben, North Sea (Murillo et al., 2013).

For the Snøhvit field, Duran et al. (2013a) estimated a contribution from the Jurassic Hekkingen Formation of 69%, while the contribution percentages of the Triassic Snadd and Kobbe formations are 22% and 9%, respectively. The data of this study, also suggest that the main contributor of hydrocarbons was the Upper Jurassic Hekkingen Formation. Snøhvit oils, which are in the main oil-generation stage (Fig. 3.8), show one of the heaviest $\delta^{13}C$ signatures of long chain *n*-alkanes (>C_{20}) (Fig. 10b), with average $\delta^{13}C$ values of -29.9‰ (Table 3.3). However, source rock extracts from the Hekkingen Formation, at the same maturity level, have similar average $\delta^{13}C$ values of long chain *n*-alkanes (-28.4 to -30.6‰) with a mean value of -29.8‰ (Table 3.4). The similar average $\delta^{13}C$ values of >C_{20} *n*-alkanes for Snøhvit oils and source rock extracts from the Hekkingen Formation would suggest no Triassic contribution. Nonetheless, considering that petroleum sourced from the Hekkingen, Snadd and Kobbe formations charged the main reservoirs in the Hammerfest Basin (e.g., Duran et al., 2013), and that the Triassic source rocks have more negative average $\delta^{13}C$ values of *n*-alkanes (>C_{20}) up to 4 and 6‰ (Fig. 3.17a,Table 3.4). It would be expected that the final $\delta^{13}C$ values of these *n*-alkanes in the mixed oils from the Snøhvit field would result in more negative values. The ^{13}C-enrichment of *n*-alkanes, especially long chain *n*-alkanes, found in Snøhvit oils allow different interpretations: (1) the ^{13}C-enrichment may have been caused, at least in part, by a hydrocarbon contribution with a very high maturity level; however, maturity parameters indicate that Snøhvit oils are in the peak stage of oil generation (Fig. 3.8). (2) The ^{13}C-enrichment could have been related to the carbonate-source contribution of

Upper Paleozoic source rocks; nonetheless, Ohm et al., 2008 reported negative isotope values (<-30‰) from an oil sample derived from Paleozoic source rocks in the Loppa High. This suggests that the carbonate source contribution recognized in Snøhvit oils and even in shallow oils from the Goliat field may also have caused a ^{13}C-depletion in the *n*-alkanes. (3) The ^{13}C-enrichment was caused by another source contribution with much heavier δ^{13}C signatures than those of the Upper Jurassic Hekkingen Formation, which may be associated with a younger age or with a different source facies. This last hypothesis seems to be the most plausible, however, it is important to consider if Lower Cretaceous source rocks reached enough thermal maturity to generate oils.

TABLE 3.3. *Parameters used in multivariate analysis (MVA): average values of compound-specific carbon isotopic data, ratios of Pr/Ph and 4-MDBT/Phen for oil and condensate samples from the HB.*

			Average δ^{13}C values (‰)				
Well	Pr/Ph	4-MDBT/ Phen	*n*-alkanes (C_{10}-C_{14})	*n*-alkanes (C_{14}-C_{19})	*n*-alkanes (>C_{20})	Pr and Ph	cyclic alkanes
7120/7-1	2.65	0.16	-29.3	-31.0	-31.8	-31.2	-25.5
7120/8-1	2.67	0.26	-29.9	-31.3	-32.8	-31.8	-25.2
7120/8-2	2.79	0.23	-28.8	-31.2	-32.8	-31.6	-26.0
7121/7-2	2.80	0.22	-29.1	-31.7	-33.1	-32.2	-25.7
7120/9-1	2.54	0.38	-30.7	-31.5	n.d.	-32.7	-26.1
7121/7-1	2.57	0.37	-29.7	-32.7	n.d.	-33.5	-26.8
7122/6-1	2.12	0.24	-30.8	-32.6	-33.6	-32.5	-26.1
7120/6-1	1.49	0.63	-29.9	-30.1	-29.9	-30.6	-27.5
7121/4-1	1.51	0.62	-29.9	-30.3	-29.9	-31.1	-27.6
7121/5-1	1.46	0.66	-29.6	-29.9	-29.9	-31.0	-27.1
7122/7-2	2.04	0.49	-29.8	-30.3	-30.3	-32.3	-26.8
7122/7-3 (1)	2.01	0.61	-28.5	-30.0	-30.3	-30.4	-26.5
7122/7-3 (2)	1.68	0.17	-30.7	-31.6	-31.8	-31.9	-27.8
7122/7-4 S	1.64	0.13	-31.6	-32.4	-32.5	-32.8	-27.8

Pr/Ph: pristane/phytane ratio; 4-MDBT/Phen: dibenzothiophene/phenanthrene ratio; n.d.: not determined. Standard deviations of δ^{13}C values for all the compounds reported are <0.5‰. Samples from wells 7119/12-3 and 7120/12-2 were excluded from MVA due to their very high thermal maturity level.

The Goliat oils hosted in the Snadd and Tubåen formations and the Snøhvit oils were grouped in the same family. They have comparable δ^{13}C signatures of long-chain *n*-alkanes, which can suggest similar relative contributions. Nevertheless, shallow oils from the Goliat field show a ^{13}C-depletion in *n*-alkanes (C_{25} to C_{28}), which is higher in the oil hosted in the Snadd Formation (up to 1.5‰) (Fig. 3.10b). This ^{13}C-depletion suggests a higher relative contribution of Triassic source rocks, in shallow oils from the Goliat field as compared to

those in Snøhvit oils. This higher Triassic contribution is more likely associated with a local contribution. The Kobbe Formation hosted oils from the Goliat field show up to 3‰ more negative $\delta^{13}C$ values of *n*-alkanes (>C_{14}) than the Snadd and Tubåen formation hosted oils (Fig. 3.10b), indicating different relative proportions of source contributions. Duran et al. (2013a) estimated for Goliat oils a high Triassic contribution (82%) which is similar to that estimated for Askeladd condensates. However, *n*-alkanes (C_{10}-C_{14}), pristane and phytane are more ^{13}C-depleted in Kobbe Formation hosted oils from the Goliat field (up to 3‰ and 1‰, respectively) than those in Askeladd condensates (Fig. 3.10a and b). Though the deep oils from the Goliat field seem to have a higher Triassic contribution than shallower oils, they, especially the oil from well 7122/7-4S, also show even more negative $\delta^{13}C$ values of *n*-alkanes (C_{14}-C_{16}) than extracts from Jurassic and Triassic source rocks, with isotope variation up to 4‰ as compared with Triassic source rocks (Fig. 3.17c). This ^{13}C-depletion might be attributed in part to the hydrocarbon contribution of low thermal maturity level; nonetheless, the high isotope variations (4‰) found in deep oils from the Goliat field compared with those in shallower oils suggest more likely an additional Paleozoic-source contribution.

TABLE 3.4. *Average $\delta^{13}C$ values of n-alkanes and regular isoprenoids for Jurassic and Triassic source rock samples from the HB.*

		Average $\delta^{13}C$ values (‰)		
Well	Source rock Fm.	(C_{14}-C_{19}) *n*-alkanes	(>C_{20}) *n*-alkanes	Pr-Ph
7120/8-2 (1)	Hekkingen	-31.0	-30.5	-32.8
7120/8-2 (2)	Hekkingen	-30.5	-30.6	n.d.
7120/8-2 (3)	Hekkingen	-30.2	-28.4	-31.2
7120/9-2 (1)	Hekkingen	-31.0	-29.8	-32.0
7120/6-1	Nordmela	-29.0	-31.8	-31.2
7120/9-2 (2)	Snadd	-30.0	n.d.	-32.4
7120/9-2 (3)	Kobbe	-30.3	n.d.	-32.3
7122/7-4 (1)	Kobbe	-30.4	-34.6	-31.5
7122/7-4 (2)	Kobbe	-30.9	-32.6	n.d.
7120/12-2 (1)	Kobbe	-30.2	n.d.	-30.4

Standard deviations of $\delta^{13}C$ values for all the compounds reported are <0.5‰

Condensates from the Tornerose and Northern Albatross fields have carbon isotope values of *n*-alkanes (>C_{14}) more negative than Snøhvit oils and Askeladd condensates (Fig. 3.10b). They also have isotopically lighter $\delta^{13}C$ values than extracts from the Jurassic and

Triassic source rocks, with large isotope variations up to 3‰ (Fig. 3.17c). Similar to the deep oils from the Goliat field, they further show the isotopically lightest $\delta^{13}C$ values of *n*-alkanes (C_{10}-C_{14}), and Pr and Ph (Figs. 3.10a and 3.13a), which may suggest a possible Paleozoic-source contribution.

3.6.6. Insights from Compound-Specific Carbon and Hydrogen Isotope Compositions

3.6.6.1. Effects of Secondary Processes on $\delta^{13}C$ data

Family I condensate from well 7120/7-1 (Askeladd Vest field), which shows no evidence of microbial degradation (Figs. 3.4b, 3.6), has a higher ^{13}C-enrichment of *n*-alkanes $<C_7$ and the $\delta^{13}C$ values of nC_4 and nC_5-alkane are up to 1.5‰ heavier than any other condensates from the same family (Fig. 3.10a). Family I condensate from well 7120/7-1 corresponds to the stratigraphically deepest sample from the Askeladd field (Table 3.1) and has a lower value of FI (0.7). The heaviest $\delta^{13}C$ values of *n*-alkanes $<C_7$ found in this evaporative condensate sample can be related to its higher thermal maturity level (1.0-1.1% R_o) as compared with other Family I condensates (Fig. 3.8).

Family II condensate from the Tornerose field (well 7122/6-1) shows presence of hydrocarbons at late stage of oil generation (1.0% R_o, Fig. 3.8) and evidences of biodegradation. It exhibits *n*-C_6 and *n*-C_7 alkanes enriched in ^{13}C (up to 1.7‰), possibly indicating both microbial degradation and increased thermal maturity (Fig. 3.10a). Lower concentrations and heavier $\delta^{13}C$ values of nC_6, nC_7, $2MC_5$, and $3MC_5$ in Tornerose condensate relative to those in condensates from the same family, support their microbial degradation (Fig. 3.18).

The upward inflection of the *n*-alkane profile in the C_7 to C_{12} range found in the deep oils from the Goliat field (Fig. 3.10a) could be associated with the wet gas-condensate charge (Edwards et al., 2004). Hydrocarbon contribution yielded at a high thermal maturity level (1.2 and 1.4% R_o) was recognized in the evaporative condensate from well 7120/12-2 (Alke field) and the thermally generated condensate from well 7119/12-3, respectively (Fig. 3.8). They show the heaviest $\delta^{13}C$ signatures of *n*-alkanes, Pr and Ph (Fig. 3.10a and b). The

thermally generated condensate exhibits a strong and steady enrichment of ^{13}C with decreasing carbon number in *n*-alkanes (<C_{14}) (Fig. 3.10a), which is associated with its high level of thermal maturity.

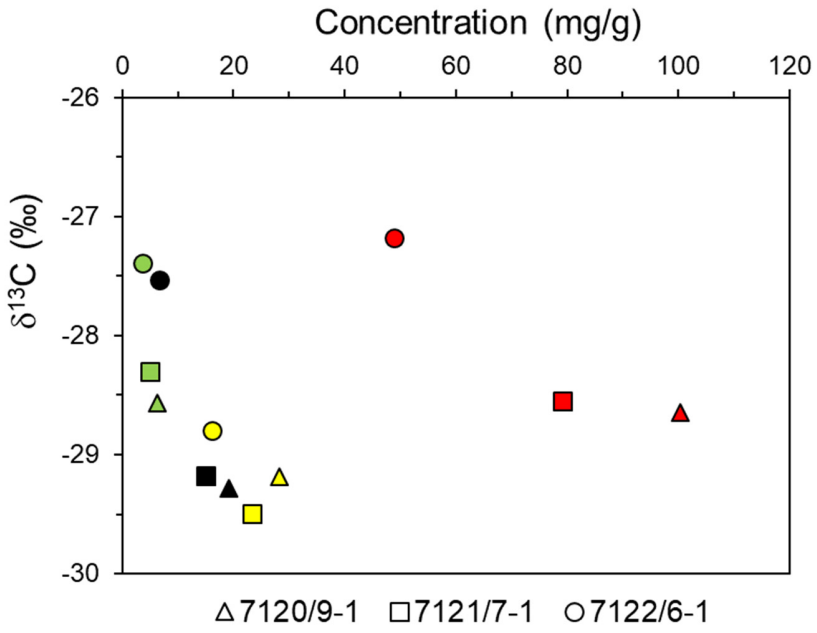

FIGURE 3.18. *Scatter plot of concentration versus stable carbon isotope composition of selected branched and n-alkanes in Family II condensates. Symbols are color-coded as follows: red - 2MC5; green - 3MC5; black - nC6; yellow – nC7.*

3.6.6.2. Effects of Secondary Processes on δD data

- ***D/H ratios of individual n-alkanes***

The δD values increase linearly with *n*-alkane carbon number in evaporative and thermally generated condensate samples and oils from wells 7122/7-2 and 7122/7-4 in the Goliat field (Fig. 3.19a). In contrast, the isotopic profiles for Goliat oils hosted in the Snadd and Kobbe formations (well 7122/7-3) and Snøhvit oils hosted in the Stø Formation (wells 7120/6-1, 7121/4-1 and 7121/5-1) display flat patterns of δD versus carbon number (Fig. 3.19a), which range from -125 to -140‰. These δD values correlate with those of source rock extracts analyzed from the Kobbe, Nordmela and Hekkingen formations, which show similar values and range from -120 to -150‰ (Fig. 3.19b).

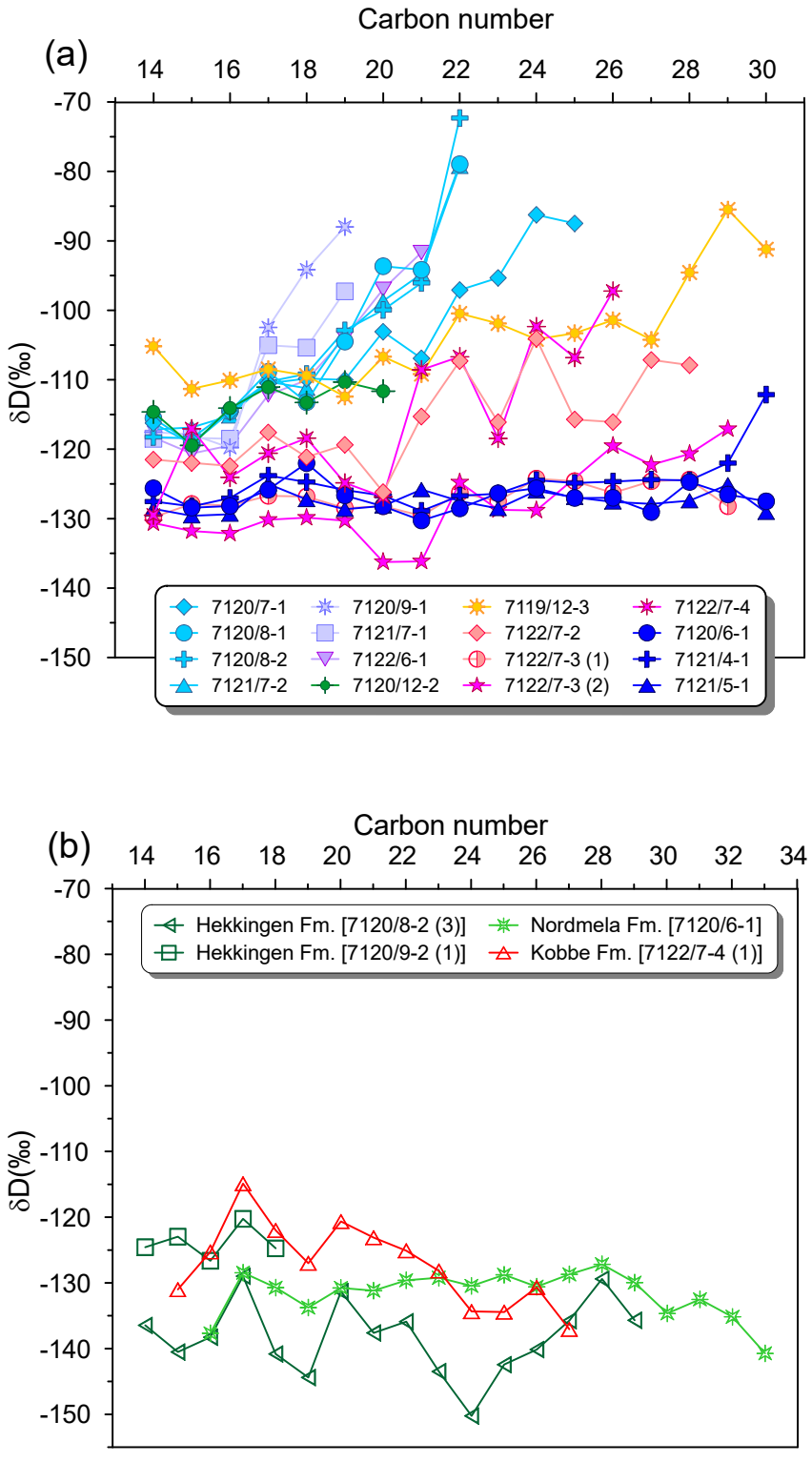

FIGURE 3.19. *(a) δD profiles of (>C_{14}) n-alkanes for hydrocarbon samples; (b) δD profiles of (>C_{14}) n-alkanes for source rock extracts.*

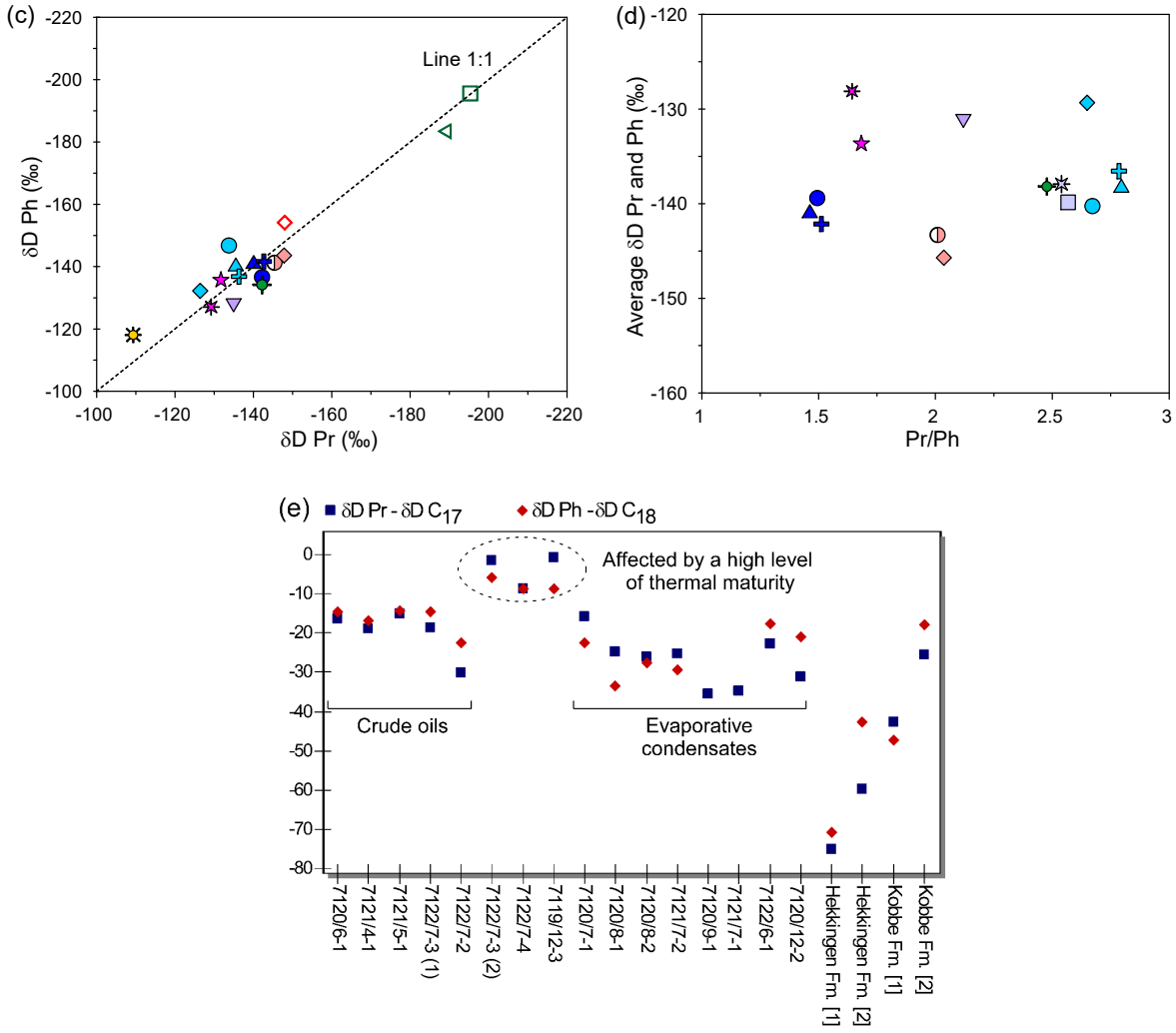

FIGURE 3.19. *Continued (c) δD values of Ph versus δD values of Pr; (d) average δD values of Pr and Ph versus Pr/Ph ratio for oil and condensate samples from the HB; (e) differences in δD values between pristane and n-C17 alkane and between phytane and n-C18 alkane for oils, condensates and source rock extracts from the HB.*

The strong and constant D-enrichment of *n*-alkanes with chain length, in condensates resulting from evaporative fractionation, is consistent with isotopic fractionations caused by physical processes as evaporation. During the course of vaporization, more volatile compounds (short-chain *n*-alkanes) become depleted in D relative to less volatile compounds (long-chain *n*-alkanes) (e.g., Kiss et al., 1972; Huang et al., 1999; Wang and Huang, 2001). Other authors have attributed the D-depletion of short-chain molecules with the D-enrichment of the long-chain ones to kinetic isotope effects during hydrocarbon generation (Rigby et al., 1981; Schoell et al., 1983). Enrichment in D with increasing chain length of *n*-alkanes was also observed during artificial thermal maturation (Tang et al., 2005).

Alternatively, Schimmelmann et al. (1999, 2001) proposed the hydrogen transfer from formation water to organic compounds during maturation reactions for explaining the increase in δD values. Wang et al. (2009) also explained this enrichment as a result of equilibrium fractionation.

To study evaporation phenomena, the slopes of δD values *versus* carbon number of *n*- alkanes (C_{15}-C_{20}) were calculated for each condensate. Condensates from the Askeladd, Albatross and Tornerose fields exhibit positive slopes with average R^2 value of 0.92, which indicate a linear increase in δD with chain length. In addition, evaporative condensates, with similar maturity, from the Askeladd and southern Albatross fields (Family I) show comparable slopes of regression lines, which reflect an average D-enrichment of 3.9‰ per carbon number (Fig. 3.19a). D-enrichment with carbon number is of 4.8‰ in the condensate sample from the Tornerose field, and ranges from 5.5 to 8.5‰ in northern Albatross condensates. The Askeladd and Alke condensates (wells 7120/7-1 and 7120/12-2, respectively), which show a higher thermal maturity (1.1-1.2% R_o), exhibit lower slopes (Fig. 3.19a). δD values of *n*-alkanes >C_{14}, in the thermally generated condensate from well 7119/12-3 (~1.4% R_o), also increase linearly with carbon number. This D-enrichment (1.3‰), however, is not as strong as that for evaporative condensates (3.7-8.5‰), which show δD profiles with steeper slopes (Fig. 3.19a).

In order to assess the effect of secondary oil migration on δD values of *n*-alkanes, the δD values of *n*-alkanes >C_{14} in oils from the Snøhvit field (located close to the mature source kitchen in the northern margin of the HB) and oils from the Goliat field (south-eastern part of the HB) were compared. The fact that oils hosted in the Snadd and Kobbe formations of the Goliat field (well 7122/7-3) have δD values of *n*-alkanes >C_{14} similar to oils from the Snøhvit field seems to indicate a negligible effect of secondary migration on δD values of *n*-alkanes in the HB. The weighted average δD values of *n*-alkanes >C_{14} in oils from the Snøhvit and Goliat fields show very small variation (4-5‰). A similar case in oils from the western Canada Basin was reported by Li et al. (2001). The authors found very little changes (4‰) in δD values of *n*-alkanes with secondary oil migration.

- ***D/H ratios of oil components***

Yeh and Epstein (1981) and Waseda (1993) documented small differences in δD values between whole oils and their fractions in unaltered oils. More recently, Schimmelmann et al. (2004) reported similarity between δD values of *n*-alkanes calculated as a weighted-mean value from compound-specific isotopic ratios and those from whole oil and saturated fractions in oils generated mainly from single sources. They concluded, on one hand, that these correlations would be unlike in mixed oils and, on the other, that isotopic measurements of *n*-alkanes would be useful for quantitative estimation of oil sources. However, mixed oils from the HB show an exceptional correlation between the weighted average δD values of the C_{14}-C_{30} *n*-alkanes and δD values of saturated fractions (R^2=0.95) (Table 3.5). These close isotopic relationships are more likely related to similar δD values of *n*-alkanes found in source rock extracts from Triassic and Jurassic ages (Fig. 3.19b).

TABLE 3.5. *Comparison between the bulk δD values of saturated fractions and weighted-mean δD values of n-alkanes from compound-specific isotopic data.*

Well	δD values of saturated fraction (‰)	Weighted δD values of *n*-alkanes (‰)	Delta δD (δD values of sat. fraction – δD values of *n*-alkanes) (‰)
7119/12-3	-99	-109	-10
7120/6-1	-119	-128	-9
7120/12-2	-113	-121	-8
7121/4-1	-124	-127	-3
7121/5-1	-121	-129	-8
7122/7-3 (1)	-123	-128	-5
7122/7-3 (2)	-124	-131	-8

- ***D/H ratio of pristane and phytane***

In all hydrocarbon samples and source rock extracts, pristane and phytane have similar δD values within the limits of uncertainty (Fig. 3.19c). This is attributed to a similar origin for the isoprenoids. In addition, the variations of δD values between *n*-alkanes with similar boiling points (*n*-C_{17} and *n*-C_{18}) are less than 9‰. The average δD values of Pr and Ph range from -135 to -145‰ and are similar for oils and condensates with similar thermal maturity (Fig. 3.19d). In contrast, the Kobbe Formation hosted oils from the Goliat field and the condensate samples from the Tornerose and Askeladd fields (wells 7122/6-1 and 7120/7-1, respectively), which show an additional contribution of hydrocarbons found in the late

stage of oil generation, have slightly more positive average δD values of Pr and Ph (-128 to -134‰). However, this D-enrichment of Pr and Ph is very small (~10‰). Greater differences in δD values of regular isoprenoids and *n*-alkanes were observed in evaporative condensates, especially in the Albatross field. These differences are probably related to D-enrichment of *n*-alkanes with carbon number due to evaporation. The differences in δD values between Pr and *n*-C_{17} alkane and between Ph and *n*-C_{18} alkane range from 15 to 35‰ in evaporative condensates (Fig. 3.19e). In contrast, the smallest variations in δD values between Pr and *n*-C_{17} and between Ph and *n*-C_{18} (less than 9‰) were observed in oils from the Goliat field, affected by a secondary charge of gas-condensate, and in the sample of the thermally generated condensate. The slight variations between δD values of the *n*-alkanes and regular isoprenoids in these hydrocarbon samples are consistent with previous studies, which indicate that pristane and phytane are more rapidly enriched in D relative to the *n*-alkanes due to isotopic exchange reactions associated with thermal maturation (Dawson et al., 2005; Pedentchouk et al., 2006). The differences in δD values between regular isoprenoids and *n*-alkanes range from 15 to 20‰ in Snøhvit oils and 18-75‰ in source rock extracts (Fig. 3.19e). However, these differences are substantially smaller than those from fatty acids and Phytol (>150‰), (e.g., Li et al., 2001). Schimmelmann et al. (2004) proposed that small differences in δD values between isoprenoids and *n*-alkanes indicate alteration of primary δD values, because these compounds should preserve notably different δD values in absence of exchange.

3.7. Conclusions

A comprehensive assessment of biomarkers and compound-specific carbon isotope composition indicated that petroleum in the HB consists of mixtures of hydrocarbons derived mainly from Paleozoic, Triassic and Jurassic source rocks. Distinct petroleum mixing processes involving source, age and maturity variations were recognized in Jurassic and Triassic reservoirs. Mixtures resulted from hydrocarbons derived from type-III and type-II kerogen-rich source rocks with small maturity variation within the main stage of oil generation or between the peak and late oil generation stages. Nevertheless, mixtures of hydrocarbons yielded from distinct source rocks at diverse stages of oil generation were

identified in the Goliat field. Furthermore, diamondoid maturity parameters indicate that a late gas charge has occurred throughout the basin. Several petroleum alteration processes affected the Jurassic and Triassic reservoirs in the HB, including microbial degradation (Goliat and Tornerose fields), water-washing (Alke, Goliat and Tornerose fields), migration-fractionation (Askeladd, Albatross, Alke and Tornerose fields), gas-condensate charge (Goliat field) and high level of thermal maturation (well 7119/12-3). The presence of evaporative condensates and gas-condensate charges may indicate the existence of deeper, undiscovered petroleum accumulations. Light hydrocarbon and biomarker ratios were unable to discriminate well the different mixed oil families in the HB. Nonetheless, compound-specific stable carbon isotope ratios were useful to identify compositional variations related to their contributing source rocks. The $\delta^{13}C$ of long chain *n*-alkanes were suitable for quantitative assessment of oil source contributions, allowing a good differentiation on Triassic vs. Jurassic contributions. Physical and thermal processes, such as evaporation and maturation, caused a D-enrichment of *n*-alkanes with carbon number $>C_{14}$. Nevertheless, evaporative condensates exhibited a stronger and constant D-enrichment of *n*-alkanes with increasing carbon number relative to the thermally generated condensate. Furthermore, the thermally generated condensate showed an abrupt and regular ^{13}C-enrichment of short-chain *n*-alkanes with decreasing carbon number. Even though the thermal maturation and evaporative fractionation alter the δD values of *n*-alkanes, secondary oil migration does not seem to have had any significant effect.

3.8. Acknowledgements

W.A.M thanks the German Academic Exchange Service (DAAD) for a doctoral fellowship, which supported this research. Thanks also to the Organic Geochemistry section at GFZ and its technical staff for providing analytical support. We are also grateful to the Norwegian Petroleum Directorate for the kind contribution of samples, and the Institute of Earth and Environmental Science of Potsdam University, particularly Yannick Garcin and Dirk Sachse, for hydrogen isotope measurements of source rock extracts. W.A.M is grateful to Jesus A. Pinto for comments, which helped to improve the English of the manuscript. Two anonymous referees are also thanked for their suggestions that resulted in improvements of the manuscript.

3.9. Appendix

3.9.1. Appendix A

Published in http://dx.doi.org/10.1016/j.marpetgeo.2015.11.009 (Murillo, W.A et al. (2016): *Marine and Petroleum Geology* 70, 119-143)

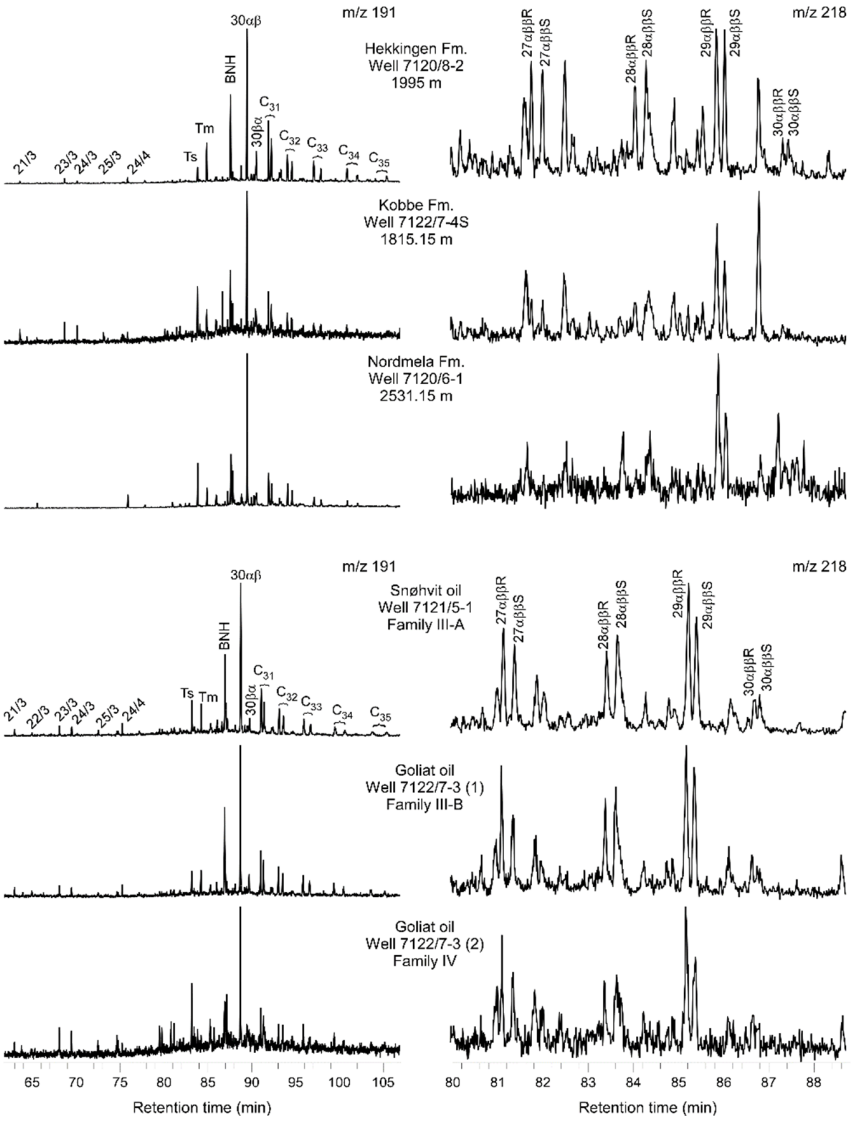

FIGURE. A.1. *Representative mass chromatograms (m/z 191 and 218) for typical source rock extracts from the Hekkingen, Kobbe and Nordmela Fms. and oil families in the HB. Selected peaks are identified in the mass chromatograms. Key: m/z 191: 21/3 to 25/3: C_{21} to C_{25} tricyclic terpanes; 24/4: C_{24} tetracyclic terpane; Ts: C_{27} 18α(H)-22,29,30-trisnorneohopane; Tm: C_{27} 17α(H)-22,29,30-trisnorhopane, BNH: C_{28} 17α(H),21β(H)-28,30-bisnorhopane; 30ab:C_{30} 17α(H),21β(H)-hopane; 30b,a: C_{30} 17β(H),21α(H)-moretane; C_{31} to C_{35}: C_{31} to C_{35} 17α(H),21β(H),22(S)+(R) homohopanes. m/z 218: 27αββR: C_{27} 5α(H),14β(H),17β(H)20Rcholestane;27αββS:C_{27} 5α(H),14β(H),17β(H) 20S cholestane; 28αββR: C_{28} 5α(H),14β(H),17β(H) 20R ergostane; 28αββS: C_{28} 5α(H),14β(H),17β(H) 20S ergostane; 29αββR: C_{29} 5α(H),14β(H),17β(H) 20R stigmastane; 29αββS: C_{29} 5α(H),14β(H),17β(H) 20S stigmastane. 30αββR: C_{30} 5α(H),14β(H),17β(H) 20R; 30αββS: C_{30} 5α(H),14β(H),17β(H) 20S.*

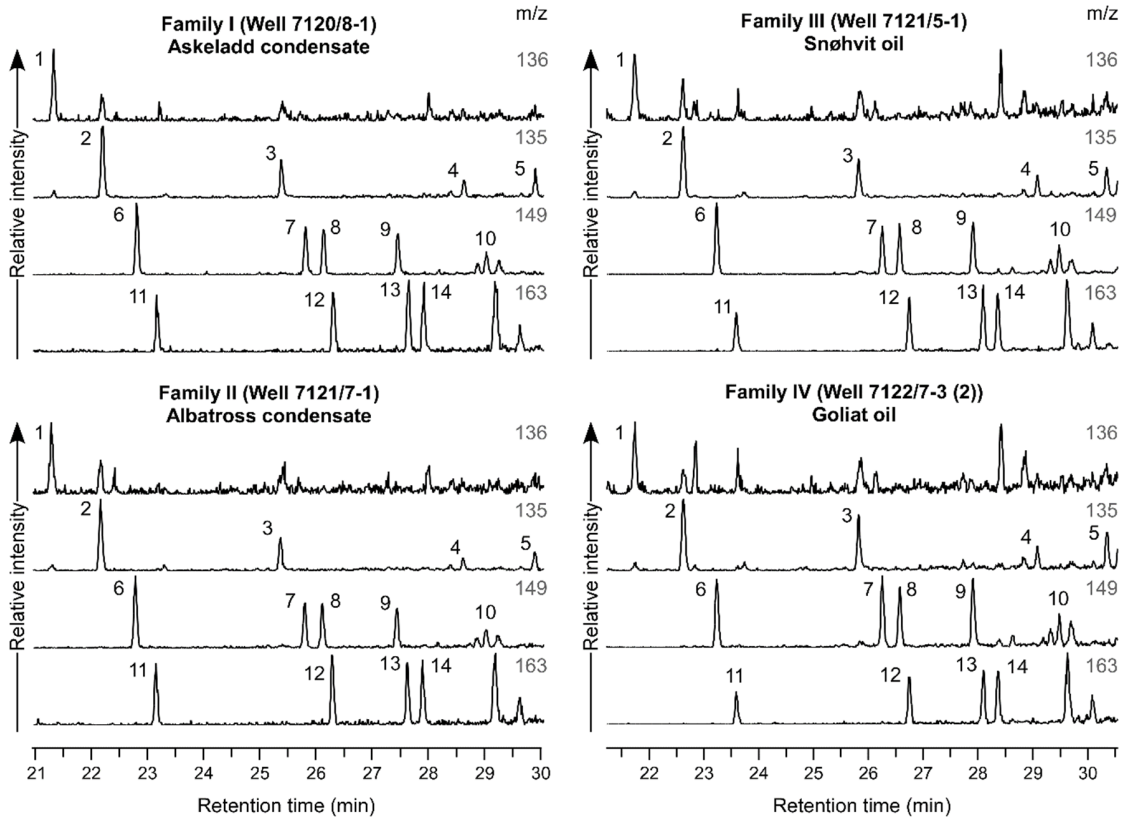

FIGURE. A.2. *Representative mass chromatograms of m/z 136, 135, 149,163 showing distribution and elution order of adamantanes for oils and condensates from the HB. 1. Adamantane; 2. 1-methyladamantane (1MA); 3. 2-methyladamantane (2-MA); 4. 1-ethyladamantane (1EA); 5. 2-ethyladamantane; 6. 1,3-dimethyladamantane; 7. 1,4-dimethyladamantane(cis); 8. 1,4-dimethyl-adamantane(trans); 9. 1,2-dimethyladamantane; 10. 1-ethyl,3-methyladamantane; 11. 1,3,5- trimethyladamantane; 12. 1,3,6-trimethyladamantane; 13. 1,3,4-trimethyladamantane(cis); 14. 1,3,4- trimethyladamantane (trans). All of the mass chromatograms are represented with the same relative intensity.*

3.9.2. Appendix B

TABLE B.1. *Parameters of source, oil source rock depositional environments and lithologies for oils, condensates and source rock extracts from the HB.*

(Data published in http://dx.doi.org/10.1016/j.marpetgeo.2015.11.009 (Murillo, W.A et al. (2016): Marine and Petroleum Geology 70, 119-143)

Well	Pr/ Ph	Pr/ C_{17}	Ph/ C_{18}	%C_{27} St	%C_{28} St	%C_{29} St	%C_{30} St	Dia/ Reg	BNH%	C_{30} Mor/ Hop	C_{35}S/ C_{34}S Hop	%Ret	%Cad	%ip-IHMN	HPP	DBT/ Phen	MDBT/ Mphen	4MDBT/ Phen
7120/7-1*	2.65	0.61	0.29	n.d.	n.d.	n.d.	n.d.	n.d.	n.d.	n.d.	n.d.	20.12	79.88	n.d.	0.20	0.12	0.09	0.16
7120/8-1*	2.67	0.70	0.36	n.d.	n.d.	n.d.	n.d.	n.d.	n.d.	n.d.	n.d.	24.94	75.06	n.d.	0.25	0.25	0.15	0.26
7120/8-2*	2.79	0.69	0.35	n.d.	n.d.	n.d.	n.d.	n.d.	n.d.	n.d.	n.d.	22.50	77.50	n.d.	0.22	0.19	0.17	0.23
7121/7-2*	2.80	0.75	0.35	n.d.	n.d.	n.d.	n.d.	n.d.	n.d.	n.d.	n.d.	24.64	75.36	n.d.	0.25	0.24	0.17	0.22
7120/9-1*	2.54	0.91	0.52	n.d.	n.d.	n.d.	n.d.	n.d.	n.d.	n.d.	n.d.	21.22	78.78	n.d.	0.21	0.39	0.26	0.38
7121/7-1*	2.57	0.92	0.57	n.d.	n.d.	n.d.	n.d.	n.d.	n.d.	n.d.	n.d.	19.73	80.27	n.d.	0.20	0.35	0.24	0.37
7122/6-1*	2.12	0.97	0.63	n.d.	n.d.	n.d.	n.d.	n.d.	n.d.	n.d.	n.d.	17.16	74.42	8.41	0.19	0.31	0.32	0.24
7120/6-1*	1.49	0.85	0.57	32.68	21.55	45.77	9.70	1.09	4.13	0.07	0.48	58.20	22.01	19.79	0.73	0.50	0.24	0.63
7121/4-1*	1.51	0.86	0.58	33.16	22.05	44.80	9.77	1.16	3.90	0.07	0.44	64.40	19.68	15.92	0.77	0.47	0.26	0.62
7121/5-1*	1.46	0.84	0.58	32.29	23.04	44.67	10.19	1.20	4.56	0.06	0.59	58.90	19.75	21.35	0.75	0.51	0.28	0.66
7122/7-2*	2.04	1.00	0.53	35.17	24.38	40.45	9.17	1.24	7.42	0.07	0.62	52.96	29.30	17.74	0.64	0.45	0.38	0.49
7122/7-3 (1)*	2.01	0.91	0.49	31.54	22.16	46.30	10.02	1.20	4.16	0.07	0.48	50.21	25.34	24.46	0.66	0.50	0.27	0.61
7122/7-3 (2)*	1.68	1.25	0.87	30.98	20.72	48.30	9.34	1.84	1.76	0.09	0.88	59.69	31.23	9.08	0.66	0.19	0.10	0.17
7122/7-4 S*	1.64	1.17	0.80	32.42	24.08	43.50	10.37	1.77	2.66	0.07	0.65	66.29	28.04	5.67	0.70	0.17	0.12	0.13
7120/12-2*	2.48	0.95	0.52	n.d.	n.d.	n.d.	n.d.	n.d.	n.d.	n.d.	n.d.	13.21	65.70	21.09	0.17	0.30	0.22	0.31
7119/12-3*	2.24	0.33	0.16	n.d.	n.d.	n.d.	n.d.	n.d.	n.d.	n.d.	n.d.	n.d.	n.d.	n.d.		0.08	0.02	0.10
7120/8-2 (1)**	1.96	1.47	0.72	31.59	26.69	41.71	12.45	0.85	4.73	0.15	0.49	85.21	3.15	11.64	0.96	n.d	n.d	n.d
7120/8-2 (2)**	1.22	1.88	1.58	26.98	15.30	57.73	8.88	1.25	1.39	0.14	0.41	79.62	10.87	9.51	0.88	n.d	n.d	n.d
7122/7-4S (1)**	1.69	0.92	0.63	16.79	18.84	64.37	4.70	1.51	18.45	0.11	0.55	73.87	18.02	8.11	0.80	n.d	n.d	n.d
7122/7-4S (2)**	1.11	1.83	1.74	17.32	18.81	63.87	4.31	1.10	8.95	0.18	0.43	83.76	9.06	7.19	0.90	n.d	n.d	n.d
7120/6-1**	3.20	0.60	0.15	17.61	21.10	61.29	7.25	1.26	0.33	0.05	0.38	80.15	17.44	2.41	0.82	n.d	n.d	n.d

Oil and condensate sample (*), source rock sample (**). Pr/Ph: Pristane/Phytane ratio; Pr/*n*-C_{17}: Pristane/*n*-C_{17}; Ph/*n*-C_{18}: Phytane/*n*-C_{18}; %C_{27} St, %C_{28} St, %C_{29} St: relative percentages of C_{27}, C_{28} and C_{29} ααββ regular steranes within C_{27} to C_{29} regular steranes, measured in m/z (372, 386, 400) → 217; %C_{30} St: C_{30}/(C_{27}-C_{30}) steranes measured in m/z 414 → 217; Dia/Reg: (total C_{27} to C_{29} 13β,17α(H) 20S + 20R diasteranes)/(total C_{27} to C_{29} 5α,14β,17β(H) and 5α,14α,17α(H) 20S + 20R) steranes) steranes; BNH%: 17α(H),21β(H)-28,30-bisnorhopane/17α(H),21β(H) 28,30-bisnorhopane+17α(H),21β(H) hopane measured in m/z (384, 412) → 191; C_{30} Mor/Hop: 17β(H),21α(H) moretane/17α(H),21β(H) hopane measured in m/z 412→ 191; C_{35}S/C_{34}S Hop: C_{35} 17α(H), 21β(H),22S hopane/ C_{34} 17α(H), 21β(H),22S hopane; %Ret: relative percentage of retene; %Cad: relative percentage of cadalene; %ip-IHMN: relative percentage of 6-isopropyl-1-isohexyl-2-methylnaphthalene; HPP: (retene/(retene+cadalene)); DBT/Phen: dibenzothiophene/phenanthrene; MDBT/MPhen: methyldibenzothiophene/methylphenanthrene; 4MDBT/Phen: 4-methyldibenzothiophene/phenathrene. n.d. - not determined.

TABLE B.2. *Fractionation index (FI) and Halper C_7 ratios used in star diagrams to differentiate hydrocarbon samples.*

(Data published in http://dx.doi.org/10.1016/j.marpetgeo.2015.11.009; Murillo, W.A et al. (2016): Marine and Petroleum Geology 70, 119-143)

Well	FI	Tr1	Tr2	Tr3	Tr4	Tr5	Tr6	Tr7	Tr8	C1	C2	C3	C4	C5
7120/7-1	0.69	28.90	15.53	5.14	4.91	10.05	2.57	1.51	3.10	0.14	0.44	0.22	0.13	0.08
7120/8-1	1.01	30.54	15.28	5.56	5.38	10.95	2.68	1.56	3.10	0.14	0.42	0.23	0.13	0.08
7120/8-2	1.14	31.66	16.53	5.51	5.19	10.70	2.87	1.65	3.16	0.12	0.45	0.22	0.13	0.08
7121/7-2	1.01	25.26	15.56	5.18	4.97	10.15	2.92	1.82	3.03	0.13	0.43	0.22	0.12	0.09
7120/9-1	2.75	20.34	17.97	6.30	5.79	12.09	3.41	1.94	3.32	0.12	0.46	0.22	0.11	0.09
7121/7-1	2.67	20.32	17.83	6.28	5.72	12.00	3.52	1.94	3.19	0.12	0.46	0.21	0.11	0.09
7122/6-1	0.93	2.09	7.03	3.81	3.53	7.34	2.22	1.13	2.73	0.16	0.44	0.22	0.11	0.08
7120/6-1	0.08	22.89	13.54	5.43	4.76	10.20	3.71	1.97	2.89	0.13	0.46	0.20	0.14	0.08
7121/4-1	0.11	18.43	13.83	5.75	5.04	10.79	3.98	1.96	3.14	0.14	0.49	0.21	0.09	0.07
7121/5-1	0.08	23.96	13.36	5.17	4.55	9.72	3.53	1.89	2.91	0.13	0.46	0.20	0.14	0.07
7122/7-2	n.d.	16.57	0.29	1.13	0.77	1.90	4.03	2.16	0.56	0.11	0.50	0.23	0.06	0.10
7122/7-3 (1)	n.d.	9.85	0.33	0.22	0.34	0.56	3.92	2.13	0.17	0.11	0.48	0.22	0.08	0.11
7122/7-3 (2)	0.16	2.69	7.50	4.33	3.97	8.30	2.43	1.44	2.48	0.16	0.35	0.29	0.12	0.08
7122/7-4 S	0.25	3.56	8.92	4.44	4.10	8.54	2.48	1.50	2.82	0.18	0.40	0.25	0.11	0.06
7120/12-2	1.72	4.17	11.99	5.66	5.53	11.19	2.50	1.43	3.14	0.17	0.40	0.23	0.12	0.09
7119/12-3	0.21	69.43	17.78	9.43	9.46	18.89	1.95	1.20	2.89	0.20	0.36	0.22	0.14	0.08

TABLE B.3. *Parameters of thermal maturity based on light hydrocarbons, biomarkers, polycyclic aromatic hydrocarbons (PAHs) and diamondoids for condensate and oil samples from the HB.*

(Data published in http://dx.doi.org/10.1016/j.marpetgeo.2015.11.009; Murillo, W.A et al. (2016): Marine and Petroleum Geology 70, 119-143)

	Light Hydrocarbons					**Biomarkers**					**PAHs**						**Diamondoids**		
Well	%Rc (V)	%Rc (J)	2,2-DMC$_4$/ 2,3-DMC$_4$	q/(q+t) C$_7$ isohep	isoC$_5$/ *n*C$_5$	20S	ββ	22S	MA(I)/ MA (I+II)	TA(I)/ TA (I+II)	DNR-3	TNR-2	MDR	%Rc (1)	%Rc (2)	%Rc (3)	%Rc (4)	%Rc (5)	%Rc (6)
7120/7-1	0.79	1.11	0.44	0.27	0.75	-	-	-	-	-	14.35	0.93	7.26	0.82	1.04	0.91	2.19	2.53	2.11
7120/8-1	0.88	1.13	0.45	0.26	0.72	-	-	-	-	-	12.79	0.87	5.33	0.76	0.92	0.80	2.19	2.57	2.15
7120/8-2	0.83	1.09	0.40	0.24	0.68	-	-	-	-	-	10.68	0.85	4.82	0.74	0.91	0.76	2.22	2.46	2.19
7121/7-2	0.80	1.05	0.45	0.25	0.71	-	-	-	-	-	11.17	0.85	4.80	0.71	0.87	0.74	2.16	2.43	2.18
7120/9-1	0.96	1.07	0.43	0.23	0.70	-	-	-	-	-	9.59	0.83	4.03	0.70	0.81	0.64	2.17	2.20	2.17
7121/7-1	0.93	1.06	0.44	0.23	0.70	-	-	-	-	-	8.88	0.84	4.37	0.70	0.82	0.67	2.23	2.27	2.25
7122/6-1	0.61	1.07	0.44	0.27	0.88	-	-	-	-	-	6.30	0.81	2.96	0.66	0.82	0.68	2.25	2.44	2.15
7120/6-1	0.75	0.97	0.56	0.26	0.78	0.49	0.59	0.57	15.12	29.23	5.06	0.79	3.81	0.83	0.82	0.77	2.04	2.35	2.08
7121/4-1	0.76	0.98	0.56	0.24	0.81	0.47	0.59	0.60	11.63	30.28	5.22	0.75	3.53	0.83	0.82	0.77	2.08	2.33	2.13
7121/5-1	0.71	0.97	0.54	0.26	0.75	0.52	0.62	0.59	16.15	31.03	5.21	0.77	3.60	0.81	0.80	0.76	2.06	2.34	2.10
7122/7-2	-	-	0.36	0.17	-	0.47	0.55	0.57	12.48	21.60	6.52	0.82	3.71	0.77	0.86	0.76	2.01	2.43	2.05
7122/7-3 (1)	-	-	0.40	0.19	-	0.47	0.59	0.58	11.07	16.54	5.40	0.81	3.76	0.84	0.88	0.79	2.04	2.31	2.10
7122/7-3 (2)	0.85	1.04	0.64	0.29	1.10	0.40	0.57	0.55	18.94	28.69	4.98	0.79	3.74	0.79	0.85	0.78	1.92	2.16	2.05
7122/7-4 S	0.86	1.04	0.63	0.29	1.09	0.44	0.56	0.55	23.17	34.01	5.93	0.80	3.40	0.72	0.80	0.72	1.91	2.34	1.99
7120/12-2	1.03	1.18	0.75	0.30	0.96	-	-	-	21.11	-	4.15	0.63	3.55	0.85	0.93	0.96	2.30	2.38	2.25
7119/12-3	1.22	1.54	0.84	0.34	1.29	-	-	-	-	-	16.15	0.95	-	0.99	1.33	1.21	2.26	2.82	2.22

%Rc (V): 1.0 + 1.8 log V, V: C$_7$ paraffins/ naphthenes; %Rc (J): 0.84 + 1.1 log J, J: (2-methylhexane+3-methylhexane)/(1,2-(cis + trans)- + 1,3 (cis + trans) dimethylpentanes); 2,2-DMC$_4$/2,3-DMC$_4$: 2,2-dimethylbutane/2,3-dimethylbutane; q/(q+t) C$_7$ isohep: (2,2-DMP + 3,3-DMP)/ (2,2-DMP + 3,3-DMP + 3-EP + 2,3-DMP + 2,4-DMP); isoC$_5$/*n*C$_5$: isopentane/ *n*-pentane; 20S: 20S/(20S + 20R) ratio for C$_{29}$-ααα steranes; ββ: αββ/(ααα + αββ) ratio for C$_{29}$ steranes; 22S: 22S/(22S + 22R) for C$_{32}$-homohopanes; MA(I)/MA(I+II): C$_{21}$ + C$_{22}$ monoaromatic steroids as MA(I), C$_{27}$-C$_{29}$ monoaromatic steroids as MA(II); TA(I)/TA(I+II): C$_{20}$ and C$_{21}$ triaromatic steroids as TA(I), C$_{26}$-C$_{28}$ (20S + 20R) triaromatic steroids as TA(II); DNR-3: 2,6-DMN/1,8-DMN; TNR-2: (1,3,7-TMN + 2,3,6-TMN)/ (1,3,5-TMN + 1,3,6-TMN + 1,4,6-TMN); MDR: 4-MDBT/1-MDBT; %Rc (1): %R$_C$ MPI-1: 0.6 MPI-1 + 0.4, MPI-1: 1.5 (2-MP + 3-MP)/ (P+1-MP+9-MP); %Rc (2): %Rc MPDF1: -0.166 + 2.242 F1, F1: (2-MP + 3-MP)/(2-MP + 3-MP + 1-MP + 9-MP); %Rc (3): %Rc MPDF2: -0.112 + 3.739 F2, F2: 2-MP/ 2-MP + 3-MP + 1-MP + 9-MP. The %Rc (4), %Rc (5) and %Rc (6) correspond to the % Rc DMAI-1, %Rc EAI and %Rc TMAI-1, respectively. They were obtained using plots reported by Fang et al., 2012. DMAI-1: 1,3-DMA/ (1,2-DMA + 1,3-DMA); EAI: 2-EA/ (1-EA + 2-EA); TMAI-1: 1,3,5-TMA/(1,3,5-TMA + 1,3,4-TMA). DMP: dimethylpentane; EP: ethylpentane; DMN: dimethylnaphthalene; TMN: trimethylnaphthalene; MDBT: methyldibenzothiophene; MP: methylphenanthrene; DMA: dimethyladamantane; EA: ethyladamantane; TMA: trimethyladamantane.

Chapter 4

Unraveling Petroleum Mixtures from the South Viking Graben, North Sea: A Study based on $\delta^{13}C$ of Individual Hydrocarbons and Molecular Data

4.1. Abstract

Mixtures of compositionally different petroleum occur in the Norwegian North Sea, one of the world's major oil-producing regions. The objective of this contribution was to appraise the source, maturity, in-reservoir mixing and alteration processes in a set of condensate and oil samples covering the main producing areas in the South Viking Graben (SVG). Furthermore, this study focused on unraveling complex mixtures of petroleum and quantifying mixing ratios of hydrocarbons generated from Jurassic source rocks. The present research was based on a multiparameter approach that comprised the molecular composition of light hydrocarbons and heterocyclic and polycyclic aromatic compounds as well as the $\delta^{13}C$ values of individual hydrocarbons in oils, condensates and Upper and Middle Jurassic source rock extracts from the SVG. According to the relative contribution of oils from Type-III kerogen-rich source rocks, seven populations (A-G) of mixed petroleum were identified by combining source-related ratios of heterocyclic and non-heterocyclic aromatic hydrocarbons and $\delta^{13}C$ values of *n*-alkanes, pristane (Pr) and phytane (Ph). The heterocyclic and polycyclic aromatic hydrocarbons provided a useful means of discriminating mixed hydrocarbons from source rocks of distinct organic matter types, depositional environments

This chapter has been published as: Murillo, W.A., Horsfield, B., Vieth-Hillebrand, A., 2019. Unraveling petroleum mixtures from the South Viking Graben, North Sea: A study based on $\delta^{13}C$ of individual hydrocarbons and molecular data. Organic Geochemistry, 137. https://doi.org/10.1016/j.orggeochem.2019.103900.

and lithologies in the SVG. The ^{13}C-enrichment of (C_{10}-C_{14}) *n*-alkanes and Pr and Ph were good indicators of the scale of the terrigenous source contribution and allowed the quantitative determination of the proportions of Jurassic source contributions enriched in Type-II and Type-III kerogens in complex petroleum mixtures from the southern part of the SVG.

4.2. Introduction

The North Sea Graben of northwestern Europe, comprising the Central and Northern North Sea, is one of the world's greatest petroleum provinces. This research is focused on the South Viking Graben (SVG), located in the Norwegian sector of the Northern North Sea, whose petroleum systems include source rocks deposited mainly during the Late Jurassic to earliest Cretaceous. Previous studies (Isaksen et al., 2002; Justwan et al., 2005, 2006a) assessed the geochemical properties of the potential Jurassic source rocks and oils in the SVG based on their carbon isotopic composition (δ^{13}C) obtained from the bulk aliphatic and aromatic fractions and biomarker composition. These authors reported an upward increase in oil-prone Type II material from Middle to Upper Jurassic source rocks. Likewise, they identified several hydrocarbon families in the SVG that correlated with different facies of the Draupne Formation, the Heather Formation and the Middle Jurassic Sleipner and Hugin formations. Hydrocarbon gases were interpreted to have originated from coals and coaly shales of the Sleipner and Hugin formations. Furthermore, Isaksen et al. (1998); Isaksen et al. (2002); Justwan et al. (2006b) noted that petroleum traps in the Greater Sleipner Area can be charged from different directions and from Jurassic source rocks with differing organic matter composition, producing complex in-reservoir mixing.

In basins with multiple source rocks and complex charging history as for the North Sea, mixing of oils can make oil-oil and oil-source correlations difficult. For this reason, employing a multiparameter approach is of paramount importance. The present research, added different petroleum components that were not considered in previous studies (namely light hydrocarbons and heterocyclic and polycyclic aromatic hydrocarbons), to establish genetic links between different oils and between oils and source rocks. Importantly, δ^{13}C values for individual *n*-alkanes were used rather than those for whole oils or subfractions as

compound-specific isotope analysis (CSIA) provides more resolution than bulk methods (e.g., Pedentchouk and Turich, 2017). CSIA has become a powerful tool to assess multiple organic matter sources in oils, source rock extracts and kerogen pyrolysates (e.g., Freeman et al. 1990, Hayes et al. 1990, Rieley et al. 1991) and has been used to study the mixing of oils (e.g., He et al., 2012; Jia et al., 2013; Murillo et al., 2016).

Light hydrocarbons are a useful means of typing oils and of evaluating alteration of oils, maturity and oil mixtures (e.g., Thompson, 1983; Mango, 1990; BeMent et al., 1995; Halpern, 1995, ten Haven, 1996; Obermajer et al., 2000; Jarvie, 2001; Murillo et al., 2018). In addition, many C_7 hydrocarbon parameters likely reflect differences in kerogen type and can be used for oil-oil correlation studies (Mango, 1987, 1990; Halpern, 1995). Furthermore, the distribution and relative abundance of certain polycyclic aromatic hydrocarbons (PAHs), along with their methyl derivatives, in bitumens and crude oils have been used as source indicators (e.g., Simoneit, 1977; Strachan et al., 1988; Alexander et al., 1992). Relative abundances of some isomers of alkylnaphthalenes and alkylphenanthrenes have been associated with specific natural precursors and applied to differentiate terrigenous from marine source input (e.g., Püttmann and Villar, 1987; Strachan et al., 1988; Budzinski et al., 1995). One example is 1,2,5-trimethylnaphthalene (1,2,5-TMN), which can be used to indicate higher-plant source input since it is a common product of aromatization of terpenoid precursors, such as bicyclic diterpenoids and pentacyclic triterpenoids (Strachan et al., 1988). Similarly, 1,6-dimethylnaphthalene (1,6-DMN) and 1,6-dimethyl-4-isopropylnaphthalene (cadalene) are proposed to be derived from fossil resins (e.g., Simoneit et al., 1986; Radke et al., 1986; van Aarssen et al., 1992). Van Aarssen et al. (1990, 1992) identified the polycadinene as a probable source of cadalene. The dominance of 1,2,5-TMN and cadalene has been used to assess the presence of conifer resin in marginally mature rocks (Radke et al., 1986; Alexander et al., 1988). Apart from the alkylnaphthalenes, the distribution of methyl, dimethyl and trimethylphenanthrenes is influenced by the type of organic matter and the environment in which it was deposited (Fan et al., 1990 and Budzinski et al., 1995). The dominance of 1-methylphenanthrene (1-MP) has been associated with Type-III kerogen (Heppenheimer et al., 1992), whereas abundant 9-methylphenanthrene (9-MP) is related to Type-II and Type-I kerogens (Isaksen, 1991). Moreover, the predominance of 1,7-

dimethylphenanthrene (1,7-DMP) has been attributed to a biomarker of the pimarane type present in resins (Simoneit, 1977).

On the other hand, the distributions of dibenzothiophene, dibenzofuran and fluorene and their methyl derivatives are controlled by source rock lithology and depositional environment (Hughes, 1984; Fan et al., 1990). Since these compounds have similar basic skeletons, it has been proposed that they originate from the same precursor (Huang, 1987). Previous authors have proposed that dibenzofuran may originate from polysaccharides (Pastorova et al., 1994) or phenols in the lignin of woody plants (e.g., Born et al., 1989; Fenton et al., 2007). Whereas sulfur-containing heterocyclic aromatic hydrocarbons (i.e., dibenzothiophene and alkyldibenzothiophenes) are abundant in marine carbonate source rocks (Hughes, 1984; Fan et al., 1990), abundant oxygen-containing heterocyclic aromatic hydrocarbons (i.e., dibenzofuran and alkyldibenzofurans) as well as fluorene and alkylfluorenes have been associated with source rocks from oxic/fresh water environments (e.g., Fan et al., 1990; Radke et al., 2000). Hughes et al. (1995) reported that the ratio of dibenzothiophene to phenanthrene (DBT/P) and the ratio of pristane to phytane (Pr/Ph) provide a convenient way to infer crude oil source rock depositional environments and lithologies. Similarly, Chakhmakhchev and Suzuki (1995) used the ratio 4-methyldibenzothiophene to phenanthrene (4-MDBT/P) to evaluate the relative concentration of aromatic sulfur compounds (ASC) in oils from source rocks with different lithologies. They observed that carbonate sources produce oils enriched in ASC that show the highest 4-MDBT/P ratio, whereas clay-rich sources generate petroleum with a very low concentration of ASC and the lowest 4-MDBT/P ratio. Radke et al. (2000) pointed that determination of the ratio of alkyl-DBTs to alkyl-DBFs improved the interpretation of terrestrial depositional environments.

In recent publications, increasing attention has been given to the identification and quantification of relative contributions from different source rocks to oil pools with multiple sources. This has become an issue of interest for reservoir studies, to better understand multiple petroleum systems and thus, to reduce hydrocarbon exploration and production risk. Peters et al. (1989) used $\delta^{13}C$ values of whole oils and source rocks extracts to estimate the

contributions of Jurassic and Devonian source rocks to the mixed Beatrice oils from the inner Moray Firth area, North Sea. Chen et al. (2003) estimated the relative contributions of Permian, Triassic and Jurassic source rocks to reservoirs from the Cainan oil field of the eastern Junggar Basin, NW China. They used mathematical calculations based on whole-oil carbon isotopic composition and the absolute concentrations of selected saturated biomarkers. Arouri and McKirdy (2005) estimated mixing ratios based on a simple mass balance approach using absolute concentrations of individual aromatic hydrocarbons from the Eromanga Basin, Australia. Peters et al. (2008) applied least squares to concentration data for biomarkers in the range C_{19}-C_{35} to de-convolute mixtures of oils from the Prudhoe Bay field, North Slope, Alaska. More recently, Murillo et al. (2016) employed $\delta^{13}C$ of individual *n*-alkanes to estimate Jurassic and Triassic source contributions to mixed petroleum from the Askeladd field of the Hammerfest Basin, NW Barents Sea.

The aims of the present research are to: (1) apply multivariate statistics to classify mixed petroleum using molecular data of heterocyclic and polycyclic aromatic hydrocarbons, C_7 hydrocarbons and $\delta^{13}C$ data of individual petroleum hydrocarbons, (2) better constrain oil-to-oil and oil-to-source correlations, (3) appraise petroleum alteration processes and thermal maturity and (4) estimate the relative contributions of Type-II and Type-III kerogen-rich Jurassic sources to mixed petroleum accumulations in the SVG, using compound-specific stable carbon isotope data.

4.3. Study Area and Geological Setting

The North Sea Graben system constitutes one of the largest oil provinces of Western Europe and encompasses three sub-basins, (1) the Viking Graben located between the East Shetland Platform and the Horda Platform and Fenno-Scandian Shield in the northern part of the North Sea Graben, (2) the Central Graben located in the southernmost part of the North Sea Graben and (3) the Moray Firth/Witch Ground structure located at the junction of the Central and Viking Grabens (Fig. 4.1a). The SVG forms a narrow rift basin at the southern end of the Viking Graben (Fig. 4.1a), whose structural configuration is mainly the result of two major phases of extension during the Permo-Triassic and the Late Jurassic (Ziegler, 1992). The graben is flanked to the west by the Fladen Ground Spur and to the east by the

Utsira High, and merges to the south with the Witch Ground Graben and Central Graben rift systems (Fig. 4.1a). The study area covers an area between 60°15' and 58°N in the southern part of the Norwegian Viking Graben (Fig. 4.1b) and comprises several oil and gas accumulations, such as the Sygin, Varg, Sleipner Øst, Sleipner Vest, Vølve, Glitne, Balder, Vale, Frøy and Lille Frøy fields.

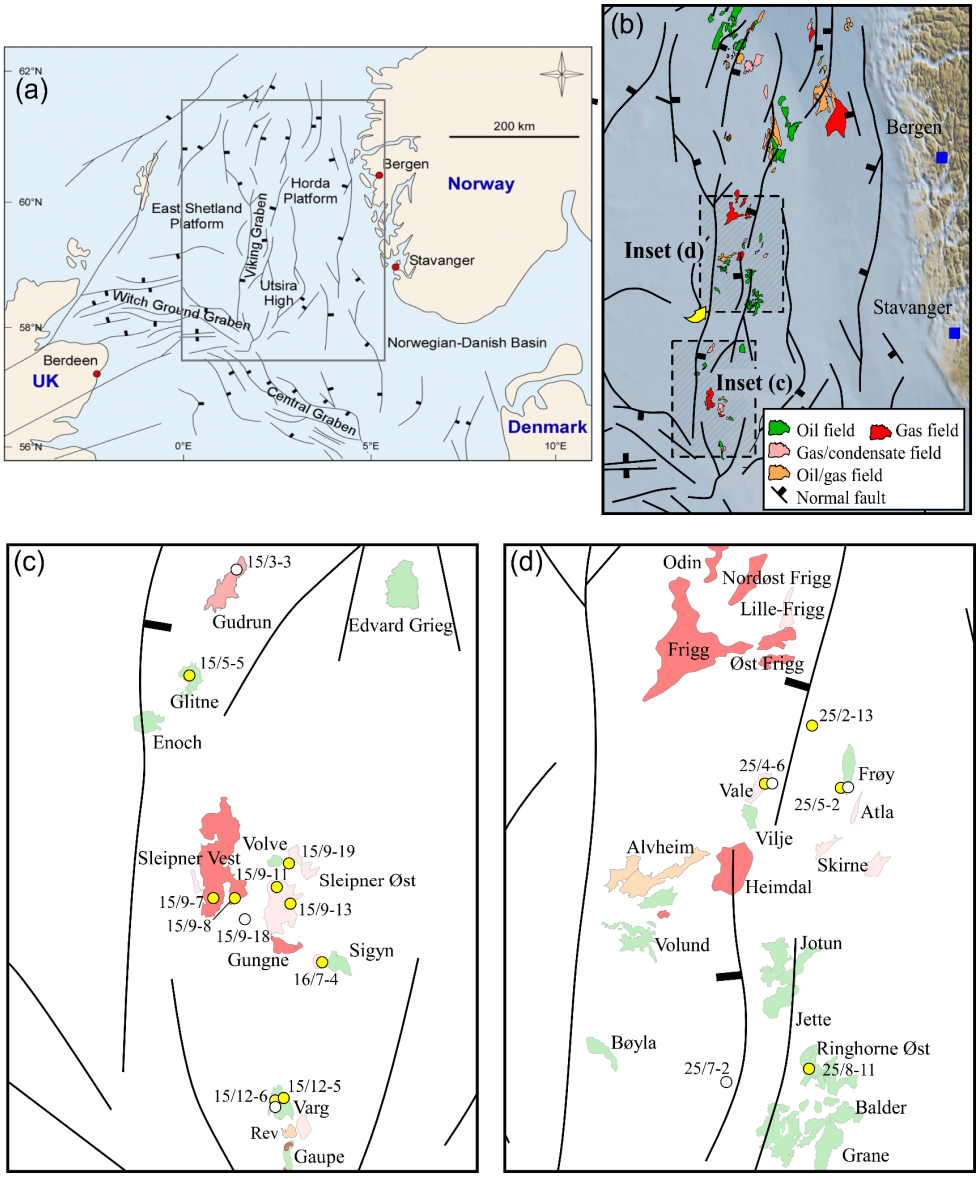

FIGURE 4.1. *(a) Index map showing major structural elements of the Northern North Sea geological province (Cockings et al., 1992); (b) location of the southern part of the SVG (Inset c) and the northern part of the SVG (Inset d); (c) and (d) well location maps with the major structural elements, fields, discoveries and sampled wells for fluids (yellow circles) and rocks (white circles) in the SVG study area.*

A detailed discussion of the tectonic evolution and geologic history of the northern North Sea is beyond the scope of this paper and the reader is referred to other papers that discuss these subjects in more detail (e.g., Thomas et al. (1985); Ziegler and Van-Hoorn (1989); Miller (1990); Fraser et al. (2003)). In this article, however, some key aspects about the petroleum systems have been summarized as follows:

The source rocks are the shales of the Upper Jurassic Draupne and Heather formations and the shales and coals of the Middle Jurassic Hugin and Sleipner formations (Fig. 4.2a). The best source rock in terms of richness, thickness and type was deposited during Late Jurassic to earliest Cretaceous time (e.g., Dore et al., 1985; Cooper and Barnard, 1984; Cornford, 1998). This source rock interval, herein referred to as the Draupne Formation, is the main hydrocarbon source in the Viking Graben. This formation is commonly classified as a Type-II oil-prone source rock deposited in a marine environment under restricted anoxic conditions (e.g., Goff, 1983; Cooper and Barnard, 1984; Thomas et al., 1985). Some authors have identified two organic facies within this formation; an upper Draupne marine Type-II facies and a lower Draupne Type-II/III facies (e.g., Field, 1985; Telnaes et al., 1997; Isaksen and Ledje, 2001; Justwan et al., 2005). The Draupne Formation siliciclastic shales grade into calcareous shales, especially during periods of maximum transgression and low siliciclastic input to the graben (e.g., Isaksen et al., 1998). The underlying marine shales of the Upper Jurassic Heather Formation are mostly a gas-prone source; however, in some areas the Heather Formation may contain oil-prone intervals (e.g., Thomas et al., 1985). This formation was deposited under dysoxic to oxic conditions, whose final deposition was characterized by an increasing oxygenation accompanying a progressive transgression (e.g., Thomas et al., 1985). The Middle Jurassic Sleipner and Hugin formations were deposited in a coastal plain to offshore marine setting and consist of coals and coaly shales (e.g., Vollset and Dore, 1984). These Middle Jurassic source rocks have the potential to generate gas and volatile oil (Isaksen et al., 1998). Even though most petroleum accumulations were generated mainly from shales of the Draupne Formation (Barnard and Cooper, 1981; Cornford, 1998; Justwan et al., 2005), they occur within reservoir rocks of various ages. Migration pathways are usually short, and mostly occur in tilted fault blocks (Goldsmith et al., 2003; Fraser et al., 2003). The oldest Jurassic reservoirs are marginal-marine to non-marine fluvial sediments of

the Statfjord Formation, which are overlain by marine shales of the Dunlin Group. Overlying the Statfjord Formation and the Dunlin Group are strata of the Brent Group, which together with their correlatives are the most important hydrocarbon reservoir sequence within the North Sea Basin (e.g., Morton et al., 1992).

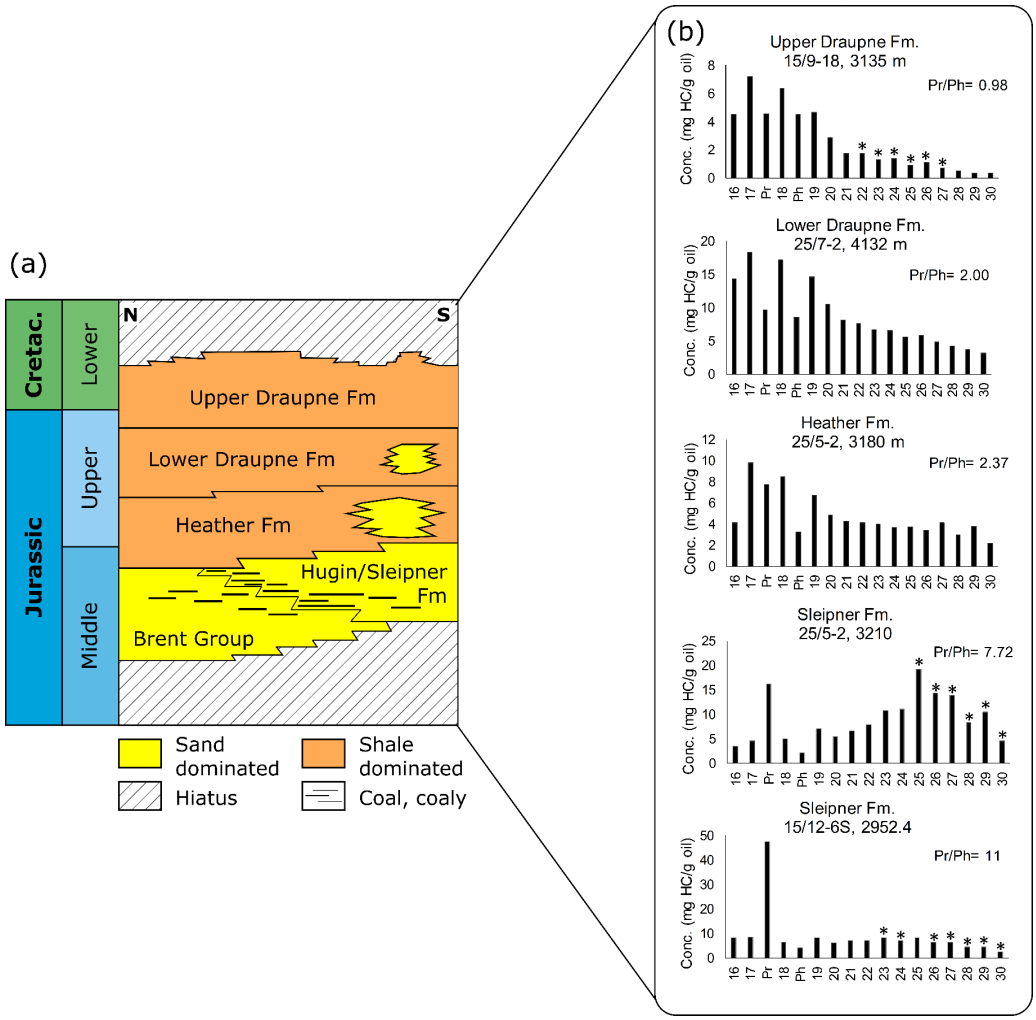

FIGURE 4.2. *(a) Upper and Middle Jurassic lithostratigraphy of the South Viking Graben (taken from Justwan et al., 2006b); (b) concentration of n-alkanes (C_{16}-C_{30}) in source rock extracts from the SVG.*

For most fields of the SVG, Middle and Upper Jurassic sandstones and Paleocene sandstones are the main petroleum reservoirs (Pegrum and Spencer, 1990; Gautier, 2005). In the Middle Jurassic reservoirs of the Viking Graben, traps are sealed vertically by unconformably overlying Jurassic and Cretaceous shales, and laterally by the juxtaposition

of shales and reservoir sandstones at fault contacts (e.g., Gautier, 2005). Altered and fractured basement rocks act as reservoir and possible migration pathways for hydrocarbons in the Utsira High (Edvard Grieg and Johan Sverdrup fields) (Riber et al., 2015). In well 16/1-12, oil was detected in weathered and faulted/fractured granitic basement (Norwegian Petroleum Directorate, 2019a).

4.4. Samples

The petroleum samples used in this study (Table 4.1) were provided by the Norwegian Petroleum Directorate (NPD). They include a total of 15 crude oils and condensates from 13 wells located in the SVG (Fig. 4.1c and d). Moreover, 22 cuttings and core samples were collected from the core repository of the NPD. They were taken from different depth intervals within the Upper Jurassic Draupne and Heather formations and the Middle Jurassic Sleipner Formation in seven wells (Table 4.2) located in the SVG (Fig. 4.1c and d).

TABLE 4.1. *Sample details and assigned families for analyzed oils and condensates from the SVG.*

Well	Test	Depth MD (m)	Field/Discovery	Reservoir Fm.	Age	Population
15/5-5	T1	2154-2183	Glitne	Heimdal Fm.	Paleocene	A
15/9-19A	T2	3826-3865	Volve	Hugin Fm.	Middle Jurassic	B
15/9-13	T1	2765-2769	Sleipner Øst	Hugin Fm.	Middle Jurassic	C
15/12-5	-	2935	Varg	Hugin Fm.	Middle Jurassic	C
15/12-6S	T2	2875-2895	Varg	Vestland Gp.	Middle Jurassic	C
25/8-11	T1	1893-1910	Balder	Statfjord Gp.	Early Jurassic	D
25/2-13	T2B	2706-2713	Lille Frøy	Hardrade Fm.	Cretaceous	D
25/4-6S	T1	3802-3819	Vale	Hugin Fm.	Middle Jurassic	D
25/5-2	T2	3196-3201	Frøy	Sleipner Fm.	Middle Jurassic	D
15/9-11	T1	2797-2807	Sleipner Øst	Hugin Fm.	Middle Jurassic	E
15/9-7	T3	3555-3565	Sleipner Vest	Hugin Fm.	Middle Jurassic	F
15/9-8	T1	3450-3460	Sleipner Vest	Hugin Fm.	Middle Jurassic	F
15/9-13	T2	2422-2427	Sleipner Øst	Heimdal Fm.	Paleocene	G
15/9-11	T2	2410-2432	Sleipner Øst	Heimdal Fm.	Paleocene	G
16/7-4	T1	2590-2597	Sigyn	Skagerrak Fm.	Triassic	G

TABLE 4.2. *List of source rock samples sorted by well, formation and depth. Total organic content (TOC), Pr/Ph ratio and values of vitrinite reflectance calculated from the methylphenanthrene index (MPI-1), methylphenanthrene distribution factors (F1 and F2) and methyldibenzothiophene ratio (MDR) for the investigated source rock extracts.*

Well	Source Rock Fm.	Type	Depth MD (m)	TOC (%)	Pr/Ph	%Rc (MPI-1)	%Rc ($MPDF_1$)	%Rc ($MPDF_2$)	%Rc (MDR)
15/3-3 (1)	Draupne	cuttings	4070	11.50	1.09	0.72	0.67	0.65	0.72
15/3-3 (2)	Draupne	cuttings	4095	5.40	0.90	0.73	0.65	0.64	0.79
15/3-3 (3)	Draupne	cuttings	4120	4.60	0.85	0.74	0.62	0.62	0.80
15/3-3 (4)	Draupne	cuttings	4145	6.80	0.93	0.73	0.61	0.63	0.78
15/9-18 (1)	Draupne	cuttings	3120	1.78	1.01	0.74	0.67	0.61	0.56
15/9-18 (2)	Draupne	cuttings	3135	8.23	0.98	0.68	0.69	0.60	0.56
15/9-18 (3)	Draupne	cuttings	3162.5	5.15	1.42	0.64	0.69	0.62	0.58
15/9-18 (4)	Draupne	cuttings	3185	6.01	1.60	0.63	0.63	0.55	0.58
25/7-2(1)	Draupne	core	4132.3	3.87	2.00	0.70	0.60	0.65	0.92
25/7-2(2)	Draupne	core	4149.83	3.61	2.10	0.71	0.72	0.74	0.96
25/7-2(3)	Draupne	core	4162.33	5.48	2.34	0.79	0.76	0.76	1.07
25/7-2(4)	Heather	core	4343.3	2.31	2.61	0.78	0.75	0.74	1.31
25/7-2(5)	Heather	core	4346.3	2.79	2.43	0.79	0.73	0.72	1.33
15/12-6S(1)	Heather	core	2839.6	1.09	2.37	0.69	0.75	0.65	0.58
25/4-6S	Heather	core	3713.5	2.76	2.47	0.73	0.79	0.78	0.75
25/5-2 (1)	Heather	core	3179.8	3.62	2.54	0.67	0.79	0.79	0.61
25/5-2 (2)	Heather	core	3180	1.86	2.37	0.69	0.80	0.80	0.62
15/12-6S(2)	Sleipner	core	2951.07	37.90	10.40	0.73	0.80	0.78	0.62
15/12-6S(3)	Sleipner	core	2951.55	73.00	11.00	0.75	0.81	0.80	0.62
15/12-6S(4)	Sleipner	core	2952.4	73.90	11.10	0.75	0.79	0.80	0.64
25/5-2 (3)	Sleipner	core	3210.25	46.60	7.72	0.71	0.83	0.80	0.68
25/5-2 (4)	Sleipner	core	3215.94	80.00	7.08	0.73	0.83	0.83	0.68

%Rc: calculated reflectance of vitrinite. $\%R_C$ (MPI-1): 0.6(MPI-1)+0.4; MPI-1: 1.5 (2-MP+3-MP)/(P+1-MP+9-MP) (Radke and Welte, 1983); %Rc ($MPDF_1$): -0.166+2.242 F1; F1: (2-MP+3-MP)/(2-MP+3-MP+1-MP+9-MP); %Rc ($MPDF_2$): -0.112+3.739 F2; F2: 2-MP/2-MP+3-MP+1-MP+9-MP (Kvalheim et al., 1987); $\%R_c$ (MDR)=(0.51+(0.073 MDR)), MDR= 4-MDBT/1-MDBT (Radke, 1988). Cuttings samples are from wells with water-based drilling mud.

4.5. Methods

4.5.1. Analytical Methods

The analytical methods were described in the methodology section, see details of specific techniques, methods and tools in Chapter 2.

4.5.2. Multivariate Statistics

Multivariate statistic was performed using Past version 3.25 software, after all values for each parameter were normalized to the standard deviation of the variables. Computational and graphical display of the data was carried out using hierarchical cluster analysis and principal component analysis (PCA). Hierarchical clustering was based on the unweighted

pair-group average (UPGMA) algorithm method. The similarity-association matrix was computed using Euclidean distances. Multivariate statistical analyses (MVA) were performed using four data sets. The first data set comprised the average $\delta^{13}C$ values of Pr and Ph, and *n*-alkanes in the ranges from C_{26}-C_{29} and from C_{10}-C_{14} together with the ratio of Pr to Ph and ratios of heterocyclic and non-heterocyclic aromatic compounds in the range of molecular weight from 178 to 198 (Table 4.3), measured for 15 oil and condensate samples.

TABLE 4.3. *Average $\delta^{13}C$ values of n-alkanes (>C_{10}), Pr and Ph and source and depositional environment-related ratios based on composition of regular isoprenoids (Pr and Ph) and heterocyclic and polycyclic aromatic hydrocarbons.*

	*Average $\delta^{13}C$ values (‰)				Heterocyclic & Polycyclic Aromatic Hydrocarbon ratios								
Well	*Pr/ Ph	*n*-alkanes (C_{10}-C_{14})	*n*-alkanes (C_{26}-C_{29})	Pr & Ph	*1	*2	*3	*4	*5	*6	7	8	9
15/5-5	0.98	-30.8	-31.4	-31.1	0.51	1.60	0.73	0.44	0.27	0.29	0.80	0.41	2.15
15/9-19A	0.67	-29.8	-30.9	-27.4	0.87	1.78	0.79	0.48	0.27	0.25	0.73	0.42	2.46
15/9-11 T1	1.38	-27.8	n.d.	-27.4	0.95	0.71	0.71	0.32	0.45	0.23	0.63	0.37	2.45
15/9-13 T2	3.98	-25.9	n.d.	n.d.	0.24	0.11	0.21	0.08	0.72	0.20	0.79	0.52	2.49
15/12-5	1.45	-28.7	-29.8	-28.8	0.26	0.80	0.38	0.29	0.37	0.34	0.77	0.43	2.11
15/12-6S	1.41	-29.1	-30.1	-29.1	0.25	0.86	0.41	0.31	0.36	0.34	0.76	0.41	2.46
25/8-11	2.07	-28.5	-29.6	-28.3	0.17	0.61	0.27	0.21	0.34	0.45	0.71	0.35	1.87
15/9-7	2.18	-27.5	-27.4	-28.2	0.18	0.19	0.18	0.11	0.57	0.31	0.86	0.64	2.63
15/9-8	2.53	-27.4	-27.6	-27.7	0.18	0.18	0.17	0.10	0.57	0.32	0.78	0.55	2.85
15/9-11 T2	3.49	-26.0	n.d.	n.d.	0.20	0.10	0.14	0.06	0.65	0.29	0.71	0.50	2.46
15/9-13 T1	1.46	-29.7	n.d.	-30.1	0.30	0.67	0.41	0.24	0.36	0.39	0.74	0.40	1.97
16/7-4	3.84	-25.7	-26.8	-25.7	0.47	0.25	0.30	0.16	0.65	0.19	0.88	0.71	3.32
25/2-13	3.14	-28.6	-28.0	-28.9	0.08	0.32	0.11	0.11	0.34	0.55	0.70	0.34	1.58
25/4-6S	2.94	-27.8	-29.0	-28.8	0.11	0.41	0.15	0.13	0.32	0.55	0.72	0.35	1.81
25/5-2	2.39	-28.4	-28.8	-28.6	0.14	0.38	0.15	0.15	0.39	0.46	0.69	0.35	2.43

*1: MDBTs/MPs; *2: MDBTs/MDBFs; *3: 4-MDBT/P; *4: MDBTs/Y; *5: MDBFs/Y; *6: MFs/Y, Y=∑MDBTs+MDBFs+MFs; 7: 1-MP/9-MP; 8: 1,7-DMP/X, X= (1,3-+3,9-+2,10-+3,10-DMP); 9: 1,2,5-TMN/1,2,7-TMN. Pr/Ph: pristane/phytane ratio; MDBTs, methyldibenzothiophenes; MPs, methylphenanthrenes; MDBFs, methyldibenzofurans; MFs, methylfluorenes, 4-MDBT, 4-methyldibenzothiophene; P, phenanthrene; DMP, dimethylphenantrene; TMN, trimethylnaphthalene. Standard deviations of $\delta^{13}C$ for all the compounds reported are <0.5‰. n.d. - not determined. Parameters used for MVA are marked with (*).

The second data set included Mango's ratios (Mango, 1987, 1990) and the $\delta^{13}C$ values of gasoline-range hydrocarbons listed in Table 4.4. The third data set comprised the concentrations of dibenzothiophene, dibenzofuran, phenanthrene and their methyl and dimethyl homologs together with the average $\delta^{13}C$ values of *n*-alkanes, in the selected carbon intervals, and of Pr and Ph (Appendix Table 1). The fourth data set comprised the concentrations of C_7 hydrocarbons and $\delta^{13}C$ values of *n*(C_5-C_9)-alkanes, branched and cyclic alkanes (Appendix Table 2).

TABLE 4.4. *Average $\delta^{13}C$ values of gasoline-range hydrocarbons and Mango's parameters.*

	*Average $\delta^{13}C$ values (‰)												
Well	*n*-alkanes (C_5-C_9)	Branched alkanes	Cyclic alkanes	*1	*2	*3	*4	*5	*6	7	8	9	10
15/5-5	-31.8	-29.9	-29.8	1.01	0.35	0.26	0.40	0.25	0.29	0.29	0.08	0.08	0.23
15/9-19A	-32.4	-29.0	-27.7	1.02	0.29	0.29	0.42	0.22	0.22	1.96	1.17	0.85	0.19
15/9-11 T1	-27.8	-25.9	-25.3	1.13	0.42	0.23	0.35	0.17	0.18	1.13	0.69	1.02	0.47
15/9-13 T2	-26.0	-25.4	-24.7	1.20	0.46	0.21	0.33	0.14	0.16	1.41	0.83	1.56	2.01
15/12-5	-28.1	-26.3	-26.7	1.06	0.41	0.23	0.36	0.16	0.20	1.47	0.63	0.95	0.17
15/12-6S	-28.5	-26.8	-27.1	1.07	0.41	0.23	0.36	0.17	0.21	1.06	0.55	0.81	0.16
25/8-11	-28.5	-27.7	-26.6	1.07	0.41	0.26	0.33	0.20	0.20	0.28	0.37	0.49	0.19
15/9-7	-26.3	-25.3	-25.5	1.19	0.49	0.19	0.33	0.11	0.14	2.17	1.08	2.41	0.24
15/9-8	-25.9	-25.0	-25.1	1.20	0.49	0.19	0.32	0.11	0.14	2.27	1.03	2.37	0.22
15/9-11 T2	-25.6	-25.0	-24.7	1.22	0.48	0.20	0.32	0.14	0.17	0.85	0.60	1.26	0.37
15/9-13 T1	-	-	-	-	-	-	-	-	-	-	0.54	1.43	0.15
16/7-4	-25.3	-24.9	-24.9	1.24	0.50	0.16	0.33	0.16	0.20	0.33	0.29	0.78	0.28
25/2-13	-28.2	-27.4	-26.1	1.09	0.48	0.25	0.27	0.14	0.16	1.08	0.38	0.67	0.21
25/4-6S	-27.3	-26.7	-25.8	1.09	0.46	0.24	0.30	0.14	0.16	1.78	0.63	1.06	0.19
25/5-2	-28.4	-27.2	-26.0	1.08	0.47	0.22	0.32	0.14	0.19	1.15	0.41	0.76	0.20

(*1) K_1; (*2) N_1^6/X; (*3) P_1/X; (*4) P_2+ P_3+N_1^5/X; (*5) 2MH+3MH/Y; (*6) DMP+DMCP/Y; (7) Bz/3-MP; (8) Tol/MCH; (9) Tol/*n*-hep; (10) FI: *n*-C_{10}/Σ(*n*-C_{16}+*n*-C_{25}) (Dzou and Hughes, 1993). Where K_1: (2-MH+2,3-DMP)/(3-MH+2,4-DMP); P_1: *n*-heptane, P_2: 2-MH+3-MH, P_3: 2,2-DMP+2,3-DMP+2,4-DMP+3,3-DMP+EP+2,2,3-TMB, N_1^5: ECP+1,trans-2-DMCP, N_2^5: 1,1-DMCP+1,trans-3-DMCP+1,cis-3-DMCP, N_1^6: MCH+Tol (Mango (1987,1990)). ∑DMP+DMCP: (2,2-DMP+2,3-DMP+2,4-DMP+3,3-DMP+1,1-DMCP+1,cis-3-DMCP+1,trans-3-MCP+1,trans-2-DMCP). MH, methylhexane; CH, cyclohexane; MCH, methylcyclohexane; DMP, dimethylpentane; DMCP, dimethylcyclopentane; EP, ethylpentane, TMB, trimethylbutane; Tol, toluene. X: P_1+P_2+P_3+N_1^5+N_2^5+N_1^6, Y: 2-MH+3-MH+∑(DMP+DMCP)+MCH+Tol. Standard deviations of $\delta^{13}C$ values for all the compounds reported are <0.5‰. Parameters used for MVA are marked with (*). Data of LHCs for altered oil from well 15/9-13T1 were excluded for MVA.

4.6. Results and Discussion

4.6.1. Geochemistry of Jurassic Source Rock Extracts

A total of 24 cuttings and core source rock extracts from the Upper Jurassic Draupne and Heather formations and the Middle Jurassic Sleipner Formation (Table 4.2) of six wells located in the SVG (Fig. 4.1c and d) were analyzed in this study. These wells are near but not directly located in the pods of active source rocks as these areas are sparsely drilled (Justwan et al., 2006a,b). Vitrinite reflectance values calculated (%R_c) from the methylphenanthrene index, MPI-1 (Radke and Welte, 1983) and methylphenanthrene distribution factors ($MPDF_1$ and $MPDF_2$) (Kvalheim et al., 1987) suggest that most source rock samples cover a range from early to peak oil generation window (0.6-0.8% R_o) (Table 4.2). However, analyzed source rock samples from well 25/7-2 show the highest values of %R_c from the methyldibenzothiophene ratio, MDR (Radke, 1988) (Table 4.2), which indicate a late stage of oil generation. Similarly, values of measured vitrinite reflectance (%R_o) range from 0.9 to 1.2% in well 25/7-2 (Norwegian Petroleum Directorate, 2019b). Source rock extracts were evaluated using the molecular and $\delta^{13}C$ data of *n*-alkanes and regular isoprenoids (Pr, Ph) together with the molecular composition of heterocyclic and polycyclic

aromatic hydrocarbons, such as the alkyl homologs of naphthalene (N), phenanthrene (P), fluorene (F), dibenzofuran (DBF) and dibenzothiophene (DBT).

4.6.1.1. Normal and Isoprenoid Alkanes

Source rock extracts from the Upper Jurassic Draupne Formation (wells 15/3-3 and 15/9-18), which cover a maturity range (0.6-0.8% R_o), show low CPI (0.95-1.15) and a unimodal distribution with a predominance of *n*-C_{16} to *n*-C_{20} alkanes (Fig. 4.2b), which is consistent with input from marine phytoplankton (Blumer et al., 1971). Their low values of Pr/Ph ratio (0.8-1.4) indicate deposition under anoxic to dysoxic conditions. The upper Draupne Formation extracts from well 15/9-18 show a slight predominance of even-numbered *n*-alkanes (C_{22}-C_{26}) typical of calcareous source facies (Moldowan et al., 1985) (Fig. 4.2b). Nevertheless, the *n*-alkanes of source rock extracts from the lower Draupne Formation in well 25/7-2 (0.9-1.0% R_o), located west of the Utsira basement high, tend to exhibit a bimodal distribution biased toward shorter chain lengths (*n*-C_{15} to *n*-C_{20}). Similarly, source rock extracts from the Upper Jurassic Heather Formation in well 25/5-2 (0.7-0.8% R_o) exhibit a bimodal *n*-alkane distribution with maxima at *n*-C_{17} and *n*-C_{27} and a bias toward lower chain lengths, which can be interpreted as a sign of mixed input of marine and terrigenous source material (Fig. 4.2b). In comparison with extracts from the upper Draupne Formation, extracts from the Heather Formation and lower Draupne Formation have higher Pr/Ph ratios (2.0-2.6) that are interpreted to represent more oxic depositional conditions. In contrast, the Middle Jurassic Sleipner Formation (0.6-0.8% R_o) shows higher CPI values (1.2-1.4) and a distribution of *n*-alkanes biased toward higher chain lengths (*n*-C_{21} to *n*-C_{30}) with maxima at *n*-C_{25} (Fig. 4.2b). Abundant long chain *n*-alkanes (C_{27}, C_{29} or C_{31}) (Fig. 4.2b) are consistent with waxes of terrigenous plants (e.g., Collister et al., 1994). In addition, Middle Jurassic Sleipner Formation extracts show an odd-over-even carbon number predominance of *n*-(C_{21}-C_{25}) alkanes (Fig. 4.2b), which can be related to aquatic macrophytes (Filley et al., 2001), suggesting that the Sleipner Formation coals may have contributions from both terrigenous and aquatic plants. The highest ratios of Pr/Ph (7-11) (Table 4.2) and Pr/*n*-C_{17} (4-12) (Fig. 4.3a) also support their terrigenous source and highly oxic depositional conditions.

The short chain *n*-alkanes (C_{15}-C_{19}), which are generally derived from both bacterial and algal biomass (Gelpi et al., 1970; Cranwell et al., 1987), tend to show the highest carbon isotopic variations among source rock extracts (Figs. 4.3b, 4.4a-d). A particularly good differentiation among Jurassic source rock extracts from the Type-II kerogen rich Draupne, Heather and Sleipner formations is achieved with a cross plot of the average $\delta^{13}C$ values of *n*-(C_{15}-C_{19}) alkanes and the average $\delta^{13}C$ values of Pr and Ph (Fig. 4.3b).

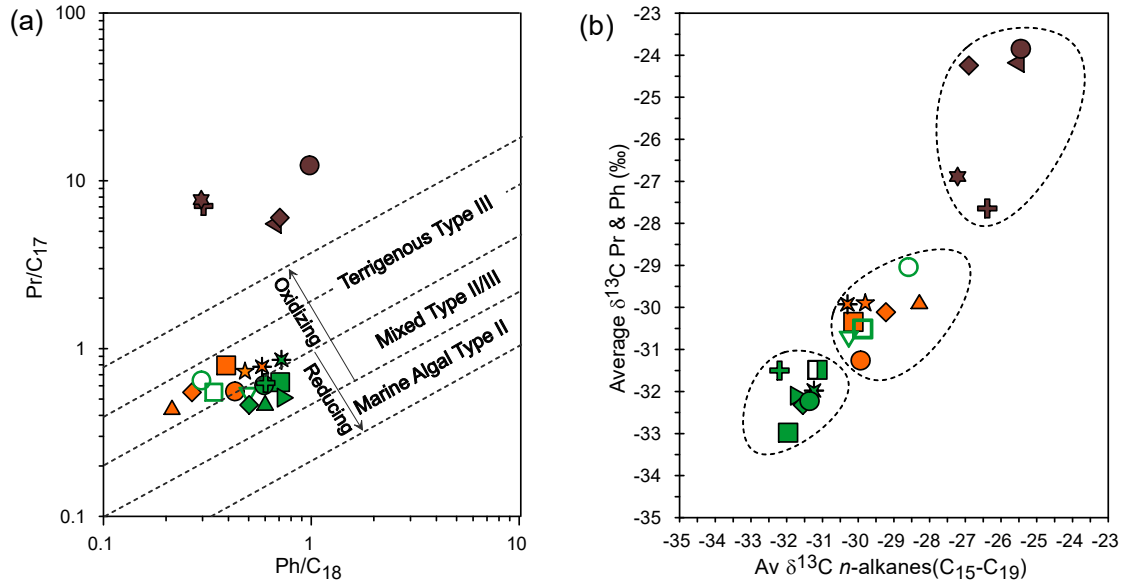

FIGURE 4.3. *(a) Plot of Pr/n-C_{17} versus Ph/n-C_{18}; (b) average $\delta^{13}C$ values of Pr and Ph versus average $\delta^{13}C$ values of n-alkanes (C_{15}-C_{19}) for source rock extracts from the SVG. Symbol color indicates the source rock formations as follows: green-the Draupne Fm; orange-the Heather Fm; brown-the Sleipner Fm. (For interpretation of the references to color in this figure legend, the reader is referred to the web version of this article).*

Extracts from the upper Draupne Formation, enriched in Type-II kerogen (wells 15/3-3 and 15/9-18), have the most negative $\delta^{13}C$ values of Pr and Ph (-32 to -33‰), and *n*-alkanes >C_{14} (-30 to -36‰) that show a ^{13}C-depletion with increasing carbon number (Fig. 4.4a). Extracts from the lower Draupne Formation (well 25/7-2), however, exhibit more positive $\delta^{13}C$ values of *n*-alkanes (-28 to -31‰) and Pr and Ph (-30 to -31‰) that tend to be comparable to those from most Heather Formation samples (Fig. 4.4b and c). The similarities in the $\delta^{13}C$ data of individual hydrocarbons for both lower Draupne and Heather formation extracts are consistent with a slight variability in organic facies. Nonetheless, some Heather Formation extracts from wells 25/5-2 (3180 m) and 25/7-2 show ^{13}C-depletion of *n*-alkanes (>C_{21}) up to 4‰ (Fig. 4.4c).

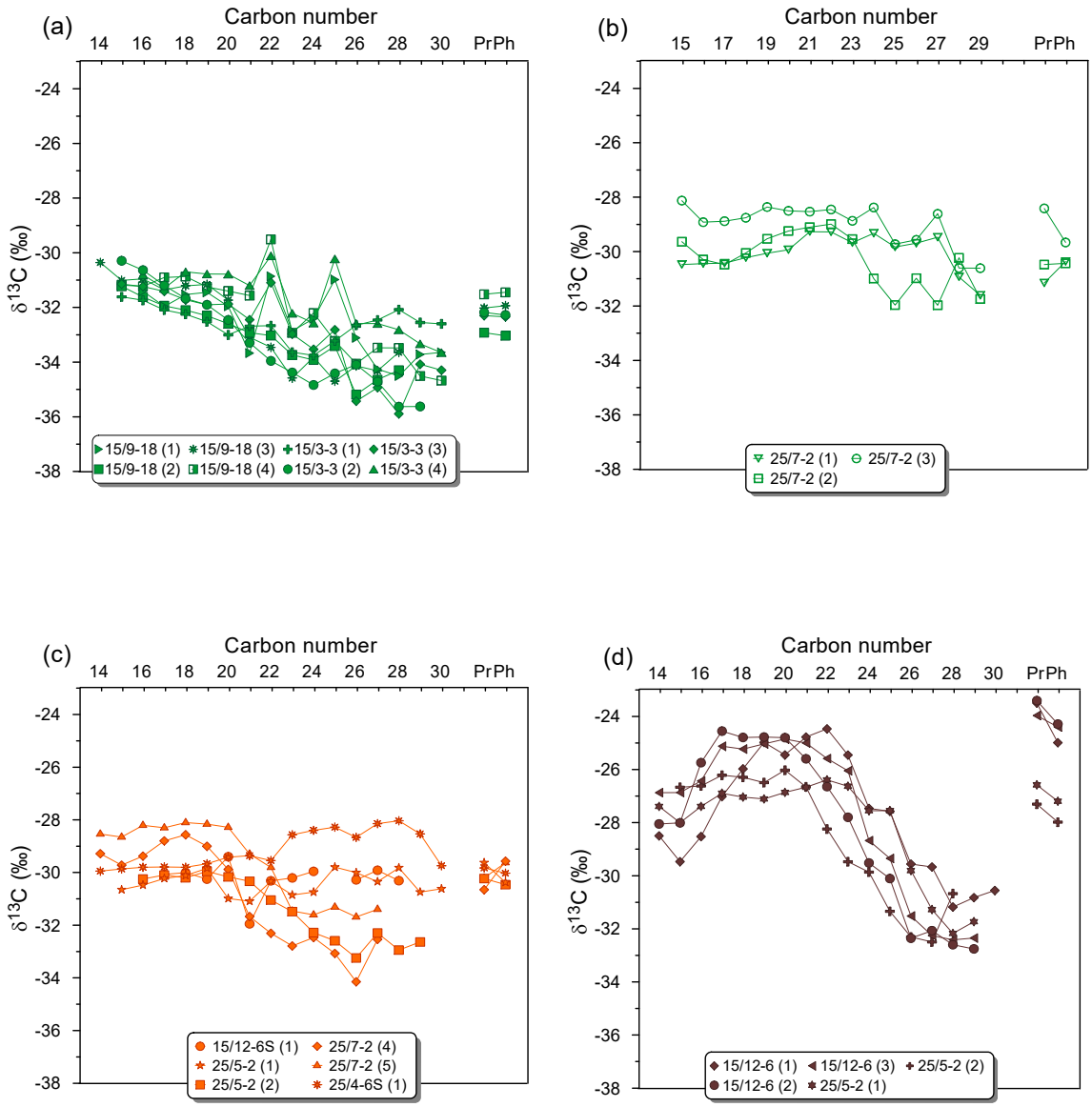

FIGURE 4.4. *$\delta^{13}C$ values of individual n-alkanes, Pr and Ph for source rock extracts from (a) the upper Draupne Fm.; (b) the lower Draupne Fm.; (c) the Heather Fm. and (d) the Sleipner Fm.*

The *n*-alkanes of Middle Jurassic coaly sources (40-80% TOC) are the most enriched in ^{13}C and exhibit a singular concave-down pattern of $\delta^{13}C$ values *versus* carbon number (Fig. 4.4d). This pattern shows a ^{13}C-enrichment with carbon numbers from C_{15} to C_{20} and even to C_{23}, together with a strong ^{13}C-depletion from C_{21}-C_{27} or from C_{24}-C_{27}, while the longer-chain *n*-alkanes tend to show no significant isotopic variations (Fig. 4d). In addition, the

Middle Jurassic Sleipner Formation shows the most positive $\delta^{13}C$ values of Pr and Ph (-23 to -28‰) (Figs. 4.3b, 4.4d).

4.6.1.2. Heterocyclic and Polycyclic Aromatic Hydrocarbons

The concentration of alkylnaphthalenes can be controlled by a combination of source and maturation effects (Alexander et al., 1985; Radke et al., 1994). The fairly broad variations obtained in the relative concentrations of agathalene (1,2,5-TMN) and 1,6-DMN between extracts from source rocks of Middle and Late Jurassic age (Fig. 4.5a and b), which have comparable thermal maturity (0.6-0.8 $\%R_o$), suggest that their abundance can be mainly related to terrigenous higher plant material. Coaly source extracts of the Middle Jurassic Sleipner Formation have higher relative concentrations of cadalene, 1,2,5-TMN and 1,6-DMN compared to Upper Jurassic Draupne and Heather formation extracts, showing a predominance of cadalene. In contrast, shales of the Heather and lower Draupne formations exhibit a dominance of 1,6-DMN over cadalene and 1,2,5-TMN (Fig. 4.5a). The abundance of phenanthrene and alkylphenanthrene have been used to differentiate aquatic *vs*. terrigenous input (e.g., Budzinski et al., 1995, Fan et al., 1990). In the Viking Graben, Jurassic source rock extracts with small maturity variations exhibited variations in the phenanthrene and alkylphenanthrene content (Fig. 4.6a and b). Phenanthrene and methylhomologs show the lowest relative concentrations in source rock extracts from the upper Draupne Formation, whereas the Heather and lower Draupne formations have the highest relative concentrations (Fig. 4.6a). Although coals of the Sleipner Formation in the Vestland Group have terrigenous dominated sources, they have lower abundances of phenanthrene series compounds compared to shales of the Heather and lower Draupne formations (Fig. 4.6a). A low relative abundance of phenanthrene was also found in coal samples by Mastalerz et al. (1997). In addition, Middle Jurassic coals of the Sleipner Formation show a higher content of 1-MP relative to other methylphenanthrene isomers (Fig. 4.6a and b), which is consistent with terrigenous sources (Heppenheimer et al., 1992). In contrast, Upper Jurassic shales of the lower Draupne and Heather formations have higher content of 9-MP (Fig. 4.6a and b) and show lower 1-MP/9-MP ratios (0.7-0.8) compared with Middle Jurassic coals (1.0-1.5).

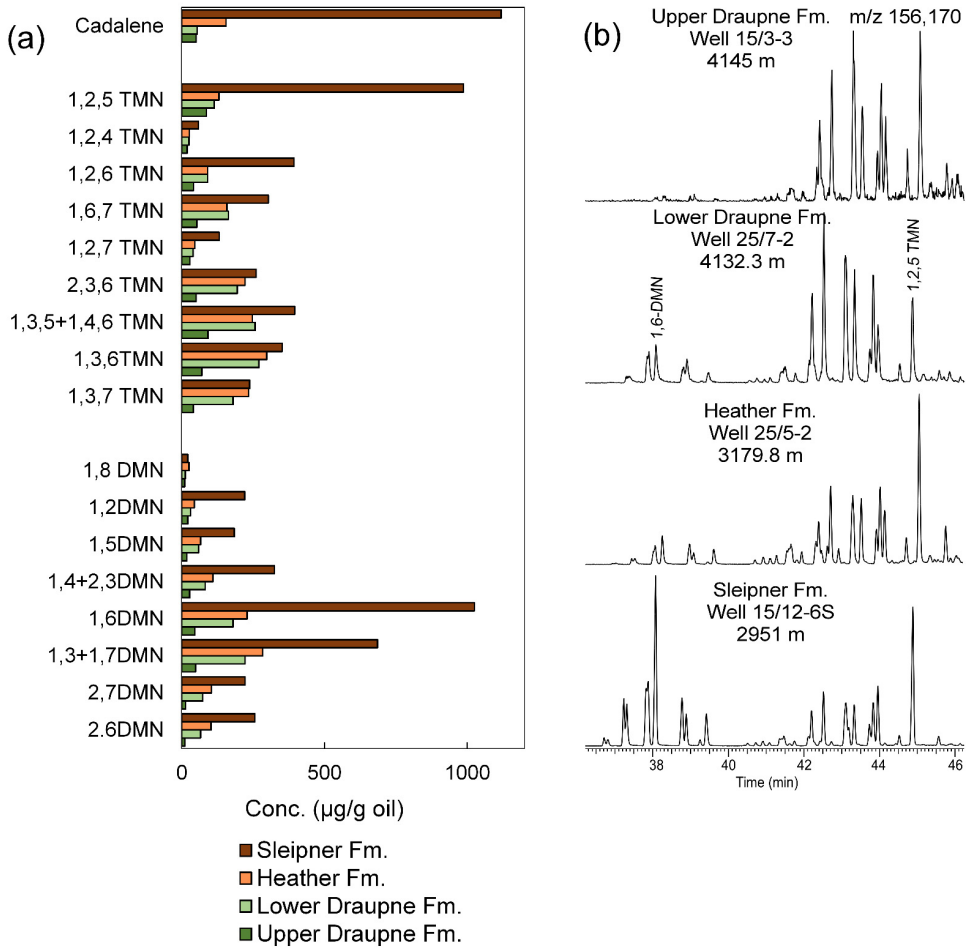

FIGURE 4.5. *(a) Relative concentration of dimethyl-naphthalene (DMN), trimethyl-naphthalene (TMN) isomers and cadalene; (b) GC-MS extracted ion profiles of alkylhomologs of naphthalenes (m/z 156+186; DMNs and TMNs) for source rock extracts.*

Similarly, higher ratios of 1,7-DMP to "X" ("X" is defined as the sum of 1,3+2,10+3,9+3,10-DMP) were found in Middle Jurassic coals (0.5-1.0) compared with those in Upper Jurassic shales (0.3-0.5). Abundant 1,7-DMP has also been associated with resins (Simoneit et al., 1986). Although 1-MP/9-MP and 1,7-DMP/"X" ratios were useful to discriminate Middle Jurassic coals from Upper Jurassic shales, they were not able to be used to differentiate among Upper Jurassic source rocks. Another alkylphenanthrene with high relative abundance in coals of the Sleipner Formation is retene (1-methyl-7-isopropyl phenanthrene) (Fig. 4.6a), which has been related to input from coniferous plants (e.g., Simoneit, 1977; Simoneit et al., 1986). Although Type III-kerogen rich source rocks of Upper

Jurassic age (the Heather and lower Draupne formations) show isotopic similarities (Fig. 4.4b and c), the relative abundances of higher plant biomarkers (retene and cadalene) were useful to distinguish them. Compared with lower Draupne formation extracts, higher relative concentrations of cadalene and retene were identified in Heather Formation extracts (Figs. 4.5a, 4.6a).

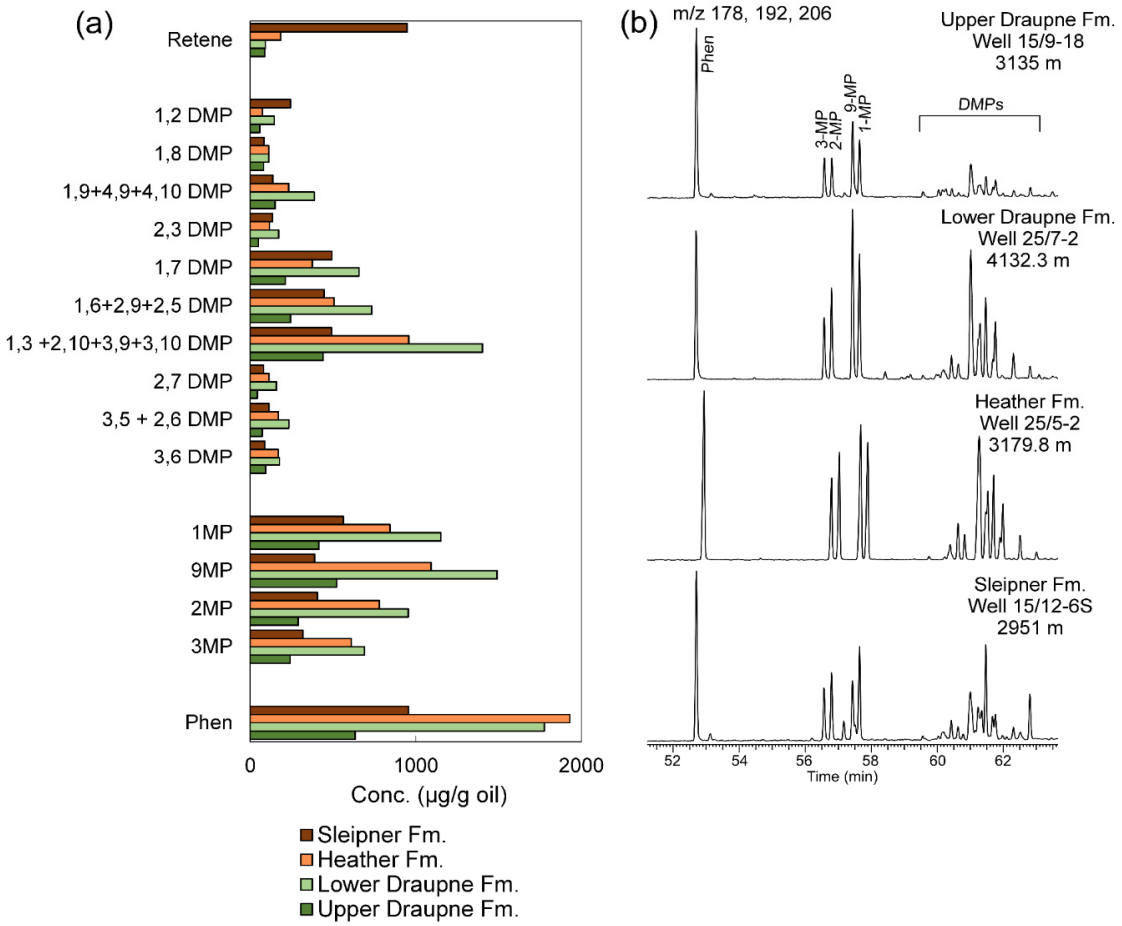

FIGURE 4.6. *(a) Relative concentration of phenanthrene (Phen), methylphenanthrene isomers (MP), dimethylphenanthrene isomers (DMP) and retene; (b) GC-MS extracted ion profiles of alkylhomologues of phenanthrenes (m/z 178+192+206; Phen, MPs and DMPs) for source rock extracts.*

In contrast to PAHs, the heterocyclic aromatic hydrocarbons were suitable for clearly distinguishing Upper Jurassic source rocks with different OM source types, depositional environment and lithology. The contents of methylfluorenes (MFs), methyldibenzofurans (MDBFs) and methyldibenzothiophenes (MDBTs) were plotted in a ternary diagram (Fig.

4.7a), which clearly discriminates source rock extracts from the Draupne, Heather and Sleipner formations. Extracts from the Draupne Formation have the highest amount of MDBTs and the lowest content of MDBFs, whereas Sleipner Formation extracts show a pronounced predominance of MDBFs and the lowest amount of MDBTs (Fig. 4.7a). Comparable relative abundances of MFs were found in extracts from both the Heather and Sleipner formations, which tend to be higher than those in Draupne Formation extracts (Fig. 4.7a).

A very good differentiation among all Jurassic source rock extracts was obtained using a plot of the ratio alkyl-DBTs to alkyl-DBFs *vs*. Pr to Ph ratio (Fig. 4.7b). This plot clearly discriminates the different organic facies into the Draupne Formation (the Type-III and Type-II kerogen rich facies). In addition, a plot of 3-+2-MDBT/ 4-MDBT *vs*. 1-MDBT/ 4-MDBT (Fig. 4.7c) allows the differentiation between siliciclastic and calcareous source facies of the Type-II kerogen rich Draupne Formation (0.6-0.8% R_o) in wells 15/3-3 and 15/9-18. Extracts from the upper Draupne Formation in well 15/9-18, between the Sleipner Øst and Vest fields (Fig. 4.1c), also showed a distinctive "V" shape distribution pattern of MDBTs (4-methyl>2-+3-methyl<1methyl) and a dominance of the even carbon numbers from *n*C_{22} to *n*C_{27}-alkanes (Fig. 4.7c), indicating calcareous source facies (Hughes, 1984; Moldowan et al., 1985). In contrast, extracts from the Draupne Formation in well 15/3-3 showed a stair-step distribution pattern of MDBTs (4-methyl>2-+3-methyl≥1methyl) (Fig. 4.7c), which are consistent with those of siliciclastic shales (Hughes, 1984). Source rock extracts show an increasing relative content of MDBTs together with a decreasing relative content of MDBFs from Middle Jurassic to Upper Jurassic formations (Fig. 4.7d). The variation in the amount of sulfur- and oxygen-containing PAHs indicates a trend of decreasing oxygenation during deposition of source rocks, which is associated with an increasing input of marine source material upwards. Justwan et al. (2006a) reported a decrease in the ratios of Pr/Ph, C_{34}/C_{35} homohopanes, C_{29}/C_{27} regular steranes and C_{30} moretane/C_{30} hopane for source rocks from Middle Jurassic to the Upper Jurassic age.

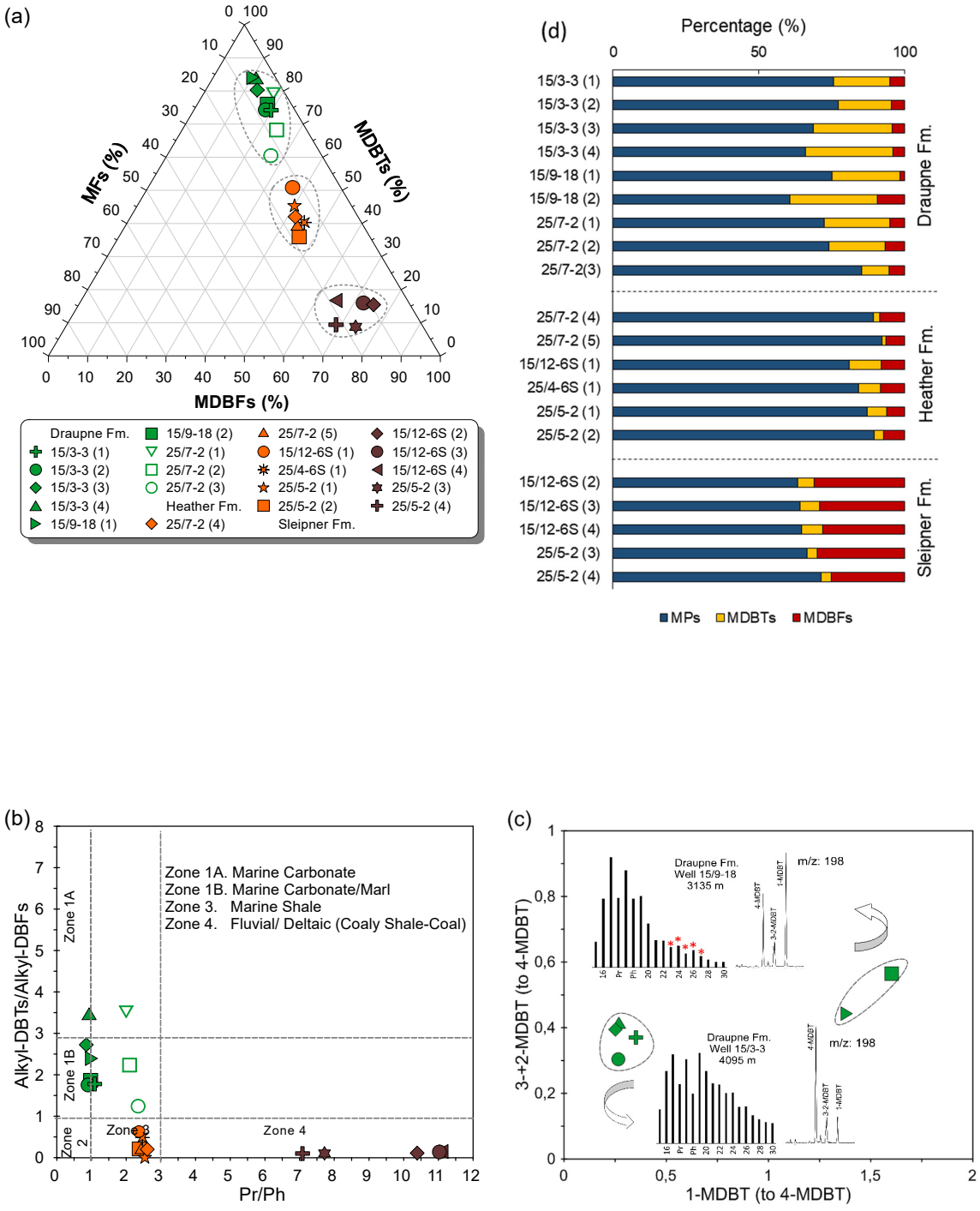

FIGURE 4.7. *(a) Ternary plot of the content of methyldibenzothiophenes (MDBTs), methyldibenzofurans (MDBFs) and methylfluorenes (MFs); (b) plot of alkyl-DBTs to alkyl-DBFs versus Pr to Ph ratio (Radke et al., 2000); (c) plot of 3+2-MDBT/4-MDBT versus 1-MDBT/4-MDBT ratios, showing a distinction between calcareous and siliciclastic source facies of the Draupne Fm. GC-MS extracted ion profiles of MDBTs (m/z 198) and GC for extracts of the Draupne Fm. (d) Bar plot of the relative content of MPs, MDBTs and MDBFs.*

4.6.2. Geochemistry of Oils

4.6.2.1. Assessment of Thermal Maturity

Maturity contrasts between light- and heavy-ends are useful to assess mixtures of petroleum. For that, various maturity parameters based on PAHs, biomarkers and light hydrocarbons were examined in this study. Thermal maturity parameters based on the distributions of methylhomologs of P, N and DBT are useful for establishing maturity levels, especially in late mature crude oils and condensates (e.g., Radke et al., 1982, Radke and Welte, 1983, Alexander et al., 1985, Radke et al., 1986). $\%R_c$ from the MDR shows the lowest values (0.58% R_o) for the oil sample from the Vølve field (Table 4.5), which corresponds to an early mature oil-expulsion phase. Equivalent vitrinite reflectance values of 0.55% R_o were reported for the Vølve oil using maturity data from des-methylsteranes and triterpanes (Isaksen et al., 1998). Moreover, $\%R_c$ values using the MPI-1 and MDR indicate that most analyzed oils were generated in the main oil-generative window (0.7-0.8% R_o) (Table 4.5), distinguishing higher maturity oils from the Balder, Vale and Lille Frøy fields in the northern half of the SVG study area (0.8-0.9% R_o). The slight northward increase of thermal maturity can also be supported by higher values of 3-methylphenanthrene/retene (3MP/Ret) and trimethylnaphthalene ratios (TNR-1 and TNR-2) (Table 4.5). In addition, $\%R_c$ values from MPI-1, MPDF1 and MPDF2 (Table 4.5) indicate a higher maturity for the Sleipner Øst oil from well 15/9-13T1 (~0.9% R_o) relative to the Varg oils from wells 15/12-5 and 15/12-6S (0.7-0.8% R_o). The oil sample from well 15/9-13T1 has higher values of triaromatic steroid (TA/TA(I+II)) and 3MP/Ret ratios (Table 4.5) that may further support the contention of higher maturity.

Biomarker ratios for assessing maturity in mixtures of oils are not reliable because biomarker have different orders of magnitude of concentrations in end member oils and their concentrations vary greatly with maturation (Li et al., 1995, Jiang and Li, 2002 and Wilhelms and Larter, 2004). However, they are useful to detect oil charges generated at the early stage of oil generation (Wilhelms and Larter, 2004). Biomarker maturity parameters based on sterane isomerization and even those of mono- and triaromatic steroids suggest that all hydrocarbons in the SVG are in the main stage of oil generation (Table 4.5). In addition, the 22S/(22S+22R) ratios for 17α-homohopanes have reached endpoint values (Table 4.5), even

in the oil sample of early maturity sourced from a Type-IIS kerogen in the Vølve field (well 15/9-19A) (Isaksen et al., 1998). Köster et al. (1997) reported that high values of 22S/(22S+22R) ratio in crude oils generated from low mature, organic sulfur-rich carbonate-marlstone source rocks may be controlled by the release of sulfurized hopanoids from the kerogen rather by isomerization during early maturation.

Mango (1987, 1990); BeMent et al. (1995); Chung et al. (1998) proposed the ratio 2,4-DMC$_5$/2,3-DMC$_5$ as a reliable maturity indicator that is independent of the source. The average generation/expulsion temperatures estimated using the 2,4-DMC$_5$/2,3-DMC$_5$ ratio together with the equation of Mango (1997), which include the distribution of calculated temperatures by BeMent et al. (1995), indicate an early oil-generation stage for oils from the Glitne and Vølve fields (Fig. 4.8a, Table 4.5).

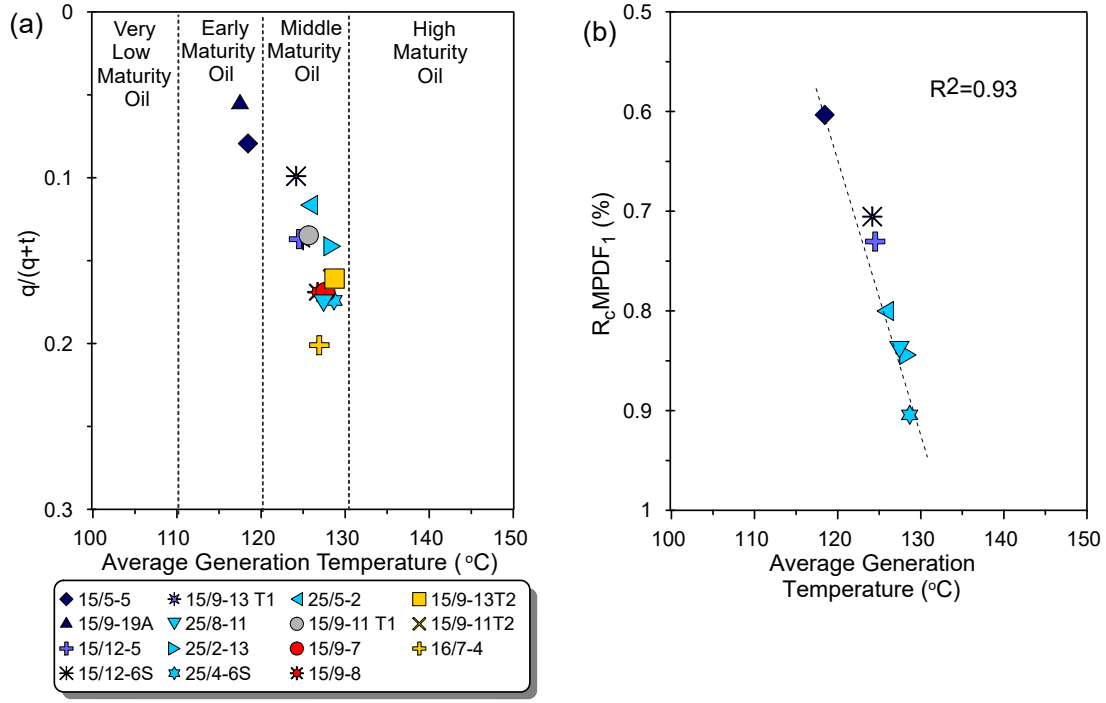

FIGURE 4.8. *(a) Plot of generation temperature versus q/(q+t) C$_7$ isoheptanes ratio, described as: q=(2,2-DMP+3,3-DMP), t=(2,4-DMP+2,3-DMP+3-EP) (Hunt et al., 1980), and Generation Temperature (°C)=140+15(ln[2,4-DMP/2,3-DMP]) (BeMent et al., 1995; Mango, 1997)., where q: quaternary, t: tertiary carbon species, DMP: dimethylpentane, EP: ethylpentane. (b) Vitrinite reflectance values estimated from methylphenanthrene distribution factor, F1 (%R$_{cMPFD1}$) vs. the average generation temperature for oils. %R$_{c(MPDF1)}$: -0.166+2.242F1, F1:(2-MP+3-MP)/(2-MP+3-MP+1-MP+9-MP), where MP: methylphenanthrene. Good linear correlations were obtained using mixed oils derived from Upper Jurassic source rocks.*

TABLE 4.5. *Thermal maturity of SVG oils and condensates from molecular ratios of light hydrocarbons, biomarkers and heterocyclic and polycyclic aromatic hydrocarbons.*

	Light Hydrocarbons					Biomarkers							PAHs				
Wells	1	2	3	4	5	6	7	8	9	10	11	12	13	14	15	16	17
15/5-5	1.03	1.24	0.13	0.24	0.10	0.42	0.61	0.58	11.19	19.25	0.41	0.64	0.66	0.69	0.59	0.53	1.72
15/9-19A	1.23	1.28	0.09	0.22	0.03	0.45	0.58	0.60	13.81	8.82	0.50	0.71	0.58	0.72	0.71	0.65	1.83
15/9-11 T1	0.86	1.34	0.16	0.38	0.08	0.49	0.58	0.60	7.83	14.76	0.55	0.73	0.61	0.73	0.75	0.68	n.d.
15/9-13 T2	0.74	1.26	0.19	0.47	0.10	n.d.	n.d.	n.d.	n.d.	n.d.	0.68	0.83	0.70	0.76	0.88	0.83	1.85
15/12-5	0.82	1.14	0.21	0.36	0.12	0.46	0.57	0.59	n.d.	18.59	0.61	0.74	0.68	0.77	0.73	0.67	2.28
15/12-6S	0.84	1.17	0.20	0.35	0.12	0.40	0.53	0.59	12.81	18.67	0.61	0.74	0.67	0.77	0.71	0.65	2.00
25/8-11	0.97	1.58	0.33	0.43	0.17	0.51	0.61	0.54	12.75	30.36	0.71	0.79	0.81	0.81	0.82	0.74	6.90
15/9-7	0.64	1.17	0.19	0.44	0.10	0.50	0.58	0.59	20.47	18.80	0.70	0.82	0.72	0.77	0.83	0.78	0.86
15/9-8	0.62	1.17	0.18	0.41	0.10	0.50	0.58	0.59	14.97	16.05	0.70	0.82	0.73	0.77	0.83	0.77	0.76
15/9-11 T2	0.67	1.23	0.18	0.47	0.10	0.44	0.51	0.61	12.64	14.53	0.62	0.81	0.75	0.71	0.85	0.76	0.76
15/9-13 T1	0.58	1.02	n.d	0.37	0.13	0.44	0.55	0.56	15.83	32.76	0.72	0.75	0.77	0.86	0.91	0.87	6.77
16/7-4	0.62	1.23	0.18	0.42	0.10	0.39	0.48	0.60	26.37	9.78	0.50	0.73	n.d.	0.72	0.72	0.67	2.25
25/2-13	0.71	1.24	0.17	0.46	0.15	0.44	0.58	0.53	15.57	60.19	0.83	0.91	0.87	0.81	0.85	0.77	10.87
25/4-6S	0.78	1.38	0.28	0.47	0.15	0.52	0.59	0.55	n.d.	41.80	0.86	0.90	0.84	0.84	0.89	0.80	8.50
25/5-2	0.67	1.04	0.18	0.39	0.11	0.45	0.59	0.54	25.34	n.d.	0.71	0.87	0.68	0.80	0.80	0.73	2.49

(1) V= C_7 paraffins/naphtalenes; (2) J= (2-MH+3-MH)/(1,2(*cis*+*trans*)-+1,3(*cis*+*trans*)-DMC5); (3) 2,2-DMC_4/2,3-DMC_4; (4) 2,4-DMC_5/2,3-DMC_5, (5) 1,1-$DMCyC_5$/∑$DMCyC_5$; (6) 20S= 20S/(20S+20R) ratio for C_{29}-ααα steranes; (7) ββ= αββ/(ααα+αββ) ratio for C_{29}-steranes; (8) 22S= 22S/(22S+22R) for C_{31}-homohopanes; (9) %MA= MA(I)/MA(I+II), where MA(I): C_{21}+C_{22} monoaromatic steroids and MA(II): C_{27}-C_{29} monoaromatic steroids; (10) %TA= TA(I)/TA(I+II), where TA(I): C_{20} and C_{21} triaromatic steroids and TA(II): C_{26}-C_{28} (20S+20R) triaromatic steroids; (11) TNR-1= (2,3,6-TMN)/(1,3,5-TMN+1,4,6-TMN); (12) TNR-2= (1,3,7-TMN+2,3,6-TMN)/(1,3,5-TMN+1,3,6-TMN+1,4,6-TMN); (13) $\%R_c$ (MDR)= (0.51+(0.073MDR)), MDR= 4-MDBT/1-MDBT; (14) $\%R_C$ (MPI-1)= 0.6(MPI-1)+0.4, MPI-1= 1.5(2-MP+3-MP)/(P+1-MP+9-MP); (15) $\%R_c$ ($MPDF_1$)= -0.166+2.242 F1, F1= (2-MP+3-MP)/(2-MP+3-MP+1-MP+9-MP); (16) $\%R_c$ ($MPDF_2$)= -0.112+3.739 F2, F2= 2-MP/2-MP+3-MP+1-MP+9-MP; (17) 3-MP/Ret. MH: methylhexane; DMC_4: dimethylbutane; DMC_5: dimethylpentane; $DMCyC_5$: dimethylcyclopentane; TMN: trimethylnaphthalene; MDBT: methyldibenzothiophene; MP: methylphenanthrene; Ret: retene; n.d. - not determined.

Hunt et al. (1980, 1984) reported that the light hydrocarbon ratios of quaternary to tertiary carbon species increase with depth in mature sediments. The highest ratios of quaternary to tertiary carbon species, such as 2,2-DMC_4/2,3-DMC_4 (0.28-0.33), were found in light oils and condensates from the Vale and Balder fields (northern part of the SVG) (Table 4.5). The slightly highest maturity detected in the northern part of the SVG is in agreement with the highest gas-oil ratios reported in this area, which corresponds to the deepest part of the graben (Justwan et al., 2006b). In contrast, oils from the Vølve and Glitne fields have the lowest ratios of quaternary to tertiary carbon species (Table 4.5). These ratios, however, suggest a higher maturity for the Glitne oil relative to the Vølve oil (Table 4.5) that may indicate an early to peak oil generation stage as was suggested by $\%R_c$ from MDR (0.66% R_o) (Table 4.5). In this study, other C_7-maturity parameters, such as Schaefer parameters V and J (Schaefer and Littke, 1988) were not used to evaluate oil maturity because no correlation was observed between them, nor between 2,4-DMC_5/2,3-DMC_5 and Schaefer ratios (Table 4.5). Chung et al. (1998) pointed that they depend on source-rock organofacies. Nevertheless, the 2,4-DMC_5/2,3-DMC_5 ratio and thus the average generation/expulsion temperatures correlate well with $\%R_c$ values from methylphenanthrene distribution factors (R^2>0.9) (Fig. 4.8b, Table 4.5) for mixed oils derived mainly from Upper Jurassic source rocks (the Draupne and Heather formations). Maturity parameters indicate that most mixtures comprise oils of comparable maturity within the oil-generative window, suggesting a slightly higher maturity in oils from the northern half of the SVG study area. Advanced levels of thermal maturity were not detected using maturity parameters based on aromatic compounds, nor light hydrocarbons.

4.6.2.2. Assessment of Petroleum Alteration Processes

In the Sleipner Øst field, the condensate sample (well 15/9-13T1) from Middle Jurassic reservoirs, measured temperature of 98ºC (Norwegian Petroleum Directorate, 2019c), has the lowest concentrations of *n*-alkanes <C_{10} (Fig. 4.9). The very low concentration of *n*-alkanes (<C_{10}) can be related to an evaporative loss of light ends that may be caused by improper storage. Isaksen et al. (2002) proposed that condensates in the Paleocene Heimdal Formation of Sleipner Øst could be fractionated products from the condensate in the Jurassic Hugin Formation. However, condensates hosted in Paleocene

reservoirs (wells 15/9-13 T2 and 15/9-11 T2) show $\delta^{13}C$ values of *n*-alkanes >C_{10} up to 4‰ more positive than those in Jurassic reservoirs (wells 15/9-13 T1 and 15/9-11 T1) (Fig. 4.10a and b), indicating a different origin. Nonetheless, the condensate sample from well 15/9-13 T2 has the highest value of fractionation index (Dzou and Hughes, 1993), FI (2.01) (Table 4.4) that may indicate phase fractionation.

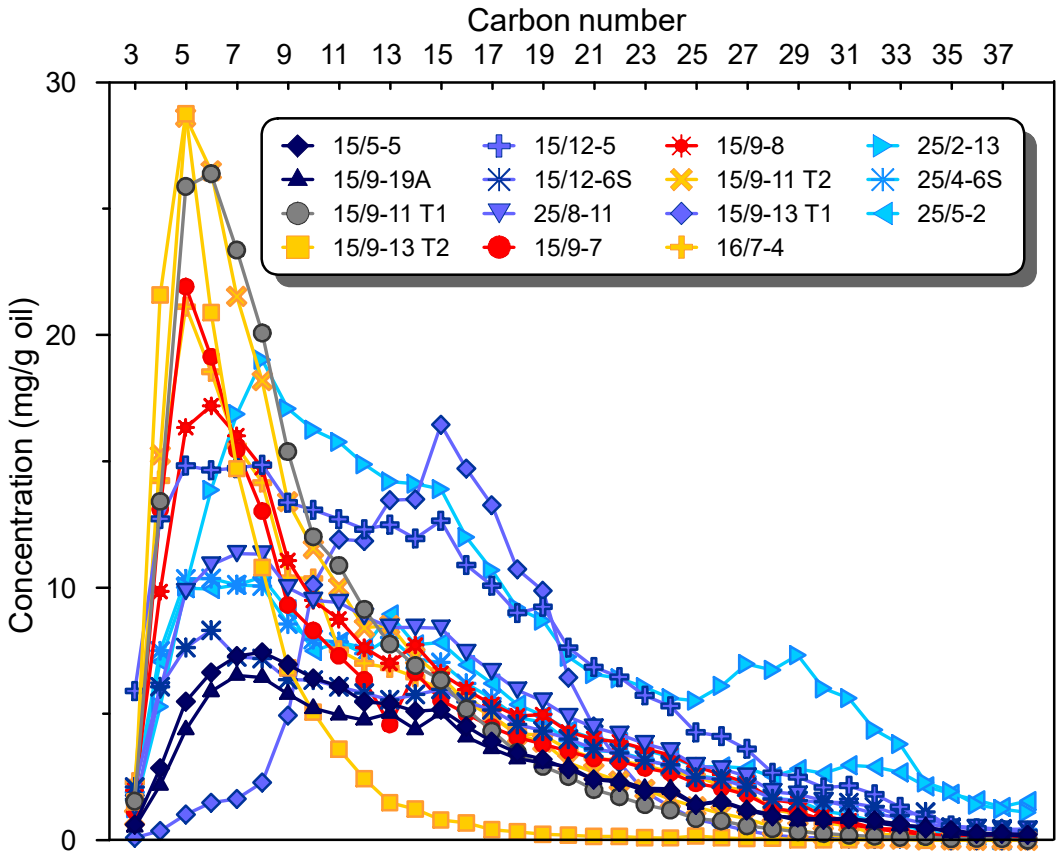

FIGURE 4.9. *Relative concentration of n-alkanes (C_4 to C_{37}) for oils and condensates from the SVG.*

The high aromaticity ratio found in condensates from Paleocene sandstones (Table 4.4) can be associated with a high terrigenous organic matter input. The oil sample from the Paleocene Heimdal Formation sandstones of the Glitne field (well 15/5-5) has the lowest concentrations of aromatic hydrocarbons, such as benzene, toluene, ethylbenzene and xylenes (BTEX) and the lowest Bz/3-MC_5 and Tol/$MCyC_6$ ratios (Table 4.4), which can be due to water washing. The Glitne oil sample, however, does not show loss of *n*-alkanes (Fig. 4.9), indicating absence of bacterial degradation.

4.6.2.3. Genetic Classification of Hydrocarbons

Since most of the analyzed hydrocarbon samples seem to have been generated during the main stage of oil generation and considering that moderate maturity levels do not significantly affect the distribution of sulfur- and oxygen-containing aromatic hydrocarbons (e.g., Chakhmakhchev et al., 1997; Radke et al., 2000), heterocyclic aromatic compounds were used to differentiate petroleum mixtures. Genetic correlations among petroleum mixtures based mainly on $\delta^{13}C$ values of individual hydrocarbons and source-related ratios of light and heavy petroleum components, such as C_7 hydrocarbons and heterocyclic and polycyclic aromatic hydrocarbons. Cluster and PCA were performed to measure the degree of compositional similarity or dissimilarity among analyzed oil and condensate samples and to establish which parameters contribute more to the variation in the data set.

The first data set employed for MVA includes the average $\delta^{13}C$ values of Pr and Ph, and *n*-alkanes in the ranges from C_{10}-C_{14} and C_{26}-C_{29}, which showed isotopic variations among mixed oils (Fig. 4.10a and b), and source-related ratios of heterocyclic and non-heterocyclic aromatic compounds (Table 4.3). As a result, cluster and PCA identified seven populations of mixed petroleum (Populations from A to G) (Fig. 4.11a and b). PC_1 and PC_2 account for 62% and 26% of the variance in the first data set. The second data set comprises molecular and stable carbon isotope ratios of light hydrocarbons (Table 4.4), distinguishing three main groups of petroleum mixtures by cluster and PCA (Figs. 4.11d-e). The total variance in the second data set (92%) is explained by the first and second principal components (PC_1= 82% and PC_2= 10%). Cluster and PCA obtained from third and fourth data sets (Fig. 4.11g and h, j and k), which include relative concentrations of heterocyclic and polycyclic aromatic hydrocarbons and C_7 hydrocarbons together with the average $\delta^{13}C$ values of individual hydrocarbons (Appendix Tables 1 and 2), support previous classifications based on molecular ratios. PC loadings were used to indicate which parameters are responsible for the largest variation in the studied data sets using different petroleum components. The PC_1 and PC_2 loadings for analyzed data are shown in Fig. 4.11 c, f, i and l.

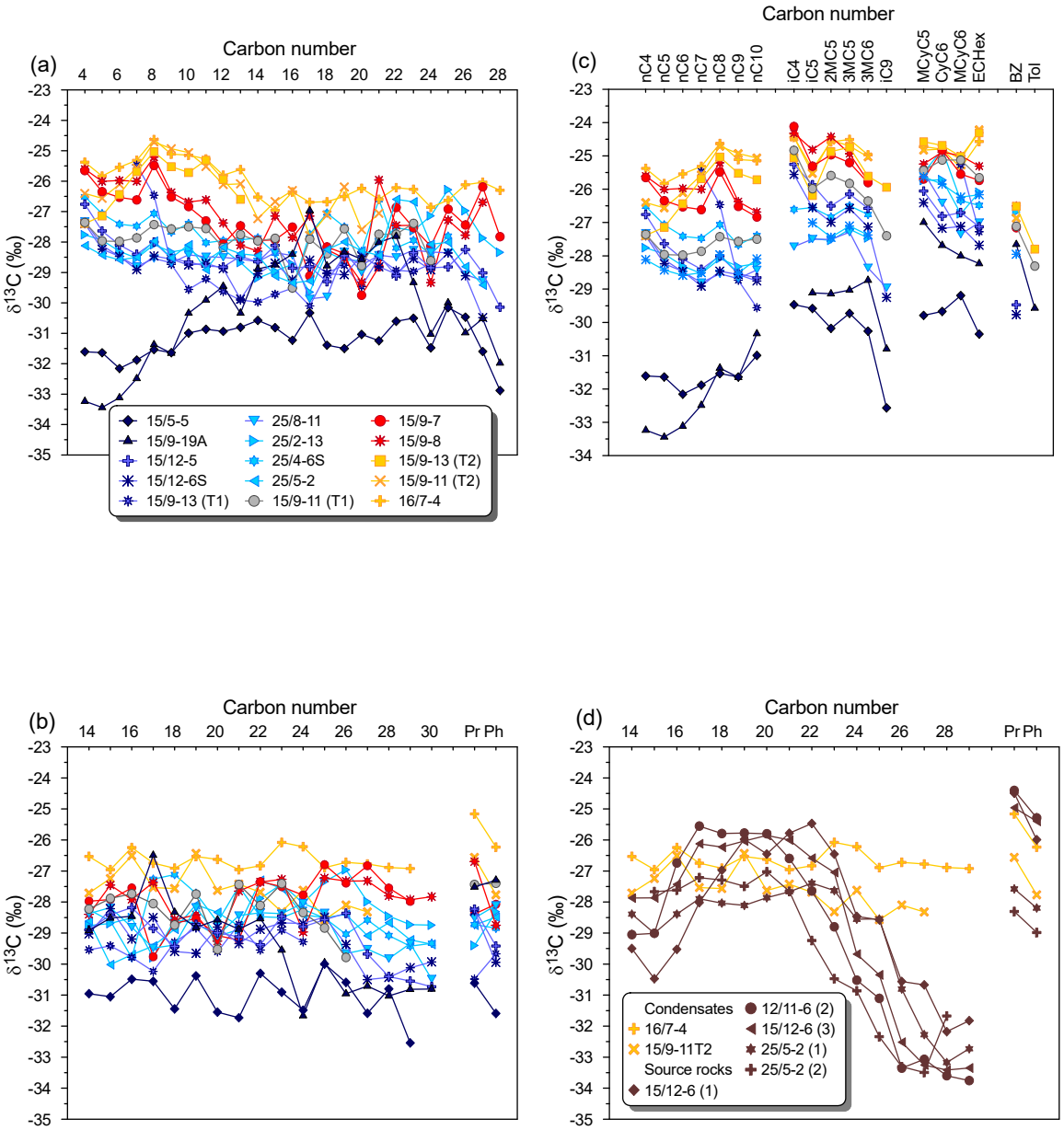

FIGURE 4.10. *$\delta^{13}C$ values of individual n-alkanes, Pr and Ph for source rock extracts from (a) the upper Draupne Fm.; (b) the lower Draupne Fm.; (c) the Heather Fm. and (d) the Sleipner Fm.*

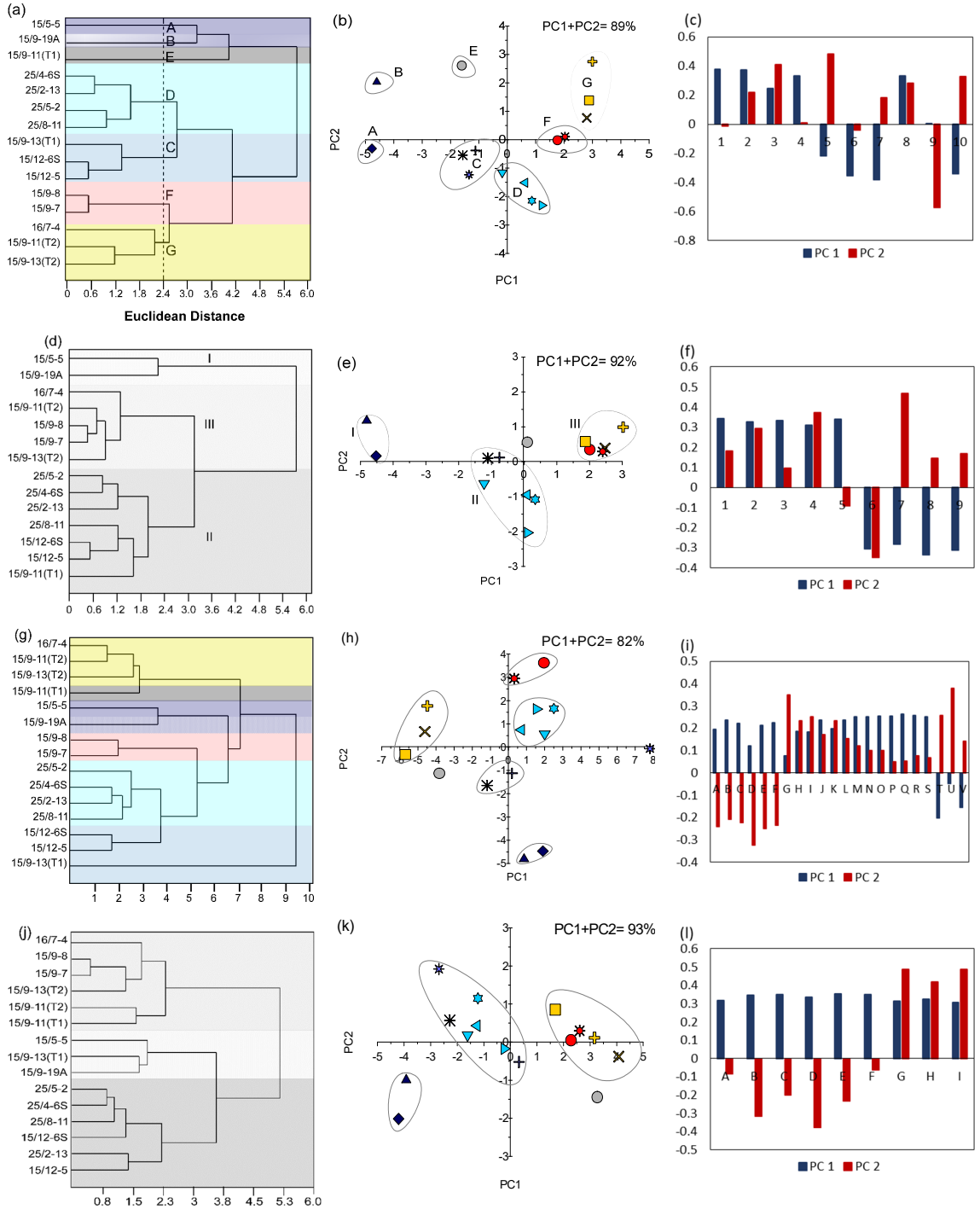

FIGURE 4.11. C*lassification of genetic populations of mixed petroleum using (a) and (b) cluster and PCA based on* $\delta^{13}C$ *values of alkanes and PAH ratios (data set I); (c) loading plots using data set I; (d) and (e) cluster and PCA based on* $\delta^{13}C$ *of LHCs and LH ratios (data set II); (f) loading plots using data set II; (g) and (h) cluster and PCA based on* $\delta^{13}C$ *of alkanes and concentration of DBT, DBF and P and their alkylhomologues (data set III); (i) loading plots using data set III; (j) and (k) cluster and PCA based on* $\delta^{13}C$ *of LHCs and concentration of* C_7 *HCs (data set IV); (l) loading plots using data set IV.*

Geochemical Characteristics of Petroleum based on Ratios of Heterocyclic and Polycyclic Aromatic Hydrocarbons and Molecular and $\delta^{13}C$ Compositions of n-Alkanes and Regular Isoprenoids

- ***Populations A and B***

Population A is represented by the oil sample hosted in the Paleocene Heimdal Formation of the Glitne field (well 15/5-5), while the Population B comprises the oil sample from the sandstones of the Middle Jurassic Hugin Formation in the Vølve field (well 15/9-19A), Table 4.1, Fig. 4.1c. Both oils show a predominance of *n*-alkanes (C_{10}-C_{20}) (Fig. 4.12) commonly indicative of marine phytoplankton source materials (Blumer et al., 1971) and typical features of oils from calcareous source facies such as a dominance of the even over odd carbon numbers in the range of *n*C_{20} to *n*C_{25}-alkanes and a distinctive "V" shape distribution pattern of MDBTs (i.e., 4-methyl>2-+3-methyl<1-methyl) (Fig. 4.12) (Hughes, 1984; Moldowan et al., 1985). Furthermore, Population A and B oils contain the highest amount of DBTs, which predominates over Fs and DBFs (Fig. 4.13a) and the highest 4-MDBT/P ratio (Table 4.3), suggesting also a contribution from calcareous marine source facies. Isaksen et al. (1998, 2002) reported that the Vølve oil sourced from a marine calcareous shale with a Type-II to IIS kerogen, possibly from a more restricted, anoxic facies of the Draupne Formation deposited in a sub-basin located between Sleipner Vest and Øst. Justwan et al. (2006a) found in both oils a pronounced dominance of C_{27} regular steranes over the C_{29} homologs, C_{30} hopane over C_{30} moretane, the lowest C_{19}/C_{23} tricyclic terpane and C_{34}/C_{35} homohopane ratios as well as a very high content of 28,30-bisnorhopane, all of which also indicate inputs from marine dominated-source facies deposited under highly reducing conditions.

Although Glitne and Vølve oils have similar bulk $\delta^{13}C$ data for saturate and aromatic fractions (Justwan et al., 2006a), both oils show mainly differences in $\delta^{13}C$ values of individual hydrocarbons (Fig. 4.10a and b). The Glitne oil tends to show the most negative $\delta^{13}C$ values of *n*-alkanes, Pr and Ph (<-30 ‰) (Fig. 4.10a and b). In contrast, the Vølve oil has an unusual isotopic pattern that exhibits $\delta^{13}C$ values of *n*(C_{10}-C_{24})-alkanes and isoprenoids (Pr and Ph) up to 3‰ more positive than the oil sample from the Glitne field (Fig. 4.10a and b), which may indicate an input from terrigenous source material. In addition,

its wet gas components, such as *n*(C_4-C_5)-alkanes are depleted in ^{13}C (-31 to -34‰) (Fig. 4.10a), suggesting that oil and gas might not be associated. Differentiation of Populations A and B was also achieved using a cross plot of the MDBT/MP ratio *vs*. MDBT/MDBF ratio (Fig. 4.13b). The Vølve oil has slightly higher relative concentrations of DBT and methyl homologs (Fig. 4.14a), a lower Pr/Ph ratio (0.67) (Table 4.3) as well as the lowest diasterane/sterane ratio (0.35) (Justwan et al., 2006a), whereas the Glitne oil shows higher ratios of Pr/Ph (0.98) (Table 4.3) and diasterane/sterane (0.88) (Justwan et al., 2006a).

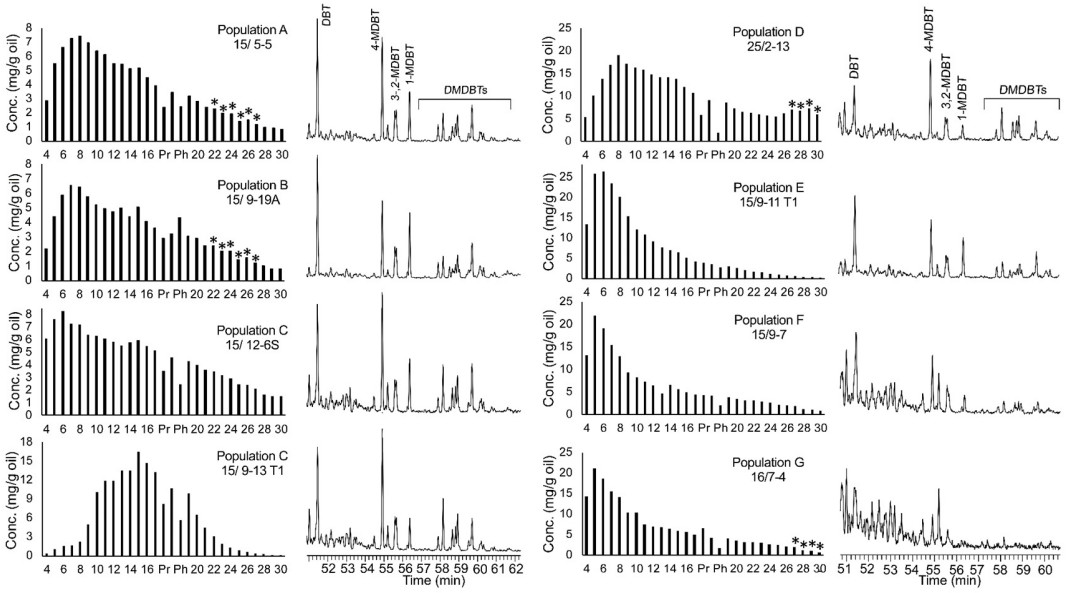

FIGURE 4.12. *Distribution of the relative concentration of n(C_4-C_{30})-alkanes and GC-MS extracted ion profiles of alkylhomologues of dibenzothiophenes (m/z 184+198+212; DBT; MDBTs; DMDBTs) for identified oil populations from the SVG.*

- ***Population C***

Population C comprises three oil samples hosted in Lower and Middle Jurassic reservoirs of the Varg field (wells 15/12-5 and 15/12-6S) and the Sleipner Øst field (well 15/9-13 T1) (Table 4.1, Fig. 4.1c). In contrast to Populations A and B, oils of Populations C show more positive $\delta^{13}C$ values of *n*-alkanes, Pr and Ph up to 3‰ (Fig. 4.10 a and b) and have higher values of Pr/Ph (1.4-1.5) (Table 4.3), lower relative content of DBTs and higher relative content of DBFs and Fs (Fig. 4.13a), suggesting contributions from less marine-dominated sources deposited under less reducing conditions. Moreover, higher C_{34}/C_{35}

homohopane ratios, lower bisnorhopane contents and lower ratios of C_{27} to C_{29} regular steranes were found in Population C oils (Justwan et al., 2006a), which may also indicate an anoxic to dysoxic source with less marine input. Population C oils also exhibit an increment in relative concentrations of alkylnaphthalenes with increasing in methyl substitution, i.e. TMN>DMN>MN (Fig. 4.14b), suggesting they derived mainly from a Type-II kerogen rich source. The same distribution pattern of alkylnaphthalenes have been shown in marine oils from the Potwar basin (Asif and Fazeelat, 2012). All Population C oils show comparable Pr/Ph, MDBT/MP and MDBT/MDBF ratios, as well as similar relative content of DBTs, Fs and DBFs (Table 4.3, Fig. 4.13a and b). Nonetheless, Justwan et al. (2006a) reported a greater contribution from more marine algal-dominated facies for the oil sample from the Sleipner Øst field based on a higher relative abundance of C_{27} over C_{29} regular steranes and C_{30} hopanes over C_{30} moretanes. In this study, the oil sample from the Sleipner Øst field exhibits $\delta^{13}C$ values of Pr, Ph and *n*-alkanes (C_{10}-C_{17}) slightly more negative (1-1.5‰) than oils from the Varg field (Fig. 4.11a), which may also suggest greater marine input. However, similar source-related ratios of heterocyclic and polycyclic aromatic hydrocarbons tend to classify this oil into the same Population C.

- ***Population D***

Population D includes oil samples from sandstones of Early-Middle Jurassic (wells 25/4-6S, 25/5-2 and 25/8-11) and Cretaceous ages (well 25/2-13) in the Vale, Frøy, Lille Frøy and Balder fields located in the northern part of the study area (Table 4.1, Fig. 4.1d). Although both Populations C and D tend to show similar $\delta^{13}C$ values of *n*-alkanes (C_{10}-C_{25}) and regular isoprenoids (Pr, Ph) (Fig. 4.10a and b), ratio of Pr to Ph and source-related ratios based on heterocyclic and PAH composition (Table 4.3, Fig. 4.13a and b) indicate variations in the source contribution. Unlike Population C oils, Population D oils show a bimodal *n*-alkane distribution (Fig. 4.12) and contain a higher Pr/Ph ratio (2.1-3.2) (Table 4.3), higher relative concentrations of P, DBF, F and their alkyl homologs together with lower relative amounts of DBT and alkyl-DBTs (Fig. 4.14b). All of these features are interpreted as a sign of a greater relative contribution of oils from a source with stronger terrigenous influence that was deposited under more oxidizing conditions. This can also be supported by the dominance of C_{29} over C_{27} regular steranes (lower C_{27}/C_{29} sterane ratio), a higher C_{19}/C_{23}

tricyclic terpane ratio, higher C_{30} moretane/hopane and C_{34}/C_{35} homohopane ratios and low amounts of bisnorhopane (Justwan et al., 2006a), as well as the ^{13}C-enrichment (up to 3‰) of long-chain *n*-alkanes from Population D oils relative to those from Population C oils (Fig. 4.10b). Furthermore, both Populations C and D exhibit different distribution patterns of alkylnaphthalenes. Higher relative concentrations of methyl- and especially dimethylnaphthalenes relative to trimethylnaphthalenes (Fig. 4.14b) found in Population D oils, may also indicate a higher relative input from a Type-III kerogen rich source. Radke et al. (1994) reported an enhanced dimethylnaphthalene concentration in oils of terrigenous origin compared with oils of marine origin. Population D oils show a stair-step distribution pattern of MDBTs (i.e., 4-methyl>2-+3-methyl>1-methyl) (Fig. 4.12), which have been associated with predominantly siliciclastic source rocks (Hughes, 1984). The very high ratios of diasteranes/steranes (Justwan et al., 2006a) together with the distribution pattern of MDBT isomers and the lack of preference for even-numbered *n*-alkanes (Fig. 4.12) suggest contributions from clay-rich sources and likely absence of calcareous input in Population D oils.

- ***Population E***

Population E includes a condensate sample hosted in the Middle Jurassic Hugin Formation of the Sleipner Øst field (15/9-11 T1) (Table 4.1, Fig. 4.1c). Population E shows $\delta^{13}C$ values of $n(C_{10}\text{-}C_{14})$-alkanes and especially Pr and Ph more positive than oils in Populations A, B, C and D (Fig. 4.10a and b). Justwan et al. (2006a) reported that saturated biomarker ratios in Population E are comparable to those in the oil sample of Population C from well 15/9-13 T_1 (Sleipner Øst field). They suggested a strong input from a marine-dominated source in Population E, evidenced by the highest C_{27}/C_{29} sterane ratio and one of the lowest C_{30} moretane/hopane ratios; thus, both hydrocarbons were grouped in the same population. In this study, however, more positive $\delta^{13}C$ values of Pr, Ph and $n(C_{10}\text{-}C_{14})$-alkanes up to 2.5‰ (Fig. 4.10a and b) as well as a higher relative percentage of MDBFs (Fig. 4.13a) suggest a higher relative input from terrigenous source material in the mixed hydrocarbon sample of Population E, which was not recognized on the basis of saturated biomarker ratios. Also, a lower relative concentration of MPs, and a higher ratio of MDBTs to MPs (Figs. 4.13b,4.14b) distinguished Population E from Population C.

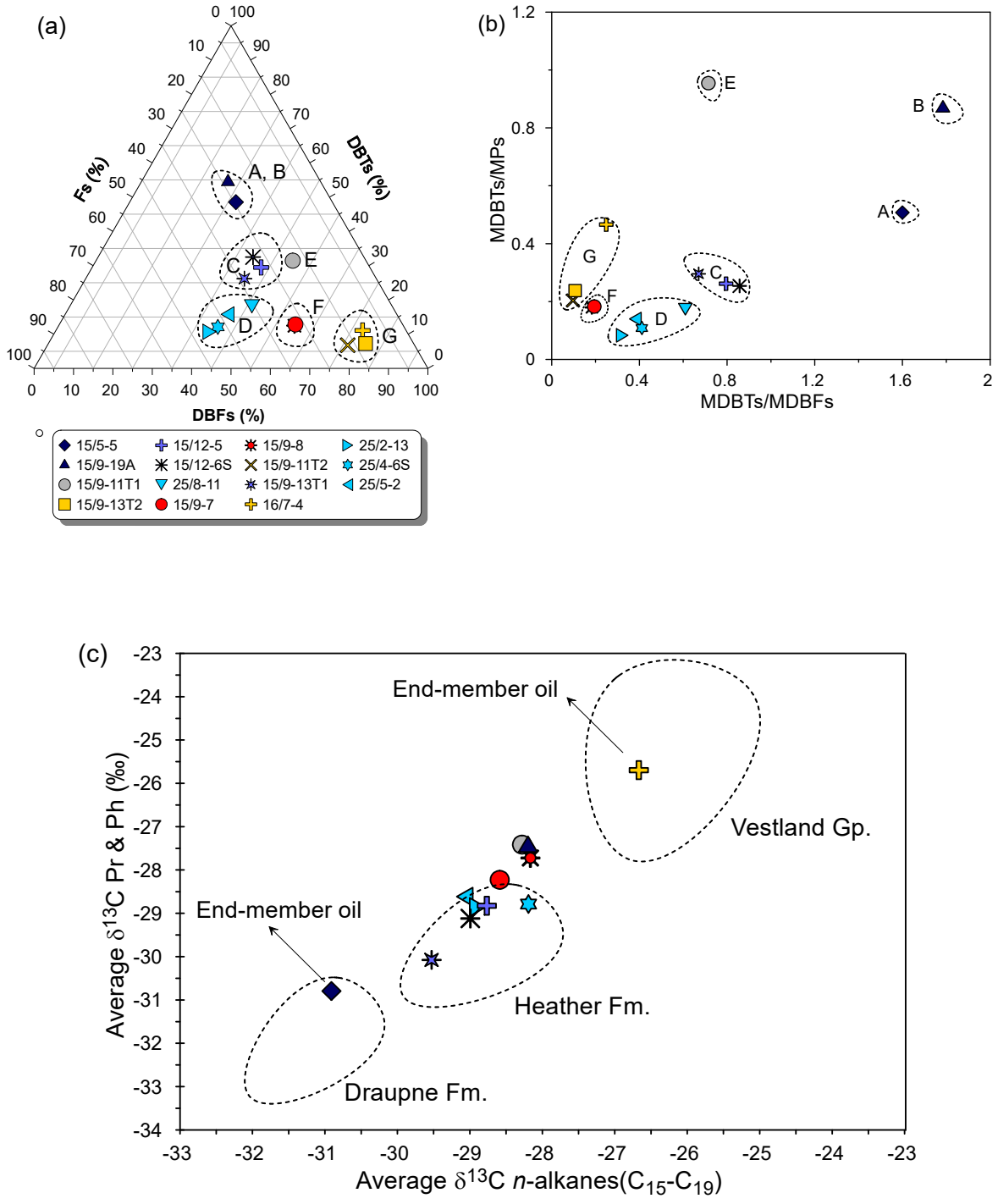

FIGURE 4.13. *(a) Ternary plot of relative amounts of DBTs, DBFs and Fs; (b) cross-plot of MDBTs/MPs vs MDBTs/MDBFs; (c) plot of average $\delta^{13}C$ values of Pr and Ph versus average $\delta^{13}C$ values of n-alkanes (C_{15}-C_{19}) for mixed oils from the SVG, showing areas with dashed lines for the respective values of Jurassic source rocks from the SVG. Oil from Well 15/5-5 (Glitne field) is the end-member oil derived from the Type-II kerogen rich-Draupne Fm., whereas condensate from Well 16/7-4 (Sigyn field) is the end-member oil derived from the Vestland Gp. DBTs: Σ(DBT+MDBTs); DBFs: Σ(DBF+MDBFs); Fs: Σ(F+MFs).*

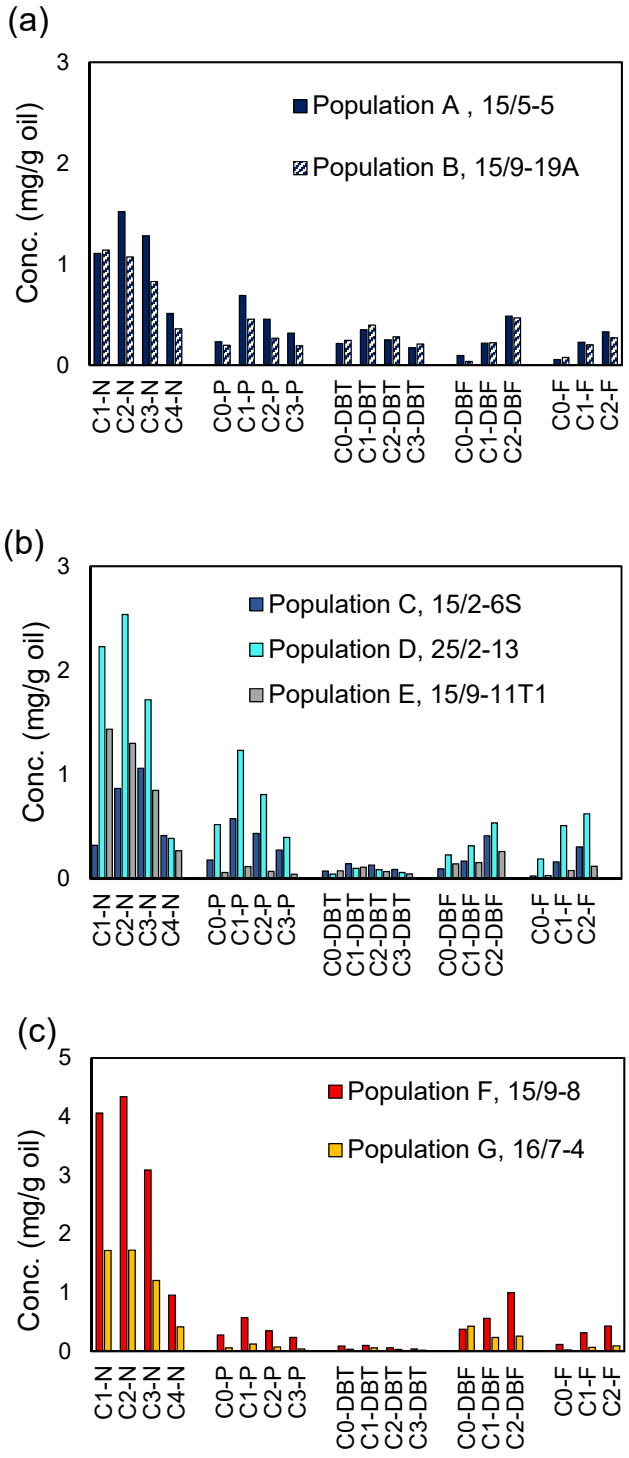

FIGURE 4.14. *Relative concentration of alkylated PAH homologs for (a) Populations A and B; (b) Populations C, D and E; (c) Populations F and G. N, P, DBT, DBF, F represent naphthalene, phenanthrene, dibenzothiophene, dibenzofuran and fluorene, respectively; 0-3 represent carbon numbers of alkyl groups in alkylated PAH homologs.*

- ***Population F***

Population F comprises two condensate samples from Middle Jurassic sandstones in the southern part of the Sleipner Vest field (wells 15/9-7 and 15/9-8) (Table 4.1, Fig. 4.1c). More positive $\delta^{13}C$ values of *n*-alkanes in the ranges from C_{10} to C_{14} and C_{27} to C_{29} (-26 to -28‰) were found in Population F relative to Populations A, B, C, D and E (Fig. 4.10a and b). Compared with other oil populations in the Greater Sleipner area (A, B, C and E), Population F shows higher values of Pr/Ph (2.2-2.5) (Table 4.3), higher relative concentrations of alkylnaphthalenes with a dominance of dimethylnaphthalenes (Fig. 4.14c), lower relative content of DBTs, higher relative amount of DBFs, lower ratios of MDBTs to MPs and MDBTs to MDBFs (Fig. 4.13a and b), as well as one of the highest ratios of 1,7-DMP to "X" (see Table 4.3). All these characteristics, together with higher $\delta^{13}C$ values of individual hydrocarbons (Fig. 4.10a and b), suggest a greater relative contribution of hydrocarbons from Type-III kerogen-containing source rocks deposited under oxic-suboxic conditions. In addition, higher C_{30} moretane/hopane and C_{19}/C_{23} tricyclic terpane ratios, as well as a lower C_{27}/C_{29} regular sterane ratio (Justwan et al., 2006a) are also consistent with a high terrigenous source input. Population F hydrocarbons also exhibit a slight predominance of even-numbered *n*-alkanes (C_{20}-C_{28}) (Fig. 4.12), which might also suggest a contribution from calcareous shales. Nevertheless, a "V" shape distribution pattern of MDBTs was not seen in this population (Fig. 4.12).

- ***Population G***

Population G includes condensate samples from Paleocene reservoirs (wells 15/9-13 T_2 and 15/9-11 T_2) in the Sleipner Øst field and Triassic reservoirs in the Sigyn field (well 16/7-4) (Table 4.1, Fig. 4.1c). Population G condensates have the most positive $\delta^{13}C$ values of Pr, Ph and *n*-alkanes, especially in the range from C_{10} to C_{14}, with values varying from -24 to -27‰ (Fig. 4.10a and b). The highest $\delta^{13}C$ values, as well as the greatest relative content of DBFs (Fig. 4.13a), indicate a very high relative input from terrigenous higher-plant source material in Population G condensates. Similar to Population F, Population G has the highest ratios of 1,7-DMP to "X" (Table 4.3) that can be attributed to higher plant diterpenoid precursors in coals (Alexander et al., 1995; Bastow et al., 2001). Furthermore, an odd over even predominance of *n*(C_{20}-C_{30})-alkanes (Fig. 4.12), common of terrigenous plant waxes

(e.g., Eglinton and Hamilton, 1967), as well as the highest Pr/Ph ratio (3.5-4) (Table 4.3), high values of C_{34}/C_{35} homohopane ratio, high relative abundances of C_{30} moretane and the highest C_{19}/C_{23} tricyclic terpane ratio (Justwan et al., 2006a) support a strong terrigenous-higher plant contribution to the correlated source rocks that were deposited under highly oxidizing conditions. Within Population G, the condensate sample from the Sygin Field (well 16/7-4) shows a strong predominance of C_{29} over C_{27} regular steranes with the lowest C_{27}/C_{29} sterane ratio (Justwan et al., 2006a), the most positive $\delta^{13}C$ values of *n*-alkanes and regular isoprenoids (Pr, Ph) (Fig. 4.10a and b) as well as the greatest ratios of 1,7-DMP/"X", 1-MP/9-MP and 1,2,5-TMN/1,2,7-TMN (Table 4.3), which are consistent with a very high terrigenous source input.

Geochemical Characteristics of Petroleum based on Molecular and $\delta^{13}C$ Compositions of Gasoline-Range Hydrocarbons

In the SVG, C_7 hydrocarbons were not helpful to detect small compositional variations in oil mixing cases, whereas the heterocyclic and polycyclic aromatic hydrocarbons were more useful as source indicators (Murillo et al., 2017). Nevertheless, they allowed discrimination of three main groups of oils and condensates. Group I corresponds to hydrocarbons of Populations A and B derived mainly from a Type-IIS kerogen (calcareous shales), Group II includes hydrocarbons of Populations C, D and E sourced mainly from Type-II and Type-III/II kerogens (siliciclastic shales) and Group III comprises hydrocarbons of Populations F and G derived mainly from a Type III kerogen (coals/ coaly shales) (Fig. 11d and e). Even though MVA includes Population E condensate in the Group II, some light hydrocarbon source-related parameters indicate that Population E has intermediate values between Group II and Group III (Fig. 15a and b).

The highest heptane ratio and the lowest preference of six carbon ring compounds (methylcyclohexane and toluene) found in early mature oils from the Vølve and Glitne fields are interpreted as a result of a high relative contribution from Type-IIS kerogen associated with marine calcareous source facies (Fig. 15a). Mixed hydrocarbons that show the greatest relative contribution from Type-III kerogen, related to coals and/or coaly shales (Populations F and G), have the lowest heptane ratios (11 to 18) and are enriched in six-carbon ring

compounds (Fig. 15a). Mixed oils of Populations C and D show intermediate values (Fig. 15a) whereas Population E tends to show similar concentration of six-carbon ring compounds to Populations F and G.

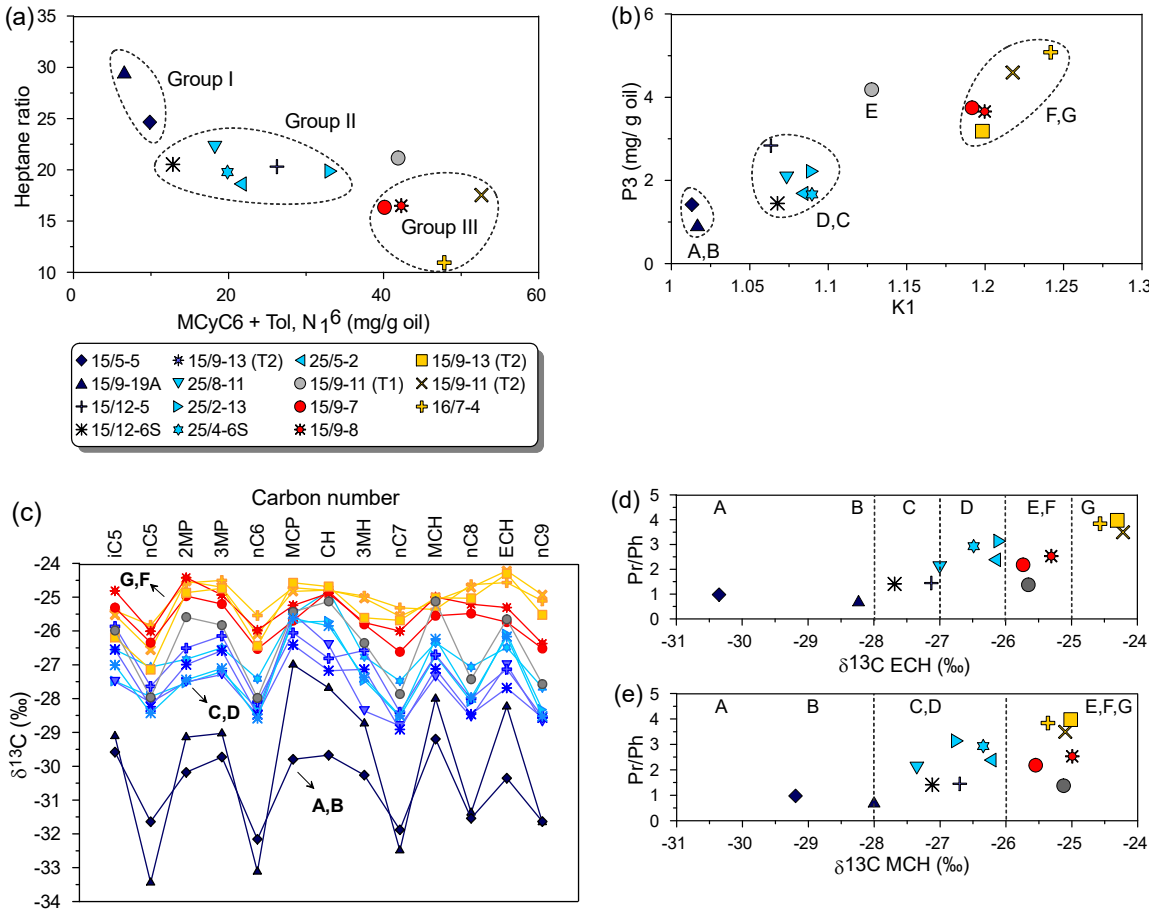

FIGURE 4.15. *(a) Cross-plot of heptane ratio versus the relative concentration of the (N_1^6), MCH+Tol; (b) cross-plot of the relative concentration of P_3 versus K_1, where K_1:(2-MH+2,3-DMP)/(3-MH+2,4-DMP); (c) $\delta^{13}C$ values of gasoline-range hydrocarbons supporting the three main groups of hydrocarbons; (d) Pr/Ph ratio vs. $\delta^{13}C$ of ECH and (e) Pr/Ph ratio vs. $\delta^{13}C$ of MCH.*

Mango (1987, 1990) attributed the variance in the isoheptane ratio (K_1) between sets of oils to different kerogen types. In the SVG, the K_1 supports the previous classification and allows separation of the mixed hydrocarbon sample of Population E from other oils (Table 4, Fig. 15b). Likewise, Mango's parent-daughter parameters also provided evidence for classifying mixtures of oils in the SVG (Table 4, Fig. 15b). In addition, the $\delta^{13}C$ values of gasoline-range paraffinic, branched and cyclic hydrocarbons distinguished the same three

main groups of mixed petroleum (Fig. 15c). In general, branched and cyclic alkanes are more enriched in ^{13}C than gasoline-range paraffins (Fig. 15c). The isotopically heaviest $\delta^{13}C$ values of gasoline-range hydrocarbons correspond to mixed oils with the highest relative input from coaly kerogen Type-III (Populations F and G), while the isotopically lightest $\delta^{13}C$ values are consistent with mixed oils that show the greatest relative input from Type-IIS kerogen (Populations A and B). Intermediate $\delta^{13}C$ values are associated with mixed oils of Populations C and D sourced mainly from Type-II and Type-III/II kerogens in different mixing ratios (Fig. 15c). All three main groups are characterized by different molecular and carbon isotopic data for gasoline range (C_5-C_9) hydrocarbons. However, some exceptions were observed in $\delta^{13}C$ values of some gasoline range hydrocarbons. For instance, Population B (Vølve oil) shows $\delta^{13}C$ values of alkylcycloalkanes up to 3‰ more positive than Population A (Glitne oil), and Population E has also $\delta^{13}C$ values of alkylcycloalkanes more positive than Populations C and D, which may indicate contribution from coaly sources (Fig. 15c). Although the $\delta^{13}C$ values of cyclic, branched and *n*-alkanes in the gasoline range show no significant differences between Populations C and D, both mixed oil populations were differentiated by the $\delta^{13}C$ values of benzene with isotopic variation up to 3‰ (Fig. 10c). Both populations were also distinguished using the bulk $\delta^{13}C$ values of aromatic fraction (Justwan et al., 2006a). Some authors have noted a ^{13}C-enrichment of alkylcycloalkanes in oils derived from higher-plant source material. Murillo et al. (2016) found that alkylcyclohexanes, especially $MCyC_6$, are ^{13}C-enriched in mixed petroleum with higher contribution from Type-III kerogen rich sources in the Hammerfest Basin, SW Barents Sea. Huang et al. (2017) reported that the $\delta^{13}C$ values of $MCyC_5$, CyC_6, $MCyC_6$, benzene and toluene can be used to identify humic and sapropelic condensates. In the SVG, mixed petroleum with high relative contribution from coaly source facies, have the isotopically heaviest $\delta^{13}C$ values of $MCyC_6$ and $ECyC_6$ (Fig. 15d and e).

4.6.3. Oil to Source Correlation

To correlate oils with the main contributing source rock, source rock samples of the same level of maturation and sufficient richness were employed (Table 4.2). Even though the $\delta^{13}C$ data of *n*-alkanes in the range from C_{15} to C_{19}, which are generally derived from algae and bacterial biomass, were useful for discriminating Jurassic source rock extracts from the

Sleipner, Heather and Type II-kerogen rich Draupne formations (Figs. 4.3b, 4.4a-d), these *n*-alkanes do not show significant $\delta^{13}C$ variations in most mixed petroleum from the SVG (Fig. 4.10a and b). Nonetheless, mixed oils have greater carbon isotopic variations in *n*-alkanes from C_{10} to C_{14} and from C_{26} to C_{29} (Fig. 4.10a and b). The relative ^{13}C-enrichment of these *n*-alkanes from Population A to Population G can be interpreted as a result of the contribution from terrigenous material.

Populations A and B show evidence of a higher relative input from calcareous source facies (Fig. 4.12) associated with the upper Draupne Formation (Fig. 4.7c). The isotopically lightest $\delta^{13}C$ values of *n*-alkanes, Pr and Ph (<-30‰) in Population A (Glitne oil; Fig. 4.10a and b), correlate with those in source rock extracts from the Type II-kerogen rich Draupne Formation (Figs. 4.4a, 4.13c). These values, together with the low Pr/Ph ratio, may exclude origin from the Heather, Hugin and Sleipner formations in Population A. Population B (Vølve oil) shows a slightly higher relative concentration of dibenzothiophene series compounds and a lower concentration of phenanthrene series compounds (Fig. 4.14a), which may suggest a greater relative contribution of marine oils from calcareous source facies of the upper Draupne Formation. However, *n*-alkanes (C_{10}-C_{23}), Pr and Ph are ^{13}C-enriched up to 3‰ (Fig. 4.10a and b), suggesting also a possible input from Type-III kerogen-rich sources. The isotopically heavy average $\delta^{13}C$ values of Pr and Ph (-27.4‰) in the Vølve oil (Fig. 4.10b) tend to correlate with those in Middle Jurassic source rock extracts (>-28‰) (Figs. 4.4d, 4.13c). Therefore, a minor contribution from the Heather Formation and Vestland Group cannot be ruled out for the Vølve oil. Population C mixed oils show geochemical evidence of oils derived from a marine algal, anoxic to disoxic source. However, more positive $\delta^{13}C$ values of *n*-alkanes (>C_{10}), as well as Pr and Ph ranging from -28 to -29.5‰ (Fig. 4.10a and b) indicate further contribution that can be associated with Type-III kerogen rich facies into the Draupne Formation and/or Heather Formation (-28 to -30‰) (Fig. 4.13c). Although there is no distinction in the $\delta^{13}C$ data for most *n*-alkanes, Pr, Ph and gasoline-range hydrocarbons for Populations C and D oils (Fig. 4.10a-c), the latter have higher values of Pr/Ph ratios (2.1-3.2) (Table 4.3) and the highest relative concentrations of P, MPs, DMPs and TMPs (Fig. 4.14b), which can be associated with a very high input from the Heather and/or lower Draupne formations enriched in Type-III kerogen (Fig. 4.6a). A ^{13}C-enrichment

up to 3‰ for *n*-alkanes (C_{10}-C_{14}) and *n*-alkanes (C_{26}-C_{29}), (Fig. 4.10a and b) and high values of Pr/Ph ratio (2.2-2.5) (Table 4.3) suggest a higher relative contribution from Type-III kerogen rich sources in hydrocarbons of Population F relative to those of Populations A, B, C, D and E. Lower amounts of DBTs and higher contents of DBFs (Fig. 4.13a) found in Population F oils are indicative of hydrocarbon contribution from coals and/or coaly shales of the Vestland Group (Fig. 4.7d). Molecular and isotopic compositions indicate that Population F represents mixtures of hydrocarbons sourced from Upper Jurassic and Middle Jurassic source rocks. The highest Pr/Ph ratios (3.5-4.0) (Table 4.3), the highest relative content of DBF and MDBFs, the lowest relative content of DBT and MDBTs (Fig. 4.13a and b) and very low relative concentrations of P and MPs (Fig. 4.14c) clearly associate Population G with Middle Jurassic coaly sources (Fig. 4.7d). Likewise, Population G condensates exhibit the most positive $\delta^{13}C$ values of *n*-alkanes (C_{15}-C_{20}), Pr and Ph (-25 to -28‰), indicating they are sourced from Middle Jurassic source rocks (Fig. 4.10a and b). Nonetheless, the isotopic dissimilarities for *n*-alkanes (>C_{22}) between the analyzed coal extracts of the Sleipner Formation and the Population G hydrocarbons (Fig. 4.10d) provide evidence of the Middle Jurassic source heterogeneity. Population E represents a peculiar mixture of petroleum, where biomarkers suggest this oil originated mainly from a marine source (Justwan et al., 2006a) and polycyclic and heterocyclic aromatic hydrocarbons as well as light hydrocarbons indicate that Population E contains a high relative contribution of hydrocarbons sourced from terrigenous higher-plant material. The high $\delta^{13}C$ values of Pr and Ph (-27 to -28‰) tend to correlate with those in coaly sources of the Sleipner Formation (Fig. 4.13c). Although Population E shows comparable $\delta^{13}C$ values of Pr and Ph to Population B (Vølve oil) (Fig. 4.10b), it has lower content of DBT and MDBTs, one of the lowest contents of P and MPs, and a higher amount of DBF and MDBFs (Figs. 4.13a and b, 4.14b) that suggest a higher relative input of hydrocarbons sourced from coals and/or coaly shales (Figs. 4.6a, 4.7d). Population E is a good example of mixtures of end-member oils, with the concentration of specific components in each oil greatly different. In Population E, biomarker distributions are biased toward the oil with the largest concentrations of these compounds. Hence, it may be possible that the less dominant source rock (upper Draupne Formation) has much greater biomarker concentrations than the dominant source (Vestland Group).

All populations of hydrocarbons show the same distribution patterns of methyl, dimethyl and trimethylphenanthrenes (i.e., MPs>DMPs>TMPs) (Fig. 4.14a-c) and exhibit a predominance of 9-MP relative to 1-MP isomer, showing the highest 1-MP/9-MP ratios in Populations G and F (Table 4.3). In addition, mixed oils show changes in the relative concentrations of phenanthrene series compounds. The highest relative concentrations of P, MPs, DMPs and TMPs found in Population D oils can be associated with a Heather and/or lower Draupne source that shows the highest concentration of alkyl-phenanthrenes; whereas the lowest concentrations of them found in Population G are consistent with Middle Jurassic coaly sources (Figs. 4.6, 4.14b and c). The fact that some mixed oil populations in the southern part of the SVG study area, show signals consistent with inputs from calcareous source facies suggest a most widespread occurrence of hydrocarbons sourced from post rift facies of the upper Draupne Formation. In the present study, geochemical interpretations are in accordance with basin modelling results, which indicate that Quaternary subsidence rates were higher in the southern half of the study area (Justwan et al., 2006b). These higher subsidence rates allowed the shallowest and youngest source rock unit of the upper Draupne Formation to enter into the hydrocarbon generation window. Furthermore, high inputs from Middle Jurassic source rocks were found in various samples from the southern half of the SVG study area (the Greater Sleipner Area), which are likely related to the great thicknesses of Middle Jurassic coals and carbargillites reported in this area (Justwan et al., 2006b). Complex mixing of hydrocarbons derived from Upper Jurassic and Middle Jurassic sources were identified in the Greater Sleipner area, where the petroleum systems that consider these source rock units are active. Besides, a high relative contribution of oils sourced from siliciclastic shales enriched in Type-III kerogen (Heather Formation and/or lower Draupne Formation) was recognized in the northern half of the SVG study area. This is supported by Justwan et al. (2006b), who estimated the highest contribution of Heather sourced oils in the northern half of the SVG study area, especially for the Vale, Frøy and Lille Frøy fields, using a pseudo-3D modelling. Moreover, they reported a major contribution of oils from the lower Draupne Formation in the Balder field.

4.6.4. Estimation of Mixing Ratios in Reservoirs Containing Different Oil Charges from Jurassic Source Rocks in the Southern Part of the SVG

Since complex mixtures of petroleum from Upper Jurassic source rocks (the Draupne and Heather formations) and Middle Jurassic source rocks (Vestland Group) have been identified in the Greater Sleipner area, the quantitative determination of the relative contribution of each source rock to mixed oils is difficult. Typical end-member oils from all source rocks were not possible to obtain from the study data set. Therefore, an attempt was made to quantify the relative contribution of the Type-II kerogen rich-Jurassic source rock (the Draupne Formation) and Type-III kerogen rich-Jurassic source rocks (the Heather and/or lower Draupne formations and the Vestland Group) to mixed oil accumulations. In the mixtures, the total proportion of oils from Type-III kerogen rich Jurassic source rocks was defined here as the terrigenous-dominated source contribution (TSC), whereas the proportion of oils from the Type-II kerogen rich-Jurassic source rock is expressed as the marine-dominated source contribution (MSC), which is described as (1-TSC). Based on molecular and $\delta^{13}C$ data, the oil sample from the Glitne field (well 15/5-5) was identified as the end-member oil of the Type-II kerogen-rich Draupne Formation, whereas the condensate sample from the Sygin field (well 16/7-4) was selected as the end-member oil of the Middle Jurassic Vestland Group.

Considering that the average $\delta^{13}C$ values become more positive with the proportion of oils derived from Type-III kerogen rich Jurassic sources, estimations of TSC were obtained from the enrichment in ^{13}C of (C_{10}-C_{14}) *n*-alkanes and regular isoprenoids (Pr and Ph) (Table 4.6) in mixed petroleum. A very good linear correlation was found between the average $\delta^{13}C$ values of (C_{10}-C_{14}) *n*-alkanes and average $\delta^{13}C$ values of Pr and Ph (R^2= 0.98) (Table 4.6). Hence, mixed oils show a similar ^{13}C-enrichment of *n*-alkanes (C_{10}-C_{14}) and Pr and Ph with the TSC proportion (Fig. 4.16a), showing delta values generally <0.5‰. $\delta^{13}C$ values of (C_{26}-C_{29}) *n*-alkanes were not used to estimate the TSC proportion to all studied mixed oil samples because they were not able to distinguish Population F from G (Fig. 4.10a and b). However, the TSC percentages estimated from the ^{13}C-enrichment of *n*-alkanes (C_{10}-C_{14}) and Pr and Ph for oils from the Varg field (wells 15/12-5 and 15/12-6S) (Table 4.6) are quite similar to those obtained using the average $\delta^{13}C$ values of long-chain *n*-alkanes (41.8

and 34.6%, respectively). In contrast to $\delta^{13}C$ values of (C_{26}-C_{29}) *n*-alkanes, $\delta^{13}C$ values of (C_{15}-C_{19}) *n*-alkanes were useful to differentiate Populations F and G. Estimates of %TSC from ^{13}C-enrichment of (C_{15}-C_{19}) *n*-alkanes for Population F condensates in wells 15/9-7 (55.9%), 15/9-8 (69.1%), and Population G condensates in well 15/9-11T_2 (90.8%) are consistent with those obtained using the average $\delta^{13}C$ values of (C_{10}-C_{14}) *n*-alkanes and Pr and Ph (Table 4.6). Values of mixing proportions near or <10% are considered negligible (Fig. 4.16a).

TABLE 4.6. *Mixing proportions of hydrocarbons from Type-III and Type-II kerogen rich Jurassic source rocks estimated from $\delta^{13}C$ values of individual petroleum hydrocarbons in petroleum mixtures from the southern part of the SVG.*

Well	1	2	3	%TSC (1)	%TSC (2)	%TSC mean	%MSC (1)	%MSC (2)	%MSC mean
15/5-5	-30.8	-31.1	-30.4	0.0	0.0	0.0	100.0	100.0	100.0
15/12-5	-28.7	-28.8	-27.1	41.8	42.1	42	58.2	57.9	58.1
15/12-6S	-29.1	-29.1	-27.7	34.6	36.6	35.6	65.4	63.4	64.4
15/9-13 T1	-29.7	-30.1	-27.3	22.8	19.0	20.9	77.2	81.1	79.1
15/9-7	-27.5	-28.2	-25.7	64.1	53.2	58.6	35.9	46.9	41.4
15/9-8	-27.4	-27.7	-25.3	66.2	62.5	64.3	33.8	37.5	35.7
15/9-11 T2	-26.0	n.d.	-24.2	93.6	n.d.	93.6	6.4	n.d.	6.4
15/9-13 T2	-25.9	n.d.	-24.3	95.8	n.d.	95.8	4.3	n.d.	4.3
16/7-4	-25.7	-25.7	-24.6	100.0	100.0	100.0	0.0	0.0	0.0

(1): Average $\delta^{13}C$ values of (C_{10}-C_{14}) *n*-alkanes; (2): Average $\delta^{13}C$ values of Pr and Ph; (3): $\delta^{13}C$ value of $ECyC_6$. %TSC (1), %TSC (2): proportion of the terrigenous-dominated Jurassic source contribution estimated using (1) and (2), respectively. %MSC (1), %MSC (2): proportion of the marine-dominated Jurassic source contribution estimated using (1) and (2). n.d. - not determined. Percentages <10% are considered negligible (within the analytical error 0.5 ‰).

The ^{13}C-enrichment of alkylcyclohexanes (Fig. 4.15c-e) with the increment in the relative contribution of hydrocarbons from terrigenous source material may indicate that there is an important biological precursor for alkylcyclohexanes in higher plants. Isotopic variations (<0.9‰) were measured between $\delta^{13}C$ values of cyclohexane (CyC_6), methyl and ethyl cyclohexane ($MCyC_6$, $ECyC_6$) for SVG oils and condensates. This may suggest no differences in biological source for each compound. Zhou-Dong et al. (1993) proposed a mechanism of formation of alkylcyclohexanes involving direct cyclization of predominantly C_{16} and C_{18} straight-chain precursor (fatty acids or alcohols), ubiquitous in terrigenous plant material that served as organic precursors of coals. They suggested that the alkylcyclohexanes may have the same fatty acid precursors as the *n*-alkanes. Murray (1998) reported that resin compounds could strongly affect $\delta^{13}C$ of cyclic fraction. In this study,

linear correlations were found between $\delta^{13}C$ values of $ECyC_6$ and the average $\delta^{13}C$ values of (C_{10}-C_{14}) *n*-alkanes and (C_{26}-C_{29}) *n*-alkanes (R^2= 0.93, 0.88). However, TSC proportion obtained from the ^{13}C-enrichment of $ECyC_6$ tends to be over-estimated relative to those obtained using ^{13}C-enrichment of *n*-alkanes and regular isoprenoids (Pr and Ph) (Table 4.6). As the estimated proportion of oils derived from the Type-II kerogen-rich Draupne Formation in the mixtures increases, the concentrations of 4-, 3-+2-, and 9-methyldibenzothiophenes increase linearly (R^2= 0.93-0.95) (Fig. 4.16b). The lowest slope of the linear regression lines is shown in the plot of the MSC proportion *versus* the concentration of 4-MDBT (*m*= 0.58). Likewise, different mixing curves were obtained by plotting of the estimated proportion of oils sourced from the Type-II kerogen rich Draupne Formation *versus* the concentrations of alkyldibenzothiophenes in the mixed petroleum (Fig. 4.16c-e). They show a linear increase in the concentrations of organo-sulfur compounds (methyl-, dimethyl-, and trimethyl-dibenzothiophenes) with the proportion of the MSC (R^2>0.9). Furthermore, the concentration of Pr increases linearly with the proportion of oils from Jurassic source rocks enriched in Type-III kerogen and decreases with the proportion of oils derived from the Type-II kerogen rich Draupne Formation (R^2= 0.90) (Fig. 4.16f). The concentration of Ph also correlates with the proportions of TSC and MSC; however, the linear regression line shows lower R^2. The mixing curves obtained by plotting of the estimated mixing proportions *versus* the concentrations of sulfur-containing heterocyclic aromatic hydrocarbons and regular isoprenoids in mixed oils, have a linear behavior. This suggests that the average $\delta^{13}C$ values of *n*-alkanes, and Pr and Ph are useful for calculating the proportions of Jurassic source contributions enriched in Type-II and Type-III kerogens in complex petroleum mixtures from the southern part of the SVG. Estimations of individual contributions of oils originated from Type-III kerogen rich Jurassic source rocks (the Heather/lower Draupne formations and the Vestland Group) were not possible using $\delta^{13}C$ data of source rocks, because carbon isotopic variations in (C_{15}-C_{19}) *n*-alkanes are not significant in most petroleum mixtures (Fig. 4.10a and b) even though they are useful to discriminate Jurassic source rock extracts (Fig. 4.4a-d). However, petroleum mixtures with the highest estimated TSC proportions show the most positive $\delta^{13}C$ values of alkylcyclohexanes (Fig. 4.15d and e) (Table 4.6) and the highest ratios of Pr/Ph and DBFs/∑(Ps+DBFs+DBTs) (Fig. 16g), which are interpreted as a result of terrigenous higher

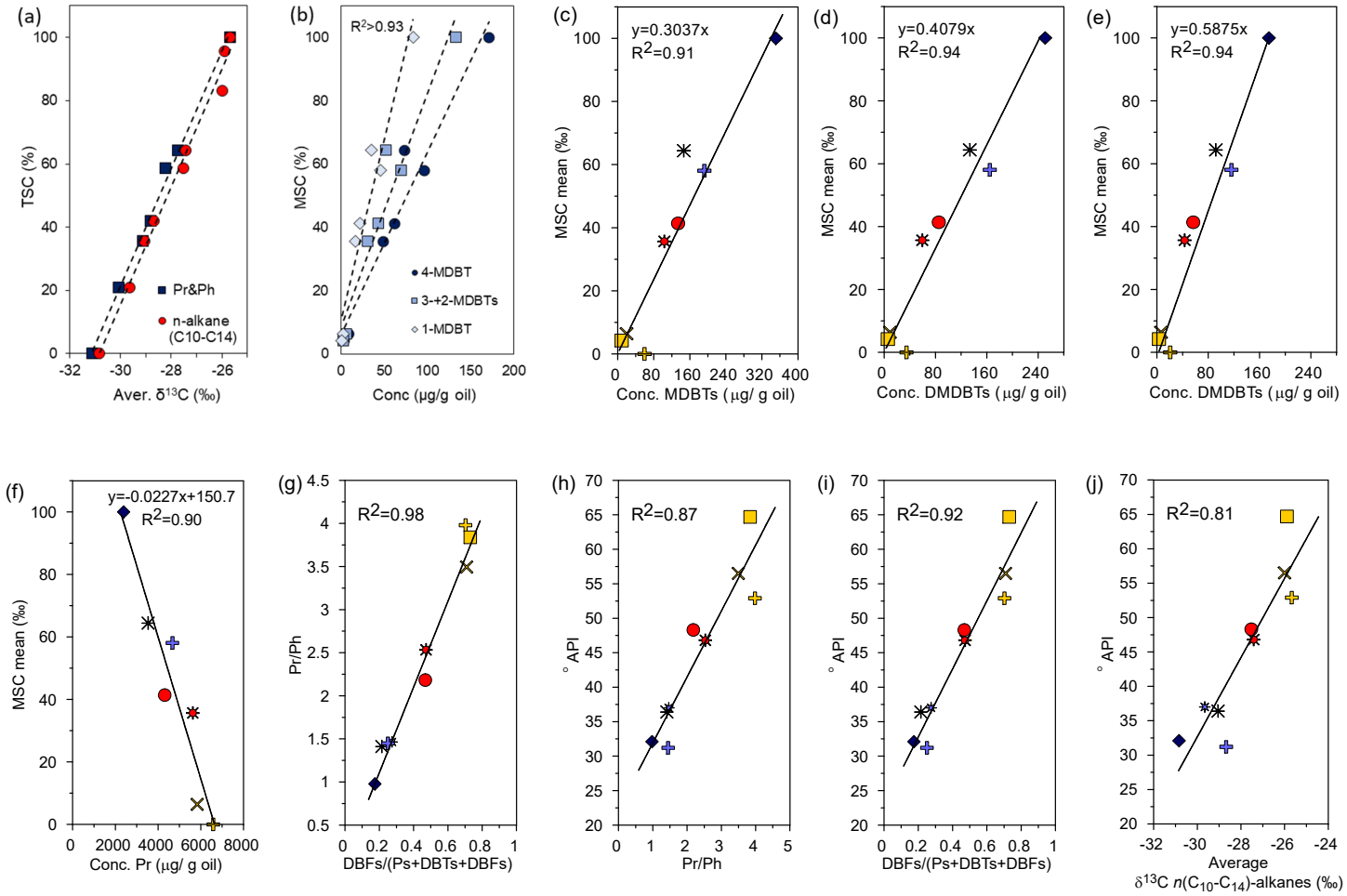

FIGURE 4.16. *Plots of (a) %TSC mean versus the average $\delta^{13}C$ values of (C_{10}-C_{14}) n-alkanes and Pr and Ph; (b) %MSC mean versus the concentration of MDBT isomers; (c) %MSC mean versus the total concentration of MDBTs; (d) %MSC mean versus the total concentration of DMDBTs; (e) %MSC mean versus the total concentration of TMDBTs; (f) %MSC mean versus the concentration of Pristane; (g) Pr/Ph vs. DBFs/Σ(Ps+DBTs+DBFs); (h) ºAPI vs. Pr/Ph; (i) ºAPI vs. DBFs/Σ(Ps+DBTs+DBFs); (j) ºAPI vs. Average $\delta^{13}C$ values of n(C_{10}-C_{14})-alkanes. ºAPI data were taken from Justwan et al. (2006a). MSC: marine-dominated Jurassic source contribution (Input from the Type-II kerogen rich Draupne Formation); TSC: terrigenous-dominated Jurassic source contribution (Input from the Heather/lower Draupne formations plus the Vestland Group).*

plant material input associated with coaly sources. Therefore, estimated proportions of TSC (59-64%) in condensates (0.7-0.8% R_o) from the southern part of the Sleipner Vest field (wells 15/9-7 and 15/9-8) can be related mainly to coaly Type-III kerogen of the Middle Jurassic Vestland group, whereas the TSC proportions (36-42%) in oils of similar maturity from the Varg field (wells 15/12-5 and 15/12-6) are associated mainly with Type-III kerogen of the Upper Jurassic Heather and/or lower Draupne formation shales. In addition, good linear correlations were obtained between Pr/Ph *vs*. DBFs/∑(Ps+DBFs+DBTs), API gravity *vs*. Pr/Ph and API gravity *vs*. DBFs/∑(Ps+DBFs+DBTs) (R^2>0.9) (Fig. 4.16g-i). Also, ºAPI increases with $\delta^{13}C$ values of *n*(C_{10}-C_{14})-alkanes in petroleum mixtures; nevertheless, the linear regression line shows lower R^2 (R^2=0.8) (Fig. 4.16j). In this study, mixtures of petroleum show an increase in ºAPI with the increase in the ratios of Pr/Ph and DBFs/∑(Ps+DBFs+DBTs) and the ^{13}C-enrichment of *n*(C_{10}-C_{14})-alkanes, which are associated with terrigenous source input. Condensates generated from Middle Jurassic coaly sources have the highest ratios of Pr/Ph (>3) and DBFs/∑(Ps+DBFs+DBTs) (>0.7) as well as the most positive $\delta^{13}C$ values (>-26‰).

4.7. Conclusions

Maturity parameters based on light hydrocarbons and polycyclic and heterocyclic aromatic hydrocarbons indicate that the oil samples in this study achieved the oil-generative window. Molecular and $\delta^{13}C$ composition of gasoline range hydrocarbons discriminates three main groups of mixed petroleum in the SVG. Group I originated mainly from Type-IIS kerogen associated with calcareous source facies, Group II originated mainly from Type-II and Type-III/II kerogens related to siliciclastic source facies and Group III originated predominantly from Type-III kerogen associated with coaly source facies. Nonetheless, the $\delta^{13}C$ data of *n*-alkanes, Pr and Ph in conjunction with the molecular composition of heterocyclic and non-heterocyclic aromatic hydrocarbons were more sensitive as source indicators, allowing small compositional variations in mixed petroleum to be detected. These molecular and $\delta^{13}C$ data identified seven populations (A-G) according to the relative contribution of hydrocarbons derived from terrigenous source material. The average $\delta^{13}C$ values of *n*-alkanes (C_{10}-C_{14}) and regular isoprenoids (Pr and Ph) were suitable for calculating the proportional contribution of hydrocarbons from Jurassic source rocks

enriched in Type-III and Type-II kerogens to petroleum accumulations in the southern part of the SVG. The estimated mixing proportions correlated linearly with the concentrations of alkyldibenzothiophenes and regular isoprenoids in petroleum mixtures of comparable maturity within the peak oil generation window. The linear behavior of these mixing curves is useful for verifying estimates of mixing ratios obtained from ^{13}C-enrichment of (C_{10}-C_{14}) *n*-alkanes, Pr and Ph in mixed petroleum from the southern part of the SVG. In addition, it can support the use of the compound-specific stable carbon isotope composition for quantitative assignment of sources in mixed oils at moderate levels of thermal maturity.

4.8. Acknowledgements

The German Academic Exchange Service (DAAD) is thanked for funding this research. The Norwegian Petroleum Directorate is gratefully acknowledged for the kind contribution of oil and source rock samples and the technical staff of the Organic Geochemistry section at GFZ for analytical support. H. Justwan is thanked for carefully reviews of this manuscript and constructive comments. K. E. Peters and anonymous peer reviewers are also thanked for their comments and suggestions that resulted in improvements of the manuscript.

4.9. Appendix

TABLE A.1. *Relative concentration of heterocyclic and polycyclic aromatic hydrocarbons in (µg/g oil) from analyzed oils and condensates from the SVG.*

Wells	DBT	4-MDBT	3+2-MDBT	1-MDBT	ΣMDBT	ΣDMDBT	DBF	4-MDBF	2-MDBF+3MDBT	1-MDBF
	A	B	C	D	E	F	G	H	I	J
15/5-5	215.87	171.13	96.49	83.47	351.10	251.06	95.95	105.48	66.28	47.70
15/9-19A	247.21	155.96	113.71	129.05	398.72	282.06	37.92	95.62	72.30	55.53
15/9-11 T1	77.72	44.64	33.90	34.20	112.74	71.25	144.86	75.91	53.32	28.55
15/9-13 T2	9.69	4.24	2.89	1.61	8.74	5.65	122.28	43.62	26.72	11.76
15/12-5	100.92	95.88	50.57	45.90	192.34	164.73	184.99	110.93	81.94	48.99
15/12-6S	75.11	73.61	37.89	35.25	146.75	133.54	97.51	77.73	58.76	34.73
25/8-11	82.63	114.13	49.16	29.97	193.27	179.31	386.10	155.15	99.74	62.25
15/9-7	115.29	62.08	49.33	22.57	133.98	85.15	473.04	301.83	266.51	121.70
15/9-8	93.44	48.23	38.48	16.83	103.55	59.42	380.19	257.23	211.67	96.47
15/9-11 T2	24.23	8.80	7.74	3.22	19.76	9.06	291.55	111.67	63.13	28.99
15/9-13 T1	233.17	238.86	122.85	70.98	432.69	364.40	378.78	319.40	196.84	129.32
16/7-4	35.74	18.06	13.70	27.72	59.48	34.81	429.65	152.28	57.11	29.67
25/2-13	47.46	56.17	33.29	13.16	102.61	90.60	230.73	127.18	128.35	63.35
25/4-6S	71.10	79.58	44.18	20.60	144.35	119.63	372.39	157.89	120.69	72.35
25/5-2	75.41	58.76	40.95	25.21	124.91	90.82	194.84	133.36	128.68	65.40

Wells	ΣMDBF	ΣDMDBF	P	ΣMP	ΣDMP	$\delta^{13}C$ *n*-alk (C_{10}-C_{14})	$\delta^{13}C$ *n*-alk (C_{26}-C_{29})	$\delta^{13}C$ Pr&Ph
	K	L	M	R	S	T	U	V
15/5-5	219.47	485.49	233.17	691.49	456.92	-30.8	-31.4	-31.1
15/9-19A	223.45	468.24	198.01	455.76	266.22	-29.8	-30.9	-27.4
15/9-11 T1	157.78	263.81	62.59	118.13	72.53	-27.8	n.d.	-27.4
15/9-13 T2	82.10	91.64	20.32	36.72	18.43	-25.9	n.d.	n.d.
15/12-5	241.86	545.36	249.62	734.83	535.27	-28.7	-29.8	-28.8
15/12-6S	171.21	413.57	181.18	577.92	436.06	-29.1	-30.1	-29.1
25/8-11	317.14	606.56	425.46	1114.57	715.80	-28.5	-29.6	-28.3
15/9-7	690.04	1049.73	339.12	732.61	475.51	-27.5	-27.4	-28.2
15/9-8	565.37	1001.46	281.50	576.38	352.72	-27.4	-27.6	-27.7
15/9-11 T2	203.79	240.06	62.10	96.92	44.97	-26.0	n.d.	n.d.
15/9-13 T1	645.57	1224.36	575.57	1462.99	864.56	-29.7	n.d.	-30.1
16/7-4	239.06	258.77	59.68	127.63	75.96	-25.7	-26.8	-25.7
25/2-13	318.88	538.28	522.13	1233.54	810.79	-28.6	-28.0	-28.9
25/4-6S	350.93	584.55	544.82	1330.85	818.82	-27.8	-29.0	-28.8
25/5-2	327.44	707.55	388.43	892.58	550.46	-28.4	-28.8	-28.6

TABLE A.2. *Relative concentration of C_7 hydrocarbons in (µg/g oil) for analyzed oils and condensates from the SVG.*

Wells	P_1	P_2	P_3	N_1^5	N_2^5	N_1^6	$\delta^{13}C$ *n*-alk (C_5-C_9)	$\delta^{13}C$ Branched alkanes	$\delta^{13}C$ Cyclic alkanes
	A	B	C	D	E	F	G	H	I
15/5-5	7287.42	4637.65	1442.15	3034.97	2147.42	8465.68	-31.8	-30.0	-29.8
15/9-19A	6528.67	4060.79	943.74	3052.67	1615.51	10271.24	-32.4	-29.0	-27.7
15/9-11 T1	23362.81	15439.68	4263.85	8894.30	6776.22	58077.97	-27.8	-25.9	-25.3
15/9-13 T2	14706.02	10120.28	3297.17	5540.58	4977.80	50619.84	-26.0	-25.4	-24.7
15/12-5	14726.35	9071.51	2923.37	5866.33	4814.77	36049.54	-28.1	-26.3	-26.7
15/12-6S	7259.21	4550.45	1525.94	2837.26	2386.70	16642.71	-28.5	-26.8	-27.1
25/8-11	11342.52	6711.97	2122.09	2782.95	2937.95	20535.39	-28.5	-27.7	-26.6
15/9-7	15449.71	10833.68	3829.78	6500.19	5753.51	71915.32	-26.3	-25.3	-25.5
15/9-8	16012.48	10987.98	3750.17	6737.03	5824.96	74665.95	-25.9	-25.0	-25.1
15/9-11 T2	21527.66	14571.50	4727.84	8136.27	7374.36	72322.85	-25.6	-25.0	-24.7
15/9-13 T1	1629.18	1321.54	573.50	911.75	860.14	6649.03	-	-	-
16/7-4	15606.43	12919.00	5281.74	7273.48	6429.67	53341.78	-25.3	-25.0	-24.9
25/2-13	16869.40	7889.11	2271.78	4004.97	4468.14	40650.41	-28.2	-27.4	-26.1
25/4-6S	10112.58	5712.98	1725.13	2667.71	2847.21	27801.23	-27.3	-26.7	-25.8
25/5-2	10136.15	5689.02	1689.98	3776.42	3450.32	26557.04	-28.4	-27.2	-26.0

Chapter 5

Compound-Specific δ^2H and $\delta^{13}C$ values of *n*-Alkanes as a Tool to Unravel Complex Petroleum Mixtures in the South Viking Graben, Norway

5.1. Abstract

In order to resolve oil mixtures and for oil-source correlation purposes, both hydrogen (δ^2H) and carbon isotope compositions ($\delta^{13}C$) of *n*-alkanes and acyclic isoprenoid alkanes have been determined in petroleum mixtures and extracts from Jurassic source rocks of distinct organic matter type, depositional setting and lithology in the South Viking Graben (SVG), Norway. δ^2H values vary from -80 to -140‰ for *n*-alkanes and from -130 to -165‰ for pristane (Pr) and phytane (Ph) in oil and condensate samples. At the same maturity level, in the main oil generative window, individual *n*-alkanes from most oils and condensates show a ^2H-enrichment with *n*-alkane chain length by 15 to 50‰. With the increase in the estimated input of hydrocarbons from terrigenous source material to petroleum mixtures, the *n*-alkanes (>C_{20}) exhibit a higher ^2H-enrichment while *n*-alkanes (C_{10}-C_{14}) show a higher ^{13}C-enrichment. δ^2H values of *n*-alkanes (>C_{20}) are useful to discriminate mixed oils that were not well differentiated by $\delta^{13}C$ data. δ^2H values of individual *n*-alkanes from oils suggest a possible exchange of C-bound H with other hydrogen during their generation from precursor molecules. We find that δ^2H values of *n*-alkanes from Jurassic source rock extracts, at the onset of oil generation, were mainly controlled by the isotopic composition of biosynthetic

This chapter has been published as: Murillo, W.A, Horsfield, B., Garcin, Y., Vieth, A., Sachse, D., 2021. Compound-specific δ^2H and $\delta^{13}C$ values of n-alkanes as a tool to unravel complex petroleum mixtures in the South Viking Graben, Norway. Organic Geochemistry - In Press, published online. https://doi.org/10.1016/j.orggeochem.2020.104167.

precursors and varied from -100 to -150‰. Combination of carbon and hydrogen isotope com-positions of *n*-alkanes proved to be a useful tool to discriminate Jurassic petroleum mixtures from distinct sources in the Norwegian South Viking Graben.

5.2. Introduction

Compound-specific isotope analysis (CSIA) allows a rapid and precise determination of the stable carbon and hydrogen isotope ratios of individual organic compounds ($^{13}C/^{12}C$ and $^{2}H/^{1}H$ expressed as $\delta^{13}C$ and $\delta^{2}H$, respectively). *n*-Alkanes are among the most abundant lipid molecules derived from diverse precursors produced by a broad range of organisms (algae, bacteria and terrestrial vascular plants) (e.g., Eglinton and Hamilton, 1967; Gelpi et al., 1970; Cranwell et al., 1987; Collister et al., 1994; Ficken et al., 2000). Stable carbon isotopic analysis of individual alkanes has become an effective analytical technique to assess multiple organic matter sources in oils, source rock extracts, kerogen pyrolysates (e.g., Freeman et al., 1990; Hayes et al., 1990; Rieley et al., 1991) and even in complex mixtures of petroleum (e.g., He et al., 2012; Jia et al., 2013; Murillo et al., 2016, 2019). In recent years, there has been a renewed interest in the use of $^{2}H/^{1}H$ ratios as proxies for paleoenvironmental and climatic conditions (e.g., Sachse et al., 2004, 2006; Sauer et al., 2001; Yang et al., 2011); the understanding of biogeochemical processes (e.g., Sessions et al., 1999; Chikaraishi and Naraoka, 2005; Chikaraishi et al., 2005; Jones et al., 2008; Li et al., 2009); correlation studies in marine and terrestrially sourced petroleum systems (e.g., Li et al., 2001; Boreham et al., 2004; Schimmelmann et al., 2004); thermal maturity assessments (e.g., Dawson et al., 2005; Radke et al., 2005; Tang et al., 2005; Pedentchouk et al., 2006) and evaluation of in-reservoir alteration processes (e.g., Li et al., 2001; Sun et al., 2005; Asif et al., 2009; Murillo et al., 2016).

In general, $\delta^{2}H$ values of sedimentary hydrocarbons are mainly controlled by four factors: the $\delta^{2}H$ values of the hydrogen source or organic substrates (Sessions et al., 1999; Sachse et al., 2012); physiologic and metabolic processes in organisms that transfer water derived hydrogen into organic molecules (e.g., Sternberg, 1988; Sessions et al., 1999; Sauer et al., 2001; Chikaraishi et al., 2005; Li et al., 2009; Kahmen et al. 2013); hydrogen exchange processes after deposition that involve water (e.g., Schimmelmann et al., 1999, 2001;

Sessions et al., 2004; Dawson et al., 2005; Pedentchouk et al., 2006) and/or clay minerals (Alexander et al., 1982, 1984); and kinetic isotopic fractionations that occur during liquid hydrocarbon generation (Tang et al., 2005). $^2H/^1H$ ratios of petroleum-derived hydrocarbons of marine origin are more strongly influenced by the isotopic compositions of the biosynthetic precursors, because the $^2H/^1H$ ratio of the oceans varies very little over most of Earth's history (Lécuyer et al., 1998). Hence, $^2H/^1H$ ratios in marine systems provide an advantage over analogous studies on terrigenous systems in the understanding of relevant biochemical controls on lipid $^2H/^1H$ ratios (Li et al., 2009). Although the variability in $^2H/^1H$ ratios of marine-sourced oils is limited, Li et al. (2001) reported that the δ^2H values of individual *n*-alkanes in marine oils from Western Canada were useful for oil-source correlation. Nonetheless, oils originated from terrigenous organic matter are expected to exhibit a larger variability in δ^2H values than those originated from marine material due to large variations in δ^2H values of environmental water in terrestrial environments (Dansgaard, 1964). Schimmelmann et al. (2004) reported that the broad $^2H/^1H$ variability in terrestrially-derived oils from Australian petroleum basins is useful as a geochemical parameter for oil-source correlation. Boreham et al (2004) found the $^2H/^1H$ ratios of *n*-alkanes are critical in distinguishing two oil populations derived from two distinct Early Cretaceous coaly source rocks in the Otway Basin, Australia. Even though these previous studies have examined the δ^2H values of *n*-alkanes as a tool for correlating oils, they focused mainly on oils sourced from a single source, so that cases of mixtures have hardly been studied. In contrast, the $\delta^{13}C$ values of *n*-alkanes have been widely applied to unravel the mixing of oils (e.g., He et al., 2012; Jia et al., 2013; Murillo et al., 2016, 2019).

Due to the large relative mass difference between deuterium and protium, hydrogen isotope ratios exhibit greater variability in natural systems (Bigeleisen, 1965) compared to carbon isotope ratios (Tang and Jenden, 1995). Therefore, hydrogen CSIA could prove to be a powerful tool to discriminate petroleum mixtures derived from multiple sources. This circumvents the problem that the carbon isotope signatures of *n*-alkanes in differently sourced petroleum are overlapping, preventing a clear unmixing. Furthermore, this paper reports the combination of hydrogen and carbon isotopic data of *n*-alkanes could improve the unraveling of complex petroleum mixtures.

This study represents the second part of an integrated study that focused on a multiparameter approach by the combination of molecular and isotope compositions to differentiate petroleum mixtures from the South Viking Graben (SVG). In the first part, Murillo et al. (2019) characterized and classified samples of mixed oils and condensates from the SVG into well-defined populations by assessing of the molecular composition of light hydrocarbons and heterocyclic and polycyclic aromatic hydrocarbons as well as $\delta^{13}C$ values of individual petroleum hydrocarbons (gasoline-range hydrocarbons, *n*-alkanes and regular isoprenoids). This previous study proved that the use of carbon CSIA rather than bulk $\delta^{13}C$ values of whole oils and sub fractions enable to differentiate sources of complex mixtures. Murillo et al. (2019) also demonstrated the importance of integrating source-related molecular markers across different fractions of oils and source rock extracts in order to perform meaningful oil-oil and oil-source correlations rather than simply relying on classical correlation protocols based on biomarkers. In addition, $\delta^{13}C$ values of individual petroleum hydrocarbons were used to estimate mixing proportions of Jurassic source contributions enriched in Type-II and Type-III kerogens to reservoirs containing complex petroleum mixtures.

In the current study, hydrogen CSIA measurements are applied to better understand sources of complex mixtures of petroleum generated from multiple Jurassic source rocks of distinct organic matter types, lithologies and depositional environments previously identified in the SVG, especially in the Greater Sleipner Area (Isaksen et al., 1998a, 2002; Justwan et al., 2006a; Murillo et al., 2019). Thus, the main objectives of this study are to: (1) evaluate the δ^2H values of individual alkanes as geochemical parameters for oil-source correlation and mixed oil discrimination, (2) assess the combination of $\delta^{13}C$ and δ^2H values of *n*-alkanes to resolve complex mixtures of petroleum, and (3) identify the main factors that may control the δ^2H values of *n*-alkanes and regular isoprenoids in oils, condensates and analyzed extracts of Jurassic source rocks from the SVG.

5.3. Study Area and Geological Setting

The North Sea Graben of northwestern Europe, comprising the Central and Northern North Sea, is one of the world's largest petroleum provinces. The Norwegian sector of the Northern North Sea Basin is dominated by the Viking Graben structure. The South Viking Graben (SVG) forms a narrow rift basin, located at the southern end of the Viking Graben system, which is characterized by extensional graben tectonics (Ziegler, 1992). The study area covers an area between 60°15' and 58°N in the southern part of the Norwegian Viking Graben (Fig. 5.1) and comprises several oil and gas accumulations, such as the Sygin, Varg, Sleipner Øst, Sleipner Vest, Vølve, Glitne, Balder, Vale, Frøy and Lille Frøy fields. Cornford (2018) reported very low values of gas/oil ratio (GOR) (<200 m^3/m^3) for the Utsira High oil fields and the Glitne, Vølve and Varg oil fields, and high GOR values (>1800 m^3/m^3) in the Sleipner gas fields.

A detailed description of the tectonic evolution and geologic history of the northern North Sea is beyond the scope of this paper, therefore the reader is referred to other papers and references therein (e.g., Thomas et al., 1985; Ziegler and Van-Hoorn, 1989; Miller, 1990; Glennie and Underhill.1998). Herein is a brief summary of the depositional settings that prevailed during deposition of the Jurassic source rock system. The Middle Jurassic Sleipner Formation was deposited in an alluvial plain and peat-swamp setting, where land plant input to sediments was substantial. The Sleipner Formation is transgressively overlain by the Hugin Formation, deposited in a nearshore marine setting (e.g., Vollset and Dore, 1984; Cockings et al., 1992). Haq et al. (1987) and Fält et al. (1989) reported a continuing rise in relative sea level, which coincided with a second syn-rift phase of extension in the SVG that initiated in the late Bathonian and continued during the Oxfordian (Cockings et al., 1992). Both Sleipner and Hugin formations (Bathonian to earliest Oxfordian) consist mainly of coals and coaly shales and have the potential to generate gas and condensates (Isaksen et al., 1998a). The Heather Formation shales, deposited in an offshore marine setting, contain relatively little land-plant material. The shales are mainly a gas-prone source, but there are intervals that also generate oils (e.g., Thomas et al., 1985). The Heather Formation is diachronously overlain by the Draupne Formation, which is the main hydrocarbon source in the Viking Graben (e.g., Goff, 1983; Cooper and Barnard, 1984; Thomas et al., 1985).

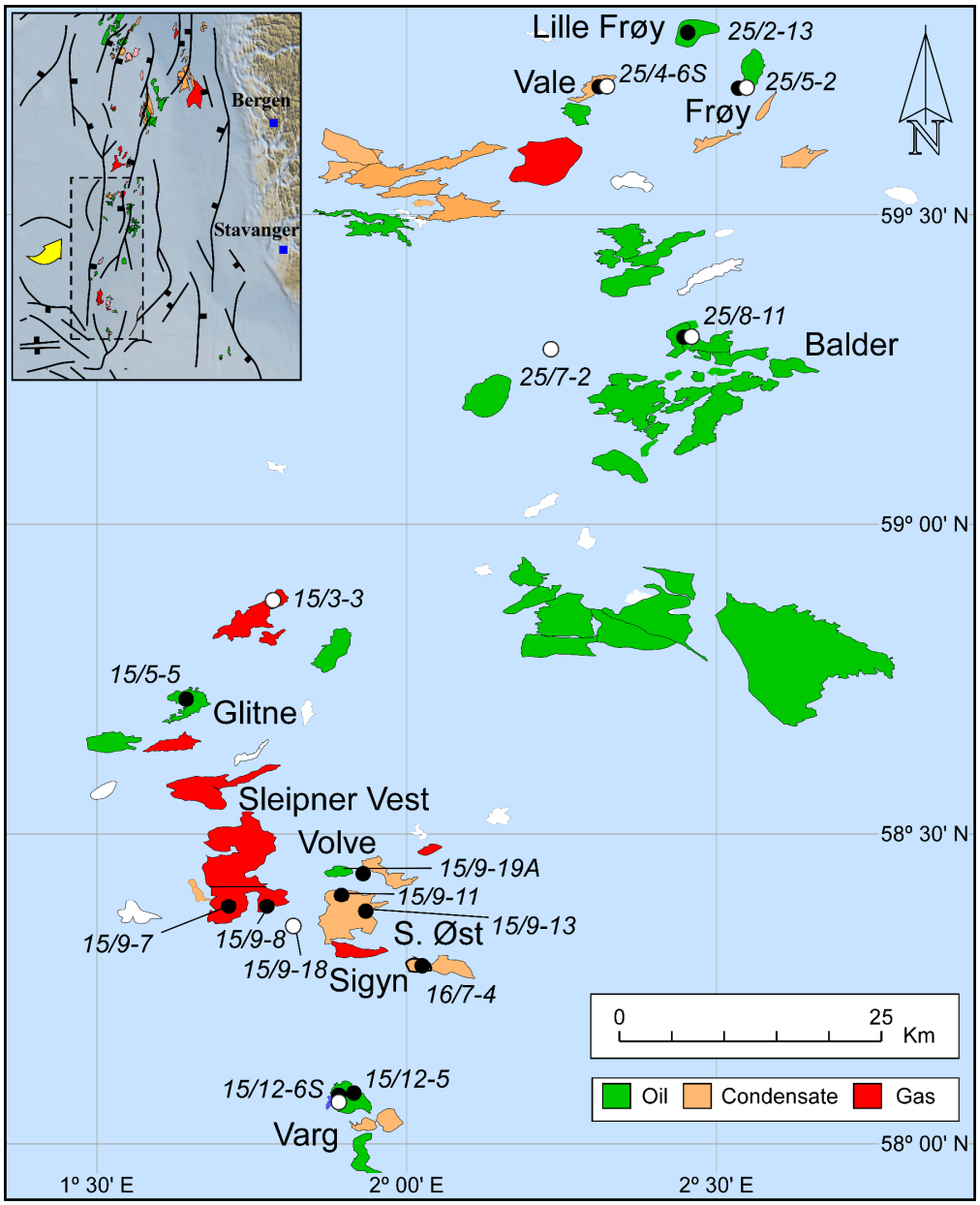

FIGURE 5.1. *Index map showing fields, discoveries and sampled wells for fluids (black circles) and source rocks (white circles) in the SVG, Norwegian North Sea.*

The Draupne Formation contains two organic facies: the Type-II and Type-II/III facies that correspond to the upper and lower sections of the Draupne Formation, respectively (e.g., Field, 1985; Isaksen and Ledje, 2001; Justwan et al., 2005). Like the Heather Formation, the lower Draupne Formation (middle Callovian to early Kimmeridgian) was deposited in an offshore marine setting. Restricted anoxic conditions, however, have likely

prevailed during deposition of the upper Draupne Formation shales (late Kimmeridgian-Ryazanian), favoring incorporation of sulfur into the organic matter (Isaksen et al., 2002). During periods of maximum transgression and low siliciclastic input to the graben, the Draupne Formation siliciclastic shales grade into calcareous shales (Isaksen et al., 1998a).

5.4. Samples

In this study, a total of 15 oil and condensate samples from 13 wells located in the SVG (Fig. 5.1) (Table 5.1) were analyzed. Liquid hydrocarbons from wells 15/9-13 and 15/9-11 were sampled from two DSTs (DST1 and DST2) (Table 5.1). Most oils and condensates represent mixtures of petroleum derived from the upper Jurassic Draupne and Heather formations and/or the Middle Jurassic Sleipner and Hugin formations (The Vestland Group). A brief sample description and assigned populations for analyzed oils and condensates (Murillo et al., 2019) are given in Table 5.1. In addition, 22 cuttings and core samples were taken from different depth intervals within the Upper Jurassic Draupne and Heather formations and the Middle Jurassic Sleipner Formation in seven wells (Murillo et al., 2019) (Table 5.2) located in the SVG (Fig. 5.1). These wells are near but not directly located in the pods of active source rocks as these areas are sparsely drilled (Justwan et al., 2006a,b).

TABLE 5.1. *Sample details and assigned populations according to the main contributing source rock for analyzed oils and condensates from the SVG.*

Well	Test	Depth MD (m)	Field/Discovery	Reservoir Fm.	Age	Oil Population	°API
15/5-5	T1	2154-2183	Glitne	Heimdal Fm.	Paleocene	A	32.1
15/9-19A	T2	3826-3865	Volve	Hugin Fm.	Middle Jurassic	B	27.5
15/9-13	T1	2765-2769	Sleipner Øst	Hugin Fm.	Middle Jurassic	C	37.0
15/12-5	-	2935	Varg	Hugin Fm.	Middle Jurassic	C	31.2
15/12-6S	T2	2875-2895	Varg	Vestland Gp.	Middle Jurassic	C	36.4
25/8-11	T1	1893-1910	Balder	Statfjord Gp.	Early Jurassic	D	39.6
25/2-13	T2B	2706-2713	Lille Frøy	Hardrade Fm.	Cretaceous	D	38.1
25/4-6S	T1	3802-3819	Vale	Hugin Fm.	Middle Jurassic	D	42.5
25/5-2	T2	3196-3201	Frøy	Sleipner Fm.	Middle Jurassic	D	35.9
15/9-11	T1	2797-2807	Sleipner Øst	Hugin Fm.	Middle Jurassic	E	53.4
15/9-7	T3	3555-3565	Sleipner Vest	Hugin Fm.	Middle Jurassic	F	48.3
15/9-8	T1	3450-3460	Sleipner Vest	Hugin Fm.	Middle Jurassic	F	46.8
15/9-13	T2	2422-2427	Sleipner Øst	Heimdal Fm.	Paleocene	G	64.7
15/9-11	T2	2410-2432	Sleipner Øst	Heimdal Fm.	Paleocene	G	56.5
16/7-4	T1	2590-2597	Sigyn	Skagerrak Fm.	Triassic	G	52.9

API gravity (°API) are from Justwan et al. (2006a). Fluids with API gravity above 40° are referred to as condensates.

Most oils and condensates represent mixtures of petroleum derived from the upper Jurassic Draupne and Heather formations and/or the Middle Jurassic Sleipner and Hugin formations (The Vestland Group). A brief sample description and assigned populations for analyzed oils and condensates (Murillo et al., 2019) are given in Table 5.1. In addition, 22 cuttings and core samples were taken from different depth intervals within the Upper Jurassic Draupne and Heather formations and the Middle Jurassic Sleipner Formation in seven wells (Murillo et al., 2019) (Table 5.2) located in the SVG (Fig. 5.1). These wells are near but not directly located in the pods of active source rocks as these areas are sparsely drilled (Justwan et al., 2006a,b).

5.5. Methods

The analytical methods were described in the methodology section, see details of specific techniques, methods and tools in Chapter 2.

5.6. Results

5.6.1. Total Organic Carbon (TOC) and Rock-Eval Pyrolysis

In order to evaluate organic richness, kerogen type, thermal maturity and petroleum generation potential, total organic carbon (TOC) and Rock-Eval analysis were undertaken on 22 core and cuttings samples from the Upper Jurassic Draupne and Heather formations and the Middle Jurassic Sleipner Formation (Table 5.2). In this study, vitrinite reflectance values (%R_o) were estimated using T_{max} data and the following equation: R_o (%) = (0.0180*T_{max}) - 7.16 (Jarvie et al., 2001). The %R_o values calculated from T_{max} indicate that most samples cover a maturity range from 0.6 to 0.8% R_o (Table 5.2), while two deeper source rock samples of the Heather Formation from well 25/7-2 have reached the late stage of oil generation (Table 5.2). The highest maturity in these samples from well 25/7-2 is also supported by measured %R_o values (1.2% R_o) (Norwegian Petroleum Directorate, 2019). Interpretation of Rock-Eval pyrolysis parameters was performed according to the standard guidelines proposed by Peters and Cassa (1994). The upper Jurassic Draupne Formation contains widely variable TOC and S1+S2 values ranging from 1.8 to 11.5 wt% (average of 5.7 wt%) and from 3.4 to 35.4 mg HC/g rock (average of 12.4 mg HC/g rock) (Table 5.2, Fig. 5.2a), respectively, which indicate good to excellent source rock quality. The Heather Formation has TOC values

that ranged from 1.1 to 3.6 wt% with an average of 2.4 wt%, and a total yield (S1+S2) ranging from 1.1 to 5.0 mg HC/g rock (average of 3.8 mg HC/g rock) (Fig. 5.2a). The lower Draupne Formation samples (well 25/7-2) have TOC values <5.5 wt% and petroleum generation potential similar to those obtained in Heather Formation samples, which suggest fair to good quality for these source rocks (Fig. 5.2a). The kerogen types in the source rocks are differentiated using the modified van Krevelen diagram of hydrogen index (HI) versus oxygen index (OI) (Peters and Cassa, 1994) (Fig. 5.2b). Most of the upper Draupne Formation samples show the highest HI values that suggest a Type-II kerogen and support its oil-prone nature (Fig. 5.2b), whereas samples from the lower Draupne and Heather formations contain both Type-III and Type-III/II kerogens (Fig. 5.2b), suggesting a potential to generate both oil and gas. The coals of the Sleipner Formation have TOC contents ranging from 38 to 80 wt%. Their HI values ranged from 180 to 350 mg HC/g TOC (Fig. 5.2b), which tend to be similar to those for the upper Draupne Formation. Isaksen et al. (1998b) (2002) suggested that coals of the Middle Jurassic Vestland Group (the Hugin and Sleipner formations) are mainly gas prone but have the capability to expel aliphatic-rich volatile oil. Nonetheless, high resinite concentration can lead to an overprediction of oil potential in coals as resinite contributes significantly to the HI value (Horsfield et al., 1988).

5.6.2. δ^2H values of n-Alkanes, Pristane and Phytane from Jurassic Oils, Condensates and Source Rock Extracts

The δ^2H values of individual *n*-alkanes (C_{15}-C_{29}) and regular isoprenoids (Pr, Ph) from hydrocarbon samples ranged from -80 to -140‰ and -130 to -165‰, respectively (Table 5.3, Fig. 5.3a). In source rock extracts, the average δ^2H values of individual *n*-alkanes and δ^2H values of regular isoprenoids ranged from -100 to -150‰ and -140 to -210‰ for upper Draupne Formation extracts; from -100 to -110‰ and -130 to -145‰ for lower Draupne Formation extracts; from -95 to -145‰ and -115 to -175‰ for Heather Formation extracts, and from -115 to -145‰ and -140 to -190‰ for coal extracts of the Sleipner Formation (Fig. 5.4a, c, e and g). The *n*-alkanes and regular isoprenoids from source rock extracts of the Heather Formation (well 25/7-2), at the late oil generation window, are more enriched in ^2H (Fig. 5.4c) and show δ^2H values that ranged from -90 to -110‰ for individual *n*-alkanes, and from -115 to -130‰ for pristane and phytane.

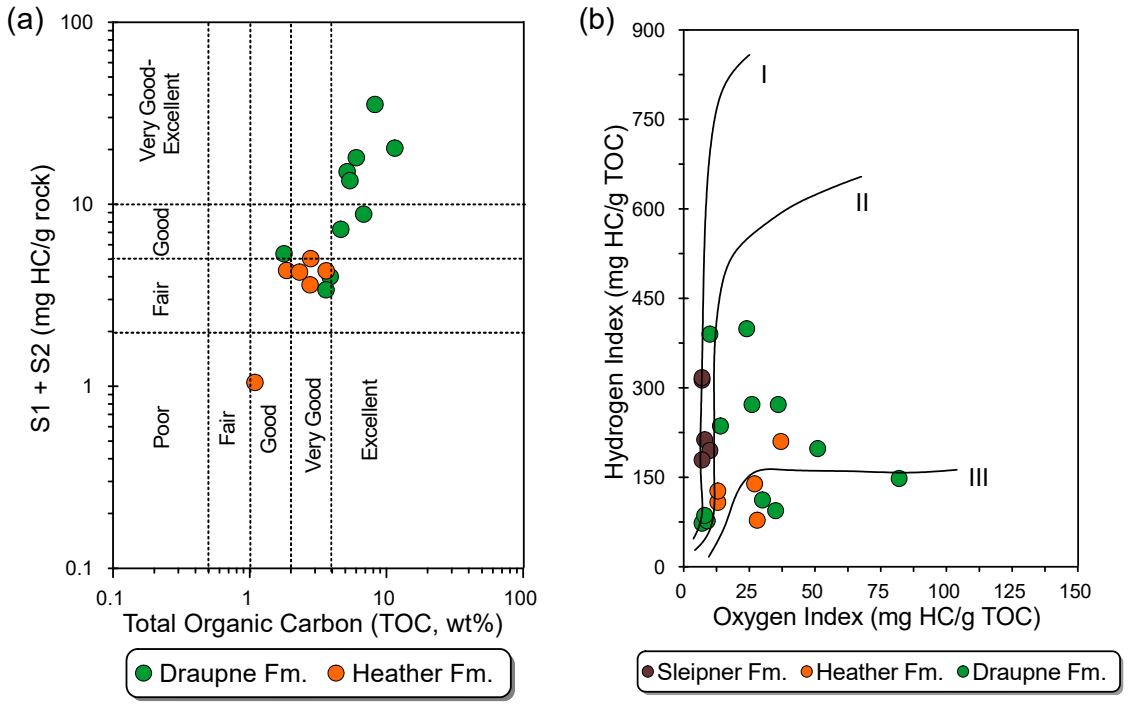

FIGURE 5.2. *(a) Plot of TOC versus petroleum generation potential (S1 + S2) showing good to very good potential for the upper Draupne Formation samples compared to the fair potential for shales samples of the lower Draupne Formation and the Heather Formation. Coal extracts of the Middle Jurassic Sleipner Formation have high values of S1+S2>100 mg/g; (b) data set of source-rock hydrogen and oxygen indices plotted on a pseudo van-Kravelen diagram for source rock samples from the SVG. The Draupne Formation contains mainly Type-II/ III kerogen whereas samples from the Heather Formation have Type-III and Type-II/III kerogens. Symbol color indicates the source rock formation as follows: green – the Draupne Formation; orange – the Heather Formation; brown – the Sleipner Formation. (For interpretation of the references to color in this figure legend, the reader is referred to the web version of this article).*

5.6.3. Biological Markers

The higher-plant derived biomarker ratio (retene to retene plus cadalene) as well as sterane and triterpane biomarker ratios, which are indicative of source organic matter type, redox conditions of the depositional environment and lithology for Jurassic source rock extracts and samples of oils and condensates are listed in Tables 5.4 and 5.5. Jurassic source rock extracts showed a decreasing input of terrigenous organic matter from Middle Jurassic to Upper Jurassic age, which is evidenced by an upward decrease of Pr/Ph ratio together with an increase of C_{27}/C_{29} regular sterane and C_{23} tricyclic terpane/ C_{24} tetracyclic terpane ratios (Table 5.4, Fig. 5.5). The high abundance of C_{24} tetracyclic terpane relative to C_{23} tricyclic terpane found in source rock extracts of the Heather Formation allowed to differentiate them from those of the Type-III kerogen rich Draupne Formation (Fig. 5.5).

TABLE 5.2. *List of source rocks sorted by well, formation and depth. Total organic content (TOC), pyrolysis oven temperature during maximum generation of hydrocarbons (T_{max}) and values of vitrinite reflectance calculated from T_{max}, methylphenanthrene index (MPI-1), methylphenanthrene distribution factors ($MPDF_1$ and $MPDF_2$) and methyldibenzothiophene ratio (MDR) for the studied source rock extracts.*

Well	Source Rock Fm.	Type	Depth MD (m)	TOC (%)	PI	S1+S2 (mg/g)	T_{max} (°C)	%Rc T_{max}	%Rc MPI-1*	%Rc MPDF1*	%Rc MPDF2*	%Rc MDR*
15/3-3 (1)	Draupne	cuttings	4070.00	11.5	0.16	20.4	428	-	0.72	0.67	0.65	0.72
15/3-3 (2)	Draupne	cuttings	4095.00	5.4	0.21	13.5	436	-	0.73	0.65	0.64	0.79
15/3-3 (3)	Draupne	cuttings	4120.00	4.6	0.29	7.3	432	-	0.74	0.62	0.62	0.80
15/3-3 (4)	Draupne	cuttings	4145.00	6.8	0.28	8.8	426	-	0.73	0.61	0.63	0.78
15/9-18 (1)	Draupne	cuttings	3120.00	1.8	0.05	5.4	426	-	0.74	0.67	0.61	0.56
15/9-18 (2)	Draupne	cuttings	3135.00	8.2	0.07	35.4	422	-	0.68	0.69	0.60	0.56
15/9-18 (3)	Draupne	cuttings	3162.50	5.2	0.07	15.1	426	-	0.64	0.69	0.62	0.58
15/9-18 (4)	Draupne	cuttings	3185.00	6.0	0.09	18.0	424	-	0.63	0.63	0.55	0.58
25/7-2(1)	Draupne	core	4132.30	3.6	0.17	3.4	439	0.74	0.70	0.60	0.65	0.92
25/7-2(2)	Draupne	core	4149.83	3.9	0.18	4.0	441	0.78	0.71	0.72	0.74	0.96
25/7-2(3)	Draupne	core	4162.33	5.5	0.14	4.6	442	0.80	0.79	0.76	0.76	1.07
25/7-2(4)	Heather	core	4343.30	2.3	0.31	4.2	453	0.99	0.78	0.75	0.74	1.31
25/7-2(5)	Heather	core	4346.30	2.8	0.23	5.0	457	1.07	0.79	0.73	0.72	1.33
15/12-6S(1)	Heather	core	2839.60	1.1	0.19	1.1	431	0.60	0.69	0.75	0.65	0.58
25/4-6S	Heather	core	3713.50	2.8	0.17	3.6	433	0.63	0.73	0.79	0.78	0.75
25/5-2 (1)	Heather	core	3179.80	3.6	0.15	4.3	432	0.62	0.67	0.79	0.79	0.61
25/5-2 (2)	Heather	core	3180.00	1.9	0.10	4.3	432	0.62	0.69	0.80	0.80	0.62
15/12-6S(2)	Sleipner	core	2951.07	37.9	0.05	126.6	436	0.69	0.73	0.80	0.78	0.62
15/12-6S(3)	Sleipner	core	2951.55	73.0	0.08	141.6	432	0.62	0.75	0.81	0.80	0.62
15/12-6S(4)	Sleipner	core	2952.40	73.9	0.07	154.3	433	0.63	0.75	0.79	0.80	0.64
25/5-2 (3)	Sleipner	core	3210.25	46.6	0.08	107.5	428	0.54	0.71	0.83	0.80	0.68
25/5-2 (4)	Sleipner	core	3215.94	80.0	0.04	261.5	432	0.62	0.73	0.83	0.83	0.68

Samples from wells 15/3-3 and 15/9-18 correspond to the upper Draupne Fm. Samples from well 25/7-2 (4132-4162m) comprise the lower Draupne Fm. % Rc T_{max}: (0.0180 T_{max})-7.16 (Jarvie et al., 2001); % Rc MPI-1: 0.6 MPI-1 + 0.4, MPI-1: 1.5 (2-MP + 3-MP)/ (P+1-MP+9-MP) (Radke and Welte, 1983); %Rc MPDF1: -0.166 + 2.242 F1, F1: (2-MP + 3-MP)/(2-MP + 3-MP + 1-MP + 9-MP); %Rc MPDF2: -0.112 + 3.739 F2, F2: 2-MP/ (2-MP + 3-MP + 1-MP + 9-MP) (Kvalheim et al., 1987) and %Rc MDR: (0.51+(0.073 MDR)), MDR: 4-MDBT/1-MDBT (Radke, 1988). (*) Data from Murillo et al. (2019). TOC: Total Organic Carbon; T_{max}: pyrolysis oven temperature during maximum generation of hydrocarbons; PI: Production Index, PI=S1/(S1+S2). Petroleum generation potential, (S1+S2). S1: the amount of free hydrocarbons in the sample, S2: the amount of hydrocarbons generated through thermal cracking. %Rc: calculated values of reflectance of vitrinite. Cuttings samples are from wells with water-based mud. The low T_{max} values (424-428 ºC) in most cuttings samples of the Draupne Formation can be related to different kerogen type (Type-II to Type-IIS). Source rock extracts from the upper Draupne Fm. (Well 15/9-18) showed a "V" shape distribution pattern of MDBTs, and a dominance of even carbon number *n*-alkanes (Murillo et al., 2019) consistent with calcareous shale source facies. Pyrolysis T_{max} values at the threshold of oil generation vary significantly for a Type-IIS kerogen (Tissot et al., 1987). Vitrinite reflectance values calculated from pyrolysis T_{max} values are not reliable for a Type-IIS kerogen. Coals defined here as having more than 40 wt%TOC.

TABLE 5.3. *Measured δ^2H values (‰) of individual n-alkanes and isoprenoid alkanes (Pr and Ph) in analyzed oils and condensates.*

Wells	15/5-5	15/9-19A	15/12-5	15/12-6S	15/9-13T1	25/8-11	25/2-13	25/4-6S	25/5-2	15/9-11T1	15/9-7	15/9-8	15/9-11T2	15/9-13T2	16/7-4
Pop.	A	B	C	C	C	D	D	D	D	E	F	F	G	G	G
n-C_{11}	-138	-123	-142	-143	-127	-124	-131	-131	-136	-126	-134	-132	-124	-126	-128
n-C_{12}	-129	-120	-137	-139	-124	-123	-130	-128	-134	-120	-128	-125	-123	-121	-124
n-C_{13}	-123	-111	-132	-133	-123	-118	-126	-127	-131	-115	-124	-122	-130	-114	-122
n-C_{14}	-123	-108	-128	-134	-121	-118	-124	-124	-129	-112	-121	-120	-118	-114	-119
n-C_{15}	-127	-110	-130	-133	-120	-118	-122	-123	-132	-120	-122	-122	-119	-112	-121
n-C_{16}	-121	-114	-132	-135	-122	-119	-124	-123	-127	-115	-118	-120	-117	-115	-119
n-C_{17}	-120	-109	-127	-132	-117	-114	-120	-118	-127	-109	-118	-117	-112	-110	-114
n-C_{18}	-116	-107	-126	-131	-117	-116	-120	-117	-125	-108	-117	-118	-108	-	-113
n-C_{19}	-122	-114	-132	-134	-120	-117	-120	-117	-125	-123	-115	-116	-109	-101	-113
n-C_{20}	-118	-107	-128	-131	-114	-115	-119	-118	-123	-118	-114	-119	-106	-	-110
n-C_{21}	-121	-109	-134	-132	-111	-117	-116	-117	-124	-121	-113	-116	-101	-	-109
n-C_{22}	-121	-105	-126	-128	-109	-113	-115	-115	-121	-106	-113	-112	-102	-	-109
n-C_{23}	-119	-109	-129	-131	-105	-114	-114	-109	-120	-92	-108	-109	-104	-	-108
n-C_{24}	-118	-108	-126	-129	-100	-121	-115	-115	-122	-102	-107	-109	-98	-	-106
n-C_{25}	-117	-103	-126	-128	-92	-115	-112	-115	-117	-98	-109	-111	-101	-	-106
n-C_{26}	-118	-107	-130	-128	-89	-112	-112	-110	-118	-94	-105	-107	-100	-	-103
n-C_{27}	-122	-105	-133	-127	-	-112	-114	-109	-116	-	-106	-105	-90	-	-104
n-C_{28}	-113	-	-117	-126	-	-115	-114	-108	-116	-	-104	-102	-84	-	-97
n-C_{29}	-124	-	-125	-140	-	-112	-113	-98	-116	-	-97	-102	-	-	-103
Pr	-145	-154	-154	-159	-141	-135	-129	-134	-146	-141	-148	-152	-148	-147	-152
Ph	-140	-151	-158	-162	-139	-136	-138	-136	-145	-139	-147	-150	-147	-	-150

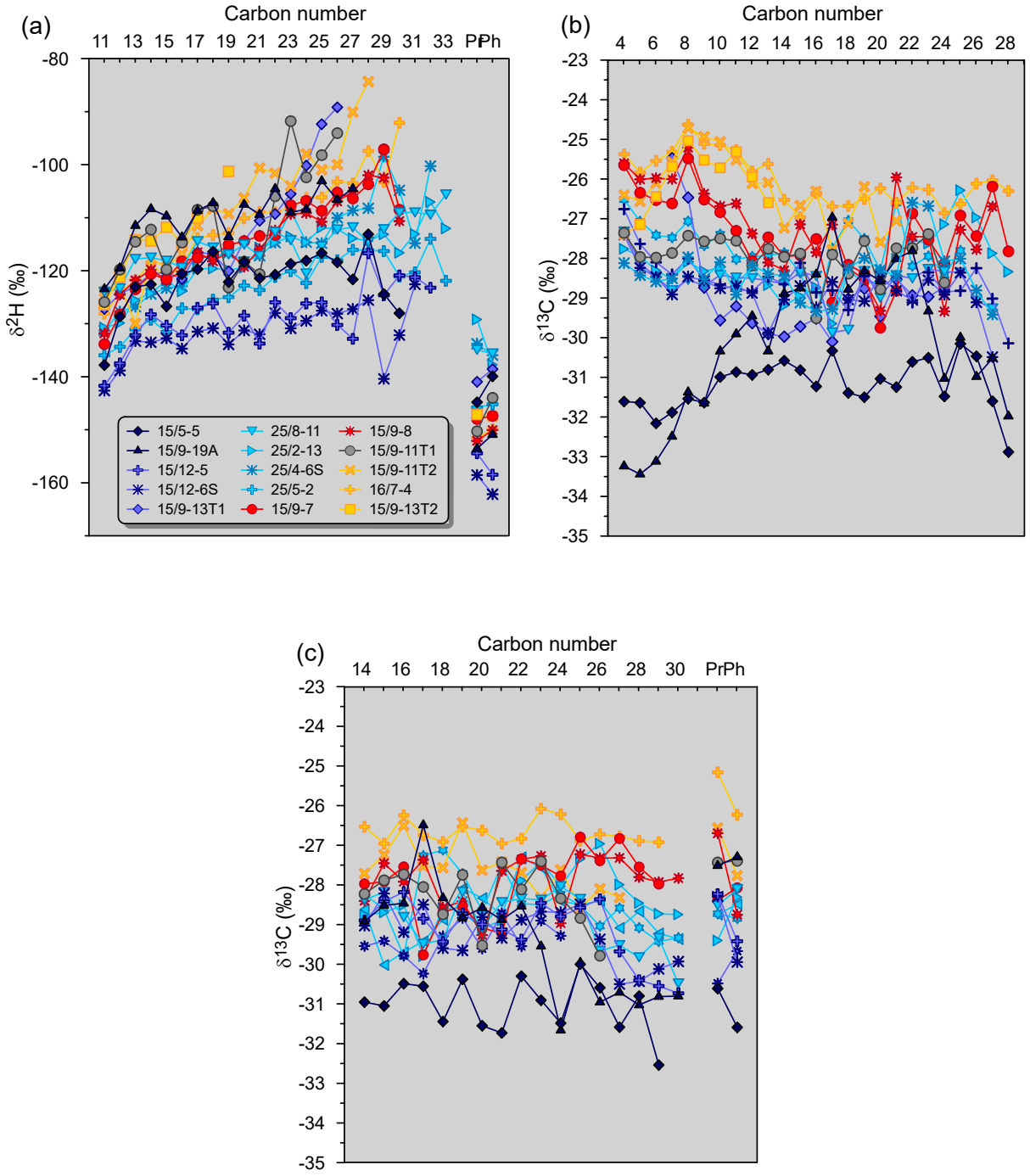

FIGURE 5.3. *Compound-specific δ^2H and $\delta^{13}C$ signatures for identified oil populations in the SVG (a) δ^2H values of n-alkanes, Pr and Ph in saturated fraction versus carbon number; (b) $\delta^{13}C$ values of n-alkanes in whole oils versus carbon number; (c) $\delta^{13}C$ values of n-alkanes, Pr and Ph in saturated fraction versus carbon number. Profiles of $\delta^{13}C$ values of n-alkanes, Pr and Ph versus carbon number redrawn from Murillo et al. (2019). Symbol color indicates the petroleum populations as follows: dark blue – Populations A (well 15/5-5) and B (well 15/9-19A), intermediate blue – Population C (wells 15/12-5, 15/12-6S, 15/9-13T1), light blue – Population D (wells 25/8-11, 25/2-13, 25/4-6S, 25/5-2), grey – Population E (15/9-11 T1), red – Population F (wells 15/9-7, 15/9-8), yellow – Population G (15/9-13T2, 15/9-11T2, 16/7-4). (For interpretation of the references to color in this figure legend, the reader is referred to the web version of this article).*

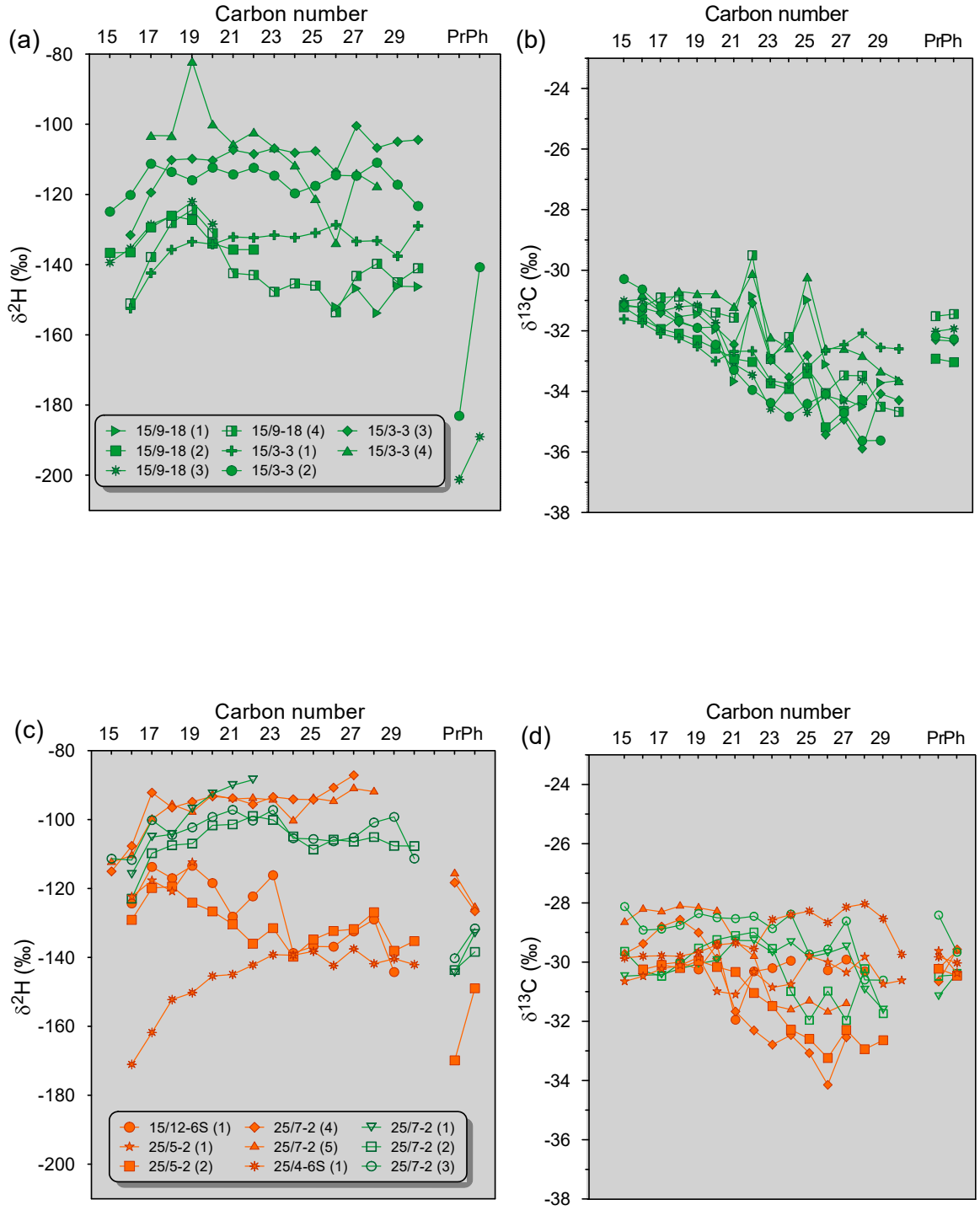

FIGURE 5.4. *δ^2H and $\delta^{13}C$ signatures of individual n-alkanes, Pr and Ph for Jurassic source rock extracts from (a) and (b) the upper Draupne Formation; (c) and (d) the Heather/lower Draupne formations.*

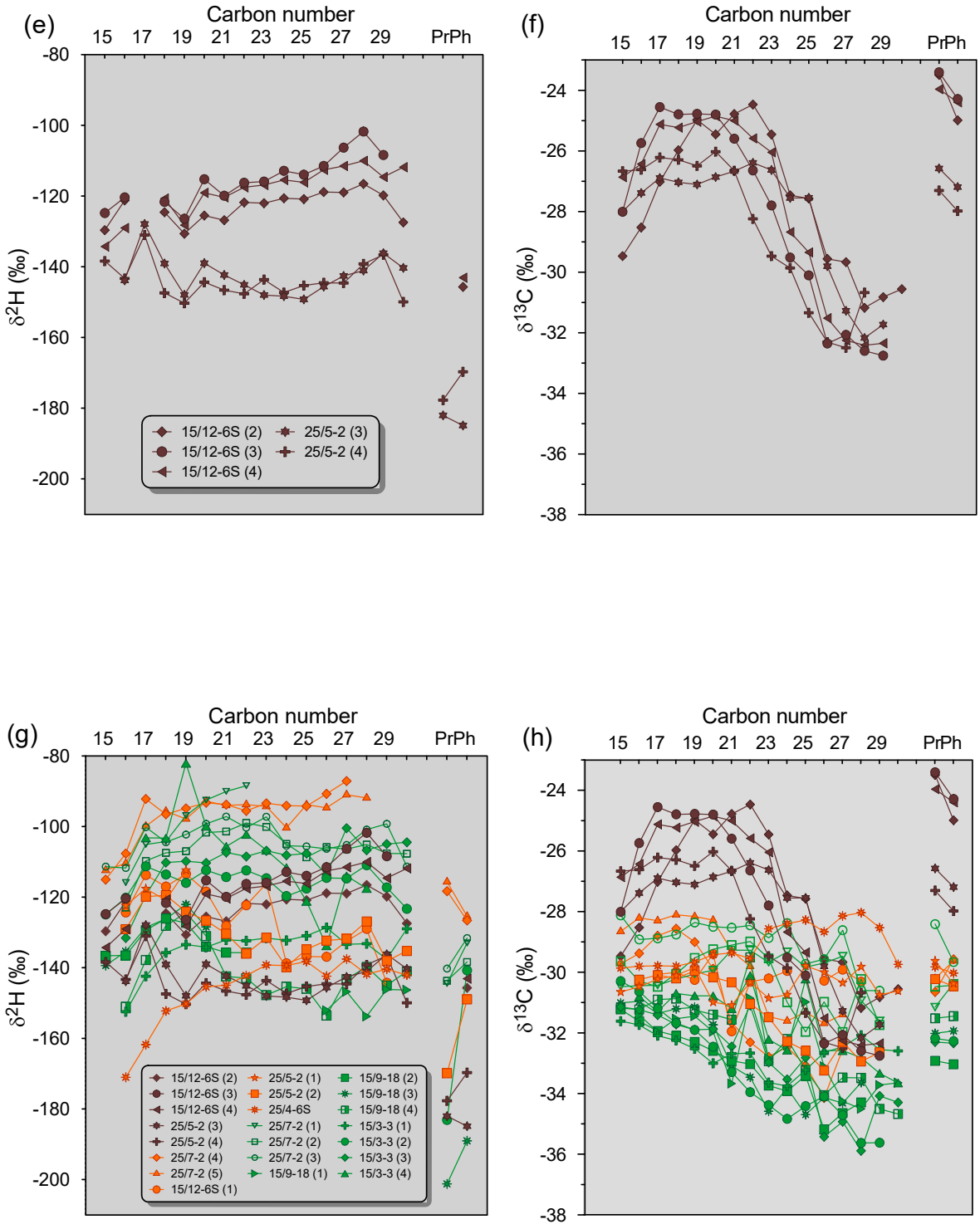

FIGURE 5.4. *(continued), (e) and (f) the Sleipner Formation; (g) and (h) all formations (the upper Draupne, lower Draupne, Heather and Sleipner formations. $\delta^{13}C$ profiles of n-alkanes, Pr and Ph are redrawn from Murillo et al. (2019).*

TABLE 5.4. *Source-related biomarker data for analyzed source rock extracts from the Upper Jurassic Draupne and Heather formations, and the Middle Jurassic Sleipner Formation.*

Wells	Source Rock Fm.	Pr/ Ph	%C_{27} St	%C_{28} St	%C_{29} St	C_{27}/C_{29} St	Reg St/ 17α-Hopanes	$C_{23\text{-}3}/C_{24\text{-}4}$	Ts/ (Ts+Tm)	Diast/ St	C_{30}-Mor/ Hop	BNH (%)	Ret/ Ret+Cad
15/3-3 (1)	Draupne	1.09	40.66	25.98	33.37	1.22	0.17	1.22	0.69	1.81	0.08	25.50	0.73
15/3-3 (2)	Draupne	0.90	36.62	31.01	32.37	1.13	0.17	1.22	0.77	1.98	0.05	28.63	0.68
15/3-3 (3)	Draupne	0.85	36.58	30.44	32.98	1.11	0.21	1.16	0.78	1.41	0.06	29.99	0.69
15/3-3 (4)	Draupne	0.93	39.61	26.50	33.89	1.17	0.23	0.96	0.87	1.52	0.07	20.76	0.69
15/9-18 (1)	Draupne	1.01	41.55	28.96	29.49	1.41	0.36	1.30	0.35	1.25	0.14	29.69	0.65
15/9-18 (2)	Draupne	0.98	41.27	27.16	31.57	1.31	0.26	1.35	0.31	1.44	0.11	24.40	0.46
15/9-18 (3)	Draupne	1.42	37.38	25.99	36.63	1.02	0.30	1.15	0.25	1.22	0.17	16.09	0.73
15/9-18 (4)	Draupne	1.60	37.45	27.78	34.77	1.08	0.27	1.45	0.35	1.39	0.16	29.05	0.87
25/7-2 (1)	Draupne	2.00	33.70	27.47	38.84	0.87	0.37	0.83	0.95	4.60	0.20	7.07	0.64
25/7-2 (2)	Draupne	2.10	33.34	26.93	39.72	0.84	0.20	1.36	0.80	2.64	0.12	6.04	0.57
25/7-2 (3)	Draupne	2.34	26.30	22.62	51.08	0.51	0.06	1.32	0.71	2.00	0.09	2.29	0.72
25/7-2 (4)	Heather	2.61	34.92	25.60	39.47	0.88	n.d.	0.50	n.d.	4.33	0.29	19.22	0.25
25/7-2 (5)	Heather	2.43	33.29	28.21	38.51	0.86	n.d.	0.41	n.d.	4.47	0.37	n.d.	0.34
15/12-6S (1)	Heather	2.37	41.38	17.37	41.25	1.00	0.08	n.d.	0.13	1.69	0.17	3.16	0.18
25/4-6S	Heather	2.47	37.86	18.51	43.63	0.87	0.05	0.31	0.50	2.18	0.08	1.21	0.61
25/5-2 (1)	Heather	2.54	39.21	20.58	40.21	0.97	0.06	0.44	0.10	2.10	0.21	66.34	0.78
25/5-2 (2)	Heather	2.37	39.37	18.80	41.83	0.94	0.08	0.43	0.15	2.36	0.17	57.75	0.85
15/12-6S (2)	Sleipner	10.39	5.03	14.39	80.58	0.06	0.02	0.17	0.02	0.58	0.27	11.01	0.34
15/12-6S (3)	Sleipner	11.03	6.24	20.18	73.57	0.08	0.02	0.16	0.02	0.59	0.28	13.09	0.42
15/12-6S (4)	Sleipner	11.11	5.10	17.92	76.98	0.07	0.03	0.14	0.01	0.62	0.27	10.93	0.32
25/5-2 (3)	Sleipner	7.72	4.51	16.26	79.23	0.06	0.18	0.08	0.05	0.05	1.20	46.49	0.72
25/5-2 (4)	Sleipner	7.08	2.50	11.03	86.47	0.03	0.15	0.09	0.05	0.04	0.93	33.82	0.66

Pr/Ph: Pristane/phytane ratio; %C_{27} St, %C_{28} St, %C_{29} St: relative percentages of C_{27}, C_{28} and C_{29} αββ regular steranes within C_{27} to C_{29} regular steranes; Reg St/17α-Hopane: (C_{27}, C_{28} and C_{29} ααα(20S+20R) and αββ(20S+20R))/ (α,β C_{29} hopane, α,β C_{30} hopane+22S and 22R epimers for C_{31}-C_{35} homologs); Dia/Reg steranes: (total C_{27} to C_{29} 13β,17α(H) 20S + 20R diasteranes)/(total C_{27} to C_{29} 5α,14β,17β(H) and 5α,14α,17α(H) 20S+20R) steranes); BNH%: 17α(H),21β(H)-28,30-bisnorhopane/17α(H), 21β(H) 28,30-bisnorhopane+17α(H), 21β(H) hopane; C_{30} Mor/Hop: 17β(H),21α(H) moretane/17α(H),21β(H) hopane; $C_{23\text{-}3}/C_{24\text{-}4}$: C_{23} tricyclic terpane/ C_{24} tetracyclic terpane; Ts/(Ts+Tm), Tm: C_{27} 17α-22,29,30-trisnorhopane, Ts: C_{27} 18α-22,29,30-trisnorhopane. Ret/Ret+Cad: retene to retene plus cadalene ratio.

TABLE 5.5. *Source-related biomarker data for studied samples of oils and condensates from the SVG.*

Wells	Pop.	Pr/Ph	%C_{27} St	%C_{28} St	%C_{29} St	C_{27}/ C_{29} St	Reg St/ 17α-hop	$C_{23\text{-}3}$/ $C_{24\text{-}4}$	Ts/ (Ts+Tm)	Diast/ St	C_{30}-Mor/ hop	BNH (%)	Ret/ Ret+Cad
15/5-5	A	0.98	40.29	27.83	31.88	1.26	0.18	1.36	0.61	1.58	0.07	17.85	0.83
15/9-19A	B	0.67	40.57	24.87	34.56	1.17	0.32	0.81	0.31	0.46	0.05	33.09	0.57
15/12-5	C	1.45	37.65	26.00	36.35	1.04	0.16	1.13	0.49	1.28	0.07	3.42	0.69
15/12-6S	C	1.41	38.34	27.26	34.40	1.11	0.16	0.96	0.57	1.34	0.08	4.12	0.73
15/9-13T1	C	1.46	40.73	26.24	33.03	1.23	0.32	1.95	0.56	1.02	0.07	13.96	0.30
25/8-11	D	2.07	33.27	27.84	38.89	0.86	0.18	0.63	0.58	1.85	0.07	11.31	0.45
25/2-13	D	3.14	38.26	19.90	41.84	0.91	0.25	1.18	0.64	2.11	0.08	3.65	0.47
25/4-6S	D	2.94	36.52	22.00	41.48	0.88	0.25	0.50	0.63	2.06	0.08	7.42	0.58
25/5-2	D	2.39	37.62	24.71	37.67	1.00	0.16	0.81	0.60	1.95	0.10	9.41	0.68
15/9-11 T1	E	1.38	46.51	23.60	29.88	1.56	0.34	n.d.	n.d.	0.89	0.05	25.87	0.19
15/9-7	F	2.18	38.16	23.35	38.49	0.99	0.20	0.67	0.40	1.40	0.09	16.53	0.73
15/9-8	F	2.53	34.70	26.16	39.13	0.89	0.17	0.69	0.40	1.55	0.10	18.38	0.71
15/9-13T2	G	3.84	n.d.	n.d.	n.d.	n.d	0.13	n.d.	n.d.	1.33	0.19	13.84	0.18
15/9-11T2	G	3.49	38.02	24.72	37.26	1.02	0.20	0.61	0.49	2.39	0.14	20.88	0.18
16/7-4	G	3.98	36.26	20.97	42.77	0.85	0.17	0.86	0.36	1.49	0.14	21.63	0.05

Pr/Ph: Pristane/phytane ratio; %C_{27} St, %C_{28} St, %C_{29} St: relative percentages of C_{27}, C_{28} and C_{29} αββ regular steranes within C_{27} to C_{29} regular steranes; Reg St/17α-Hopane: (C_{27}, C_{28} and C_{29} ααα(20S+20R) and αββ(20S+20R))/ (α,β C_{29} hopane, α,β C_{30} hopane+22S and 22R epimers for C_{31}-C_{35} homologs); Dia/Reg steranes: (total C_{27} to C_{29} 13β,17α(H) 20S + 20R diasteranes)/(total C_{27} to C_{29} 5α,14β,17β(H) and 5α,14α,17α(H) 20S+20R) steranes); BNH%: 17α(H),21β(H)-28,30-bisnorhopane/17α(H),21β(H) 28,30-bisnorhopane+17α(H),21β(H) hopane; C_{30} Mor/Hop: 17β(H),21α(H) moretane/17α(H),21β(H) hopane; $C_{23\text{-}3}$/$C_{24\text{-}4}$: C_{23} tricyclic terpane/ C_{24} tetracyclic terpane; Ts/(Ts+Tm), Tm: C_{27} 17α-22,29,30-trisnorhopane, Ts: C_{27} 18α-22,29,30-trisnorhopane. Ret/Ret+Cad: retene to retene plus cadalene ratio.

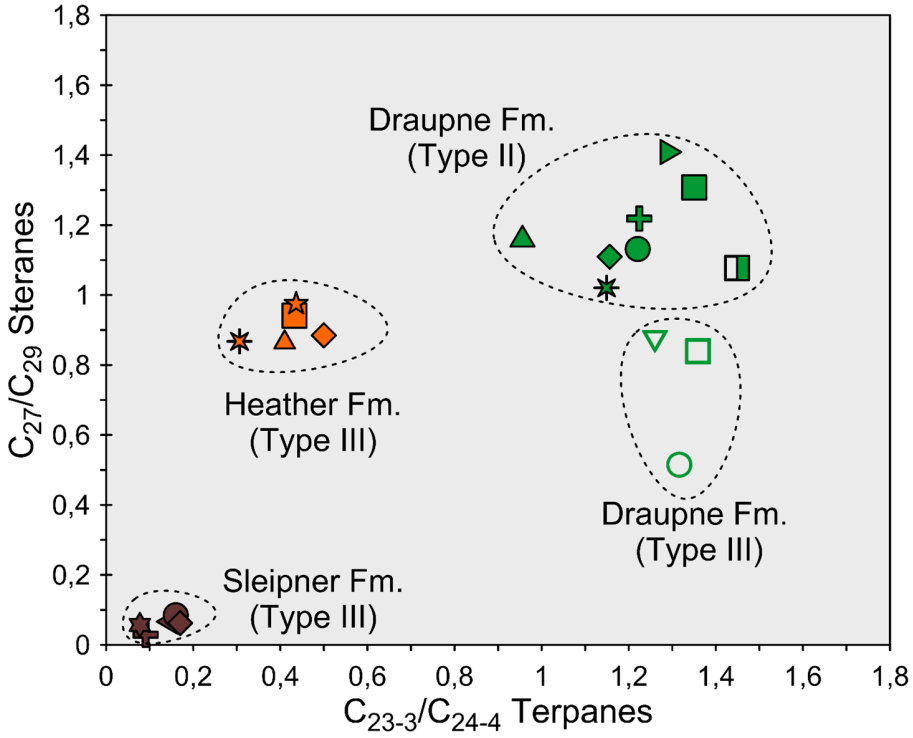

FIGURE 5.5. *Cross-plots of C_{27}/C_{29} regular steranes versus C_{23} tricyclic/C_{24} tetracyclic terpanes.*

5.7. Discussions

5.7.1. Evaluation of Thermal Maturity in Jurassic Oils, Condensates and Source Rock Extracts

Since T_{max} values at the threshold of oil generation can vary due to differences in OM type (Peters, 1986), maturity estimates in source rock extracts based on T_{max} values were supported by vitrinite reflectance values calculated from the methylphenanthrene index (%R_c MPI-1), methylphenanthrene distribution factors (%R_c MPDF1 and %R_c MPDF2) and methyldibenzothiophene ratio (%R_c MDR) published by Murillo et al., 2019. %R_c values from MPI-1, MPDF1, MPDF2 and MDR also suggest that most source rock samples cover a range from early to peak oil generation stages (0.6-0.8% R_o) (Table 5.2). Similar to %R_o values estimated from T_{max} (1.1% R_o), values of %R_c MDR (~1.3% R_o) suggest that deeper samples (4343 and 4346 m) of the Heather Formation from well 25/7-2 have higher thermal maturity (Murillo et al., 2019). The highest thermal maturity of these samples is also confirmed by measured %R_o values (1.2% R_o) (Norwegian Petroleum Directorate, 2019).

Maturity parameters based on %R_c MPI-1 and %R_c MDR (Murillo et al., 2019) show that most mixtures comprise oils of comparable maturity within the main oil generative window. Values of %R_c from MPI-1 ranged from 0.70 to 0.80% R_o, and %R_c from MDR from 0.66 to 0.80% R_o (Fig. 5.6a). A slight increase of maturity (0.8-0.9% R_o) was observed in oils from the northern half of the SVG (wells 25/8-11, 25/2-13, 25/4-6S, 25/5-2) (Fig. 5.6a). The slight maturity increase was also supported by higher light hydrocarbon ratios of quaternary to tertiary carbon species, and triaromatic steroid ratio (Murillo et al., 2019) (Fig. 5.6b and c); however, these populations of oils and condensates are within the main oil generative window. The lowest light hydrocarbon ratios of quaternary to tertiary carbon species along with the lowest values of %R_c from MDR (0.58% R_o) (Murillo et al., 2019) indicate an early mature oil-expulsion phase for the oil sample from well 15/9-19A in the Vølve field (Fig. 5.6a, b), followed by the mixed hydrocarbon sample from well 15/9-11T_1 in the Sleipner Øst field that shows early-mature oil input (Fig. 5.6a-c). The oil sample from well 15/5-5 in the Glitne field reached the onset of the oil generation window (0.66 %R_o) (Fig. 5.6a). Advanced levels of thermal maturity (%R_o>1.2%) were not detected in oil and condensate samples from the SVG.

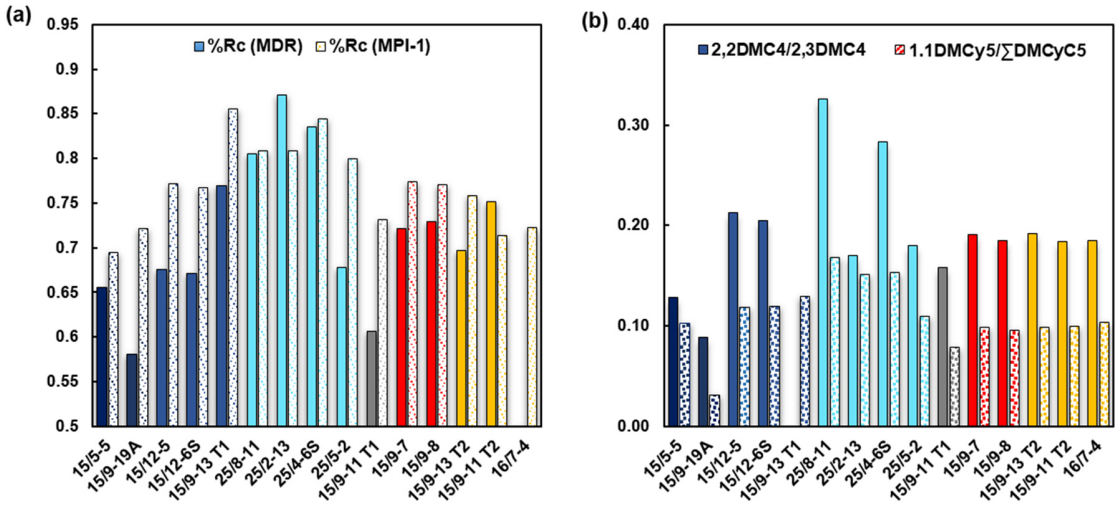

FIGURE 5.6. *Bar plots of maturity-related parameters for SVG oils and condensates based on (a) vitrinite reflectance values calculated from methyldibenzothiophene ratio (MDR) and methylphenanthrene index (MPI-1); (b) light hydrocarbon ratios of quaternary to tertiary carbon species.*

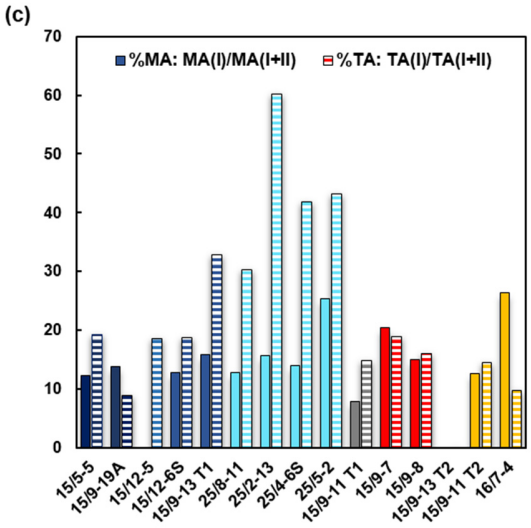

FIGURE 5.6. *Continued (c) monoaromatic and triaromatic steroid ratios (Data from Murillo et al., 2019).*

5.7.2. $\delta^{13}C$ and δ^2H values of Individual n-Alkanes to Discriminate Jurassic Petroleum Mixtures in the SVG

Based on source-related ratios and concentrations of heterocyclic and polycyclic aromatic hydrocarbons together with $\delta^{13}C$ values of *n*-alkanes, pristane and phytane, Murillo et al. (2019) recognized seven populations (A-G) of petroleum according to the relative contribution of hydrocarbons from Type-III kerogen-rich Jurassic source rocks to reservoirs containing oil mixtures in the SVG. Correlation studies indicated that Population A and B generated mainly from calcareous shale source facies of the Type-II kerogen rich Draupne Formation. Populations C and D mixed oils originated from the Type-II kerogen rich Draupne Formation and the Type-III kerogen rich Draupne/Heather Formation in different mixing ratios. Population D has a higher relative contribution of oils from siliciclastic shales of the Type III-kerogen rich Draupne/Heather Formation. Population E, F and G showed a high contribution of hydrocarbons from coals/coaly shales of the Vestland Group (coaly Type-III kerogen). In contrast, saturated biomarker ratios were not useful for discriminating most mixed oils and condensates (Table 5.5), however, oils with high contribution from marine source facies (Population A, B and C) showed the lowest Pr/Ph ratios (0.7-1.5) and high values of C_{27}/C_{29} regular sterane (1.1-1.3) and $C_{23\text{-}3}/C_{24\text{-}4}$ terpane ratios (1.0-2.0) (Table 5.5), while condensates generated from Middle Jurassic coaly sources (Population G) showed

the highest Pr/Ph ratios (3.5-4.0), and a high predominance of C_{29} regular steranes over the C_{27} homologs, especially in the condensate samples from well 16/7-4 (Table 5.5).

Mixed oil and condensate samples from the SVG showed an overall range of $\delta^{13}C$ values of *n*-alkanes (>C_{11}) from -25 to -32‰ (Murillo et al., 2019) and δ^2H values of *n*-alkanes (>C_{11}) ranging from -80 to -140‰ (Fig. 5.3a-c). The $\delta^{13}C$ values of shorter and longer chain *n*-alkanes in the ranges from C_{10} to C_{14} and C_{26} to C_{29} enabled discrimination among some mixed oil populations in the SVG (Murillo et al., 2019) (Fig. 5.3b and c). In contrast, $\delta^{13}C$ signatures of *n*-alkanes in the ranges from C_{15}-C_{19} and C_{20}-C_{25} are overlapping in most mixed hydrocarbons (Fig. 5.3b and c). Although $\delta^{13}C$ values of *n*(C_{10}-C_{14})-alkanes allowed to differentiate most mixed oil populations, in the southern part of the SVG, with the increase in the hydrocarbon input from terrigenous source material (Fig. 5.3b); in this study, δ^2H values of *n*-alkanes for the same carbon number range showed no significant isotopic variations, especially in mixed oil populations that contain a high input from terrigenous organic matter (Fig. 5.3a). However, the *n*-alkanes (>C_{20}), and specifically those of higher molecular weight, exhibited a greater ^2H-enrichment and their δ^2H values showed higher isotopic variations among mixed oils (Fig. 5.3a). Overall, the *n*-alkanes in the carbon number ranges from C_{10}-C_{14} and C_{26}-C_{29} exhibited a ^{13}C-enrichment between 2 and 6‰ (Fig. 5.3b and c) with hydrocarbon input generated from Type-III kerogen rich Jurassic source rocks (the Heather/ lower Draupne Formation and/or the Vestland Group) from Population A to G (Murillo et al, 2019). Whereas, *n*-alkanes (>C_{20}) become more enriched in ^2H (15 to 50‰) with the increasing contribution of hydrocarbons from terrigenous source material (Fig. 5.3a).

Population C mixed oils from the Varg field, generated predominantly from the Type-II kerogen-rich Draupne Formation, depicted the most negative δ^2H values of *n*-alkanes (>C_{20}) (-125 to -135‰) (Fig. 5.3a). In contrast, Population G condensates, originated mainly from Middle Jurassic coaly source rocks (the Vestland Group), exhibited the most positive δ^2H values of *n*-alkanes (>C_{20}) (-80 to -110‰) (Fig. 5.3a). Although Glitne and Vølve oils originated mainly from marine organic matter, they showed a ^2H-enrichment of *n*-alkanes up to 30‰ relative to oils of Population C (Fig. 5.3a). Schimmelmann et al. (1999) found that

the influence of water-derived hydrogen on the $^2H/^1H$ ratios of organic hydrogen is related to kerogen chemistry. Previous authors reported that the oil sample from the Vølve field generated mainly from marine, calcareous shales of the Upper Jurassic Draupne Formation characterized by a Type-IIS kerogen based on saturated biomarkers and a relatively high bulk organic sulfur content (Isaksen et al., 2002, Justwan et al., 2006a). In addition, Murillo et al. (2019) reported that oils from both Glitne and Vølve fields generated mainly from marine calcareous source facies based on the "V" shape distribution pattern of methyldibenzothiophenes, the highest concentrations of aromatic sulfur compounds as well as a dominance of the even carbon number *n*-alkanes (C_{22}-C_{26}). Therefore, the ^2H-enrichment observed in individual *n*-alkanes of both the Glitne and Vølve oils, showing a particular ^2H-enrichment in the oil sample from the Vølve field, may likely be related to the highly reactive kerogen Type-IIS that favors the isotopic transfer of water-derived hydrogen to organic matter (Schimmelmann et al.,1999).

Considering the standard deviation (σ) of 0.3‰ and 3‰ for $\delta^{13}C$ and δ^2H measurements of *n*-alkanes(>C_{10}) in oils and condensate samples, and an uncertainty (3σ) of 0.9‰ for $\delta^{13}C$ and 9‰ for δ^2H measurements of *n*-alkanes(>C_{10}), the $\delta^{13}C$ profiles of *n*-alkanes (C_{10}-C_{15}) enabled a better discrimination among mixed oil populations (E, F and G) that have the highest contribution of hydrocarbons from terrigenous higher plant source material (Middle Jurassic coals/coaly shales) (Fig. 5.3b). In contrast, δ^2H profiles of *n*-alkanes (C_{20}-C_{29}) allowed to distinguish better mixed oil populations, which have a high relative contribution of hydrocarbons from marine source material (Population A from Population B), and and especially to distinguish an increase in terrigenous source contribution (Population C from Population D) (Fig. 5.3a). δ^2H values of *n*-alkanes (>C_{20}) enabled to discriminate populations of petroleum mixtures that were not well differentiated by $\delta^{13}C$ data. Hence, the combination of δ^2H and $\delta^{13}C$ values for different carbon number ranges of *n*-alkanes allowed a clearer differentiation among mixed oil populations rather than using isotope values alone (Figs. 5.3a-c and 5.7a-c). One case study is represented by mixed oils from wells (15/12-5 and 15/12-6S) located in the southern half of the SVG (Population C), which derived mainly from the Type-II kerogen rich-Upper Jurassic Draupne Formation, and mixed oils from wells (25/8-11, 25/2-13, 25/4-6S and 25/5-2) located in the northern half

of the SVG (Population D) that sourced mainly from the Upper Jurassic Heather and/or lower Draupne formations enriched in Type III-kerogen. Similar to biomarkers (Justwan et al., 2006a) and heterocyclic and polycyclic aromatic hydrocarbon composition (Murillo et al., 2019), the weighted average δ^2H values of *n*-alkanes (>C_{20}) and regular isoprenoids (Pr and Ph) distinguished Population C from Population D, with isotopic variations of up to 20 and 30‰ (Fig. 5.7a-d). Both mixed oil populations, however, were not well distinguished by $\delta^{13}C$ data, which show small carbon isotopic variations of 1‰ (Fig. 5.3a-c and 5.7a-d).

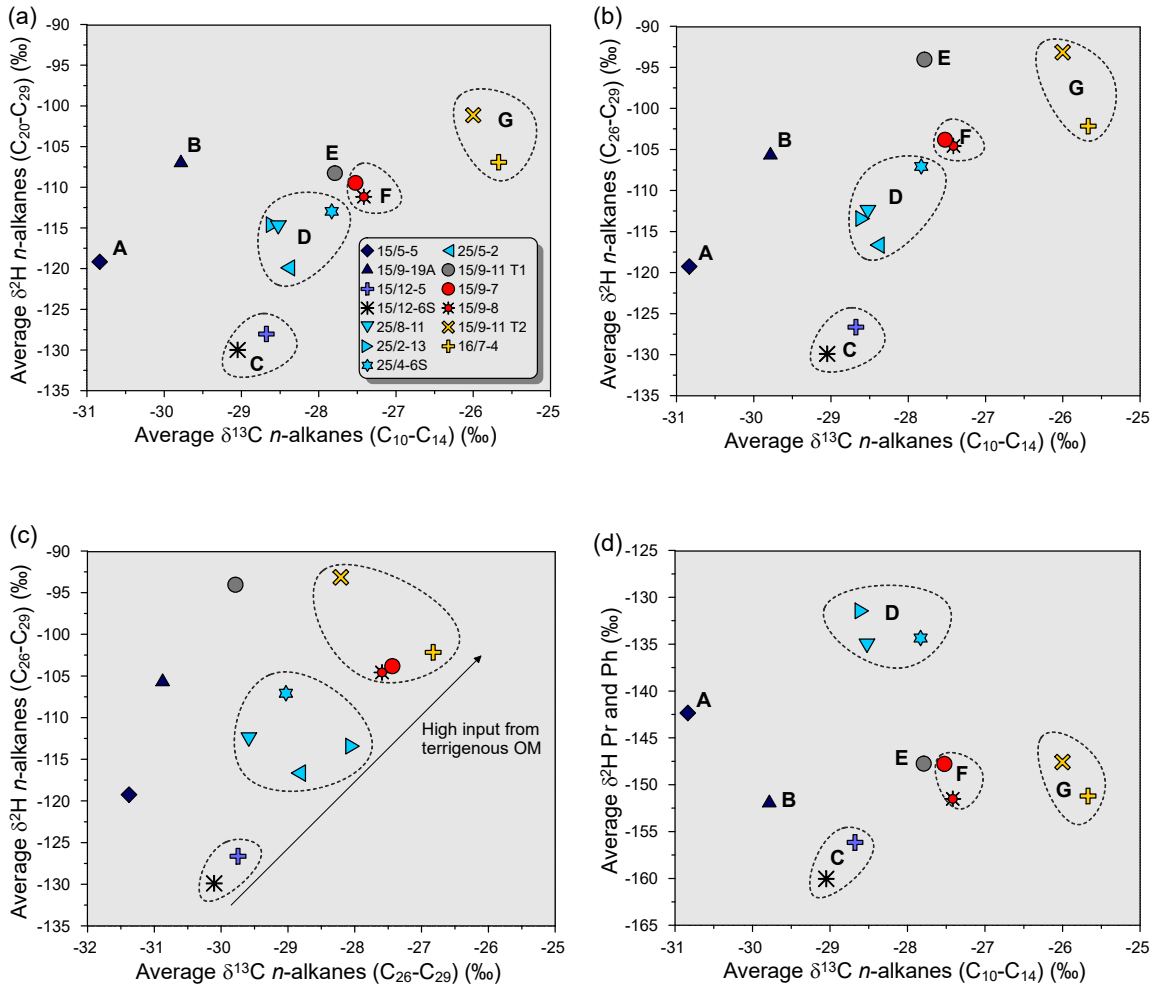

FIGURE 5.7. *Cross-plots of the average $\delta^{13}C$ and δ^2H values of n-alkanes for distinguishing mixed oil populations in the SVG. (a) Weighted average δ^2H values of n-alkanes (C_{20}-C_{29}) versus average $\delta^{13}C$ values of n-alkanes (C_{10}-C_{14}); (b) weighted average δ^2H values of n-alkanes (C_{26}-C_{29}) versus average $\delta^{13}C$ values of n-alkanes (C_{10}-C_{14}); (c) weighted average δ^2H values of n-alkanes (C_{26}-C_{29}) versus average $\delta^{13}C$ values of n-alkanes (C_{26}-C_{29}); (d) weighted average δ^2H values of Pr and Ph versus average $\delta^{13}C$ values of n-alkanes (C_{10}-C_{14}). The weighted average δ^2H values were calculated from compound-specific isotope data using the mass-peak area as the weighting factor.*

Another case illustrating the use of δ^2H values to differentiate terrigenous source contribution, corresponds to the condensate sample from well 15/9-11T1 (Population E). Population E condensate represents a particular mixture of end-member oils, where the concentration of specific components in each oil seems to be greatly different (Murillo et al., 2019). Population E shows one of the most positive δ^2H values of *n*-alkanes (Fig. 5.3a), which may indicate a dominant Middle Jurassic source contribution. This prevalent Middle Jurassic source input was not suggested by saturated biomarker ratios (Table 5.5), which seem to be biased toward the oil with the largest concentrations of these compounds (early mature oil). However, it was recognized by concentrations and source-related ratios of heterocyclic and polycyclic aromatic hydrocarbons and light hydrocarbons, which indicated a high relative contribution of hydrocarbons from terrigenous higher-plant source material (Murillo et al., 2019). This hydrocarbon mixture also shows input from a marine-dominated source as revealed by the highest C_{27}/C_{29} sterane ratio (Table 5.5) as well as a high 4-MDBT/P ratio (Murillo et al., 2019), which suggest a further contribution from the upper Draupne Formation that can be plausible due to its proximity to the Vølve field. This peculiar mixture displayed a distinctive δ^2H profile, showing a ^2H-depletion for *n*-alkanes from C_{19} to C_{21} (-118 to -125‰), which can be associated with contribution from marine source material (Type-II kerogen rich Draupne Formation) since similar δ^2H values were found in the Glitne oils (Fig. 5.3a). Whereas, a strong ^2H-enrichment is seen for *n*-alkanes ($>C_{22}$), showing δ^2H values (-90 to -110‰) similar to those for condensates from Middle Jurassic coaly sources (Fig. 5.3a).

Furthermore, Populations A and B were differentiated by the weighted average δ^2H values of *n*-alkanes ($>C_{20}$), however the hydrogen isotopic variation is subtle (15‰). Both populations differ by more than three standard deviations (>9%). More positive weighted average δ^2H value for long chain *n*-alkane was observed for the Vølve oil (-105‰) relative to that for the Glitne oil (-120‰) (Fig. 5.7a-c). In contrast, $\delta^{13}C$ values of *n*-alkanes in the carbon number ranges from C_{10}-C_{14} and C_{26}-C_{29} exhibited very small isotopic variations of up to 1‰. Nonetheless, the $\delta^{13}C$ values of *n*-alkanes (C_{14}-C_{23}), and Pr and Ph are more positive (up to 3‰) (Fig. 5.3c) for the Vølve oil (Murillo et al., 2019). On the other hand, $\delta^{13}C$ values of *n*-alkanes (C_{10}-C_{14}) enabled differentiation between Populations F and G by

1.5 and 2‰, whereas the weighted average δ^2H value for *n*-alkanes in the carbon number ranges from C_{20}-C_{29} and C_{26}-C_{29} showed subtle isotopic variations (tens of ‰) (Fig. 5.7a,b). In general, cross-plots of the average $\delta^{13}C$ values of shorter chain *n*-alkanes (C_{10}-C_{14}) *versus* the weighted average δ^2H values of long chain *n*-alkanes (C_{26}-C_{29}) and cross-plot of the average $\delta^{13}C$ values of long-chain *n*-alkanes (C_{26}-C_{29}) *versus* the weighted average δ^2H values of long chain *n*-alkanes (C_{26}-C_{29}) (Fig. 5.7b and c) depicted that these *n*-alkanes become more enriched in ^{13}C and ^2H with the increasing contribution of hydrocarbons generated from Type-III kerogen rich Jurassic source rocks. Therefore, mixtures of oils from multiple Jurassic source rocks enriched in Type-II and Type-III kerogens were clearly distinguished by the combination of carbon and hydrogen isotope compositions of *n*-alkanes. The subtle isotopic differences observed in the weighted average δ^2H values of *n*-alkanes for some mixed petroleum can be related to the limited variability in the δ^2H values of individual *n*-alkanes from most source rock extracts (Fig. 4g), which seem to be mainly controlled by the δ^2H values of biological precursors.

5.7.3. δ^2H signatures of Individual n-Alkanes in Petroleum Mixtures: Comparison of Isotope Slopes

With the exception of oils from the Glitne and Vølve fields, which are generated mainly from Type-II to Type-IIS kerogen, a consistent pattern of increasing δ^2H values with carbon number of *n*-alkanes (>C_{20}) (Fig. 5.3a) was observed for mixtures of petroleum at the main oil-generative window (0.7-0.9% R_o) (Fig. 5.6a). Schimmelmann et al. (2004), and Tang et al. (2005) published that this isotope slope can be attributed to kinetic fractionation during oil generation, which cause lower molecular weight *n*-alkanes to become regularly depleted in ^2H whereas higher homologues become progressively enriched. However, Tang et al. (2005) reported that the slope of the curve increases above $\%R_o \sim 1.0$ to 1.1, point at which the onset of significant *n*-alkane cracking occurs under the experimental conditions. In the present study, oils with calculated $\%R_o<1.0$ show increasing slopes which is likely related to mixing. The isotope slopes, representing the ^2H-enrichment per carbon number, tend to increase from mixed hydrocarbons generated mainly from Type-II kerogen rich Jurassic source rock (Population C oils from the Varg field) to those generated mainly from Type-III kerogen rich Jurassic source rocks (Populations D, F and G) (Fig. 5.8). Most of

mixed petroleum (0.7-0.9% R_o) exhibited a linear increase in δ^2H values of *n*-alkanes (C_{20}-C_{28}) with increasing chain length, showing R^2>0.9 (Fig. 5.8). A possible explanation may likely be related to the fact that Type-III kerogen has a higher proportion of organic hydrogen in the form of readily exchangeable aromatic hydrogen that can favor hydrogen exchange processes (Alexander et al., 1984; Schimmelmann et al., 1999) between organic hydrogen and other hydrogen derived from water and/or organic compounds during generation of oils. On the other hand, the ^2H-enrichment of longer chain *n*-alkanes (>C_{27}) seen in some petroleum derived mainly from land-plant source material (Fig. 5.3a) may also be related to evapotranspiration in plant leaf waxes that results in ^2H-enrichment of longer-chain *n*-alkanes (>C_{27}) (Chikaraishi and Naraoka, 2003; Yang and Huang, 2003). Nonetheless, this cannot explain the consistent ^2H-enrichment with carbon number of *n*-alkanes that have lower molecular weight.

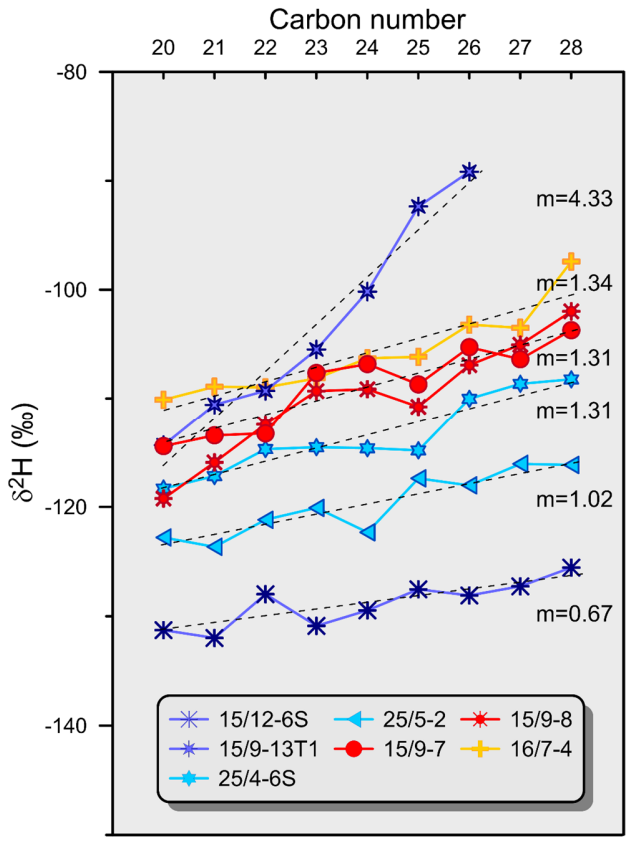

FIGURE 5.8. *Slopes of δ^2H profiles of n-alkanes (C_{20}-C_{28}) for some mixed petroleum generated mainly from Jurassic source rocks enriched in Type-II kerogen (the upper Draupne Formation - Population C from the Varg field) and Type-III kerogen (the Heather/lower Draupne Formation - Population D) and (the Vestland Group coaly sources - Populations F and G). Slope (m): delta δ^2H values/ delta carbon number.*

In contrast, the Population C oil sample from the Sleipner Øst Field (well 15/9-13T_1), originated mainly from marine organic matter, exhibits the strongest ^{2}H-enrichment of *n*-alkanes (>C_{20}) with carbon number (*m*= 4.3) (Fig. 5.8). This hydrocarbon sample has a very high ratio of C_{27} to C_{29} regular steranes and C_{23} tricyclic terpane to C_{24} tetracyclic terpane (Table 5.4) as well as more negative $\delta^{13}C$ values of Pr, Ph and *n*-alkanes (C_{10}-C_{17}) (-28.5 to -30‰) (Fig. 5.3b), indicating input from marine organic matter. Murillo et al. (2019) reported that petroleum from well 15/9-13T_1 (~0.9% R_o) shows an evaporative loss of light ends (Fig. 5.9a). Also, it shows a high relative concentration of *n*-alkanes from C_{10} to C_{20} and a very low concentration of *n*-alkanes >C_{23} (Fig. 5.9a) (Murillo et al., 2019), suggesting that this oil may likely be affected by phase fractionation. Therefore, the strong and constant ^{2}H-enrichment of *n*-alkanes with chain length observed in this sample may be associated with isotopic fractionations caused by evaporation/phase separation. Evaporation of hydrocarbons is explained by an "inverse" deuterium isotope effect, where the vapor phase is ^{2}H-enriched relative to the liquid (Hopfner, 1969; Kiss et al., 1972). Therefore, during evaporation of petroleum hydrocarbons, more volatile compounds (shorter-chain *n*-alkanes) will become depleted in ^{2}H relative to less volatile compounds (e.g., Wang and Huang, 2001, 2003). Murillo et al. (2016) reported a strong and constant ^{2}H-enrichment of *n*-alkanes with chain length, showing slopes of regression lines from 3.5 to 8.5 for condensates resulting from evaporative fractionation in the Hammerfest Basin, southwestern Barents Sea. In the Hammerfest Basin case study, the steeper slopes in δ^2H profiles of *n*-alkanes (>C_{15}) were observed in condensates with the highest parafinicity ratios and fractionation index, reflecting the impact of evaporative fraccionation.

5.7.4. Differential Changes in δ^2H values of n-Alkanes and Regular Isoprenoids to Assess Terrigenous Source Contribution to Jurassic Petroleum Mixtures

Even though condensates generated from Middle Jurassic coaly sources (Population G) showed one of the most positive δ^2H values of *n*-alkanes (-80 to -120‰), they displayed more negative average δ^2H values of Pr and Ph (-147 to -151‰) (Fig. 5.3a). Hence, they exhibited very high differences between the weighted average δ^2H values of *n*-alkanes (C_{20}-C_{29}) and regular isoprenoids (Pr and Ph), which ranged from 44 to 46‰ (Fig. 5.10). Similarly,

petroleum mixtures in the southern part of the Sleipner Vest field, which have the greatest hydrocarbon contribution from Middle Jurassic coaly sources (Population F), showed high differential changes in δ^2H values between *n*-alkanes and regular isoprenoids (38 to 40‰) (Fig. 5.10). In the SVG, very high differences between the weighted average δ^2H values of *n*-alkanes and the weighted average δ^2H values of Pr and Ph were also obtained in mixed petroleum from the Vølve field (Population B) (45‰) and from the Sleipner Øst field (Population E) (40‰).

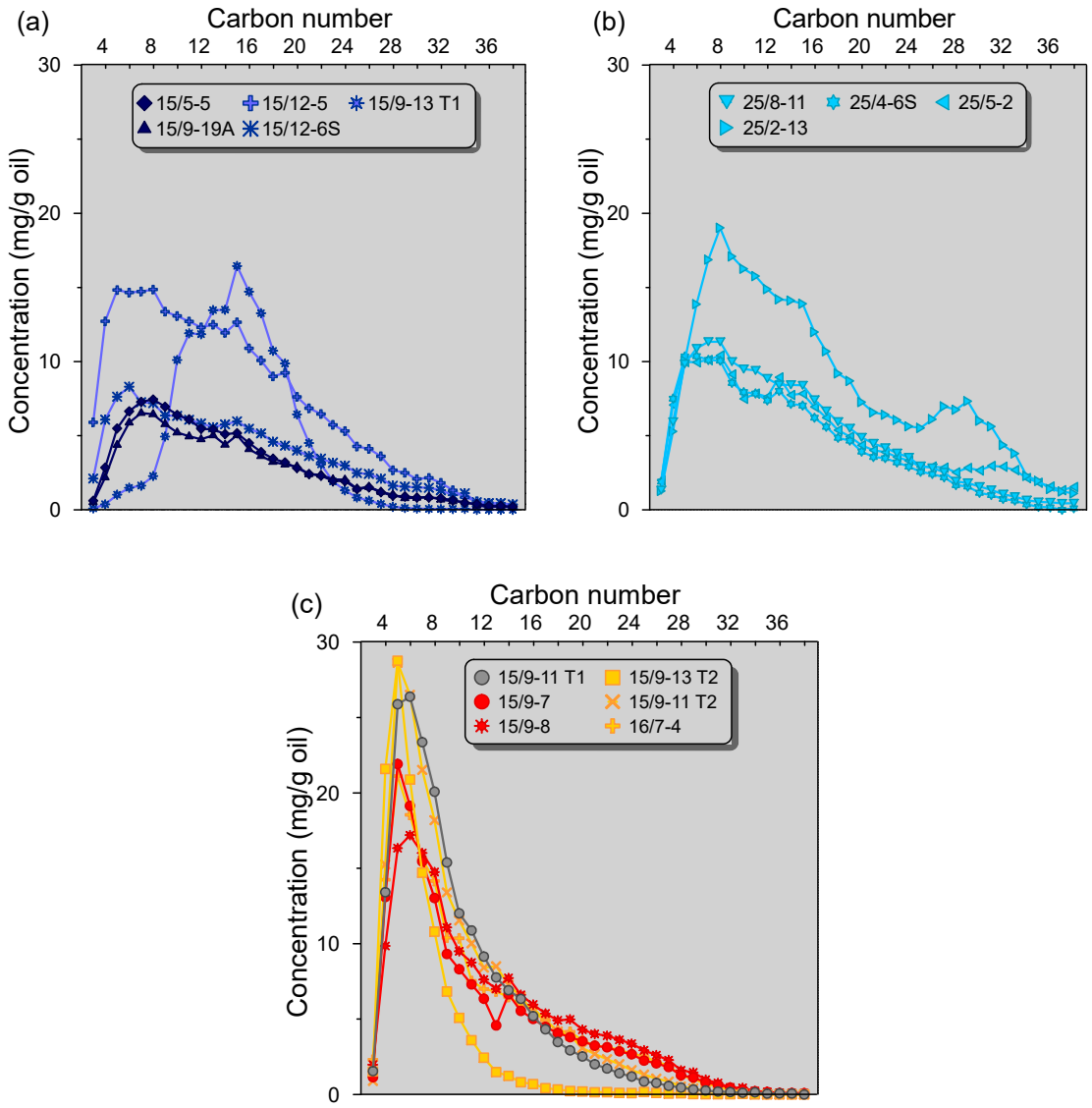

FIGURE 5.9. *Relative concentrations of n-alkanes (C_4 to C_{37}) in (a) Populations A, B and C oils; (b) Population D oils; and (c) Populations E, F and G condensates. Redrawn from Murillo et al., 2019*

For these two particular petroleum mixtures, the high differential changes observed in δ^2H values of *n*-alkanes and regular isoprenoids can be mainly associated with the ^2H-enrichment of *n*-alkanes due to the main input from calcareous shales of the Type-IIS kerogen rich Draupne Formation (Population B) and the main input from coaly sources of the Middle Jurassic Vestland Group (Population E). In addition, lower thermal maturity (early mature oils) may also cause that δ^2H values of Pr and Ph become slightly more negative. Although, the hydrocarbon sample from the Sleipner Øst field (well 15/9-13 T1) (Population C) showed a strong ^2H-enrichment of *n*-alkanes with chain length (Figs. 5.3a and 5.8), which is thought to be associated with evaporation, it also showed a ^2H-enrichment of Pr and Ph (Fig. 5.3a). Thus, the variation in δ^2H values between *n*-alkanes and regular isoprenoids in this sample is smaller than those in condensates from Middle Jurassic coaly sources and tends to be comparable to those for the same population (Population C) (Fig. 5.10).

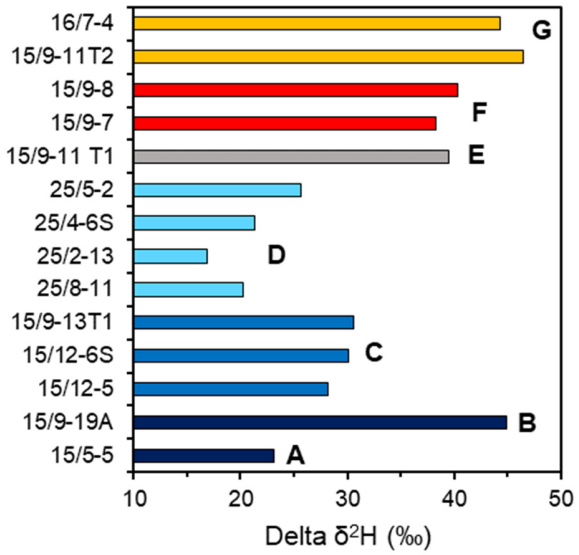

FIGURE 5.10. *Delta δ^2H values (weighted average δ^2H values of n-alkanes (C_{20}-C_{29}) – average of δ^2H values of Pr and Ph) for oils and condensates from the SVG.*

In Jurassic petroleum mixtures of similar thermal maturity (0.7-0.8% R_o) from the southern part of the SVG, the $\delta^{13}C$ values of *n*-alkanes (C_{10}-C_{14}) become more positive with the contribution of oils derived from terrigenous source material (Murillo et al., 2019). Based on the ^{13}C-enrichment of *n*-alkanes from C_{10} to C_{14}, Murillo et al. (2019) estimated the mixing

proportions of liquid hydrocarbon contribution from Jurassic source rocks enriched in Type-II and Type-III kerogens to petroleum mixtures. These mixing proportions correlated linearly with the concentrations of alkyl-dibenzothiophenes and regular isoprenoids. In this study, the difference between the weighted average δ^2H values of *n*-alkanes (C_{20}-C_{29}) and regular isoprenoids ($\Delta\delta^2H$ values) correlates linearly with $\delta^{13}C$ values of *n*-alkanes (C_{10}-C_{14}) (Fig. 5.11a). Thus, the differences between δ^2H values of *n*-alkanes and regular isoprenoids (Pr and Ph) become higher with the increase in mixing proportion of hydrocarbons generated from Type-III kerogen rich Jurassic source rocks (terrigenous-dominated source contribution, TSC) (Fig. 5.11b) and become smaller with the increase in mixing proportion of oils generated from the Jurassic Draupne Formation enriched in Type-II kerogen (marine-dominated source contribution, MSC) (Fig. 5.11c).

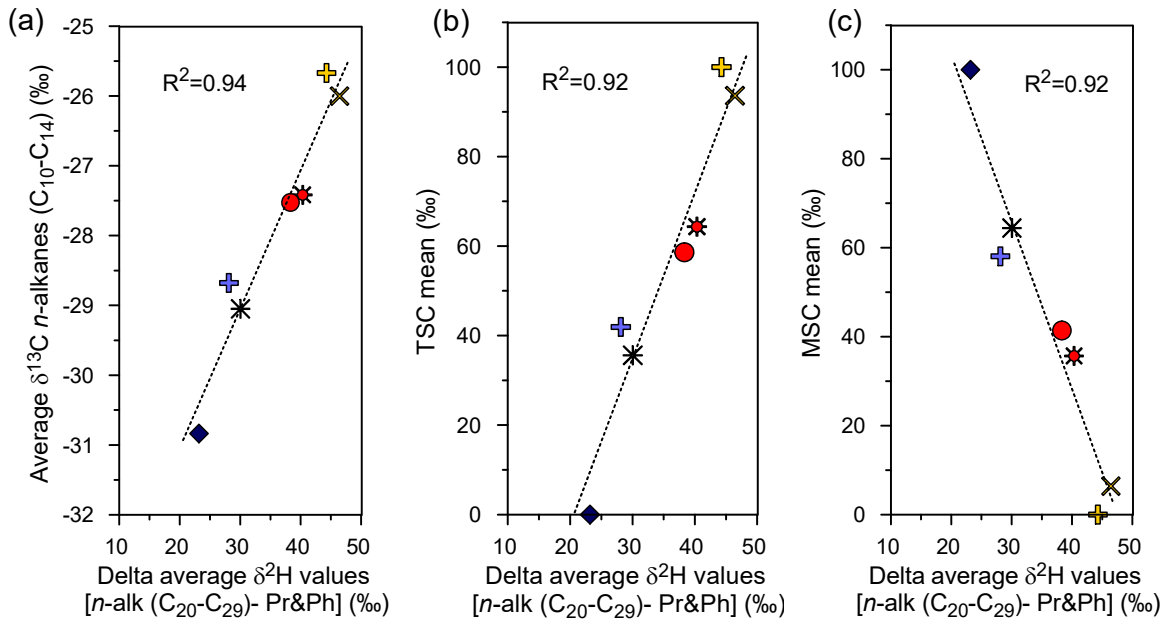

FIGURE 5.11. *Plots of (a) Average $\delta^{13}C$ values n-alkanes (C_{10}-C_{14}) versus delta δ^2H values; (b) TSC mean versus delta δ^2H values; (c) MSC mean versus delta δ^2H values for petroleum from the southern part of the SVG. Delta δ^2H= difference between the average δ^2H value of the n-alkanes (C_{20}-C_{29}) and the average δ^2H value of Pr and Ph. MSC: marine-dominated Jurassic source contribution (input from the Type-II kerogen rich Draupne Formation). TSC: terrigenous-dominated Jurassic source contribution (input from the Heather/lower Draupne formations plus the Vestland Group). Percentage data of MSC and TSC are from Murillo et al. (2019). Delta δ^2H values for hydrocarbon samples affected by phase fractionation (wells 15/9-13 T2 and 15/9-13 T1) were excluded.*

5.7.5. $\delta^{13}C$ and δ^2H values of Individual n-Alkanes for Jurassic Source Rock Extracts from the SVG

The shape of the *n*-alkane carbon isotope profiles, at least in the C_{12}-C_{34} range, depends mainly on the source matter type/depositional environment (e.g., Murray et al., 1994). Evaluation and comparison of the shape of the carbon and hydrogen isotope profiles of individual *n*-alkanes (C_{15}-C_{30}) for Jurassic source rock extracts of distinct organic matter type and depositional environment was performed in the present study. The studied Jurassic source rocks included the Middle Jurassic Sleipner Formation deposited mainly in the alluvial plain and peat-swamp setting, the Upper Jurassic lower Draupne/Heather Formation deposited in an offshore marine setting and the upper Draupne Formation deposited in a marine setting with restricted bottom-water circulation.

5.7.5.1. Carbon Isotope Profiles of n-Alkanes for Jurassic Source Rock Extracts of Distinct Origin

The average $\delta^{13}C$ values of *n*(C_{15}-C_{19})-alkanes for Jurassic source rock extracts become more negative with decreasing input of terrigenous organic matter in source rocks from Middle Jurassic to Upper Jurassic age (Fig. 5.4b,d,f and h). Although the short-chain alkanes (*n*-C_{15} to *n*-C_{19}), which are derived from algae and bacterial biomass (Gelpi et al., 1970; Cranwell et al.,1987), tend to exhibit a flat carbon isotope pattern for most source rock extracts, most of the carbon isotope profiles of intermediate *n*-alkanes (*n*-C_{20} to *n*-C_{25}) for Jurassic source rocks (the Draupne, Heather and Sleipner formations) showed a trend towards isotopically lighter values with increasing chain length (Fig. 5.4h). Source rock extracts from coals/coaly shales of the Sleipner Formation depicted the steepest negative slopes (Fig. 5.4b,d and f). In contrast, long-chain *n*-alkanes (*n*-C_{26} to *n*-C_{30}) tend to have relatively constant $\delta^{13}C$ values for all of the source rock extracts (Fig. 5.4h). Murray et al. (1994) suggested that negatively sloping curves of $\delta^{13}C$ profiles of *n*-alkanes may be likely associated with bacterial and perhaps fungal reworking of the higher plant biomass. Nonetheless, Bjøroy et al. (1992) also reported ^{13}C-depletion of *n*-alkanes with chain length for carbonate source rock extracts. $\delta^{13}C$ profiles of *n*-alkanes are similar for source rock extracts from the Heather and lower Draupne formations (Fig. 4d), showing slight variability in organic facies.

Sun et al. (2000) found that typical coal extracts from the Turpan Basin (northwest China) tend to have uniform $\delta^{13}C$ values for all *n*-alkanes from C_{12} to C_{30}, while $\delta^{13}C$ values from the interbedded shales present significant isotopic differences between *n*-alkanes from C_{12} to C_{22} (^{13}C-enriched) and *n*-alkanes from C_{24} to C_{30} (^{13}C-depleted). However, Xiong et al. (2005) found that *n*-alkanes from both coals and coal interbedded mudstones in the Turpan Basin display negatively sloping carbon isotope profiles. Coals of the Middle Jurassic Sleipner Fm. (38-80% TOC) (Table 5.2) also showed a ^{13}C-depletion of *n*-alkanes with increasing length from C_{20} or C_{22} to C_{27}, along with a ^{13}C-enrichment of odd carbon-numbered *n*-alkanes relative to even carbon-numbered *n*-alkanes (C_{25}-C_{29}) (Fig. 5.4f). This strongly negative sloping $\delta^{13}C$ profiles of *n*-alkanes are consistent with a predominant land plant source (Bjorøy et al., 1991; Dzou and Hughes, 1993; Murray et al., 1994; Wilhelms et al., 1994). Furthermore, those zigzag patterns in $\delta^{13}C$ values of *n*-alkanes are observed in modern terrestrial plants (Collister et al., 1994; Chikaraishi and Naroaka, 2003). In contrast, $\delta^{13}C$ values of *n*-alkanes in condensates sourced from Middle Jurassic coaly sources (Fig. 5.3b,c) showed profiles isotopically uniform or relatively flat over the *n(*C_{14}-C_{29}) range (Murillo et al., 2019), which is associated with a homogenous precursor that cause slight isotopic differences between long and short-chain alkanes (Eglinton, 1994; Murray et al., 1994; Sun et al., 2000).

5.7.5.2. Hydrogen Isotope Profiles of n-Alkanes for Source Rock Extracts of Distinct Origin

- ***Coal Extracts from the Middle Jurassic Sleipner Formation (Type-III Kerogen)***

Previous studies have reported negative δ^2H values of *n*-alkanes, ranging from -150 to -250‰, in coals and carbonaceous mudstones from the Turpan and Liaohe Basin, China (Xiong et al., 2005; Tuo et al., 2006). Coals and coal-bearing mudstones from the Middle Jurassic swamp facies in the Turpan basin show δ^2H values of *n*-alkanes that ranged from -200 to -250‰ (Xiong et al., 2005). In this study, however, coal extracts from the Middle Jurassic Sleipner Formation at the onset of oil generation (0.6-0.7 $\%R_o$) (Table 5.2), showed δ^2H values of *n*-alkanes that ranged from -100 to -150‰ (Fig. 5.4f). These isotopic values are similar to δ^2H values of lipids derived from modern terrestrial plants (e.g., Chikaraishi

and Naraoka, 2006; Hou et al., 2007; Sachse et al., 2012); thus the original biological signal seems to be preserved in analyzed source rock extracts. Generally, terrigenous organic matter is ^2H-enriched relative to marine organic matter because terrestrial plants fractionate $^2H/^1H$ of *n*-alkyl lipids less strongly (by 20-70‰) than marine algae (Sessions et al., 1999; Zhang and Sachs, 2007; Li et al., 2009; Sachse et al., 2012). Sessions (2016) indicated that terrestrial leaf waxes become noticeably depleted in ^2H, with δ^2H values <-200‰, relative to marine lipids when the δ^2H value of meteoric water drops below ~-70‰. However, when the supplied water has a δ^2H value of 0‰ (seawater), terrestrial leaf waxes can be enriched in ^2H relative to marine lipids, with δ^2H values ranging from -120‰ to -150‰ (Sessions, 2016). Haq et al. (1987) and Fält et al. (1989) reported a continuing rise in relative sea level, which coincided with a second syn-rift phase of extension in the SVG that initiated in the late Bathonian and continued through to the Oxfordian (Cockings et al., 1992).

Coals of the Middle Jurassic Sleipner Formation are characterized by very high ratios of Pr/Ph (7-11), the lowest ratio of C_{23} tricyclic terpane to C_{24} tetracyclic terpane and a very high abundance of C_{29} regular steranes over C_{27} homologues (C_{29}, 70-80% and C_{27}, 2-6%) (Table 5.4, Fig. 5.5), indicating a very high input of higher plant derived organic matter deposited under highly oxidizing conditions. All analyzed coal extracts from the Sleipner Formation (0.6-0.7% R_o) from wells 25/5-2 and 15/12-6S showed similar $\delta^{13}C$ values of *n*-alkanes; nonetheless they displayed differences in their δ^2H data (Fig. 5.4e and f). δ^2H values of *n*-alkanes (>C_{20}) from extracts of the Sleipner Formation in well 25/5-2 (northern part of the SVG) are more depleted in ^2H for about 30-40‰ than those in well 15/12-6S (southern part of the SVG) (Fig. 5.4f). These variations may reflect original differences in δ^2H values of leaf wax lipids due to different geographical or plant type sources. Even though coal extracts from wells 25/5-2 and 15/12-6S have similar biomarker ratios, some variations were observed in the Pr/Ph ratio and the relative abundance of higher-plant derived biomarkers, such as retene and cadalene (Table 5.4). Coal extracts from well 25/5-2 (Pr/Ph: 7-8) have higher abundance of retene relative to cadalene, showing a higher ratio of retene to retene plus cadalene (0.66-0.72), whereas coal extracts from well 15/12-6S (Pr/Ph: 10-11) show dominance of cadalene relative to retene and have a lower ratio of retene to retene plus cadalene (0.32-0.42) (Table 5.4). Simoneit (1985) and Alexander et al. (1988) indicated that

the higher plant biomarker retene is derived from compounds produced by conifers, while specific higher plant markers like cadinane has been reported as a source for cadalene (van Aarssen et al., 1990; 1992) and it is thought to be derived from gymnosperm resins (Simoneit et al., 1986) or from fragmentation of polycadinene resins produced by angiosperms (van Aarssen et al., 1990). Due to the fact that retene and cadalene represent input from a different plant type, variation in their relative abundances may reflect paleovegetation changes that may probably be associated with changes in paleoclimate (van Aarssen et al., 2000). Coal extracts from the Sleipner Formation showed a slight ^2H-enrichment in *n*(C_{27}-C_{29})-alkanes (Fig. 5.4e). This ^2H-enrichment of long-chain *n*-alkanes, derived from plant leaf waxes, can be the result of evapotranspiration (Estep and Hoering, 1980). Some coal extracts depicted a zigzag pattern of δ^2H values, however, this small enrichment and depletion in ^2H is independent of carbon number of *n*-alkanes. This zigzag distribution pattern for δ^2H values of *n*-alkanes has been related to waxes from terrestrial higher plants, and it has been observed in *n*-alkanes from terrigenous source rock extracts, as well as some plant leaves (e.g., Chikaraishi and Naraoka, 2003; Yang and Huang, 2003; Xiong et al., 2005).

- ***Shale Extracts from the Upper Jurassic Heather and Lower Draupne Formations Enriched in Type-III Kerogen***

The δ^2H values of *n*-alkanes from source rock extracts of the Heather Formation (4343 and 4346m) in well 25/7-2 (1.2-1.3% R_o) are up to 50‰ more positive relative to the corresponding δ^2H values for source rock extracts of the Heather Formation (0.6-0.7% R_o) from other wells. Despite the higher maturity level in source rock extracts from well 25/7-2, the δ^2H profiles of *n*-alkanes (>C_{17}) tend to be flat with a slight ^2H-enrichment of longer chain *n*-alkanes (Fig. 5.4c). However, Tang et al. (2005) observed a significant ^2H-enrichment with carbon chain length of *n*-alkanes at high level of thermal maturity. Sessions (2016) pointed out that a combination of processes may produce exagerations or cancellations of changes in hydrogen isotopic composition. Except for δ^2H data of *n*-alkanes from Heather Formation extracts in well 25/7-2 (-90 to -110‰), the δ^2H values of individual *n*-alkanes (>C_{20}) ranged from -120 to -145‰ (Fig. 5.4c) for shale extracts from the Heather Formation at the onset of oil generation (Table 5.2), which correspond to δ^2H values of leaf wax lipids (e.g., Chikaraishi and Naraoka, 2006; Hou et al., 2007; Sachse et al., 2012). The

δ^2H values of *n*-alkanes from Heather Formation extracts overlapped with the δ^2H values of those from calcareous shales of the upper Draupne Formation extracts in well 15/9-18. They also exhibited differences in the order of 20-30‰ with δ^2H values of *n*-alkanes from siliciclastic shale extracts of the upper Draupne Formation in well 15/3-3 (Fig. 5.4a, c and g), showing more negative δ^2H values. Likewise, extracts from the lower Draupne Formation from well 25/7-2 showed similar δ^2H values of *n*-alkanes (C_{15}-C_{23}) to those from Heather Formation extracts in the same well. Nonetheless, extracts from the Heather Formation, which have higher thermal maturity (Table 2), showed more positive δ^2H values of *n*-alkanes (>C_{23}) (Fig. 5.4c).

- ***Siliciclastic and Calcareous Shale Extracts from the Upper Draupne Formation Enriched in Type-II Kerogen***

The average δ^2H values of individual *n*-alkanes from analyzed marine source rock extracts and oils (-100 to -150‰) are more positive (Figs. 5.3a and 5.4a, c) than those expected values for *n*-alkyl lipids from marine organisms (marine algae), which have mean δ^2H values near -170‰ (Li et al., 2009; Sessions, 2016). Nonetheless, these δ^2H values are similar to those reported by Li et al. (2001) for marine-sourced oils from the Western Canada basin. These authors suggested that these differences between δ^2H values of *n*-alkanes from marine-sourced oils and δ^2H values of *n*-alkyl lipids derived from marine planktonic sources may be attributed to isotopic exchange of ^2H-depleted organic matter with formation waters, which are typically ^2H-enriched relative to organic hydrogen, during thermal maturation. Sessions et al. (2004) and Wang et al. (2009) reported that this variation range in δ^2H values is consistent with equilibrium $^2H/^1H$ fractionation between water and *n*-alkanes.

Even though the $\delta^{13}C$ values of individual *n*-alkanes are similar for source rock extracts from siliciclastic and calcareous shale facies of the Type-II kerogen rich-Draupne Formation in wells 15/3-3 and 15/9-18, the δ^2H values of *n*-alkanes displayed variations between both of them (Fig. 5.4a and b). Source rock extracts from the Type-II kerogen rich-Draupne Formation in wells 15/3-3 and 15/9-18 showed the lowest Pr/Ph ratio (0.9-1.6), the highest C_{27}/C_{29} sterane (1.0-1.4) and $C_{23\text{-}3}/C_{24\text{-}4}$ (1-1.5) ratios and a high BNH content (20-30%) typical of marine organic matter deposited under reducing condition (Table 5.4, Fig.

5.5). In addition, they showed very low ratios of regular steranes/17α-hopane (0.17-0.36), which are slightly higher for source rock extracts from well 15/9-18 (0.27-0.36) (Table 5.4). The ratio of regular steranes to 17α-hopane is useful to assess input of eukaryotic (algae and higher plants) *versus* prokaryotic (bacteria) organisms to the source rock (Moldowan et al., 1985). The low values of steranes/hopanes (<1) found in the Draupne Formation source rock extracts and oils generated mainly from the Draupne Formation (Tables 5.4 and 5.5) are indicative of bacterial input or microbially reworked organic matter (e.g., Tissot and Welte, 1984).

Overall, δ^2H values for *n*-alkyl lipids derived from marine planktonic sources are typically in the range from -150 to -200‰, with a mean near -175‰ (e.g., Li et al., 2009). Jones et al. (2008) observed that bacterial fatty acids were often enriched in ^2H relative to those from phytoplankton, showing δ^2H values that ranged from -73 to -132‰ for the most ^2H-enriched compounds. Li et al (2009) also reported that several bacterial lipids (fatty acids and hopanols) tend to be ^2H-enriched relative to similar eukaryotic products by 30‰ or more. Also, aerobic bacteria growing heterotrophically tend to be ^2H-enriched relative to plants and algae (Osburn, 2013, Heinzelmann et al., 2015). In this study, *n*-alkanes from analyzed extract samples of the Type-II kerogen-rich Draupne Formation, characterized by a major bacterial input, are enriched in ^2H and showed δ^2H values from -100 to -150‰, which overlapped with the δ^2H values of *n*-alkanes from the Type-III kerogen rich Heather and Sleipner formations (Fig. 5.4g). The siliciclastic shale extracts from well 15/3-3 of the Type-II kerogen rich Draupne Formation showed more positive δ^2H values of *n*-alkanes, which ranged from -100 to -120‰; whereas calcareous shale extracts from well 15/9-18 exhibited more negative δ^2H values (-120 to -150‰) (Fig. 5.4a). Even though source rock extracts from both wells showed similar thermal maturity, with $\%R_c$ from MPI-1 (~ 0.65-0.75% R_o), within the main oil generative window (Table 5.2); higher ratios of Ts/Ts+Tm (0.7-0.9) and Diast/St ratios (1.4-2.0) were found in extracts from siliciclastic shale facies of the upper Draupne Formation (well 15/3-3) relative to those from calcareous shale facies (well 15/9-18), which show Ts/Ts+Tm and Diast/St ratios ranging from 0.2 to 0.4 and from 1.2 to 1.4, respectively (Table 5.4). Both parameters appear to be sensitive to clay-catalyzed reactions (McKirdy et al., 1983; Rullkötter et al., 1985; Rubinstein et al., 1975), thus variation in

Ts/Ts+Tm and Diast/St ratios can be associated with lithological changes into the Draupne Formation. In addition, source rock extracts from well 15/9-18, located between the Sleipner Vest and Sleipner Øst fields, showed a predominance of even-numbered *n*-alkanes (C_{22}-C_{27}) together with a distinctive "V" shape distribution pattern of MDBTs (4-methyl > 2-+3-methyl < 1methyl) typical of calcareous source facies (Murillo et al., 2019). δ^2H variations among *n*-alkanes homologues (>C_{20}) for siliciclastic and calcareous shale facies of the upper Draupne Formation ranged from 18 to 43‰ and averaged 30‰ (Fig. 5.4a). Therefore, the ^2H-enrichment seen in *n*-alkanes from siliciclastic shale facies into the Draupne Formation from well 15/3-3 may likely be due to a greater influence of clay catalyzed hydrogen exchange processes (Alexander et al., 1982,1984) and may also reflect changes in the physiologic and metabolic processes in organisms that fix water hydrogen into organic molecules (e.g., Li et al., 2009; Sessions et al., 1999).

5.7.6. $\delta^{13}C$ and δ^2H values of Pristane and Phytane for Jurassic Oils, Condensates and Source Rock Extracts

In general, Jurassic petroleum and source rock extracts from the SVG that represent a wide variety of redox conditions from anoxic to oxic, showed very similar carbon and hydrogen isotope compositions for pristane and phytane (Fig. 5.12a-d). The differences between $\delta^{13}C$ values of Pr and Ph ranged from 0.04 to 1.6‰ with an average of 0.4‰, whereas variations in δ^2H values between Pr and Ph are within the analytical error, averaging 3‰ in oils and condensates that exhibit very low (0.7) to very high (4.0) ratios of Pr to Ph. In addition, the differences in $\delta^{13}C$ values of these two isoprenoids ranged from 0.04 to 1.50‰ (average of 0.3‰) for Jurassic source rock extracts that represent a very wide range of Pr/Ph ratios (0.9 to 11). Likewise, most of Jurassic source rock extracts exhibited small differences in δ^2H values of Pr and Ph, which ranged from 3 to 12‰, with an average of 3.6‰. For analyzed oils, condensates and source rock extracts, the similar $\delta^{13}C$ values found between Pr and Ph can be consistent with common biosynthetic origin and pathways (Hayes et al., 1990). Similarly, δ^2H values of Pr and Ph also showed small isotopic variations, within the limits of uncertainty, which may support a common origin. Nonetheless, very few source rock extracts showed differences in δ^2H values of Pr and Ph (up to 42‰) that may be attributed to differences in the biosynthetic origins of lipids and/or different isotopic effects

during their derivation from a common phytol precursor (Li et al., 2001; Dawson et al., 2004). In general, Ph is enriched in ^2H relative to Pr, however samples of overmature source rock extracts of the Heather Formation from well 25/7-2 exhibited a ^2H-enrichment of Pr compared to Ph (Fig. 5.4c).

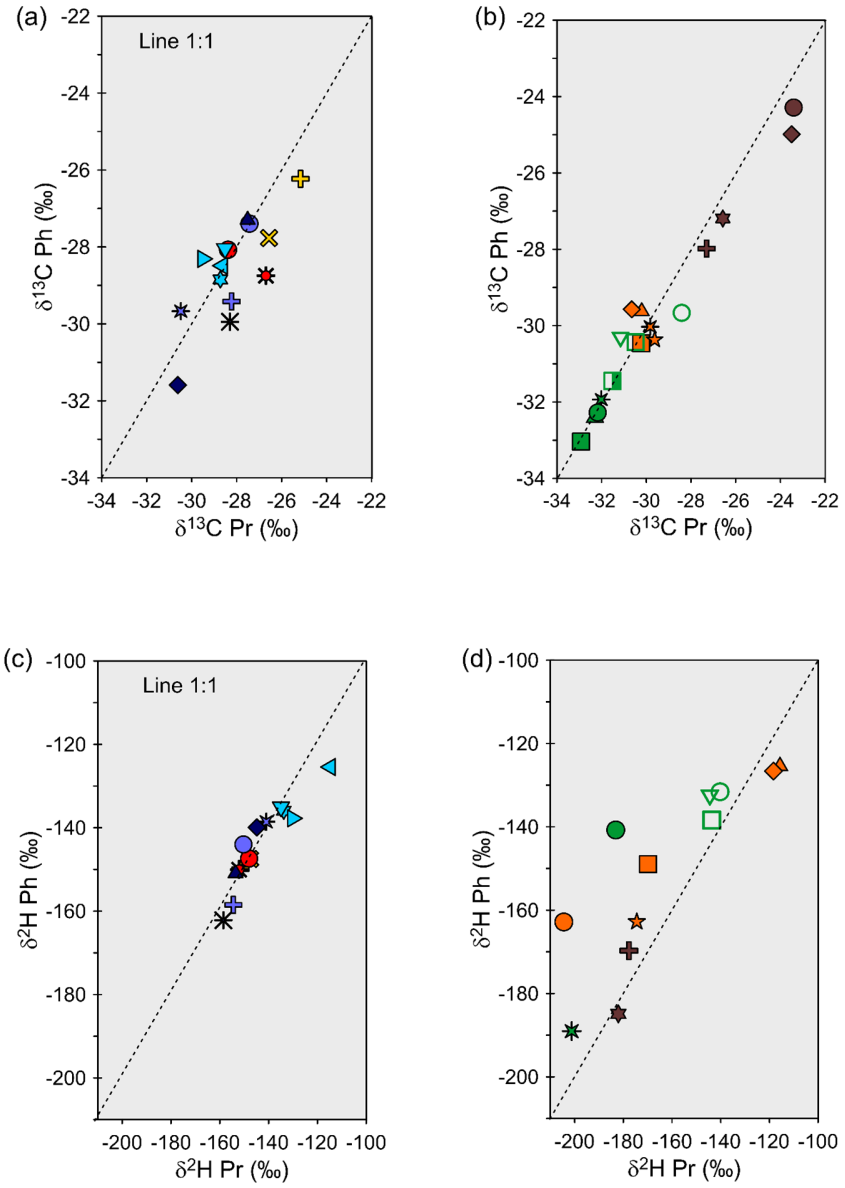

FIGURE 5.12. *Cross-plots of (a) $\delta^{13}C$ values of Pr versus $\delta^{13}C$ values of Ph for oils; (b) $\delta^{13}C$ values of Pr versus $\delta^{13}C$ values of Ph for Jurassic source rock extracts; (c) δ^2H values of Pr versus δ^2H values of Ph for oils, and (d) δ^2H values of Pr versus δ^2H values of Ph for Jurassic source rock extracts.*

The $\delta^{13}C$ values of Pr and Ph, derived from phytol side chains of the chlorophylls of algae and cyanobacteria, are robust proxies for the isotopic composition of phytoplankton (Schouten et al., 1998; Hayes, 2001), whereas the $\delta^{13}C$ values of short-chain *n*-alkanes (*n*-C_{15} to *n*-C_{19}) may represent the average isotopic composition of different sources, since these *n*-alkanes are often attributed to algae and bacterial biomass (Han et al., 1968; Gelpi et al., 1970; Cranwell et al., 1987). If short-chain *n*-alkanes derived from algae and cyanobacteria, they should be depleted in ^{13}C relative to isoprenoids by 1.5‰ (Hayes, 2001). Nevertheless, *n*-alkanes (C_{15}-C_{19}) are enriched in ^{13}C relative to pristane and phytane for the analyzed extract samples from the Upper Jurassic source rocks. The difference between the average $\delta^{13}C$ values of C_{15}-C_{19} alkanes and the average $\delta^{13}C$ values of Pr and Ph is up to 1.6‰ (Fig. 3c). The enrichment in ^{13}C for the *n*-C_{15} and *n*-C_{19} alkanes relative to Pr and Ph, in source rock extracts, have been attributed to a lower relative algal input to the OM (Dawson et al., 2007), a heterotrophic processing of primary photosynthate or a high input of isotopically heavy bacterial biomass (Summons et al., 1994; Grice et al., 2005). The pattern of ^{13}C-enrichment of C_{15}-C_{19} *n*-alkyl carbon chains compared with the $\delta^{13}C$ values of Pr and Ph seen in source rock extracts from the Upper Jurassic Draupne Formation (Fig. 4b) may indicate a dominant input of bacterial biomass. This is also suggested by their very low ratios of regular steranes to 17-α hopanes (0.1-0.4) (Table 5.4), which are typical of bacterial input or microbially reworked primary biomass (e.g., Tissot and Welte, 1984), and more positive δ^2H values of *n*-alkanes (-100 to -140‰) (Fig. 5.4a) relative to those of *n*-alkyl lipids derived from marine planktonic sources (-170‰) (Li et al., 2009; Sessions, 2016).

5.7.7. Differential Changes in δ^2H values of n-Alkanes and Regular Isoprenoids to Assess Thermal Maturation

For both Jurassic oils and source rock extracts, regular isoprenoids (Pr and Ph) are depleted in ^2H relative to *n*-alkyl compounds (Figs. 5.3a and 5.4a,c and d). The differences between the average δ^2H values of Pr and Ph and the average δ^2H values of *n*-alkanes ranged from -17 to -46‰ for mixed oils from the SVG (Fig. 5.3a, Fig. 5.10) and from -23 to -65‰ for Jurassic source rocks (Fig. 5.4g, Fig. 5.13). These differences are smaller compared to those expected from fatty acids and phytol (>150‰) (e.g., Sessions et al., 1999; Li et al., 2009). The differences in δ^2H values between *n*-alkyl and isoprenoid hydrocarbons,

therefore, indicate alteration of primary δ^2H values. Schimmelmann et al. (1999, 2001) reported that the primary δ^2H values of *n*-alkanes are typically altered during hydrocarbon generation, and suggested the transfer of ^2H-enriched hydrogen from water to organic compounds during cracking reactions. Dawson et al. (2005); Radke et al. (2005); Pedentchouk et al. (2006) indicated that pristane and phytane become more enriched in ^2H relative to the *n*-alkanes with increasing maturity. Dawson et al. (2005, 2007) suggested clay-catalyzed exchange, which involves carbocation like intermediates, proceeds faster with compounds, such as the pristane and phytane, containing tertiary carbon centers that induce hydrogen exchange at the adjacent secondary carbons.

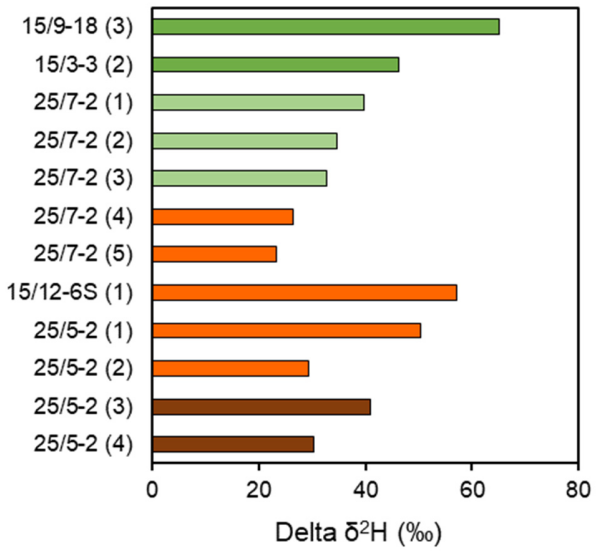

FIGURE 5.13. *Delta δ^2H values (average δ^2H values of n-alkanes (C_{15}-C_{29}) - average δ^2H values of Pr and Ph) for Jurassic source rock extracts from the SVG.*

As the differences between the δ^2H values of *n*-alkanes and regular isoprenoids decreases with increasing maturity (Dawson et al., 2005; Radke et al., 2005; Pedentchouk et al., 2006; Dawson et al., 2007), they can be used to assess thermal maturation in Jurassic oils and source rocks. In mixed oils, the average δ^2H values of Pr and Ph ranged from -130 to -165‰ (Fig. 5.7d). The most negative average δ^2H values of Pr and Ph (-155 to -165‰) corresponds to mixed oils of Population C (wells 15/12-5, 15/12-6S) sourced mainly from the Type-II kerogen rich Upper Jurassic Draupne Formation (Figs. 5.3a and 5.7d). In contrast,

Population D mixed oils that have a high contribution from the Type-III kerogen rich Upper Jurassic Heather/lower Draupne formations, located in the northern part of the SVG, showed the most positive average δ^2H values of Pr and Ph (-130 to -140‰) (Figs. 5.3a and 5.7d). In addition, they have slightly higher thermal maturity (0.8-0.9% R_o) (Fig. 5.6a-c), which may also influence in the ^2H-enrichment of Pr and Ph. Similarly, the lowest variations between the average δ^2H values of *n*-alkanes and the average δ^2H values of Pr and Ph were found in Population D mixed oils (17 to 23‰), especially in the oil sample from well 25/2-13 (17‰) (Fig. 5.10). The lowest variations are attributed to their higher values of vitrinite reflectance calculated from MPI-1 and MDR (0.8-0.9% R_o) (Fig. 5.6a).

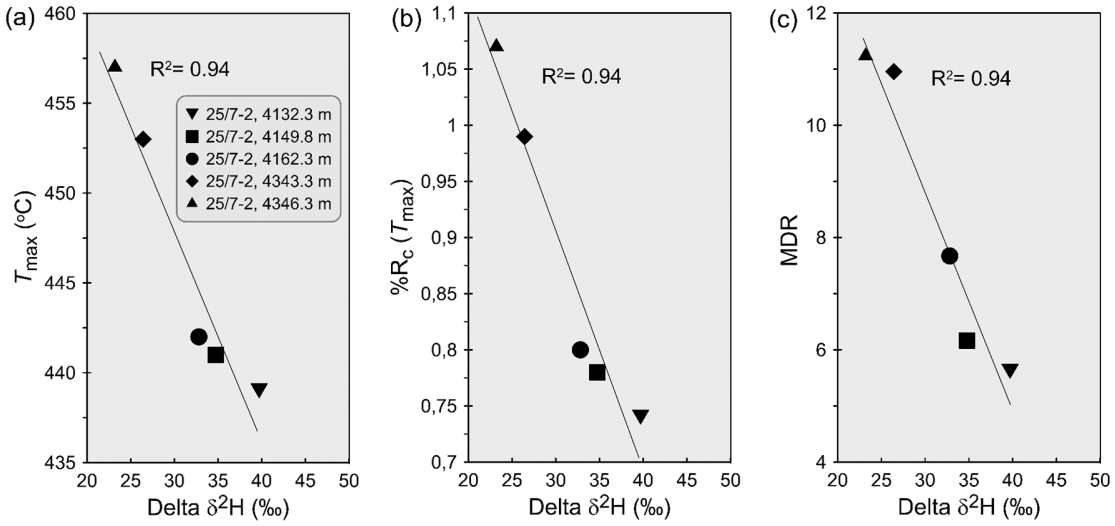

FIGURE 5.14. *Cross-plots of (a) T_{max} versus delta δ^2H values; (b) $\%R_c$ from T_{max} versus delta δ^2H values; and (c) methyldibenzothiophene ratio (MDR) versus delta δ^2H values. Delta δ^2H values= (Average δ^2H values of n-alkanes (C_{15}-C_{29}) - Average of δ^2H values of Pr&Ph).*

For Jurassic source rock extracts, the lowest variations between the average δ^2H values of *n*-alkanes and the average δ^2H values of Pr and Ph were found in deeper samples of well 25/7-2 (Fig. 5.13), which are consistent with their high values of measured vitrinite reflectance (~1.2% R_o) (Norwegian Petroleum Directorate, 2019) and high vitrinite reflectance values calculated from T_{max} and MDR (1.1-1.3% R_o) (Table 5.2). The differences between the average δ^2H values of *n*-alkanes and average δ^2H values of Pr and Ph decrease with increasing maturity in extracts from Upper Jurassic source rocks enriched in Type-III kerogen in well 25/7-2, correlating strongly with T_{max} and MDR (R^2=0.94) (Fig. 5.14).

5.8. Conclusions

Higher average δ^2H values of individual *n*-alkanes from marine source rock extracts and petroleum (-100 to -150‰) relative to those expected values for *n*-alkylipids from marine planktonic sources, can mainly be related to a high input of bacterial biomass or to microbially reworked primary biomass, and to isotopic exchange of organic matter with formation waters during thermal cracking. With the increasing input of hydrocarbons from Jurassic source rocks enriched in Type-III kerogen to petroleum mixtures, *n*-alkanes of lower molecular weight (C_{10}-C_{15}) become more enriched in ^{13}C, whereas *n*-alkanes of higher molecular weight (>C_{20}) become more enriched in ^{2}H. Likewise, differences between the weighted average δ^2H values of *n*-alkanes and the weighted average δ^2H values of Pr and Ph, in petroleum mixtures of similar thermal maturity, tend to increase. The ^{2}H-enrichment of individual *n*-alkanes from the Glitne and Vølve oils is likely related to the highly reactive kerogen Type-IIS, which favors the isotopic transfer of water-derived hydrogen to organic matter. Furthermore, the consistent pattern of increasing δ^2H values with carbon number of *n*-alkanes (C_{20}-C_{29}) seen in petroleum mixtures of similar thermal maturity and sourced mainly from terrigenous organic matter, may likely be due to higher proportion of readily exchangeable aromatic hydrogen in kerogen Type-III that can favor hydrogen exchange processes. The current study supports the use of δ^2H values of *n*-alkanes to assess the origin of the organic matter, to source-oil correlation and to differentiate mixed petroleum. Furthermore, a combined carbon and hydrogen isotope approach provided an improved resolution to resolve complex mixtures of petroleum from multiple Jurassic source rocks in the SVG.

5.9. Acknowledgements

The DAAD is thanked for funding this research. The NPD is gratefully acknowledged for the kind contribution of oil and source rock samples. We are also grateful to the technical staff of the Organic Geochemistry section at GFZ, as well as to the Isotope Laboratory of the University of Potsdam for analytical support. The Editor-in-Chief Erdem Idiz and the Associate Editor Alexei Milkov are acknowledged for editorial handling of the manuscript. C.J. Boreham and an anonymous reviewer are thanked for constructive comments and detailed suggestions, which helped to improve the manuscript.

Chapter 6

Summary and Outlook

Detailed and comprehensive studies, integrating molecular and compound-specific isotope data into a multiparameter approach, were used to unravel petroleum mixing phenomena in the Hammerfest Basin, SW Norwegian Barents Sea and the South Viking Graben, Norwegian North Sea, and the results published in peer reviewed journals. In these studies, the main scientific findings were subdivided into three sections for having implications in: (1) the assessment of secondary alteration processes; (2) the evaluation of thermal maturation, source-oil and oil-oil correlations, mixing of oils and source contribution quantification; and (3) the understanding of petroleum systems.

6.1. Summary of the Hammerfest Basin Case Study, Norwegian Barents Sea

In this research (Chapter 3) a full suite of geochemical and isotope analysis on 16 oil and condensate samples (from 15 wells) and 10 source rock extracts from the Triassic Snadd and Kobbe formations and the Jurassic Hekkingen and Nordmela formations were used to (1) examine the extent and effects of diverse petroleum alteration processes in Jurassic and Triassic reservoirs, and (2) investigate the source, maturity and mixing of oils and condensates in the HB. The multiparameter approach followed in this study included light hydrocarbons, conventional biomarkers, higher-plant derived biomarkers, polycyclic aromatic hydrocarbons, diamondoids and $\delta^{13}C$ and $\delta^{2}H$ values of individual petroleum hydrocarbons. The result of this study helped to identify hydrocarbon mixtures of distinct sources, thermal maturity levels and geological ages and diverse in-reservoir petroleum

alteration processes, providing new insights to better understand the multiple petroleum systems in the HB.

6.1.1. Assessment of Secondary Alteration Processes

Several phases of rift-related subsidence, uplift and erosion have notably changed the original composition of petroleum accumulated in reservoirs of the HB. Based on interpretations of light hydrocarbon composition as well as stable carbon and hydrogen isotope ratios of individual hydrocarbons, this research was aimed to assess petroleum alteration processes in Triassic and Jurassic reservoirs of the HB and their influence on the isotope data. Crude oils hosted in the Snadd and Tubåen formations of the Goliat field showed the lowest concentrations of *n*-alkanes ($<C_{14}$) and methyl alkanes as well as the lowest heptane (H) and isoheptane (I) ratios, which are attributed to microbial degradation. In contrast, deeper oils hosted in the Kobbe Formation exhibited high concentrations of gasoline range hydrocarbons (C_5-C_9) interpreted as a result of a secondary gas-condensate charge. Even though biomarkers and PAHs do not give information related to an increase in the maturity of these oils, maturity parameters based on light hydrocarbons containing quaternary to tertiary carbon species suggested hydrocarbon influx with a higher thermal maturity level in Goliat oils affected by a secondary gas-condensate charge in the Middle Triassic reservoir. In addition, the upward inflection of the $\delta^{13}C$ signatures for *n*-alkanes (C_7 to C_{12}) found in deep oils from the Goliat field can also support the occurrence of a wet gas-condensate charge. The Snadd Fm.-hosted condensates from the Tornerose field were also altered microbially but to a lesser degree than Goliat oils from the the Snadd and Tubåen formations. Microbial degradation in the condensate sample from the Tornerose field was evidenced by the low concentrations and isotopically heavier (more positive) $\delta^{13}C$ values of *n*-alkanes ($<C_8$) and methyl alkanes relative to those in condensates from the same family.

Condensates from the Askeladd, Albatross, Alke and Tornerose fields showed a high fractionation index (FI). Furthermore, the stratigraphically deeper condensates from the Askeladd and southern Albatross fields have a high aromaticity ratio and lower FI, while the stratigraphically shallower condensates from the northern Albatross field showed higher paraffinicity ratio and the highest FI values. All of these parameters strongly indicated

evaporative fractionation in the Askeladd and Albatross fields. The low aromaticity ratio found in condensates from the Alke and Tornerose fields can also be associated with water washing, however, their high FI also suggests evaporative fractionation. Furthermore, isotopic evidences were also reported in this study. Here, a strong and constant ^{2}H-enrichment of *n*-alkanes (>C_{14}) with increasing carbon number was found in condensates resulting from evaporative fractionation. The highest ^{2}H-enrichments of *n*-alkanes with carbon number were observed in northern Albatross condensates with the highest FI values, which are consistent with isotopic fractionations caused by evaporation. As ^{2}H-containing hydrocarbons are more volatile than those containing all H (e.g. Hopfner, 1969; Kiss et al., 1972); during evaporation of an oil, more volatile compounds (short-chain *n*-alkanes) will become depleted in ^{2}H relative to less volatile compounds (long-chain *n*-alkanes). Therefore, the impact of evaporative fractionation in reservoirs was revealed by greater ^{2}H-enrichments of *n*-alkanes with increasing carbon number shown in naturally evaporated condensates.

On the other hand, the thermally generated condensate from well 7119/12-3 located on the Ringvassøy-Loppa Fault Complex (RLFC) exhibited an abrupt and regular ^{13}C-enrichment of *n*-alkanes (<C_{14}) with decreasing carbon number that is attributed to its high level of thermal maturity (%R_o ~1.4%). In addition, δ^{2}H values of *n*-alkanes >C_{14} increased linearly with increasing carbon number in the over-mature condensate. This ^{2}H-enrichment, however, is not as strong as that observed for evaporative condensates which depicted δ^{2}H profiles with steeper slopes, showing the impact of the evaporative fractionation in the reservoirs. Although the δ^{2}H values of *n*-alkanes were altered by thermal maturation and evaporative fractionation they seem to be not affected by secondary oil migration from the northern margin of the HB to the Goliat field. This research demonstrated how the combination of isotopic and molecular data offers a robust way of assessing diverse petroleum alteration processes in reservoirs of the HB. This research provided strong evidence for the occurrence of microbial degradation (Goliat and Tornerose fields), water-washing (Alke, Goliat and Tornerose fields), evaporative fractionation (Askeladd, Albatross, Alke and Tornerose fields), gas-condensate charge (Goliat field) and advanced level of thermal maturation (well 7119/12-3, RLFC).

6.1.2. Assessment of Thermal Maturation, Oil-Source and Oil-Oil Correlations, Mixing of Oils and Source Contribution Quantification

This research identified several scenarios of hydrocarbon mixing, involving distinct organic matter source types, maturity levels and geological ages in the main accumulations of the HB. Variation of several maturity parameters based on composition of light hydrocarbons, biomarkers, and alkylated PAHs suggest that most HB oils and condensates consist of hydrocarbon mixtures with small thermal maturity variations within the main stage of oil generation or between the peak and late-oil generation stages. Maturity parameters, nevertheless, cover a relatively larger variation in mixed oils from the Goliat field. Mixed oils hosted in the Kobbe Formation of the Goliat field were formed from multiple stages of generation (early to late-oil generation stages), while mixed oils from the Snadd and Tubåen formations in the Goliat field were formed from early to peak-oil generation stages. Vitrinite reflectance values estimated from dimethyl-, trimethyl- and ethyladamantane indexes suggest an influx of dry gas.

Based on $\delta^{13}C$ data of individual petroleum hydrocarbons and a comprehensive assessment of biomarkers and heterocyclic and polycyclic aromatic hydrocarbons (dibenzothiophene and phenanthrene and their methyl homologs), mixtures of hydrocarbons derived mainly from Paleozoic, Triassic and Jurassic source rocks were recognized in the HB. Multivariate statistical analyses (MVA) of the molecular and carbon isotope data allowed to recognize four main families of mixed hydrocarbons according to their main contributing source rocks. Family I consists of condensates from the Askeladd and southern Albatross fields, Family II comprises condensates from the northern Albatross and Tornerose fields, Family III includes oils from the Snøhvit field (III-A) and oils hosted in the Snadd and Tubåen formations of the Goliat field (III-B), and Family IV consists of oils from the deeper Kobbe Formation of the Goliat field. Unlike hydrocarbons of other families, Family III showed typical features of oils derived from carbonate source facies, such as a slight even-over-odd carbon number predominance of n-C_{20} to n-C_{25}-alkanes in Snøhvit oils, lower concentrations of tricyclic terpanes >C_{26} as compared with their C_{21}-C_{25} homologs, and the highest concentrations of dibenzothiophene and alkyl-dibenzothiophenes. However, a significant amount of resin-derived biomarkers in the Snøhvit oils along with their lowest

Pr/Ph ratios demonstrate the presence of hydrocarbon mixtures derived from distinct sources. Even though oils from the Snøhvit field and shallow oils from the Goliat field have comparable $\delta^{13}C$ signatures of *n*-alkanes, some differences related to source were recognized. Snøhvit oils show a higher ratio of retene to retene plus cadalene and higher concentrations of phenanthrene and tricyclic saturated diterpanes relative to Goliat oils, especially those hosted in the Kobbe Fm. This suggests a higher terrestrial influence, which may be associated with waxy hydrocarbons probably generated from coals and coaly shales of the Nordmela Fm. In the Goliat field, the Kobbe Fm. hosted oils differ isotopically from shallower oils in the $\delta^{13}C$ values of *n*-alkanes ($>C_{14}$), which are more negative and show isotopic variations of up to 3‰.

Furthermore, $\delta^{13}C$ values of *n*-alkanes ($>C_{20}$) for Jurassic and Triassic source rock extracts are differentiated as well. Source rock extracts from the Jurassic Hekkingen Formation have $\delta^{13}C$ values of *n*-alkanes ($>C_{20}$) ranging from -28 to -31‰, while those from the Triassic Kobbe Formation showed more negative $\delta^{13}C$ values (-32 to -35‰), with isotopic differences up to 4-6‰. These variations enabled source assessment for the different petroleum families. Therefore, Jurassic contribution is higher in Family III (Goliat oils from the Snadd and Tubåen Fms. and Snøhvit oils), while Askeladd, Albatross and Tornerose condensates (Family I and II) and Goliat oils from the Kobbe Fm. likely have a greater Triassic contribution. However, though the deep oils from the Goliat field seem to have a higher Triassic contribution than shallower oils, they also showed even isotopically lighter $\delta^{13}C$ values of *n*-alkanes (C_{14}-C_{16}) than extracts from Jurassic and Triassic source rocks with isotopic variations up to 4‰ as compared with Triassic source rocks, suggesting more likely an additional Paleozoic-source contribution. Based on the average $\delta^{13}C$ values of *n*-alkanes ($>C_{20}$), a mixing model was applied to estimate the contribution of the different sources to condensates from the Askeladd field. The quantification results indicate a proportion of 18-21% for Upper Jurassic and 79-82% for Triassic derived-oils. This estimation is quite consistent with that obtained from 3D modeling by Duran et al. (2013a) and demonstrates that $\delta^{13}C$ values of *n*-alkanes can be useful for quantitative assignment of oil sources.

6.1.3. Comprehensive Understanding of the Petroleum Systems

In this study, the distribution of hydrocarbon families in the HB agrees with the 3D model of hydrocarbon charges proposed by Duran et al. (2013b), which was based on the analysis of migration pathways and drainage areas in the Basin. This study confirmed that the Albatross field was charged from both the western and northern margins of the HB, and also supported a local and long distance migration from the north to the Goliat field. This research provided molecular and isotopic evidence for a likely Paleozoic-source contribution, which support earlier findings by Ohm et al. (2008), and proved the occurrence of petroleum mixtures of Jurassic, Triassic and Paleozoic source rocks in the HB. The presence of evaporative condensates and gas-condensate charge may indicate the existence of deeper petroleum accumulations. Diamondoid maturity parameters suggested that a late gas charge may have occurred throughout the basin. Study of diamondoid quantification and CSIA of diamondoids are recommended for future works.

6.2. Summary of the South Viking Graben Case Study, Norwegian North Sea

The research results published in paper 2 (chapter 4) based on different petroleum components that were not considered in previous studies of the SVG, namely light hydrocarbons as well as heterocyclic and polycyclic aromatic aromatics (phenanthrene, fluorene, dibenzothiophene and dibenzofuran as well as their alkyl homologs). The multiparameter research approach used also included CSIA rather than bulk $\delta^{13}C$ values of whole oils and their sub-fractions. $\delta^{13}C$ data of gasoline-range alkanes, *n*-alkanes of higher molecular weight (C_{10}-C_{30}) and isoprenoid alkanes (pristane and phytane) were assessed together with molecular data to unravel mixed petroleum. The objectives of this research were to: (1) classify mixed petroleum by MVA using molecular data (ratios and concentrations) of heterocyclic and polycyclic aromatic hydrocarbons, C_7 hydrocarbons and $\delta^{13}C$ data of individual petroleum hydrocarbons; (2) better constrain oil-oil and oil-source correlations; (3) appraise petroleum alteration processes and thermal maturation; and (4) estimate the relative contributions of Type-II and Type-III kerogen-rich Jurassic source rocks to mixed petroleum accumulations in the SVG. To this end, a total of 15 oil and condensate samples from 13 wells and 22 cuttings and core samples taken from different depth intervals

within the Upper Jurassic Draupne and Heather formations and the Middle Jurassic Sleipner Formation in seven wells located in the SVG were analyzed in this study.

6.2.1. Assessment of Secondary Alteration Processes

The oil sample from the Paleocene Heimdal Formation sandstones of the Glitne field did not show loss of *n*-alkanes but showed the lowest concentration of aromatic hydrocarbons (BTEX), the lowest Bz/3-MC_5 and Tol/$MCyC_6$ ratios, suggesting water washing without microbial degradation. Isaksen et al. (2002) proposed based on Thompson's plots (aromaticity *versus* paraffinicity) that condensates in the Paleocene Heimdal Formation of Sleipner Øst could be fractionated products from the condensate in the Jurassic Hugin Formation. In this research, however, the application of CSIA improved the understanding of this case study in reservoirs of the Sleipner Øst field. Condensates hosted in Paleocene reservoirs (wells 15/9-13 T2 and 15/9-11 T2) showed $\delta^{13}C$ values of *n*-alkanes >C_{10} up to 4‰ more positive than those in Jurassic reservoirs (wells 15/9-13 T1 and 15/9-11 T1), indicating a different origin. Therefore, the high aromaticity ratio can be associated with a high input of terrigenous organic matter. Nonetheless, in the Sleipner Øst field, the condensate sample from well 15/9-13 T2 exhibited the highest value of FI, which may indicate phase fractionation. Besides, the condensate sample from well 15/9-13 T1 showed the lowest concentrations of *n*-alkanes (<C_{10}) that can be related to an evaporative loss of light ends.

6.2.2. Assessment of Thermal Maturation, Oil-Source and Oil-Oil Correlations, Mixing of Oils and Source Contribution Quantification

Maturity parameters based on methylhomologs of phenanthrene, naphthalene and dibenzothiophene, biomarkers and light hydrocarbons indicate that most mixtures comprise oils of comparable maturity within the oil generative window. The lowest light hydrocarbon ratios of quaternary to tertiary carbon species, the lowest average generation/expulsion temperature estimated using the 2,4-DMC_5/2,3-DMC_5 ratio along with the lowest values of $\%R_c$ from MDR (0.58% R_o) indicate an early-oil generation stage for the oil sample from the Vølve field, followed by the oil sample from the Glitne field that is found in the onset of the oil generation stage (0.66 $\%R_o$). Moreover, $\%R_c$ values using the MPI-1 and MDR indicate

that most analyzed oils were generated in the main oil generative window, distinguishing higher maturity oils from the Balder, Vale and Lille Frøy fields in the northern half of the SVG study area (0.8-0.9 $\%R_o$). The slight northward increase of thermal maturity can also be supported by higher values of trimethylnaphthalene ratios (TNR-1 and TNR-2) and triaromatic steroid ratio (%TA), as well as the highest light hydrocarbon ratios of quaternary to tertiary carbon species, which is in agreement with the highest gas-oil ratios reported in this area (Justwan et al., 2006b). Advanced levels of thermal maturity were not detected in oil and condensate samples from the SVG.

A particularly good differentiation among all Jurassic source rock extracts (0.6-0.8% R_o) was obtained using the contents of MFs, MDBFs and MDBTs. In addition, distribution of MDBT isomers clearly differentiated between siliciclastic and calcareous source facies of the upper Draupne Fm. Since hydrocarbon samples were not generated at advanced levels of thermal maturity and considering that moderate maturity levels do not significantly affect the distribution of sulfur- and oxygen-containing aromatic HCs (e.g., Chakhmakhchev et al., 1997; Radke et al., 2000), heterocyclic aromatic compounds were used to discriminate petroleum mixtures. Hierarchical cluster analysis (HCA) and principal component analysis (PCA) using C_7 hydrocarbon ratios together with the $\delta^{13}C$ values of gasoline range hydrocarbons distinguished three main groups of mixed petroleum in the SVG. Group I originated mainly from Type-IIS kerogen associated with calcareous source facies, Group II originated mainly from Type-II and Type-III/II kerogens related to siliciclastic source facies and Group III originated predominantly from Type-III kerogen associated with coaly source facies. Nonetheless, the $\delta^{13}C$ data of *n*-alkanes, Pr and Ph in conjunction with source-related ratios of heterocyclic and polycyclic aromatic compounds were more sensitive as source indicators, allowing small compositional variations in mixed petroleum to be detected. HCA and PCA using these data identified seven populations (Populations from A to G) of mixed petroleum according to the relative contribution of hydrocarbons derived from terrigenous source material. Furthermore, HCA and PCA using concentration data of heterocyclic and polycyclic aromatic hydrocarbons along with the average $\delta^{13}C$ values of *n*-alkanes and regular isoprenoids, and C_7 hydrocarbon concentration together with $\delta^{13}C$ values of gasoline range hydrocarbons, supported also the previous classifications based on molecular ratios.

MVA using concentration data of heterocyclic and polycyclic aromatic compounds confirmed that source-related ratios of these components are able to discriminate well mixtures of petroleum in the SVG.

With increasing relative input of oils derived from Type-III kerogen rich Jurassic source rocks to mixed oils, it is observed higher relative concentrations of methyl- and especially dimethylnaphthalenes relative to trimethylnaphthalenes, a lower relative content of DBTs and higher relative contents of DBFs and Fs. Mixed oil populations with the highest terrestrial source contributions (Populations F and G) showed higher ratios of C_{34}-to C_{35}-homohopanes, C_{24}-tetracyclic to C_{23}-tricyclic terpanes, C_{19}- to C_{23}-tricyclic terpanes, C_{30}-moretane to C_{30}-hopane and C_{29}- to C_{27}-regular steranes. In addition, they contained the highest ratios of 1,7-DMP to "X" ("X" is defined as the sum of 1,3+2,10+3,9+3,10-DMP), 1-MP/9-MP and 1,2,5-TMN/1,2,7-TMN together with the lowest heptane ratio and the highest concentration of six-carbon ring compounds ($MCyC_6$ plus toluene), which are consistent with a very high input from higher-plant source material. Although $\delta^{13}C$ values of *n*-alkanes ($<C_{25}$), regular isoprenoids (Pr and Ph), and $\delta^{13}C$ values of cyclic, branched and *n*-alkanes in the gasoline range showed no significant differences between Populations C and D, they were isotopically distinguished using $\delta^{13}C$ values of long-chain *n*-alkanes ($>C_{25}$) and benzene, which exhibited more positive values with variations of up to 3‰ in Population D oils. Similarly, both populations were discriminated based on source-related ratios of heterocyclic and polycyclic aromatic hydrocarbons, which indicated a higher input of oils sourced from terrigenous material in Population D. Populations A and B (Glitne and Vølve oils) showed evidence of a higher contribution from calcareous source facies (a dominance of the even over odd carbon numbers in *n*(C_{20}-C_{25})-alkanes, the highest concentrations of DBTs and a distinctive "V" shape distribution pattern of MDBTs). In addition, both oils have similar bulk $\delta^{13}C$ data for saturated and aromatic fractions, however, they exhibited significant differences in $\delta^{13}C$ values of *n*(C_{10}-C_{24})-alkanes, isoprenoids (Pr and Ph) and alkylcloalkanes, which are up to 3‰ more positive in the Vølve oil sample than those for the Glitne oil sample. This indicates a further oil contribution from higher-plant source material. The isotopically heavy $\delta^{13}C$ values of Pr and Ph (-27.4‰) correlate with those in Middle Jurassic coaly source rocks. Likewise, Population E (well 15/9-11T1) represents a peculiar

mixture of petroleum, while biomarkers suggested that this oil originated mainly from a marine source, heterocyclic and polycyclic aromatic HCs as well as light HCs indicated that this petroleum mixture contains a high contribution of oils sourced from terrigenous higher-plant material. That is also confirmed by the isotopically heavy $\delta^{13}C$ values of *n*-alkanes (C_{10}-C_{14}) and especially Pr and Ph, with $\delta^{13}C$ values ranging from -27 to -28‰ that also tend to correlate with those in coaly sources of the Middle Jurassic Sleipner Formation. Population E is a good example of mixtures of end-member oils, with the concentrations of specific components in each oil greatly different. In Population E, biomarker distributions are biased toward the oil with the largest concentrations of these compounds. Hence, it is possible that the less dominant source rock (the upper Draupne Fm.) has much greater biomarker concentrations than the dominant source (the Vestland Group). This study, therefore, demonstrates the importance of a combination of molecular markers across different fractions of petroleum, rather than the routinely used saturate fraction alone. This research also provided an excellent case study on the use of CSIA rather than bulk $\delta^{13}C$ values of whole oils and sub fractions to better understand sources of complex mixtures, and the importance of combining molecular composition of different petroleum fractions and $\delta^{13}C$ data of individual hydrocarbons to unravel complex petroleum mixtures from distinct organic matter types, depositional environments and lithologies.

In the southern part of the SVG, the ^{13}C-enrichment of (C_{10}-C_{14}) *n*-alkanes as well as Pr and Ph were good indicators of the scale of the terrigenous source contribution and allowed quantitative determination of the proportions of Jurassic source contributions enriched in Type-II and Type-III kerogens in complex petroleum mixtures from the southern part of the SVG. The estimated mixing proportions correlated linearly with the concentrations of alkyldibenzothiophenes and regular isoprenoids in petroleum mixtures of comparable maturity within the main oil generative window. The linear behavior of these mixing curves is useful for verifying estimates of mixing ratios obtained from ^{13}C-enrichment of (C_{10}-C_{14}) *n*-alkanes as well as Pr and Ph in mixed petroleum from the southern part of the SVG. In addition, it supports the use of the compound-specific stable carbon isotope composition for estimating source contribution to mixed oils generated at moderate levels of thermal maturity.

6.2.3. Comprehensive Understanding of the Petroleum Systems

The fact that some mixed oil populations in the southern part of the SVG study area, show signals consistent with inputs from calcareous source facies suggests a most widespread occurrence of hydrocarbons sourced from post rift facies of the upper Draupne Formation. In the present study, geochemical interpretations are in accordance with basin modelling results, which indicate that Quaternary subsidence rates were higher in the southern half of the study area (Justwan et al., 2006b). These higher subsidence rates allowed the shallowest and youngest source rock unit of the upper Draupne Formation to enter into the hydrocarbon generation window. Furthermore, in this research, hydrocarbon inputs from Middle Jurassic source rocks were identified in various samples from the southern half of the SVG study area, which are likely associated with the great thicknesses of Middle Jurassic coals and carbargillites in this area and with its proximity to Middle Jurassic source pods (Justwan et al., 2006b). Complex mixing of hydrocarbons derived from Upper Jurassic and Middle Jurassic sources were identified in the Greater Sleipner area, where the petroleum systems that consider these source rock units are active. Besides, a high relative contribution of oils sourced from siliciclastic shales enriched in Type-III kerogen (the Heather Formation and/or the lower Draupne Formation) was recognized in the northern half of the SVG study area. This is supported by Justwan et al. (2006b), who estimated the highest contribution of Heather sourced oils in the northern half of the SVG study area, especially for the Vale, Frøy and Lille Frøy fields, and a major contribution of oils from the lower Draupne Formation in the Balder field using a pseudo-3D modelling.

6.3. Summary of the Combined Appraisal of Compound-Specific δ^2H and $\delta^{13}C$ values of *n*-Alkanes as a New Tool to Unravel Oil Mixtures

In this research (Chapter 5), carbon and hydrogen CSIA were applied to better understand sources of complex mixtures of petroleum generated from multiple Jurassic source rocks of distinct organic matter types, lithologies and depositional settings previously identified in the SVG (Murillo et al., 2019). Thus, the main objectives of this study were to: (1) evaluate the δ^2H values of individual normal and isoprenoid alkanes as geochemical

parameters for oil-source correlation and mixed oil discrimination, (2) assess the combination of $\delta^{13}C$ and $\delta^{2}H$ values of *n*-alkanes to resolve complex mixtures of petroleum, and (3) identify the main factors that may control the $\delta^{2}H$ values of individual *n*-alkanes, Pr and Ph in oils, condensates and analyzed extracts of Jurassic source rocks from the SVG.

More positive $\delta^{2}H$ values of individual *n*-alkanes from marine source rocks (-90 to -150‰) relative to those expected values for *n*-alkylipids from marine planktonic sources (-150 to -200‰) can mainly be related to a high input of bacterial biomass or to microbially reworked primary biomass, and to isotopic exchange of organic matter with formation waters during thermal cracking. With the increase in the estimated input of hydrocarbons from terrigenous source material to petroleum mixtures of similar thermal maturity, the *n*-alkanes ($>C_{20}$) exhibited a higher ^{2}H-enrichment while *n*-alkanes (C_{10}-C_{14}) showed a higher ^{13}C-enrichment. Likewise, differences between the average $\delta^{2}H$ values of *n*-alkanes (C_{14}-C_{29}), especially those of higher molecular weight (C_{20}-C_{29}), and the average $\delta^{2}H$ values of Pr and Ph in petroleum mixtures tend to increase with the input of oils generated from Jurassic source rocks enriched in Type-III kerogen. Although Glitne and Vølve oils were originated mainly from marine organic matter, they showed a ^{2}H-enrichment of *n*-alkanes up to 30‰ as compared to oils of Population C. The ^{2}H-enrichment of individual *n*-alkanes for the Glitne and Vølve oils can likely be related to the highly reactive kerogen Type-IIS, which favors the irreversible isotopic transfer of water-derived hydrogen to organic matter. Furthermore, the consistent and significant pattern of increasing $\delta^{2}H$ values with carbon number of *n*-alkanes ($>C_{20}$) seen in mixed oils derived mainly from terrigenous organic matter, may likely be due to higher proportion of readily exchangeable aromatic hydrogen in Type-III kerogen that can favor hydrogen exchange processes.

This study showed that $\delta^{2}H$ values for intermediate and long chain *n*-alkanes ($>C_{20}$) were useful to discriminate mixed oils that were not well differentiated by $\delta^{13}C$ data. For example, one case study is represented by mixed oils from Population C, which derived mainly from the Type-II kerogen rich-Upper Jurassic Draupne Formation, and mixed oils from Population D that sourced mainly from the Type III-kerogen rich Upper Jurassic Heather and/or lower Draupne formations. Similar to biomarkers and heterocyclic and

polycyclic aromatic hydrocarbon composition, δ^2H values of alkanes distinguished well Population C from Population D, indicating a higher input of oils from terrigenous source material in Population D mixed oils. *n*-Alkanes, Pr and Ph from Population D showed a ^2H-enrichment of up to 20 and 30‰ relative to those from Population C. Another case study that illustrates the usefulness of δ^2H values to differentiate terrigenous source contribution, corresponds to the condensate sample from Population E. Population E shows one of the most positive δ^2H values of *n*-alkanes, which may indicate a dominant Middle Jurassic source contribution. This prevalent Middle Jurassic source input was not suggested by saturated biomarker ratios, however, it was recognized by concentrations and source-related ratios of heterocyclic and polycyclic aromatic hydrocarbons and light hydrocarbons, which suggested a high relative contribution of hydrocarbons from terrigenous higher-plant source material (Murillo et al., 2019). Hydrogen CSIA, therefore, proved to be a powerful tool to discriminate Jurassic petroleum mixtures from distinct sources. Furthermore, in this research a strong and constant ^2H-enrichment of *n*-alkanes with chain length was observed in the condensate sample generated mainly from marine source material (well 15/9-13 T1) at the main oil generative window (~0.9%R_o). This strong and regular ^2H-enrichment can likely be associated with isotopic fractionations caused by evaporation, as this condensate sample showed an evaporative loss of light ends (Murillo et al., 2019). This result may also support the evidence of greater ^2H-enrichments with increasing carbon number of *n*-alkanes in condensates affected by evaporation.

6.4. Outlook

The current research presented two excellent case studies of oil mixing in basins with multiple source rocks and complex charge histories in the Norwegian Barents Sea and North Sea. This study reinforces the importance of performing meaningful oil-oil and oil-source correlations based on a combination of source-related molecular markers across different fractions of the oils and source rock extracts, rather than classical correlation studies based on biomarkers. Furthermore, it was demonstrated how the use of CSIA of *n*-alkanes and related *n*-alkyl structures provides valuable additional information to discriminate oil families, constrain oil-oil and oil-source rock correlations and better understand in-reservoir processes that have had an impact upon hydrocarbon composition, thus strengthening a

comprehensive understanding of the multiple petroleum systems in both the HB, southwestern Barents Sea and the SVG, North Sea. Furthermore, hydrogen CSIA also proved to be a powerful tool to differentiate mixed oils, improving resolution to resolve complex mixtures of petroleum from multiple Jurassic source rocks in the SVG. Both compound-specific stable carbon and hydrogen compositions of individual *n*-alkanes provided unique new insights into the source origins of complex petroleum mixtures and the evaluation of secondary alteration processes. Therefore, for future work, the multiparameter approaches described in this study that include the molecular composition of light hydrocarbons, *n*-alkanes, biomarkers, as well as heterocyclic and polycyclic aromatic hydrocarbons combined with $\delta^{13}C$ data of individual petroleum hydrocarbons, such as gasoline-range alkanes, *n*-alkanes (>C_{10}) and isoprenoid alkanes (Pr and Ph), can be applied in many other petroleum basins around the world with multiple source systems that produce in-reservoir oil mixing.

Due to the need to develop methods for estimating the relative contributions from each effective source rock to reservoirs containing multiple oil charges, the present doctoral research addressed the issue of how best to unravel and quantify oil mixing ratios using $\delta^{13}C$ values of individual alkanes. Mixing ratios of hydrocarbons from Jurassic source rocks enriched in Type-II and Type-III kerogens were obtained from ^{13}C-enrichment of *n*(C_{10}-C_{14})-alkanes, and regular isoprenoids (Pr and Ph) in mixed petroleum of comparable thermal maturity in the SVG. The linear behavior between the estimated mixing proportions and concentration data supported the use of compound-specific stable carbon isotope composition for quantitative assignment of sources in mixed oils. Hence, further study using other quantification methods can also be applied to compare with estimates obtained from $\delta^{13}C$ values of *n*-alkanes. In addition, for future research in the HB, concentration data of diamondoids and compound-specific isotope analysis of diamondoids (CSIA-D) should be carried out to identify highly cracked components in mixed oils.

REFERENCES

Aitken, C.M., Jones, D.M., Larter, S.R., 2004. Anaerobic hydrocarbon biodegradation in deep subsurface oil reservoir. Nature, 431, 291-294

Akinlua, A., Ajayi, T.R., Adeleke, B.B., 2006. Niger Delta oil geochemistry: insight from light hydrocarbons. Journal of Petroleum Science and Engineering 50, 308-314.

Alexander, R., Kagi, R., Larcher, A., 1982. Clay catalysis of aromatic hydrogen exchange reactions. Geochimica et Cosmochimica Acta 46, 219-222.

Alexander, R., Kagi, R., Larcher, A., 1984. Clay catalysis of alkyl hydrogen exchange reactions-reaction mechanisms. Organic Geochemistry 6, 755-760.

Alexander, R., Kagi, R.I., Rowland, S.J., Sheppard, P.N., Chirila, T.V., 1985. The effects of thermal maturity on distribution of dimethylnaphthalenes and trimethylnaphthalenes in some ancient sediments and petroleums. Geochimica et Cosmochimica Acta 49, 385-395.

Alexander, R., Kagi, R.I., Rowland, S.J., Sheppard, P.N., and Chirila, T.V., 1988. The effects of thermal maturity on distributions of dimethylnaphthalenes and trimethylnaphthalenes in some ancient sediments and petroleums. Geochimica et Cosmochimica Acta 49, 385-395.

Alexander R., Larcher A. V., Kagi R. I., and Price P., 1988. The use of plant-derived biomarkers for correlation of oils with source rocks in the Cooper/Eromanga Basin system, Australia. APEA Journal 28**,** 310-328.

Alexander, R., Larcher, A.V., Kagi, R.I., Price, P.L., 1992. An oil-source correlation study using age specific plant-derived aromatic biomarkers. In: Moldowan, J.M., Albrecht, P., Philp, R.P. (Eds.), Biological Markers in Sediments and Petroleum. Prentice Hall, Englewood Cliffs, N.J., pp. 201-221.

Alexander, R., Bastow, T.P., Fisher, S.J., Kagi, R.I., 1995. Geosynthesis of organic compounds: II. Methylation of phenanthrene and alkylphenanthrenes. Geochimica et Cosmochimica Acta 59, 4259-4266.

Aquino Neto, F.R., Trendel, J.M., Restle, A., Connan, J. and Albrecht, P., 1983. Occurrence and formation of tricyclic and tetracyclic terpanes in sediments and petroleum. In Advances in Organic Geochemistry 1981 (Edited by Bjorøy, M. et al.), Wiley, Chichester, pp. 659-667.

Arouri, K.R., McKirdy, D.M., 2005. The behaviour of aromatic hydrocarbons in artificial mixtures of Permian and Jurassic end-member oils: application to in-reservoir mixing in the Eromanga Basin, Australia. Organic Geochemistry 36,105-115.

Asif, M., Fazeelat, T., 2012. Petroleum geochemistry of the Potwar Basin, Pakistan: II-Oil classification based on heterocyclic and polycyclic aromatic hydrocarbons. Applied Geochemistry 27, 1655-1665.

Asif, M., Grice, K., Fazeelat, T., 2009. Assessment of petroleum biodegradation using stable hydrogen isotopes of individual saturated hydrocarbon and polycyclic aromatic hydrocarbon distributions in oils from the Upper Indus Basin, Pakistan. Organic Geochemistry 40, 301-311.

Asif, M., Wenger, L., 2019. Heterocyclic aromatic hydrocarbon distributions in petroleum: A source facies assessment tool. Organic Geochemistry 137.

Barnard, P.C., Cooper, B.S., 1981. Oils and source rocks of the North Sea area. In: Illing, L.V., Hobson, G.D. (Eds.), Petroleum Geology of the Continental Shelf of North-West Europe. Proceedings of the 2nd Conference. Heyden and Son, London, pp. 169-175.

Bastow, T.P., Singh, R.K., van Aarssen, B.G.K., Alexander, R., Kagi, R.I., 2001. 2-Methylretene in sedimentary material: a new higher-plant biomarker. Organic Geochemistry 32, 1211-1217.

Behar, F., Vandenbroucke, M., 1987. Chemical modelling of kerogens. Organic Geochemistry, 11, 15-24.

BeMent, W.O., Levey, R.A., Mango, F.D., 1995. The temperature of oil generation as defined with a C_7 chemistry parameter (2,4-DMP/2,3-DMP). In: Grimalt, J.O., Dorronsoro, C. (Eds.), Organic Geochemistry: Developments and Applications to Energy, Climate, Environment and Human History. Proceedings of the 17th International Meeting on Organic Geochemistry, San Sebastian, September 1995, pp. 505-507.

Berglund, L.T., Augustson, J., Færseth, R., Gjelberg J. and Ramberg-Moe, H., 1986. The evolution of the Hammersfest Basin, In: Spencer, A.M. et al (eds.) Habitat of Hydrocarbons on the Norwegian Continental Shelf. Graham & Trotman, London, pp. 319-338.

Bigeleisen, J., 1965. Chemistry of isotopes. Science 147, 463-471.

Biller, P., Ross, A.B., Skill, S.C., 2015, Investigation of the presence of an aliphatic biopolymer in cyanobacteria: Implications for kerogen formation. Organic Geochemistry 81, 64-69.

Bjorøy, M., Hall, K., Gillyon, P. and Jumeau, J., 1991. Carbon isotope variations in *n*-alkanes and isoprenoids in whole oils. Chem. Geol. 93, 13-20.

Bjorøy, M., Hall, P.B., Hustad, E. and Williams, J.A., 1992. Variation in stable carbon isotope ratios of individual hydrocarbons as a function of artificial maturity. Organic Geochemistry 19, 89-105.

Bjorøy, M., Hall, P.B. and Moe, R.P., 1994. Variation in the isotopic composition of single components in the C_4-C_{20} fraction of oils and condensates. Organic Geochemistry 21, 761-776.

Blanc, P. and Connan, J., 1994. Preservation, Degradation and Destruction of Trapped Oil. In: The petroleum system- From source to trap. AAPG Memoir 60*,* L.B. Magoonand, W.G. Dow, ed, Tulsa, Oklahoma, 237-247.

Blumer, M., Guillard, R.R.L., and Chase, T., 1971. Hydrocarbons of marine plankton. Marine Biology, 8, 183-9.

Bojesen-Koefoed, J.A., Christiansen, F.G., Peter, H and Pedersen, A.K., 1999. Oil seepage onshore west Greenland: evidence of multiple source rocks and oil mixing. Geological Society, London, Petroleum Geology Conference Series, 5, 305-314.

Bordenave, M.L., 1993. Applied Petroleum Geochemistry, Éditions Technip, Paris.

Boreham, C.J., and Summons, R.E., 1999. New insights into the active petroleum systems in the Cooper and Eromanga basins, Australia: Australian Petroleum Production and Exploration Association Journal, 39, 1, 263-296.

Boreham, C.J., Dowling, L.M., Murray, A.P., 1995. Biodegradation and maturity influences on *n*-alkane isotopic profiles in terrigenous sequences. In: Abstracts of 17th International Meeting on Organic Geochemistry, San Sebastian, Spain, 539–541.

Born, J.G.P., Louw, R., and Mulder, P., 1989. Formation of dibenzodioxins and dibenzofurans in homogenous gas-phase reactions of phenols. Chemosphere 19, 401-406.

Brekke, H., Sjulstad, H.I., Magnus, C. and Williams, R.W., 2001. Sedimentary environments offshore Norway–an overview. In: Martinsen, O.J. & Dreyer, T. (eds) Sedimentary Environments Offshore Norway–Paleozoic to Recent. Elsevier, Amsterdam, NPF Special Publications, 10, 7-37.

Briggs, D.E.G., 1999. Molecular taphonomy of animal and plant cuticles: selective preservation and diagenesis. Philos. Trans. R. Soc. Lond. B 354, 7-16.

Budzinski, H., Garrigues, P., Connan, J., Devillers, J., Domine, D., Radke, M., Oudins, J.L., 1995. Alkylated phenanthrene distributions as maturity and origin indicators in crude oils and rock extracts. Geochimica et Cosmochimica Acta 59, 2043-2056.

Caldwell, M.E., Garrett, R.M., Prince, R.C., Suflita, J.M., 1998. Anaerobic biodegradation of long-chain n-alkanes under sulfate-reducing conditions. Environmental Science Technology 32, 2191.

Cao, J., Yao, S., Jin, Z., Hu, W., Zhang, Y., Wang, X., Zhang, Y., Tang, Y., 2006. Petroleum migration and mixing in the northwestern Junggar Basin (NW China): constraints from oil-bearing fluid inclusion analyses. Organic Geochemistry 37 (7), 827-846.

Carpentier, B., Ungerer, P., Kowalewski, I., Magnier, C., Courcy, J.P., Huc, A.Y., 1996. Molecular and isotopic fractionation of light hydrocarbons between oil and gas phases. Organic Geochemistry, 24, 1115-1139.

Cavanagh, A.J., di Primio, R., Scheck-Wenderoth, M. and Horsfield, B., 2006. Severity and timing of Cenozoic exhumation in the southwestern Barents Sea. Journal of the Geological Society, London, 163, 761-774.

Chaffee, A.L., Perry, J.J., and Jones, R.B., 1981. Carboxylic acids and coal structure. In Coal Structure (ed. M. L. Gorbaty and K. Ouchi); Adv. Chem. 192, pp. 113-131.

Chakhmakhchev, A. and Suzuki, M., 1995. Saturate biomarkers and aromatic sulfur compounds in oils and condensates from different source rocks lithologies of Kazakhstan, Japan and Russia. Organic Geochemistry 23, 289-299.

Chakhmakhchev, A., Suzuki, M., Kuniaki, T., 1997. Distribution of alkylated dibenzothiophenes in petroleum as a tool for maturity assessments. Organic Geochemistry 26, 7, 483-490.

Chand, S., Rise, L., Ottesen, O., Dolan, M.F.J., Bellec, V., Bøe, R., 2009. Pockmark-like depressions near the Goliat hydrocarbon field, Barents Sea: Morphology and genesis. Marine and Petroleum Geology 26, 1035-1042.

Chen, J.H., Fu, J.M., Sheng, G.Y., Liu, D.H., Zhang, J.J., 1996. Diamondoid hydrocarbon ratios: novel maturity indices for highly mature crude oils. Organic Geochemistry 25, 179-190.

Chen, J., Deng, C., Liang, D., Wang, X., Zhong, N., Song, F., Shi, X., Jin, T., Xiang, S., 2003. Mixed oils derived from multiple source rocks in the Cainan oilfield, Junggar Basin, Northwest China. Part II: artificial mixing experiments on typical crude oils and quantitative oil-source correlation. Organic Geochemistry 34, 911-930.

Chikaraishi, Y., Naraoka, H., 2003. Compound-specific δD–δ^{13}C analyses of *n*-alkanes extracted from terrestrial and aquatic plants. Phytochemistry 63, 361-371.

Chikaraishi, Y., Yamada, Y. and Naraoka, H., 2005. Carbon and hydrogen isotopic compositions of sterols from riverine and marine sediments. Limnol. Ocean. 50, 1763-1770.

Chikaraishi Y. and Naraoka H., 2005. δ^{13}C and δD identification of sources of lipid biomarkers in sediments of Lake Huruna (Japan). Geochim. Cosmochim. Acta 69, 3285-3297.

Chikaraishi Y. and Naraoka H., 2006. Carbon and hydrogen isotope variation of plant biomarkers in a plant–soil system. Chem. Geol. 231, 190-202.

Chung, H.M., Clifford, W., Buck, S. and Bingham, G., 1998. Mixed signals of the source and thermal maturity for petroleum accumulations from light hydrocarbons: an example of the Beryl field. Organic Geochemistry 29, 381-396.

Claypool, G.E., Mancini, E.A., 1989. Geochemical relationships of petroleum in Mesozoic reservoirs to carbonate source rocks of Jurassic Smackover Formation, southwestern Alabama. American Association of Petroleum Geologists 73, 904-924.

Clayton, J.L., Rice, D.D., Michael, G.E., 1991. Oil-generating coals of the San Juan basin, New Mexico and Colorado, U.S.A. Organic Geochemistry 17, 735-742.

Clayton, C.J., Bjorøy, M., 1994. Effect of maturity on ratios of individual compounds in North Sea oils. Organic Geochemistry, 21, 737-750.

Coates, J.D., Anderson, R.T., Lovley, D.R., 1996. Oxidation of polycyclic aromatic hydrocarbons under sulfate-reducing conditions. Applied and Environmental Microbiology 62, 1099-1101.

Cockings, J.H., Gifford, L.G.II., Mazza, T.A. and Riley, L.A., 1992. Bathonian to mid-Oxfordian sequence stratigraphy of the South Viking Graben, North Sea, In: Hardman, R.F.P., (Ed.), Exploration Britain: Geological insights for the next decade, Geological Society; London, Special Publication 67, 65-105.

Collister, J.W., Rieley, G., Stern, B., Eglinton, G. and Fry, B., 1994. Compound-specific δ^{13}C analyses of leaf lipids from plants with differing carbon dioxide metabolisms. Organic Geochemistry 21, 619-628.

Connan, J., 1984. Biodegradation of crude oils in reservoirs. In: Brooks, J., Welte, D. (Eds.), Advances in Petroleum Geochemistry. Academic Press, London, pp. 299-335.

Connan, J., Lacrampe-Couloume, G., 1993. The origin of the Lacq Superieur heavy oil accumulation and of the giant Lacq Inferieur gas field (Aquitaine basin, SW France). In: Bordenave, M.L. (Ed.), Applied Petroleum Geochemistry. Editions Technip, Paris, pp. 465-487.

Cooper, B.S., Barnard, P.C., 1984. Source rocks and oils of the central and northern North Sea. In: Demaison, G., Murris, R.J. (Eds.), Petroleum Geochemistry and Basin Evaluation. AAPG, Tulsa, Mem 35, pp. 303-314.

Cornford, C., 1998. Source rocks and hydrocarbons of the North Sea. In: Glennie, K.W. (Ed.), Petroleum Geology of the North Sea: Basic concepts and recent advances. Blackwell Science Geology & Petroleum Geology, Oxford, United Kingdom, pp. 376-462

Cranwell, P.A., Eglinton, G., and Robinson, N., 1987. Lipids of aquatic organisms as potential contributors to lacustrine sediments. Organic Geochemistry 11**,** 6, 513-527.

Dahl, B., and Speers, G.C., 1986. Geochemical characterization of a tar mat in the Oseberg Field Norwegian Sector, North Sea. Organic Geochemistry, 10, 547-588.

Dansgaard, W., 1964. Stable isotopes in precipitation. Tellus 16, 436-468.

Dawson, D., Grice, K., Wang, S.X., Alexander, R., Radke, J., 2004. Stable hydrogen isotopic composition of hydrocarbons in torbanites (Late Carboniferous to Late Permian) deposited under various climatic conditions. Organic Geochemistry 35, 189-197.

Dawson, D., Grice, K., Alexander, R., 2005. Effect of maturation on the indigenous delta D signatures of individual hydrocarbons in sediments and crude oils from the Perth Basin (Western Australia). Organic Geochemistry 36, 95-104.

Dawson, D., Grice, K., Alexander, R., Edwards, D., 2007. The effect of source and maturity on the stable isotopic compositions of individual hydrocarbons in sediments and crude oils from the Vulcan Sub-basin, Timor Sea, Northern Australia. Organic Geochemistry 38, 1015-1038.

de Leeuw, J. W., Versteegh, G. J. M., and van Bergen, P. F., 2006. Biomacromolecules of plants and algae and their fossil analogues. Plant Ecol. 189, 209-233.

Didyk, B.M., Simoneit, B.R.T., Brassell, S.C. and Eglinton, G., 1978. Organic geochemical indicators of paleoenvironmental conditions of sedimentation. Nature, 272, 216-222.

Dimakis, P., Braathen, B.I., Faleide, J.I., Elverhøi, A., and Gudlaugsson, S.T., 1998 Cenozoic erosion and the preglacial uplift of the Svalbard–Barents Sea region, Tectonophysics, 300, 311-327.

Doré, A., 1995. Barents Sea geology, petroleum resources and commercial potential. Arctic 48, 207-221.

Doré, A.G. and Jensen, L.N., 1996. The impact of late Cenozoic uplift and erosion on hydrocarbon exploration: offshore Norway and some other uplifted basins. Global and Planetary Change, 12, 415-436.

Doré, A.G., Vollset, J. and Hamar, G.P., 1985. Correlation of the offshore sequences referred to the Kimmeridge Clay Formation; relevance to the Norwegian sector. In: Thomas, B.M., Dore, A.G., Eggen, S.S., Home, P.C. and Larsen, R.M. (Eds), Petroleum Geochemistry in Exploration of the Norwegian Shelf. Graham and Trotman, London, 27-37.

Duran, E.R., di Primio, R., Anka, Z., Stoddart, D., Horsfield, B., 2013a. Petroleum system analysis of the Hammerfest Basin (southwestern Barents Sea): Comparison of basin modelling and geochemical data. Organic Geochemistry 63, 105-121.

Duran, E.R., di Primio, R., Anka, Z., Stoddart, D., Horsfield, B., 2013b. 3D-basin modelling of the Hammerfest Basin (southwestern Barents Sea): A quantitative assessment of petroleum generation, migration and leakage. Marine and Petroleum Geology 45, 281-303.

Durand, B., 1980. Kerogen: Insoluble organic matter from sedimentary rocks. Editions technip, Paris, 519 p.

Dzou, L.I.P. and Hughes, W.B., 1993. Geochemistry of oils and condensates, K Field, offshore Taiwan: a case study in migration fractionation. Organic Geochemistry 20, 437-462.

Edwards, D.S., Preston, J.C., Kennard, J.M., Boreham, C.J., van Aarssen, B.G.K., Summons, R.E., Zumberge, J.E., 2004. Geochemical characteristics of hydrocarbons from the Vulcan Sub-basin, western Bonaparte Basin, Australia. In: Ellis, G.K., Baillie, P.W., Munson, T.J. (eds.), Timor Sea Petroleum Geoscience: Proceedings of the Timor Sea Symposium, Darwin, Northern Territory, 19-20 June 2003. Northern Territory Geological Survey, pp. 169-201.

Eglinton, T.I., 1994. Carbon isotopic evidence for the origin of macromolecular aliphatic structures in kerogen. Organic Geochemistry 21, 721-736.

Eglinton, G., Hamilton, R.J., 1967. Leaf epicuticular waxes. Science 9, 156, 1322-1335.

Elias, V.O., Debarros, A.M.A., Debarros, A.B., Simoneit, B.R.T., and Cardoso, J.N., 1997. Sesquiterpenoids in sediments of a hypersaline lagoon: a possible algal origin. Organic Geochemistry 26, 721-730.

Ellis, L., Singh, R.K., Alexander, R., and Kagi, R.I., 1996. Formation of isohexyl alkylaromatic hydrocarbons from aromatization-rearrangement of terpenoids in the sedimentary environment: a new class of biomarker. Geochimica et Cosmochimica Acta 60, 4747-4763.

Estep, M., Hoering, T., 1980. Biogeochemistry of the stable hydrogen isotopes. Geochimica et Cosmochimica Acta 44, 1197-1206.

Faleide, J.I., Gudlaugsson, S.T. and Jacquart, G., 1984. Evolution of the western Barents Sea. Marine and Petroleum Geology 1, 123-150.

Faleide, J.I., Vagnes, E. and Gudlaugsson, S.T., 1993. Late Mesozoic–Cenozoic evolution of the south-western Barents Sea in a regional rift-shear tectonic setting. Marine and Petroleum Geology, 10,186-214.

Faleide, J.I., Bjorlykke, K., Gabrielsen, R.H., 2010. Geology of the Norwegian Continental Shelf. In: Bjørlykke, K (eds.) Petroleum Geoscience: From Sedimentary Environments to Rock Physics. Springer, pp. 467-499.

Falt, L.M., Helland, R., Wiik Jacobsen, V. and Renshaw, D., 1989. Correlation of transgressive-regressive depositional sequences in the middle Jurassic Brent/Vestland Group megacycle, Viking Graben, Norwegian North Sea. In: Collinson, J. D. (Ed.) Correlation in Hydrocarbon Exploration. Norwegian Petroleum Society, Graham & Trotman, 191-200.

Fan, P., Philp, R.P., Li, Z.X., and Ying, G.G., 1990. Geochemical characteristics of aromatic hydrocarbons of crude oils and source rocks from different sedimentary environments. Organic Geochemistry 16**,** 427-435.

Fang, C.C., Xiong, Y.Q., Liang, Q.Y. and Li, Y., 2012. Variation in abundance and distribution of diamondoids during oil cracking. Organic Geochemistry 47, 1-8.

Farquhar, G.D., Ehleringer, J.R. and Hubick, K.T., 1989. Carbon isotope discrimination and photosyntheis. Annual Review of Plant Physiology and Plant Molecular Biology, 40, 503-537.

Fenton, S., Grice, K., Twitchett, R.J., Bottcher, M.E., Looy, C.V., Nabbefeld, B., 2007. Changes in biomarker abundances and sulfur isotopes of pyrite across the Permian Triassic (P/Tr) Schuchert Dal section (East Greenland). Earth Planet. Sci. Lett. 262, 230-239.

Ficken, K.J., Li, B., Swain, D.L., and Eglinton G., 2000. An *n*-alkane proxy for the sedimentary input of submerged/floating freshwater aquatic macrophytes. Organic Geochemistry 31**,** 7-8, 745-749.

Field, J.D., 1985. Organic Geochemistry in exploration of the northern North Sea. In: Thomas, B.M., Dore, A.G., Eggen, S.S., Home, P.C. and Larsen, R.M. (Eds.), Petroleum geochemistry in exploration of the Norwegian Shelf. Graham and Trotman. London, pp. 39-57.

Filley, T.R., Freeman, K.H., Bianchi, T.S., Baskaran, M., Colarusso, L.A., Hatcher, P.G., 2001. An isotopic biogeochemical assessment of shifts in organic matter input to Holocene sediments from Mud Lake, Florida. Organic Geochemistry 32, 1153-1167.

Forsman, J.P. and Hunt, J.M., 1958. Insoluble organic matter (kerogen) in sedimentary rocks of marine origin. In: Weeks L.G. (Ed.), Habitat of Oil, American Association of Petroleum Geologists, Tulsa, Oklahoma, 747 p.

Fraser, S.I., Robinson, A.M., Johnson, H.D., Underhill, J.R., Kadolsky, D.G.A., Connell, R., Johannesen, P., Ravnas, R., 2003. Lower and middle Jurassic. In: Evans, D., Graham, C., Armour, A., Bathurst, P. (Eds.), The Millenium Atlas: Petroleum Geology of the Central and Northern North Sea. The Geological Society, London, pp. 157-189.

Freeman, K.H., Hayes, J.M., Trendel, J.M. & Albrecht, P., 1990. Evidence from carbon isotope measurements for diverse origins of sedimentary hydrocarbons. Nature 343, 254-256.

Gabrielsen, R.H., Færseth, R.B., Jensen, L.N., Kalheim, J.E., Riis, F., 1990. Structural elements of the Norwegian continental shelf. Part I: The Barents Sea Region. Norwegian Petroleum Directorate Bulletin 6, 47.

Gautier, D.L., 2005. Kimmeridgian Shales Total Petroleum System of the North Sea Graben Province. U.S. Geological Survey Bulletin 2204-C, 24 p.

Gelin, F., Boogers, I., Noordeloos, A.A.M., Sinninghe Damsté, J.S., Riegman, R., de Leeuw, J.W., 1997. Resistant biomacromolecules in marine microalgae of the classes Eustigmatophytaceae and Chlorophyceae. Geochemical implications. Organic Geochemistry 26, 659-675.

Gelpi, E., Schneider, H., Mann, J., and Oro, J., 1970. Lipids of geochemical significance in microscopic algae 1. Hydrocarbons of geochemical significance in microscopic algae. Phytochemistry 9**,** 3, 603-612.

George, S.C., Boreham, C.J., Minifie, S.A., Teerman, S.C., 2002. The effect of minor to moderate biodegradation on C_5 to C_9 hydrocarbons in crude oils. Organic Geochemistry 33, 1293-1317.

Gjelberg, J., Dreyer, T., Høie, A., Tjelland, T. and Lilleng, T., 1987. Late Triassic to Mid-Jurassic sandbody development on the Barents and Mid-Norwegian Shelf. In: J. Brooks and K. Glennie (Eds.) Petroleum Geology of North West Europe. Graham and Trotman, London, pp. 1105-1129.

Glennie, K.W. and Underhill, J.R., 1998. The development and evolution of structural styles in the North Sea. In: Glennie, K. (ed.) Introduction to the Petroleum Geology of the North Sea. Blackwell Science, Oxford, 42-84.

Goff, J.C., 1983. Hydrocarbon generation and migration from Jurassic source rocks in the east Shetland basin and Viking Graben of the northern North Sea. Journal of the Geological Society 140, 445-474.

Goldsmith, P.J., Hudson, G., van Veen, P., 2003. Triassic. In: Evans, D., Graham, C., Armour, A., Bathurst, P. (Eds.), The Millennium Atlas; Petroleum Geology of the Central and Northern North Sea. Geological Society, London, pp. 105-127.

Goth, K., de Leeuw, J. W., Puttman, W., and Tegelaar, E. W., 1998. Origin of messel oil shale kerogen. Nature 336, 759-761.

Grice, K., Cao, C., Love, G.D., Bottcher, M.E., Twitchett, R.J., Grosjean, E., Summons, R.E., Turgeon, S.C., Dunning, W., Jin, Y., 2005. Photic zone euxinia during the Permian-Triassic superanoxic event. Science 307, 706-709.

Gudlaugsson, S.T., Faleide, J.I., Jahansen, S.E., Breivik, A.J., 1998. Late Paleozoic structural development of the South-western Barents Sea. Marine and Petroleum Geology 15, 73-102.

Gupta, N.S., Steele, A., Fogel, M., Griffin, P., Adams, M., Summons, R.E., Yang, H., Cody, G.D., 2014. Experimental formation of geomacromoleculas from microbial lipids. Organic Geochemistry 67, 35-40.

Halpern, H.I., 1995. Development and applications of light-hydrocarbon-based star diagrams. American Association of Petroleum Geologist Bulletin 79, 801-815.

Han, B.J., McCarthy, E.D., van Hoeven, W., Calvin, M., Bradley, W.H., 1968. Organic geochemical studies, II. A preliminary report on the distribution of aliphatic hydrocarbons in algae, in bacteria, and in a recent lake sediment. Proceedings of the National Academy of Sciences 59, 29-33.

Haq, B.U., Hardenbol, J. & Vail, P.R., 1987. Chronology of fluctuating sea levels since the Triassic. Science, 235, 1156-1166.

Hayatsu, R., Winans, R.E., Scott, R.G., Moore, L.P., and Studier, M.H., 1978. Trapped organic compounds and aromatic units in coals. Fuel 57**,** 541–548.

Hayes, J.M., 1993. Factors controlling the ^{13}C contents of sedimentary organic compounds: principles and evidence. Marine Geology 113, 111-125.

Hayes. J.M., 2001. Fractionation of carbon and hydrogen isotopes in biosynthetic processes. In: J.W. Valley, D.R. (eds) Stable isotope geochemistry. Rev Miner Geochem 43, 225-277.

Hayes, J.M., Freeman, K.H., Popp, B.N., and Hoham, C.H., 1990. Compound-specific isotopic analyses: A novel tool for reconstruction of ancient biogeochemical processes. In Advances in Organic Geochemistry 1989 (ed. B. Durand and F. Behar); Organic Geochemistry 16, 1115-1128.

He, M., Moldowan, J.M., Nemchenko-Rovenskaya, A. & Peters, K.E., 2012. Oil families and their inferred source rocks in the Barents Sea and northern Timan–Pechora basin, Russia. American Association of Petroleum Geologists Bulletin 96, 1121-1146.

Heinzelmann, S.M., Villanueva, L., Sinke-Schoen, D., Sinninghe Damst, Ã.J.S., Schouten, S., van der Meer, M.T.J., 2015. Impact of metabolism and growth phase on the hydrogen isotopic composition of microbial fatty acids. Frontiers in Microbiology 6, 408.

Henriksen, E., Bjørnseth, H.M., Hals, T.K., Heide, T., Kiryukhina, T., Kløvjan, O.S, Larssen, G.B., Ryseth, A.E., Rønning, K., Sollid, K. and Stoupakova, A., 2011. Uplift and erosion of the greater Barents Sea: impact on prospectivity and petroleum systems. In: Spencer, A.M. et al. (eds) Artic Petroleum Geology. Geological Society, London, Memoirs 35, 271-281.

Heppenheimer, H., Steffens, K., Püttman, W., Kalkreuth, W., 1992. Comparison of resinite-related aromatic biomarker distributions in Cretaceous-Tertiary coals from Canada and Germany. Organic Geochemistry 18, 273-287.

Hilkert, A.W., Douthitt, C.B., Schluer, H.J., Brand, W.A., 1999. Isotope ratio monitoring gas chromatography/mass spectrometry of D/H by high temperature conversion isotope ratio mass spectrometry. Rapid Communication in Mass Spectrometry 13, 1226-1230.

Hoefs, J., 1997. Stable Isotope Geochemistry. 3rd Edition. Springer-Verlag, Berlin. 201 pp.

Holba, A.G., Dzou, L.I.P., Hickey, J.J., Franks A.G., May, S.J. and Lenney, T., 1996. Reservoir Geochemistry of South Pass 61 Field 61, Gulf of Mexico: Compositional Heterogeneities Reflecting Filling History and Biodegradation. Organic Geochemistry 24, 1179-1198.

Holba, A.G., Dzou, L.I.P., Masterson, W.D., Hughes, W.B., Huizinga, B.J., Singletary, M.S., Moldowan, J.M., Mello, M.R., Tegelaar, E., 1998. Application of 24-norcholestanes for constraining source age of petroleum. Organic Geochemistry 29, 1269-1283.

Holba, A.G., Ellis, L., Dzou, L.I., Hallam, A., Masterson, W.D., Francu, J., Fincannon, A. L., 2001. Extended tricyclic terpanes as age discriminators between Triassic, Early Jurassic, and Middle–Late Jurassic oils. 20th International Meeting on Organic Geochemistry: EAOG 1. Nancy, France, p. 464.

Hopfner, A., 1969. Vapor pressure isotope effects. Angewandte Chemie 8, 689-699.

Horsfield, B., Yordy, K.L. and Crelling, J.C., 1988. Determining the petroleum-generating potential of coal using organic geochemistry and organic petrology. In: Advances in Organic Geochemistry 1987. (Mattavelli, L. and Novelli, L., eds.). Pergamon Press, Oxford, pp. 121-131.

Horstad, L., Larter, S.R., Mills, N., 1992. A quantitative model of biological petroleum degradation within the Brent group reservoir in the Gullfaks Field, Norwegian North Sea. Organic Geochemistry, 19, 107-117.

Hou J. Z., D'Andrea, W. J., MacDonald, D. and Huang, Y. S., 2007. Hydrogen isotopic variability in leaf waxes among terrestrial and aquatic plants around Blood Pond, Massachusetts (USA). Org. Geochem. 38, 977-984.

Hovland, M., 1982. Pockmarks and the recent geology of the central section of the Norwegian Trench. Marine Geology 47, 283-301.

Huang, Y., Eglinton, G., Ineson, P., Latter, P.M., Bol, R., Harkness, D.D., 1997. Absence of carbon isotope fractionation of individual *n*-alkanes in a 23-year field decomposition experiment with Calluna vulgaris. Organic Geochemistry 26, 497-501.

Huang, S., Fang, C., Peng, W., Jiang, Q., Feng, Z., 2017 Stable carbon isotopic composition of light hydrocarbons and *n*-alkanes of condensates in the Tarim Basin, NW China. Journal of Natural Gas Geoscience 2, 165-177.

Huang, L., Sturchio, N.C., Abrajano, T., Heraty, L.J., Holt, B.D., 1999. Carbon and chlorine isotope fractionation of chlorinated aliphatic hydrocarbons by evaporation. Organic Geochemistry 30, 777-785.

Huc, A.Y., Nederlof, P., Debarre, R., Carpentier, B., Boussafir, M., Laggoun-Defarge, F., Lenail Chouteau, A., Bordas-Le Foch, N., 2000. Pyrobitumen occurrence and formation in a Cambro-Ordovician sandstone reservoir, Fahud Salt Basin, North Oman. Chemical Geology 168, 99-112.

Hughes, W.B., 1984. Use of thiophenic organosulfur compounds in characterizing crude oils derived from carbonate versus siliclastic sources. In: Palacas, J.B. (Ed.), Petroleum Geochemistry and Source Rock Potential of Carbonate rocks. American Association of Petroleum Geologists, Studies in Geology, pp. 181-196.

Hughes, W.B., Holba, A.G., Dzou, L.I.P., 1995. The ratios of dibenzothiophene to phenanthrene and pristane to phytane as indicators of depositional environment and lithology of petroleum source rocks. Geochimica et Cosmochimica Acta 59, 3581-3598.

Hunt, J.M., 1979. Petroleum Geochemistry and Geology, Freeman, San Francisco (1st Edition).

Hunt, J.M., Whelan, J.K. and Huc, A.Y., 1980. Genesis of petroleum hydrocarbons in marine sediments. Science 209, 403-404.

Hunt, J.M., 1984. Generation and migration of light hydrocarbons. Science 1226, 1265-1270.

Hunt, J.M., 1996. Petroleum Geochemistry and Geology, Freeman, San Francisco (2st Edition).

Isaksen, G.H., 1991. Molecular indicators of lacustrine freshwater depositional environments. In: Manning, D. (Ed), Advances and Applications in Energy and the Natural Environment. Manchester Univ. Press., pp. 361-364

Isaksen, G. H., Curry, D.J., Yeakel, J.D. and Jenssen, A.I. 1998b, Controls on the oil and gas potential of humic coals: Organic Geochemistry, v. 29, no. 1-3, p. 23-44

Isaksen, G.H. and Ledje, K.H.I., 2001. Source rock quality and hydrocarbon migration pathways within the greater Utsira High area, Viking Graben, Norwegian North Sea. American Association of Petroleum Geologists Bulletin 85, 861-883.

Isaksen, G.H., Patience, R., van Graas, G., Jenssen, A.I., 2002. Hydrocarbon system analysis in a rift basin with mixed marine and nonmarine source rocks; the South Viking Graben, North Sea. American Association of Petroleum Geologists Bulletin 86, 4, 557-591.

Isaksen, G.H., Pottorf, A. and Jenssen, A.I., 1998a. Correlation of fluid inclusions and reservoired oils in the South Viking Graben, using GC/MS/MS technology. Petroleum Geoscience 4, 41-55.

Jansen, E., Sjoholm, J., 1991. Reconstruction of glaciation over the past 6 Myr from ice-borne deposits in the Norwegian Sea. Nature, 349, 600-603.

Jarvie, D.M., 2001. Williston Basin petroleum systems: inferences from oil geochemistry and geology. The Mountain Geologist 38, 1, 19-41.

Jia, W., Wang, Q., Peng, P., Xiao, Z. & Li, B., 2013. Isotopic compositions and biomarkers in crude oils from the Tarim basin: oil maturity and oil mixing. Organic Geochemistry 57, 95-106.

Jiang, C. and Li, M. 2002. Bakken/Madison petroleum systems in the Canadian Williston Basin. Part 3: geochemical evidence for significant Bakken derived oils in Madison Group reservoirs. Organic Geochemistry, 33, 761-787.

Johansen, S.E., Ostisty, B.K., Birkeland, Ø., Fedorovsky, Y.F., Martirosjan, V.N., Bruun, Christensen O., Cheredeev, S.I., Ignatenko, E.A. & Margulis, L.S., 1992. Hydrocarbon potential in the Barents Sea region: play distribution and potential. In: T.O. Vorren et al. (eds.) Arctic Geology and Petroleum Potential. *Norwegian Petroleum Society*, Special Publication 2, pp. 273-320.

Jones, D.M., Head, I.M., Gray, N.D., Adams, J.J., Rowan, A.K., Aitken, C.M, Bennett, B., et al., 2007. Crude-oil biodegradation via methanogenesis in subsurface petroleum reservoirs. Nature, 451, 176-180.

Jones, A.A., Sessions, A.L., Campbell, B., Li, C., Valentine, D.L., 2008. D/H ratios of fatty acids from marine particulate organic matter in the California Borderland Basins. Organic Geochemistry 39, 485-500.

Judd, A.G., Hovland, M., 2007. Seabed Fluid Flow: The Impact on Geology, Biology and the Marine Environment. Cambridge University Press, Cambridge, 475 pp.

Justwan, H., 2006b. The petroleum systems of the South Viking Graben, Norway. PhD thesis, University of Bergen, 1-37.

Justwan, H., Dahl, B., Isaksen, G.H., Meisingset, I., 2005. Late to Middle Jurassic source facies and quality variations, South Viking Graben, North Sea. Journal of Petroleum Geology 28, 241-268.

Justwan, H., Dahl, B., Isaksen, G.H., 2006a. Geochemical characterisation of genetic origin of oils and condensates in the South Viking Graben, Norway. Marine and Petroleum Geology 23, 213-239.

Kahmen, A., Schefuß, E., Sachse, D., 2013. Leaf water deuterium enrichment shapes leaf wax *n*-alkane δD values of angiosperm plants I: Experimental evidence and mechanistic insights. Geochimica et Cosmochimica Acta 111, 39–49.

Karr, C., Estep, P.A., Chang, T.C.L., and Comberiati, J.R., 1967. Identification of distillable paraffins, olefins, aromatic hydrocarbons, and neutral heterocyclics from a low-temperature bituminous coal tar. BuMines Bull. 637, 1-198.

Killops, S., Stoddart, D., Mills, N., 2014. Inferences for sources of oils from the Norwegian Barents Sea using statistical analysis of biomarkers. Organic Geochemistry 76, 157-166.

Kiss, I., Jakli, G., Illy, H., 1972. Isotope effects on vapour pressure, IV. Acta Chimica Academiae Scientiarum Hungaricae 71, 59-74.

Knudsen, K., Meisingset, K.K., 1991. Evaporative fractionation effects for the oils in the Gullfaks South area. In: Manning, D. (Ed.), Organic Geochemistry Advances and Applications in Energy and the Natural Environment. Manchester University Press, pp. 162-165.

Köster, J., Van Kaam-Peters, H.M.E., Koopmans, M.P., De Leeuw, J.W., Sinninghe Damsté, J.S., 1997. Sulphurisation of homohopanoids: Effects on carbon number distribution, speciation, and 22S/22R epimer ratios. Geochimica et Cosmochimica Acta 61, 2431-52.

Krouse, H.R., Viau, C.A., Eliuk, L.S., Ueda, A., Halas, S., 1989. Chemical and isotopic evidence of thermochemical sulphate reduction by light hydrocarbon gases in deep carbonate reservoirs. Nature 333, 415-419.

Kvalheim, O.M., Christy, A.A., Telnaes, N. and Bjørseth, A., 1987. Maturity determination of organic matter in coals using the methylphenanthrene distribution. Geochimica et Cosmochimica Acta 51, 1883-1888.

Lafargue, E., Barker, C., 1988. Effect of Water Washing on Crude Oil Compositions. AAPG Bulletin 72, 263-276.

Larsen, R.M., Fjaeran, T., Skarpnes, O., 1992. Hydrocarbon potential of the Norwegian Barents Sea base on recent well results. In: Vorren, T.O. et al. (eds.) Artic Geology and Petroleum Potential. Norwegian Petroleum Society, Special Publication 2, pp.321-331.

Larssen, G.B., Elvebakk, G., Henriksen, L.B., Kristensen, S.E., Nilsson, I., Samuelsberg, T.J., Svånå, T.A., Stemmerik, L., Worsley, D., 2002. Upper Palaeozoic lithostratigraphy of the Southern Norwegian Barents Sea: NPD Bulletin 9, 76 pp.

Larter, S.R., 1990. The molecular characterization of kerogen. Applications to primary and secondary migration studies and to maturation modelling. Review of Palaeobotany and Palynology, 65, 379-391.

Larter, S., Koopmans, M.P., Head, I., Aplin, A., Li, M., Wilhelms, A., Telnaes, N., Bowen, M., Zhang, C., Tieshen, W., Yixian, Y., 2000. Biodegradation rates assessed geologically in a heavy oilfield—implications for a deep, slow (Largo) biosphere. Abstract 120, GeoCanada 2000—The Millennium Geoscience Summit, Calgary, 2000, 4 p.

Larter, S.R., Solli, H., Douglas, A.G., De Lange, F., and De Leeuw, J.W., 1979. The occurrence and significance of prist-l-ene in kerogen pyrolysates. Nature, 279, 405-408.

Lecuyer, C., Gillet, P., Robert, F., 1998. The hydrogen isotope composition of seawater and the global water cycle. Chemical Geology 145, 249-261.

Li, M., Huang, Y., Obermajer, M., Jiang, C., Snowdon, L.R., Fowler, M.G., 2001. Hydrogen isotopic compositions of individual alkanes as a new approach to petroleum correlation: case studies from the western Canada sedimentary basin. Organic Geochemistry 32, 1387-1399.

Li, M., Larter, S., Mei, B. and Wu, T., 1995. Mixed maturity signatures in oils and source rocks of the Liaohe Basin. *In:* Grimalt, J. and Dorransorro, C. (eds) Organic Geochemistry, Developments and Applications to Energy, Climate, Environment and Human History, AIGOH, Donostia, San Sebastian, 421-423.

Li, J.G., Philp, P., Cui, M.Z., 2000. Methyl diamantane index (MDI) as a maturity parameter for Lower Palaeozoic carbonate rocks at high maturity and overmaturity. Organic Geochemistry 31, 267-272.

Li, C., Sessions, A.L., Kinnaman, F.S., Valentine, D.L., 2009. Hydrogen-isotopic variability in lipids from Santa Barbara Basin sediments. Geochimica et Cosmochimica Acta 73, 4803-4823.

Li, M., Wang, T., Zhong, N., Zhang, W., Akbar, S., Li, H., 2013. Ternary diagram of fluorenes, dibenzothiophenes and dibenzofurans: Indicating depositional environment of crude oils source rocks. Energy Exploration & Exploitation 31, 569-588.

Linjordet, A., and Grung-Olsen, R., 1992. The Jurassic Snøhvit Gas Field, Hammerfest Basin, Offshore Northern Norway. In: Giant Gas and Oil Fields of the Decade 1978-1988 (ed. Halbouty, M.T.). American Association of Petroleum Geologists Memoir 54, 349-370.

Littke, R., Baker, D.R., and Rullkötter, J., 1997. Deposition of Petroleum Source Rocks. In: Tissot, B.P., Welte, D.H. (Eds.), Petroleum Formation and Ocurrence: A New Approach to Oil and Gas Exploration. Springer, Berlin, Heidelberg (2nd Edition), 699.

Losh, L., Cathles, L., Meulbroek, P., 2002. Gas-washing of oil along a regional transect, offshore Louisiana. Organic Geochemistry 33, 655-664.

Machel, H.G., Krouse, H.R., Riciputi, L.R., Cole, D.R., 1995. The Devonian Nisku sour gas play, Canada- A unique natural laboratory for study of thermochemical sulfate reduction. In: Vairavamurthy, M., Schoonen, M.A.A. (Eds.), Geochemical Transformations of Sedimentary Sulfur. American Chemical Society Symposium Series 612, pp. 439-454.

Mackenzie, A.S., 1984. Application of biological markers in petroleum geochemistry. In: Brooks, J., Welte, D.H. (Eds.), Advances in Petroleum Geochemistry, Vol.1. Academic Press, London, pp. 115-214.

Mahlstedt, N., Horsfield, B., 2012. Metagenetic methane generation in gas shales I. Screening protocols using immature samples. Marine and Petroleum Geology, 31, 1, 27-42.

Mango, F.D., 1987. An invariance in the isoheptanes of petroleum. Science 273, 514-517.

Mango, F.D., 1990. The origin of light hydrocarbons in petroleum: a kinetic test of the steady-state catalytic hypothesis. Geochimica et Cosmochimica Acta 54, 1315-1323.

Mango, F.D., 1997. The light hydrocarbons in petroleum: a critical review. Organic Geochemistry 26, 7/8, 417-440.

Mansuy, L., Philp, R.P., Allen, J., 1997. Source identification of oil spills based on the isotopic composition of individual components in weathered oil samples. Environmental Science and Technology 31, 3417-3425.

Mastalerz, M., Stankiewicz, A.B., Salmon, G., Kvale, E.P., Millard, C.L., 1997. Organic geochemical study of sequences overlying coal seams; example from the Mansfield Formation (Lower Pennsylvanian), Indiana. International Journal of Coal Geology 33, 275-299.

Masterson, W.D., Dzou, L.I.P., Holba, A.G., Fincannon, A.L., Ellis, L., 2001. Evidence for biodegradation and evaporative fractionation in West Sak, Kuparuk and Prudhoe Bay field areas, North Slope, Alaska. Organic Geochemistry 32, 411-442.

Matyasik, I., Steczko, A., Philp, R.P., 2000. Biodegradation and migrational fractionation of oil from the Eastern Carpathians, Poland. Organic Geochemistry 31, 1509-1523.

Mazeas, L., Budzinski, H., Raymond, N., 2002. Absence of stable carbon isotopic fractionation of saturated and polycyclic aromatic hydrocarbons during aerobic bacterial biodegradation. Organic Geochemistry 33, 1259-1272

McKirdy, D.M., Aldrige, A.K. and Ypma, P.J.M., 1983. A geochemical comparison of some crude oils from Pre-Ordovician carbonate rocks. In: Advances in Organic Geochemistry 1981 (M. Bjoroy, C. Albrecht, C. Cornford et al., eds.), John Wiley&Sons, New York, pp. 99-107.

Miller, R.G., 1990. A paleoceanographic approach to the Kimmeridge Clay Formation. In: Huc, A.Y. (Ed), Deposition of organic facies. American Association of Petroleum Geologists Studies in Geology 30, pp. 13-26.

Milner, C.W.D., Rogers, M.A., Evans, C.R., 1977. Petroleum transformations in reservoirs. Journal of Geochemical Exploration 7, 101-153.

Moldowan, J.M., Seifert, W.K. and Gallegos, E.J., 1985. Relationship between petroleum composition and depositional environment of petroleum source rocks. AAPG Bulletin, 69, 1255-1268.

Moldowan, J.M., Sundararaman, P. and Schoell, M., 1986. Sensitivity of biomarker properties to depositional environment and/ or source input in the Lower Toarcian of S. W. Germany. Organic Geochemistry 10, 915-926.

Morton, A.C., Haszeldine, R.S., Giles, M.R. and Brown, S., 1992. Geology of the Brent Group. Geological Society Special Publication 61, pp. 1-2.

Mösle, B., Collinson, M. E., Finch, P., Stankiewicz, B. A., Scott, A. C., and Wilson, R., 1998. Factors influencing the preservation of plant cuticles: a comparison of morphology and chemical comparison of modern and fossil examples. Org. Geochem. 29, 1369-1380.

Murillo, W.A., Horsfield, B., Vieth-Hillebrand, A., 2019. Unraveling petroleum mixtures from the South Viking Graben, North Sea: A study based on $\delta^{13}C$ of individual hydrocarbons and molecular data. Organic Geochemistry, 137, 103900. https://doi.org/10.1016/j.orggeochem.2019.103900.

Murillo, W.A., Horsfield, B., Vieth-Hillebrand, A., Wilkes, H., 2017. Source Indicators to Unravel Mixtures of Oils in the South Viking Graben, North Sea: A Study based on $\delta^{13}C$ of Individual Hydrocarbons, PAHs and Sulfur Aromatic Hydrocarbons - Conference Proceedings, AAPG Annual Convention and Exhibition, Houston, Texas, USA.

Murillo, W.A., Vieth-Hillebrand, A., Horsfield, B., 2018. Petroleum in the Gullfaks Area, Northern North Sea: A New Appraisal of Source Indicators from Molecular and Isotope Data. Second EAGE Workshop on Geochemistry in Petroleum Operations and Production, Muscat, Oman, pp. 1-5. https://doi.org/10.3997/2214-4609.201803094.

Murillo, W.A., Vieth-Hillebrand, A., Horsfield, B., Wilkes, H., 2016. Petroleum source, maturity, alteration and mixing in the southwestern Barents Sea: New insights from geochemical and isotope data. Marine and Petroleum Geology 70, 119-143.

Murillo, W.A, Wilkes, H., Horsfield, B., Vieth-Hillebrand, A., 2014. Deciphering oil mixing from Jurassic, Triassic and Paleozoic source rocks in the Hammerfest Basin, SW Barents Sea - Proceedings, AAPG International Conference & Exhibition "The Spirit Between Continents: Energy Geosciences in a Changing World", Istanbul, Turkey.

Murillo, W.A., Wilkes, H., Vieth-Hillebrand, A., 2013. Assessing the effects of primary and in-reservoir processes using biomarkers and compound-specific isotopic compositions in crude oils from the Norwegian Viking Graben, North Sea. In: Gonzalez-Perez, J.A. et al. (eds.), 26th IMOG, Costa Adeje, Tenerife Spain, pp.100-101.

Murray, A.P., 1998. Factors controlling the abundance and carbon isotopic composition of land-plant derived compounds in crude oils. PhD thesis, 179 p.

Murray, A.P., Summons, R.E., Boreham, C.J., Dowling, L.M., 1994. Biomarker and *n*-alkane isotope profiles for tertiary oils: relationship to source rock depositional setting. Organic Geochemistry 22, 521-542.

Napitupulu, H., Ellis, L., Mitterer, R.M., 2000. Post-generative effects on petroleum in the onshore Northwest Java Basin. Organic Geochemistry 31, 295-315.

Norwegian Petroleum Directorate, 2013. The Norwegian Petroleum Directorate Fact-Pages of Exploration Wellbores. http://factpages.npd.no/factpages/default.aspx? culture= en&nav1=wellbore (accessed November 2013).

Norwegian Petroleum Directorate, 2014. The Norwegian Petroleum Directorate Fact-Pages of Exploration Wellbores. http://gis.npd.no/arcgis/rest/services/FactMaps (accessed November 2014).

Norwegian Petroleum Directorate, 2019a. The Norwegian Petroleum Directorate Fact-Pages of Exploration Wellbores.http://factpages.npd.no/ReportServer?/FactPages/PageView/discovery&rs:Command=Render&rc:Toolbar=false&rc:Parameters=f&NpdId=17196400&IpAddress=200.89.46.168&CultureCode=en (accessed Jun, 2019).

Norwegian Petroleum Directorate, 2019b. The Norwegian Petroleum Directorate Fact-Pages of Exploration Wellbores. http://factpages.npd.no/pbl/geochemical_pdfs/1494_2.pdf (accessed Jun, 2019).

Norwegian Petroleum Directorate, 2019c. The Norwegian Petroleum Directorate Fact-Pages of Exploration Wellbores.http://factpages.npd.no/ReportServer?/FactPages/PageView/wellbore_exploration (accessed Jun, 2019).

Obermajer, M., Osadetz, K.G., Fowler, M.G., Snowdon, L.R., 2000. Light hydrocarbon (gasoline range) parameter refinement of biomarker-based oil-oil correlation studies: an example from Williston Basin. Organic Geochemistry 31, 959-976.

Odden, W., Barth, T. and Talbot, M.R. 2002. Compound specific carbon isotope analysis of natural and artificially generated hydrocarbons in source rocks and petroleum fluids from offshore Mid-Norway. Organic Geochemistry, 33, 47-65.

Odden, W., Patience, R.L. and van Graas, G.W., 1998. Applications of light hydrocarbons (C_4-C_{13}) to oil/source rock correlations. Organic Geochemistry 28, 823-47.

Ohm, S.E., Karlsen, D.A., Austin, T.J.F., 2008. Geochemically driven exploration models in uplifted areas: examples from the Norwegian Barents Sea. American Association of Petroleum Geologists Bulletin 92 (9), 1191-1223.

Orr, W.L., 1974. Changes in sulfur content and isotopic ratios of sulfur during petroleum maturation- study of Big Horn basin Paleozoic oils. American Association Petroleum Geologists Bulletin 58, 2295-2318.

Orr, W.L., 1977. Geologic and geochemical controls on the distribution of hydrogen sulfide in natural gas. In: Campos, R., Goni, J. (Eds.), Advances in Organic Geochemistry, Proceedings of the 7th International Meeting, Enadisma, Madrid, Spain, pp. 571-597.

Orr, W.L., 1986. Kerogen/asphaltene/sulfur relationships in sulfur-rich Monterey oils. Organic Geochemistry 10, 499-516.

Osburn, M.R., 2013. Isotopic proxies for microbial and environmental change (PhD thesis). California Institute of Technology.

Ostanin, I., Anka, Z., di Primio, R., Bernal, A., 2013. Hydrocarbon plumbing systems above the Snøhvit gas field: Structural control and implications for thermogenic methane leakage in the Hammerfest Basin, SW Barents Sea. Mar. Pet. Geol., 43, 127-146.

Ostanin, I., Anka, Z., di Primio, R., 2017. Role of Faults in Hydrocarbon leakage in the Hammerfest Basin, SW Barents Sea: Insights from Seismic Data and Numerical modelling. Geosciences, 7, 28.

Oygard, K., Larter, S.R., and Senftle, J., 1988. The Control of Maturity and Kerogen Type on Analytical Pyrolysis Data. Organic Geochemistry 13, 1153-1162.

Palmer, S.E., 1984. Effect of water washing on C_{15}^+ hydrocarbon fraction of crude oils from northwest Palawan, Philippines. AAPG Bulletin 68, 137-149.

Palmer, S.E., 1993. Effect of biodegradation and water washing on crude oil composition. In: Engel, M.H., Macko, S.A. (Eds.), Organic Geochemistry. Plenum Press, New York, pp. 511-533.Geochemistry 10, 499-516.

Pastorova, R.E., Botto, A.P.W., Boon, J.J., 1994. Cellulose char structure: a combined analytical Py–GC–MS, FTIR, and NMR study. Carbohydr. Res. 262, 27-47.

Pedentchouk, N., Freeman, K.H., Harris, N.B., 2006. Different response of δD values of *n*-alkanes, isoprenoids, and kerogen during thermal maturation. Geochimica et Cosmochimica Acta 70, 2063-2072.

Pedentchouk, N., Turich, C., 2017. Carbon and hydrogen isotopic compositions of *n*-alkanes as a tool in petroleum exploration. In: Lawson, M., Formolo, M.J. and Eiler, J.M. (Eds.), From Source to Seep: Geochemical Applications in Hydrocarbon Systems. Geological Society, London, Special Publications, 468.

Pegrum, R.M., Spencer, A.M., 1990. Hydrocarbon plays in the northern North Sea. In: Brooks, J. (Ed.), Classic Petroleum Provinces. Geological Society Special Publication 50, pp. 441-470.

Peters, K.E., 1986. Guidelines for Evaluating Petroleum Source Rock Using Programmed Pyrolysis. American Association of Petroleum Geologists Bulletin, 70, 318-329.

Peters, K.E., Cassa, M.R., 1994. Applied source rock geochemistry. In: Magoon, L.B., Dow, W.G. (Eds.), The Petroleum System-from Source to Trap. Amer. Assoc. Petrol. Geol. Mem. 60, pp. 93-120.

Peters, K.E., Creaney, S., 2004. Geochemical differentiation of Silurian from Devonian crude oils in eastern Algeria. In: Hill, R., Leventhal, J. et al. (eds) Geochemical Investigations in Earth and Space Science. The Geochemical Society Special Publications, 9, Elsevier Science, 287-301.

Peters, K.E., Fowler, M., 2002. Applications of petroleum geochemistry to exploration and reservoir management. Organic Geochemistry, 33, 5-36.

Peters, K.E., and Moldowan, J.M., 1991. Effects of source, thermal maturity, and biodegradation on the distribution and isomerization of homohopanes in petroleum. Organic Geochemistry 17 (1), 47-61.

Peters, K.E., Moldowan, J.M., 1993. The Biomarker Guide. Interpreting Molecular Fossils in Petroleum and Ancient Sediments. Prentice-Hall, Englewood Cliffs, New Jersey, 365 p.

Peters, K.E., Moldowan, J.M., Driscole, A.R., Demaison, G.J., 1989. Origin of Beatrice oil by co-sourcing from Devonian and Middle Jurassic source rocks, Inner Moray Firth, U.K. Bulletin of the American Association of Petroleum Geologists 73, 454-471.

Peters, K.E., Moldowan, J.M., McCaffrey, M.A., Fago, F.J., 1996. Selective biodegradation of extended hopanes to 25-norhopanes in petroleum reservoirs. Insights from molecular mechanics. Organic Geochemistry 24, 765-783.

Peters, K.E., Scott-Ramos, L., Zumberge, J.E., Valin, Z.C., Bird, K.J., 2008. De-convoluting mixed crude oil in Prudhoe Bay Field, North Slope, Alaska. Organic Geochemistry 39, 623-645.

Peters K.E., Walters C.C., and Moldowan J.M., 2005. The Biomarker Guide. Second edition. Cambridge University Press, UK. Vol. 2, 1155 p.

Pond, K.L., Huang, Y., Wang, Y., Kulpa, C.F., 2002. Hydrogen isotopic composition of individual *n*-alkanes as an intrinsic tracer for bioremediation and source identification of petroleum contamination. Environmental Science and Technology 36, 724-728.

Püttmann, W., Villar, H., 1987. Occurrence and geochemical significance of 1,2,5,6- tetramethylnaphthalene. Geochimica et Cosmochimica Acta 51, 3023-3029.

Radke, M., 1988. Application of aromatic compounds as maturity indicators in source rocks and crude oils. Marine and Petroleum Geology 5, 224-236.

Radke, J., Bechtel, A., Gaupp, R., Puttmann, W., Schwark, L., Sachse, D., Gleixner, G., 2005. correlation between hydrogen isotope ratios of lipid biomarkers and sediment maturity. Geochimica et Cosmochimica Acta 69, 5517-5530.

Radke, M., Rullkötter, J. and Vriend, S.P., 1994. Distribution of naphthalenes in crude oils from the Java Sea: Source and maturation effects. Geochimica et Cosmochimica Acta 58, 3675-3689.

Radke, M., Vriend, S.P., Ramanampisoa, L.R., 2000. Alkyldibenzofurans in terrestrial rocks: influence of organic facies and maturation. Geochimica et Cosmochimica Acta 64, 275-286.

Radke, M. and Welte, D.H., 1983. The methylphenanthrene index (MPI): A maturity parameter based on aromatic hydrocarbons. In: Bjorøy, M. et al. (Eds.), Advances in Organic Geochemistry 1981. London, Wiley, pp. 504-512.

Radke, M., Welte, D.H. and Willsch, H., 1982. Geochemical study on a well in the Western Canada Basin: relation of the aromatic distribution pattern to maturity of organic matter. Geochimica et Cosmochimica Acta 46, 1-10.

Radke, M., Welte, D.H., Willsch, H., 1986. Maturity parameters based on aromatic hydrocarbons: influence of the organic matter type. Organic Geochemistry 10, 51-63.

Radke, M., Willsch, H., Welte, D.H., 1980. Preparative hydrocarbon group type determination by automated medium pressure liquid chromatography. Analytical Chemistry 52, 406-411.

Renard, V., Malod, J., 1974. Structure of the Barents Sea from seismic refraction. Earth and Planetary Science Letters 24, 33-47.

Riber, L., Dypvik, H., Sørlie, R., 2015. Altered basement rocks on the Utsira High and its surroundings, Norwegian North Sea. Norwegian Journal of Geology 95, 57–89.

Rice, D. D., Claypool, G. E., 1981. Generation, accumulation and resource potential of biogenic gas. AAPG Bulletin 65, 5-25.

Rieley, G., Collier, R., Jones, D., Eglinton, G., Eakin, P. and Fallick, A., 1991. Sources of sedimentary lipids deduced from stable carbon-isotope analyses of individual compounds. Nature 352, 425-427.

Rigby, D., Batts, B.D., Smith, J.W., 1981.The effect of maturation on the isotopic composition of fossil fuels. Organic Geochemistry 3, 29-36.

Riis, F. and Fjeldskaar, W., 1992. On the magnitude of the Late Tertiary and Quaternary erosion and its significance for the uplift of Scandinavia and the Barents Sea. In: R. M. Larsen et al. (eds.) Structural and Tectonic Modelling and its Application to Petroleum Geology. Norwegian Petroleum Society, Special Publication 1, pp. 163-185.

Riis, F., Lundschien, B.A., Høy, T., Mørk, A., and Mørk, M.B., 2008. Evolution of the Triassic shelf in the northern Barents Sea region: Polar Research 27, 3, 318-338.

Rooney, M.A., 1995. Carbon isotope ratios of light hydrocarbons as indicators of thermochemical sulfate reduction. In: Grimalt, J.O., Dorronsoro, C. (Eds.), Organic Geochemistry: Developments and Applications to Energy, Climate, Environment and Human History. A.I.G.O.A, Donostia-San Sebastian, pp. 523-525.

Rubinstein, I. and Albrecht, P., 1975. The occurrence of nuclear methylated steranes in a shale. Journal of the Chemical Society, Chemical Communications, 957-8.

Rubinstein, I., Sieskind, O. & Albrecht, P. 1975. Rearranged steranes in a shale: Occurrence and simulated formation. Journal of Chemical Society, 1, 1833-1836.

Rullkötter, J., Mackenzie, A.S., Welte, D.H., Leythaeuser, D. and Radke, M., 1984. Quantitative gas chromatography-mass spectrometry analysis of geological samples. Organic Geochemistry, 6, 817-827.

Rullkötter, J., Spiro, B. and Nissenbaum, A., 1985. Biological marker characteristics of oils and asphalts from carbonate source rocks in a rapidly subsiding graben, Dead Sea, Israel. Geochimica et Cosmochimica Acta, 49, 1357-70.

Sachse, D., Billault, I., Bowen, G.J., Chikaraishi, Y., Dawson, T.E., Feakins, S.J., Freeman, K.H., Magill, C.R., McInerney, F.A., van der Meer, M.T.J., Polissar, P., Robins, R.J., Sachs, J.P., Schmidt, H. L., Sessions, A.L., White, J.W.C., West, J.B., Kahmen, A., 2012. Molecular paleohydrology: interpreting the hydrogen isotopic composition of lipid biomarkers from photosynthesizing organisms. Annual Reviews of Earth and Planetary Science 40, 221-249. 37:469-83.

Sachse, D., Gleixner, G., Wilkes, H., Kahmen, A., 2010. Leaf wax *n*-alkane δD values of field-grown barley reflect leaf water δD values at the time of leaf formation. Geochim. Cosmochim. Acta 74, 6741-50

Sachse, D., Radke, J., Gleixner, G., 2004. Hydrogen isotope ratios of recent lacustrine sedimentary *n*-alkanes record modern climate variability. Geochim. Cosmochim. Acta 68, 4877-89.

Sachse, D., Radke, J., Gleixner, G., 2006. δD values of individual *n*-alkanes from terrestrial plants along a climatic gradient—Implications for the sedimentary biomarker record. Org. Geochem. 37, 469-483.

Samuel, O.J., Cornford, C., Jones, M., Adekeye, O.A., Akande, S.O., 2009. Improved understanding of the petroleum systems of the Niger delta basin, Nigeria. Organic Geochemistry 40, 461-483.

Sauer, P.E., Eglinton, T.I., Hayes, J.M., Schimmelmann, A., Sessions, A.L., 2001. Compound-specific D/H ratios of lipid biomarkers from sediments as a proxy for environmental and climatic conditions. Geochimica et Cosmochimica Acta 65, 213-222.

Schaefer, R.G. and Littke, R., 1988. Maturity-related compositional changes in the low-molecular-weight hydrocarbon fraction of Toarcian shales. Organic Geochemistry 13, 887-92.

Schimmelmann, A., Boudou, J.P., Lewan, M.D., Wintsch, R.P., 2001. Experimental controls on D/H and $^{13}C/^{12}C$ ratios of kerogen, bitumen and oil during hydrous pyrolysis. Organic Geochemistry 32, 1009-1018.

Schimmelmann, A., Lewan, M.D., Wintsch, R.P., 1999. D/H isotope ratios of kerogen, bitumen, oil, and water in hydrous pyrolysis of source rocks containing kerogen types I, II, IIS, and III. Geochimica et Cosmochimica Acta 63, 3751-3766.

Schimmelmann, A., Sessions, A.L., Boreham, C., Edwards, D., Logan, G.A., Summons, R.E., 2004. D/H ratios in terrestrially sourced petroleum systems. Organic Geochemistry 35, 1169-1195.

Schoell, M., Hayes, J.M., 1994. Compound-specific isotope analysis in biogeochemistry and petroleum research. Organic Geochemistry 21, 1-827.

Schoell, M., Teschner, M., Wehner, H., Durand, B., Oudin, J.L., 1983. Maturity related biomarker and stable isotope variations and their application to oil/source rock correlation in the Mahakam Delta Kalimantan. In: Bjorøy, M. et al. (eds.), Advances in Organic Geochemistry 1981. Wiley, Chichester, pp. 156-163

Schouten, S., Klein Breteler, W.C.M., Blokker, P., Schogt, N., Rijpstra, W.I.C., Grice, K., Baas, M., Sinninghe Damsté, J.S., 1998. Biosynthetic effects on the stable carbon isotopic compositions of algal lipids: implications for deciphering the carbon isotopic biomarker record. Geochimica et Cosmochimica Acta 62, 1397-1406.

Seifert, W.K., Moldowan, J.M., 1978. Applications of steranes, terpanes and monoaromatics to the maturation, migration and source of crude oils. Geochimica et Cosmochimica Acta 42, 77-95.

Seifert, W.K., Moldowan, J.M., 1981. Paleoreconstruction by biological markers. Geochimica et Cosmochimica Acta 45, 783-794.

Sessions, A.L., 2016. Factors controlling the deuterium contents of sedimentary hydrocarbons. Organic Geochemistry, 96, 43-64.

Sessions, A.L., Burgoyne, T.W., Schimmelmann, A., Hayes, J.M., 1999. Fractionation of hydrogen isotopes in lipid biosynthesis. Organic Geochemistry 30, 1193-1200.

Sessions, A.L., Sylva, S.P., Summons, R.E., Hayes, J.M., 2004. Isotopic exchange of carbon-bound hydrogen over geologic timescales. Geochimica et Cosmochimica Acta 68, 1545-1559.

Sharaf, L., El Nady, M., 2006. Application of light hydrocarbon (C_7^+) and biomarker analyses in characterizing oil from wells in the north and north central Sinai, Egypt. Petroleum Science and Technology 24, 607-627.

Silverman, S. R., 1965, Migration and segregation of oil and gas, in A. Young and J. E. Galley, eds., Fluids in subsurface environments: AAPG Memoir N° 4, p. 53-65.

Simoneit, B.R.T., 1977. Diterpenoid compounds and other lipids in deep-sea sediments and their geochemical significance. Geochimica et Cosmochimica Acta 41, 463-476.

Simoneit, B.R.T., 1985. Cyclic terpenoids in the geosphere. In Methods in Geochemistry and Geophysics 25 (ed. Johns, R. B.), pp. 43-99. Elsevier.

Simoneit, B.R.T., Grimalt, J.G., Wang, T.G., Cox, R.E., Hatcher, P.G., and Nissenbaum, A., 1986. Cyclic terpenoids of contemporary resinous plant detritus and of fossil woods, ambers and coals. In: Advances in Organic Geochemistry 1985 (ed. Leythauser, D. and Rullkotter, J.). Org. Geochem. 10**,** 877-889.

Stemmerik. L. and Worsley, D., 1989. Late Paleozoic sequence correlation, North Greenland and the Barents Shelf. In: Collinson, J.D. (ed.) Correlation in hydrocarbon exploration, Graham & Trotman, Norwegian Petroleum Society, London, pp. 100-113.

Sternberg L.D.L., 1988. D/H ratios of environmental water recorded by D/H ratios of plant lipids. Nature 333, 59-61.

Strachan, M.G., Alexander, R., Kagi, R.I., 1988. Trimethylnaphthalenes in crude oils and sediments: effects of source and maturity. Geochimica et Cosmochimica Acta 52, 1255-1264.

Su, A., Liang, D., Cheng, K., 2003. Evaporative fractionation of oil and gas reservoir in Nanbaxian area of northern Qaidam Basin, China. Shiyou Xuebao 24, 31-35 (English abstract).

Summons, R.E., Jahnke, L.L., Roksandic, Z., 1994. Carbon isotopic fractionation in lipids from methanotrophic bacteria: relevance for interpretation of the geochemical record of biomarkers. Geochimica et Cosmochimica Acta 13, 2853-2863.

Sun, Y., Chen, Z., Xu, S., Cai, P., 2005. Stable carbon and hydrogen isotopic fractionation of individual *n*-alkanes accompanying biodegradation: evidence from a group of progressively biodegraded oils. Organic Geochemistry, 36, 225-238.

Tang, Y., Huang, Y., Ellis, G.S., Wang, Y., Kralert, P.G., et al., 2005. A kinetic model for thermally induced hydrogen and carbon isotope fractionation of individual *n*-alkanes in crude oil. Geochimica et Cosmochimica Acta 69, 4505-20.

Tang, Y., Jenden, P.D., 1995. Theoretical modeling of carbon and hydrogen isotope fractionations in natural gas. In: Grimalt, J.O. and Dorronsoro, C. (Eds.) Organic Geochemistry, Developments and Applications to Energy, Climate, Environment and Human History. AIGOA, Donostia-San Sebastian, p.1067-1096.

Tegelaar, E.W., de Leeuw, J.W., Derenne, S., Largeau, C., 1989. A reappraisal of kerogen formation. Geochimica et Cosmochimica Acta 53, 3103-3106.

Telnaes, N., Wilhelms, A., Hanesand, T., Rein, E., Hermansen, D., 1997. Variation in the kinetic parameters for hydrocarbon generation in Upper Jurassic source rocks offshore Norway. In: AAPG International Conference and Exhibition; abstracts. American Association of Petroleum Geologists, Tulsa, p. 1416.

Ten Haven, H.L., 1996. Applications and limitations of Mango's light hydrocarbon parameters in petroleum correlation studies. Organic Geochemistry 24, 957-976.

Theuerkorn, K., Horsfield, B., Wilkes, H., di Primio, R., Lehne, E., 2008. A reproducible and linear method for separating asphaltenes from crude oil. Organic Geochemistry 39, 929-934.

Thomas, B.M., Moller-Pedersen, P., Whitaker, M.F., Shaw, N.D., 1985. Organic facies and hydrocarbon distributions in the Norwegian North Sea. In: Thomas, B.M. et al. (Eds.), Petroleum Geochemistry in Exploration of the Norwegian Shelf. Proceedings NPF Conference, Stavanger, 1984. Graham and Trotman for Norwegian Petroleum Society, pp. 3-26.

Thompson, K.F.M., 1983. Classification and thermal history of petroleum based on light hydrocarbons. Geochimica et Cosmochimica Acta 47, 303-316.

Thompson, K.F.M., 1987. Fractionated aromatic petroleums and the generation of gas-condensates: Organic Geochemistry 11, 573-590.

Thompson, K.F.M., 1988. Gas-condensate migration and oil fractionation in deltaic systems. Marine and Petroleum Geology 5, 237-246.

Tissot, B., Durand, B., Espitalié, J. and Combaz, A., 1974. Influence of the Nature and Diagenesis of Organic Matter in Formation of Petroleum. Am. Assoc. Petr. Geol., 58, 499-506.

Tissot, B., Welte, D.H., 1978. Petroleum Formation and Occurrence: A New Approach to Oil and Gas Exploration. Springer, Berlin, Heidelberg (1st Edition), 538 p.

Tissot, B., Welte, D.H., 1984. Petroleum Formation and Occurrence: A New Approach to Oil and Gas Exploration. Springer, Berlin, Heidelberg (2nd Edition), 699 p.

Trindade, L.A.F., Brassell, S.C., Santos Neto, E.V., 1992. Petroleum migration and mixing in the Potiguar Basin, Brazil. AAPG Bulletin76 (12), 1903-1924.

Tuo, J., Zhang, M., Wang, X., Zhang, C., 2006. Hydrogen isotope ratios of aliphatic and diterpenoid hydrocarbons in coals and carbonaceous mudstones from the Liaohe Basin, China. Organic Geochemistry 37, 165-176.

van Aarssen, B.G.K., Alexander, R., Kagi, R., 2000. Higher plant biomarkers reflect palaeovegetation changes during Jurassic times. Geochimica et Cosmochimica Acta 64, 1417-1424.a

van Aarssen, B.G.K., Cox, H.C., Hoogendoorn, P., and de Leeuw, J.W., 1990. A cadinene biopolymer in fossil and extant dammar resins as a source for cadinanes and bicadinanes in crude oils from South East Asia. Geochimica et Cosmochimica Acta 54, 3021-3031.

van Aarssen, B.G.K., Hessels, J.K.C., Abbink, O.A., and de Leeuw, J.W., 1992. The occurrence of polycyclic sesqui-, tri-, and oligoterpenoids derived from a resinous polymeric cadinene in crude oils from Southeast Asia. Geochimica et Cosmochimica Acta 56, 1231-1246.

van Graas, G.W., Gilje, A.E., Isom, T.P., Tau, L.A., 2000. The effects of phase fractionation on the composition of oils, condensates and gases. Organic Geochemistry 31, 1419-1439.

van Koeverden, J.H., Karlsen, D.A., Schwark, L., Chpitsglouz, A. and Backer-Owe, K., 2010. Oil-prone Lower Carboniferous coals in the Norwegian Barents Sea: Implications for a Paleozoic petroleum system: Journal of Petroleum Geology 33, 155-181.

Volk, H., Horsfield, B., Mann, U., Suchy, V., 2002. Variability of petroleum inclusions in vein, fossil and vug cements – a geochemical study in the Barrandian Basin (Lower Paleozoic, Czech Republic). Organic Geochemistry 33, 1319-1341.

Volkman, J.K., Alexander, R., Kagi, R.I., Woodhouse, G.W., 1983. Demethylated hopanes in crude oils and their application in petroleum geochemistry. Geochimica Cosmochimica Acta 47, 1033-1040.

Vollset, J., Dore, A.G., 1984. A revised Triassic and Jurassic lithostratigraphic nomenclature for the Norwegian North Sea. Norwegian Petroleum Directorate Bulletin 3, 1-53.

Von der Dick, H., Meloche, J.D., Dwyer, J. and Gunther, P., 1989. Source-rock geochemistry and hydrocarbon generation in the Jeanne D'arc basin, grand banks, offshore eastern Canada. Journal of Petroleum Geology 12, 51-68.

Vorren, T.O., Richardsen, G., Knutsen, S.M. and Henriksen, E., 1991. Cenozoic erosion and sedimentation in the western Barents Sea. Marine Petroleum Geology 8, 317-340.

Wang, Y., Huang Y., 2001. Hydrogen isotope fractionation of low molecular weight *n*-alkanes during progressive vaporization. Organic Geochemistry 32, 991-98.

Wang, Y., Huang, Y., 2003. Hydrogen isotopic fractionation of petroleum hydrocarbons during vaporization: implications for assessing artificial and natural remediation of petroleum contamination. Applied Geochemistry 18, 1641-1651.

Wang, Y., Sessions, A.L., Nielsen, R.J., Goddard, W.A., 2009. Equilibrium $^{2}H/^{1}H$ fractionations in organic molecules. II: Linear alkanes, alkenes, ketones, carboxylic acids, esters, alcohols and ethers. Geochimica et Cosmochimica Acta 73, 7076-7086.

Waples, D.W., 2000. The kinetics of in-reservoir oil destruction and gas formation: constraints from experimental and empirical data, and from thermodynamics. Organic Geochemistry 31, 553-575.

Waples, D.W., Curiale, J.A., 1999. Oil-oil and oil-source rock correlations. In: Beaumont, E.A., Foster, N.H. (Eds.), Exploring for Oil and Gas Traps. American Association of Petroleum Geologists, Tulsa, Oklahoma, pp. 8-71.

Waseda, A., 1993. Effect of maturity on carbon and hydrogen isotopes of crude oils in Northeast Japan. Journal of the Japanese Association for Petroleum Technology 58, 199-208.

Weiss, H.M., Wilhelms, A., Mills, N., Scotchmer, J., Hall, P.B., Lind, K., Brekke, T., 2000. NIGOGA - The Norwegian Industry Guide to Organic Geochemical Analyses. Edition 4.0. http://www.npd.no/engelsk/nigoga/default.htm.

Wenger, L.M., Davis, C.L. and Isaksen, G.H., 2002. Multiple controls on petroleum biodegradation and impact on oil quality. SPE Reservoir Evaluation and Engineering 5, 375-383.

Wilhelms, A., Larter, S.R., 1994a. On the origin of tar mats in petroleum reservoirs: Part I. Introduction and case studies. Marine and Petroleum Geology 11, 418-441.

Wilhelms, A., Larter, S.R., 1994b. On the origin of tar mats in petroleum reservoirs: Part II. Formation mechanisms for tar mats. Marine and Petroleum Geology 11, 442-456

Wilhelms, A., Larter, S.R., 1995. Overview of the geochemistry of some tar mats from the North Sea and USA: Implications for tar-mat origin. Geological Society, London, Special Publications, 86, 87-101.

Wilhelms, A., Larter, S.R., Hall, K., 1994c. A comparative study of the stable carbon isotopic composition of crude oil alkanes and associated crude oil asphaltene pyrolysate alkanes. Organic Geochemistry 21, 751-759.

Wilhelms, A., Larter, S.R., Head, I., Farrimond, P., di-Primio, R. and Zwach, C., 2001. Biodegradation of oil in uplifted basins prevented by deep-burial sterilization. Nature, 411, 1034-1037.

Wilhelms, A., Larter, S.R., 2004. Shaken but not always stirred. Impact of petroleum charge mixing on reservoir geochemistry. In: Cubitt, J.M., England, W.A., Larter, S.R. (Eds.), Understanding Petroleum Reservoirs: Towards an Integrated Reservoir Engineering and Geochemical Approach. Geological Society Special Publication 237, 27-35.

Wilkes, H., Boreham, C., Harms, G., Zengler, K., Rabus, R., 2000. Anaerobic degradation and carbon isotopic fractionation of alkylbenzenes in crude oil by sulphate-reducing bacteria. Organic Geochemistry 31, 101-115.

Worden, R.H., Smalley, P.C., Oxtoby, N.H., 1995. Gas souring by thermochemical sulfate reduction at 140 °C. American Association of Petroleum Geologists Bulletin 79, 854-863.

Worsley, D., 2008. The post-Caledonian development of Svalbard and the western Barents Sea: Polar Research 27, 298-317.

Xiong, Y., Geng, A., Pan, C., Liu, D., Peng, P., 2005. Characterization of the hydrogen isotopic composition of individual *n*-alkanes in terrestrial source rocks. Applied Geochemistry 20, 455-464.

Yang, H., Huang, Y., 2003. Preservation of lipid hydrogen isotope ratios in Miocene lacustrine sediments and plant fossils at Clarkia, northern Idaho, USA. Organic Geochemistry 34, 413-423.

Yang, H., Liu, WG., Leng, Q., Hren, MT., Pagani, M., 2011. Variation in *n*-alkane δD values from terrestrial plants at high latitude: implications for paleoclimate reconstruction. Organic Geochemistry 42, 283-88

Yeh, H.W., Epstein, S., 1981. Hydrogen and carbon isotopes of petroleum and related organic matter. Geochimica et Cosmochimica Acta 45, 753-762.

Zengler, K., Richnow, H.H., Rossello -Mora, X., Michaelis, W., Widdel, F., 1999. Methane formation from long-chain alkanes by anaerobic microorganisms. Nature 401, 266-269.

Zhang, C., Li, S., Yang, J., Yang, S., Wang, J., 2004. Petroleum migration and mixing in the Pearl River Mouth Basin, South China Sea. Marine and Petroleum Geology 21, 215-224.

Zhang, Z., Sachs, J.P., 2007. Hydrogen isotope fractionation in freshwater algae: I. Variations among lipids and species. Organic Geochemistry 38, 582-608.

Zhou Dong, J., Vorkink, W.P., Lee, M.L., 1993. Origin of long-chain alkylcyclohexanes and alkylbenzenes in a coal-bed wax. Geochimica et Cosmochimica Acta 57, 837-849.

Ziegler, P.A., 1992. North Sea rift system. Tectonophysics 208, 55-75.

Ziegler, P.A., Van-Hoorn, B., 1989. Evolution of North Sea rift system. In: Tankard, A. J., Balkwill, H.R. (Eds.), Extensional Tectonics and Stratigraphy of the North Atlantic Margins. American Association of Petroleum Geologists Memoir, pp. 471-500.